Mathematical modelling of nicotinic effects and Parkinson's disease in the brain

Penney, Mark Stuart

Award date:
2000

Awarding institution:
University of Bath

Mathematical Modelling of Nicotinic Effects and Parkinson's Disease in the Brain

Submitted by Mark Stuart Penney

for the degree of Ph.D. of the University of Bath, 2000

ProQuest LLC
789 East Eisenhower Parkway
P.O. Box 1346
Ann Arbor, MI 48106-1346

Summary

The neuromodulatory effects of nicotine and the degenerative disorder of Parkinson's disease have been the subject of experimental study worldwide. As yet there has been no mathematical modelling of the effects of nicotine and Parkinson's disease at the cellular level, a process that is capable of providing great insight and a much better understanding of the mechanisms involved.

We present a variety of models that attempt to describe various aspects of nicotinic effects and of Parkinson's Disease. We first model the nicotinic-agonist induced release of transmitter from the experimental preparation of synaptosomes, the results of which we can describe well with our quantitative model which suggests that nicotinic agonists induce release from synaptosomes by prompting the repetitive firing of action potentials.

We consider the apparently pleasurable effects of tobacco smoking by modelling the burst firing pattern of mesolimbic dopamine neurons. This pattern, which is physiologically relevant to the rewarding effects of addictive drugs, can be caused by the calcium-dependent inactivation of an otherwise voltage-dependent potassium channel. Furthermore we show that for this inactivation to take place, calcium levels must be elevated by the forcing of action potentials by an external excitatory input, that nicotine can potentiate.

The modelling of the long-term effects of nicotine addresses how persistent exposure to nicotine can lead to both a functional tolerance to its effects, by a downregulation in functional receptor numbers, and a sensitisation, by the induction of a long-term potentiation-like upregulation of synaptic strength. We demonstrate that this sensitisation, once induced, can be self-sustaining and as such can be maintained indefinitely.

By modelling the neuronal network affected by Parkinson's Disease we study how the onset of this disease leads to changes in neuronal function and how this may explain some of the clinical symptoms of sufferers. In particular we can demonstrate that the model is robust to large losses of dopaminergic input before there are any changes in the dynamics, when oscillations analogous to the resting tremor in patients emerge.

Acknowledgements

There are many people I would like to thank for their contributions towards the production of this thesis, whether it has been providing technical help or making the last three years a very pleasant time. Thanks in particular must go to my supervisors, Nick and Sue. Nick's been brilliant in helping me set the project up and getting me started in the right places that has made my time here run very smoothly, needing only the occasional guiding nudge. Sue should be congratulated for taking on a non-experimentalist in the first place and I hope that I have been able to justify this and demonstrate how useful modelling may be. Her knowledge of all things neuronal and patience in explaining the workings of a subject that was initially very alien to me have been invaluable.

The department have been great; the Admin. people who let me have the money to go to Canada, USA and the Netherlands; and Computer Support for the flash PC that this thesis was written on.

Thanks go to my parents for an unwavering support (emotional and financial) whilst I have spent even more time being a student.

Cheers for the support from the old Uni. lot; Andy for just being Andy (why Tori?), Tori for the Welsh translations, Karen and Bryn for some of the juiciest gossip around and Susie for our many e-mail conversations.

I would like to mention those who have made my time here so very enjoyable, I hope I haven't missed anyone out. Graeme and Stuart for all the cups of tea we've shared and Simon for brightening everyone's day. The footballers and cricketers; new captain and fantasy league runner Git, Jock, Bob, Jon Heritage, Dim, Doc. Hobson, Hooman, Frank, Martin, Steve Langdon (and for introducing me to the delights of Bath City), Steve Benbow, Bill Browne, Jon Wilson, Paul, Matt, Stuart Humphreys, Adrian, Yoshi, Rob Scheichl (in whom Austria have a fine wicket keeper), Aaron Wilson, Alfio, Ross, Sam, Rob Laister and Orlando. The others from around the department, biology and the rest of the university ; Kathy, Andrew Falcon, Chris Sangwin, Claudia, Ivana, Vicky, Emma, Diana, Rich, Spenny, Sarah Backen, Dave Power, Ryan and Sarah, James and Helen and of course the lovely Nia.

Contents

List of Figures

List of Tables

Chapter 1

Introduction

1.1 Mathematical Modelling

1.1.1 What is a mathematical model?

A model can be considered to be any theoretical description of another system, which may be complex real life physical systems through to other models. Mathematics provides a language that is highly suited to describing such a theoretical model formally and rigorous techniques that may be used to analyse this description and tell us how our model (and by implication the original system) behaves. We can then define a mathematical model to be a formal description of a theoretical model.

1.1.2 Models are in use everywhere

Before advancing reasons as to why modelling can be a useful process it is worth stressing that models are already in use in everyday life. This is to address the point that is often made to me (and often by experimentalists) that models are not real, implying that as such they have no use. However we all use models; simple cases being such things as estimating car journey times based on average speeds, or where to put our hand to catch a ball.

We can also counter that so-called 'real' experiments are often based on artificially created 'model' preparations and the results gleaned involve measurements of parameters that are themselves based on models, such as reading from an oscilloscope. Of course such models have been extensively tested and are generally accepted to be accurate to within certain limits and so are as 'real' as we can expect. This is a process that must be done with any of our modelling; testing and discussing where its conclusions are valid.

Probably mathematical-biology's greatest success in neuroscience has been Hodgkin and Huxley's description of current in excitable cell membranes [41] (described in section 1.2.2). This is certainly a mathematical model but has proved to be so accurate that it is used today by neuroscientists as a description of how ion channels are thought to work. The parameters necessary for the model are readily measured by experiment. It has long since ceased to be considered a model and has become part of the subject it was intended to describe.

1.1.3 The Advantages of Modelling

It may not be apparent how a model can be of use. Since it represents a theoretical description it will generally be deficient in some way and is therefore wrong. So how can such a simplified model be useful? It is often the case that the preparation of study (populations of insects, bits of brain, or the motion of the planets) is terrifyingly complicated. If we wish to understand how the system functions, or to make predictions of future behaviour, we must make simplifications. This forces us to create a theoretical model and mathematics allows us to write this down in a formal way.

A simplified description will then identify the major components that cause the system to behave the way it does, minor components having been discarded (subject to justification). The act of writing down a model forces the modeller to consider the system in a very proper way, which can itself be instructive and show up any flaws in a theoretical model.

Where such a model describes the system well we can be confident that we have an accurate picture of how it computes. Conversely there may be areas in which the model is deficient, in which case we know that we may have missed a process, or have been unjustified in removing a known one. Hence the development of a model can help here; it can act to confirm the theories we propose and also reveal any holes that may exist. A good model may also be able to suggest what process is missing that plugs this hole. This makes the interesting point that even when wrong, a model may be very useful, depending on the reasons why it is wrong.

Once developed it may be possible to observe the behaviour of the model in the study of the system, rather than performing the wet experiments. The running of the model, typically by computer simulation, can be quicker, easier, less prone to experimental error and cheaper than laboratory based experiments. It may be the case that the model has a higher resolution in space or time than the wet experiments and it can therefore give results outside the experimental range. Attempts to fit the model quantitatively to experimental preparations can allow the estimation of parameters that may be otherwise unknown.

Either by some mathematical analysis, or simulation runs, the model may display some novel aspects that are not apparent in the original system. The model may then be of use in designing a suitable wet experiment that will determine whether this is a true result of the system or a false result from the modelling. Hence it may also be used to discover new features of experimentally characterised systems.

Mathematical models therefore have many advantages over wet experiments and, in descriptive terms, over the original system. However it is generally true that the development and testing of models requires results from wet experiments. Hence modelling can never totally replace experiments, but ideally the two will enjoy a synergistic relationship; experiments will enable the development and testing of models which can then refine current, or suggest new, experiments.

The advantages that modelling can bring necessarily require that the model is developed in a sensible and accountable way. These processes are detailed in the following couple of sections where we shall first describe some relevant modelling that has been performed thus far in the neurosciences. We shall then detail some of the additional techniques that we have had cause to use in our own modelling efforts.

1.2 Modelling in the Neurosciences

1.2.1 Michaelis-Menten Theory

This section will detail three important ideas that are used in our modelling; the first concerns chemical reaction rates between two reactants. The other two are the *pseudo-steady state* hypothesis, where fast effects may be considered to be at equilibrium; and the conditions when slow effects may be regarded as constant. These have important implications when considering effects that happen on very different timescales. This description is taken largely from a dealing with enzyme reactions found in Murray [66], which has the best example and explanation that we have seen.

Consider the following basic enzyme reaction, proposed by Michaelis and Menten in 1913 [62]. A substrate S reacts with an enzyme E and the compound object SE is converted to a product P and the enzyme. This is given schematically by

$$S + E \underset{k_{-1}}{\overset{k_1}{\rightleftharpoons}} SE \xrightarrow{k_2} P + E. \tag{1.1}$$

Denoting the concentrations $[S]$, $[E]$, $[SE]$ and $[P]$ by s, e, c and p we may write down a system of reaction equations describing (1.1) using the *law of mass action.* This states that the rate of a reaction is proportional to the product of the reactants. If the k's in (1.1) are the appropriate constants of proportionality we may write

$$\frac{ds}{dt} = -k_1 es + k_{-1}c, \tag{1.2}$$
$$\frac{de}{dt} = -k_1 es + (k_{-1} + k_2)c, \tag{1.3}$$
$$\frac{dc}{dt} = k_1 es - (k_{-1} + k_2)c, \tag{1.4}$$
$$\frac{dp}{dt} = k_2 c, \tag{1.5}$$

with initial conditions

$$s(0) = s_0, \quad e(0) = e_0, \quad c(0) = 0, \quad p(0) = 0. \tag{1.6}$$

Equation (1.5) is uncoupled from the rest and has solution, once $c(t)$ has been found

$$p(t) = k_2 \int_0^t c(t')dt'. \tag{1.7}$$

Furthermore E is a catalyst and so its total concentration is a constant, $e_0 = e(t) + c(t)$, enabling us to reduce our system to just two equations

$$\frac{ds}{dt} = -k_1 e_0 s + (k_1 s + k_{-1})c, \tag{1.8}$$
$$\frac{dc}{dt} = k_1 e_0 s - (k_1 s + k_{-1} = k_2)c. \tag{1.9}$$

Using the non-dimensionalisation

$$\tau = k_1 e_0 t, \quad u(\tau) = \tfrac{s(t)}{s_0}, \quad v(\tau) = \frac{c(t)}{c_0},$$
$$\lambda = \frac{k_2}{k_1 s_0}, \quad K = \tfrac{k_{-1}+k_2}{k_1 s_0}, \quad \varepsilon = \frac{e_0}{s_0} \tag{1.10}$$

we obtain

$$\frac{du}{d\tau} = -u + (u + K - \lambda)v, \tag{1.11}$$
$$\varepsilon\frac{dv}{d\tau} = u - (u + K)v, \tag{1.12}$$
$$u(0) = 1 \tag{1.13}$$
$$v(0) = 0. \tag{1.14}$$

It is noted in biological reactions that the catalytic effects of enzymes is reflected in the low concentrations needed to react with the substrate and so $0 < \varepsilon \ll 1$. Hence v changes very

rapidly compared to u. If we look for a solution of the form

$$u(\tau;\varepsilon) = \sum_{n=0} \varepsilon^n u_n(\tau), \quad v(\tau;\varepsilon) = \sum_{n=0} \varepsilon^n v_n(\tau), \tag{1.15}$$

substituting into (1.11)-(1.14) and comparing powers of ε we obtain the $O(1)$ terms

$$\frac{du_0}{d\tau} = -u_0 + (u_0 + K - \lambda)v_0, \tag{1.16}$$

$$0 = u_0 - (u_0 + K)v_0, \tag{1.17}$$

$$u(0) = 1 \tag{1.18}$$

$$v(0) = 0, \tag{1.19}$$

which we may solve to obtain

$$u_0(\tau) + K \ln u_0(\tau) = 1 - \lambda\tau \tag{1.20}$$

$$v_0(\tau) = \frac{u_0(\tau)}{u_0(\tau) + K} \tag{1.21}$$

which clearly does not satisfy $v(0) = 0$. This is because we have reduced the order of our system in setting $\varepsilon = 0$, hence we have only one constant of integration with which to attempt to satisfy both initial conditions. We need to retain the order of our system near $\varepsilon = 0$. The solution (1.20)-(1.21) is the *outer* or *non-singular* solution, valid for τ away from 0.

Changing variables to

$$\sigma = \frac{\tau}{\varepsilon}, \quad u(\tau;\varepsilon) = U(\sigma,\varepsilon), \quad v(\tau;\varepsilon) = V(\sigma,\varepsilon), \tag{1.22}$$

which serves to magnify the region close to 0, we obtain

$$\frac{dU}{d\sigma} = -\varepsilon U + \varepsilon(U + K - \lambda)V, \tag{1.23}$$

$$\frac{dV}{d\sigma} = U - (U + K)V, \tag{1.24}$$

$$U(0) = 1 \tag{1.25}$$

$$V(0) = 0. \tag{1.26}$$

Repeating as before for

$$U(\sigma;\varepsilon) = \sum_{n=0} \varepsilon^n U_n(\sigma), \quad V(\sigma;\varepsilon) = \sum_{n=0} \varepsilon^n V_n(\sigma), \tag{1.27}$$

we retain the order of the system for the $O(1)$ equations given by

$$\frac{dU_0}{d\sigma} = 0, \tag{1.28}$$

$$\frac{dV}{d\sigma} = U_0 - (U_0 + K)V_0, \tag{1.29}$$

$$U(0) = 1 \tag{1.30}$$

$$V(0) = 0, \tag{1.31}$$

with solution

$$U_0(\sigma) = 1 \tag{1.32}$$

$$V_0(\sigma) = (1+K)^{-1}\left(1-\exp(-(1+K)\sigma)\right). \tag{1.33}$$

This is the *inner* or *singular* solution and is valid for $0 < \tau \ll 1$. Note that for $\varepsilon \to 0$ (i.e. $\tau \to 0$, $\sigma \to \infty$) the solutions match; $\lim_{\sigma\to\infty} U_O = 1 = \lim_{\tau=0} u_0$ and $\lim_{\sigma\to\infty} V_O = \frac{1}{1+K} = \lim_{\tau=0} v_0$.

We have shown that the change in the substrate-enzyme complex is very fast, taking place as $\tau = O(\varepsilon)$ in dimensionless time. In dimensional time this is $O(\frac{1}{k_1 s_0})$. If this is also very fast, then the inner solution is effectively never seen (experimentally immeasurable) and the system is described by the outer solution (1.20)-(1.21) and the variable v is essentially at steady state since $\varepsilon\frac{dv}{d\tau} \approx 0$. Hence v changes so fast that it is more or less at its steady state for all time and is called the pseudo-steady state hypothesis.

Conversely when considering the fast timescales close to $\tau = 0$ our solution is given by the inner solution (1.32)-(1.33) and hence at such timescales we can consider the slow component (in this case U_0) to be constant.

1.2.2 Hodgkin and Huxley

The work of Hodgkin and Huxley [41], for which they were awarded the 1963 Nobel Prize in Physiology and Medicine, underpins much of the modelling that we perform. Chapters 2,3 and 4 all feature ion channels that are modelled using the approach of these two, first identified in their studies on the conduction of action potentials in the squid giant axon.

As one might expect, experimental neuroscience in the early part of this century was limited by the lack of equipment and techniques to study preparations with the small scale and fast kinetics of neurons. At 1mm in diameter the squid giant axon (not to be confused with the giant squid of nautical mythology) represented the most amenable preparation and by the time of the Second World War it was possible to measure the membrane potential of the axon by inserting an electrode along the inside of it.

Hodgkin and Huxley regarded the axon membrane to be acting as an electrical capacitor separating the imbalance of ions, where the membrane potential is given by

$$C_m\frac{dV}{dt} + I_{\text{ion}}(V,t) = 0 \tag{1.34}$$

where C_m is the electrical capacitance, measurable by plotting the time course of voltage for injected currents in the absence (blocking) of ionic currents [47][66]. It was proposed that the ionic currents could be separated into three; one for potassium (I_K), sodium (I_{Na}) and the other to describe the remaining currents in the axon (I_L), called the leakage. Experimentally noting that the instantaneous current-voltage relationship of the squid axon appeared to be linear they could propose that

$$I_{\text{ion}}(V,t) = I_K + I_{Na} + I_L = g_K(V,t)(V-V_K) + g_{Na}(V,t)(V-V_{Na}) + g_L(V-V_L) + I_{\text{app}} \tag{1.35}$$

where I_{app} is the applied current and the g terms describe the conductance of the other currents. Each current is proportional to the voltage gradient given by the difference between membrane potential and the Nernst potential of the ion species, such a dependence having been experimentally observed. The Nernst potential is the potential difference due to two phases of differing ionic concentration (and is derived in section 1.2.3).

With further refinement of the techniques involved, Hodgkin and Huxley were able to begin their formulation. This largely involved the use of a voltage clamp, a technique that fixes the membrane potential and then can measure the transmembrane current by recording the current necessary to maintain the clamp. The ability to fix the voltage meant that the otherwise time and voltage dependent currents measured were functions of time only. By stepping the voltage up to a fixed higher level it was observed that an initially inward current was followed by a slower developing outward current, which they considered to be mediated by sodium and potassium ions respectively.

By measuring the current in this initial inward phase they considered that they were measuring the changing sodium current. Replacing portions of the extracellular sodium ions with the relatively inert choline they were able to measure the ratio of the sodium currents and the potassium current. Hence they solved for the conductances g_{Na} and g_K for steady voltages as functions of time.

Observing that the potassium conductance had a sigmoidal increase and exponential decrease they supposed that

$$g_K(V,t) = \bar{g_K} n^4, \tag{1.36}$$

for a constant $\bar{g_K}$. The fourth power was chosen since it was the smallest power that fitted with the experimental data, where n obeys

$$\tau_n(V)\frac{dn}{dt} = n_\infty(V) - n, \tag{1.37}$$

for time constant function $\tau_n(V)$ and *steady state activation curve* $n_\infty(V)$. $n(t)$ is then known as the *potassium activation.* Supposing that at $t = 0$ the voltage is stepped from 0 to v_0 and then held constant, solving (1.37) gives

$$n(t) = n_\infty(0) + (n_\infty(v_0) - n_\infty(0)) \left[1 - \exp\left(\frac{-t}{t_n(v_0)}\right)\right], \tag{1.38}$$

which is sigmoidal in appearance when taken to the fourth power. Similarly a step decrease, from v_0 to 0 say, has solution

$$n(t) = n_\infty(0) + (n_\infty(v_0) - n_\infty(0)) \exp\left(\frac{-t}{t_n(0)}\right), \tag{1.39}$$

which has n^4 exponentially decaying.

The discrete values n_∞ and t_n could then be found by fitting (1.38) and (1.39) to the experimental data characterising g_K. Curve fitting then yielded continuous functions $n_\infty(V)$ and $\tau_n(V)$.

The sodium conductance was described in a similar way, except that it was observed that the current seemed to have two effects, one that switched on the current and the other that switched it off. This lead to the formulation

$$g_{Na}(V,t) = g\bar{_{Na}} m^3 h, \tag{1.40}$$

where $m(t)$ is called the *sodium activation* and $h(t)$ is the *sodium inactivation.* These are defined analogously to $n(t)$ and the appropriate functions derived from curve fitting as before.

The conductance of the leakage current g_L, assumed constant, is easily derived from measuring the ionic current when both the sodium and potassium currents are blocked.

The equations derived produce a mathematical model of the production of action potential generation in the squid axon. Numerical solution of these equations, some of which were produced by Huxley on a hand-cranked calculator, produced accurate traces of action potentials. Figure 1.1 shows the numerical solution of the so-called Hodgkin and Huxley equations for an applied current of 0.1nA. A key characteristic of the model is that it is excitable; for small current injections the resting potential is a stable steady state but a sufficiently large perturbation, past a threshold, can send the membrane potential off on a large deviation (an action potential) before it returns to rest. Prolonged current injection can cause the resting potential to shift above the threshold and so lead to periodic firing.

The work of Hodgkin and Huxley lays down a procedure for the experimental protocol and parameter and function derivation required to produce accurate mathematical models of

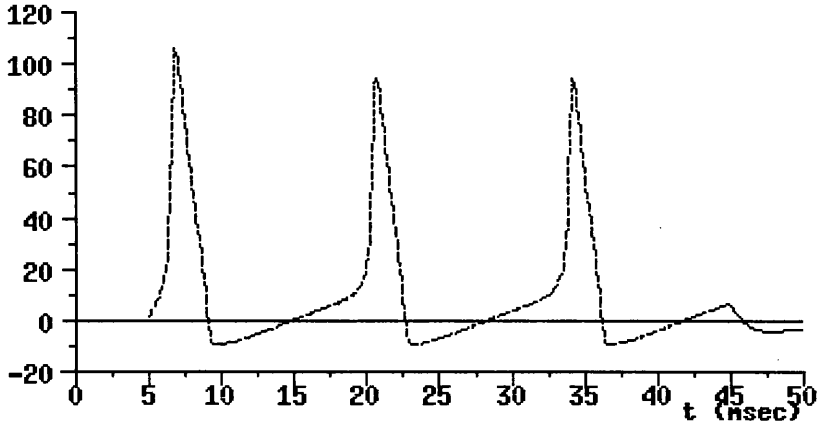

Figure 1.1: A plot of membrane potential in mV against time in ms for the numerical solution of the Hodgkin and Huxley equations in the squid giant axon, for an applied current of 0.1nA. This produces the periodic firing of action potentials. Resting potential was defined to be 0mV.

currents in excitable cells and is still used today. Many mammalian channels can be fitted to a Hodgkin and Huxley scheme by measuring for the steady state activation and time constant functions and it may also be extended to take account of dependencies on ion concentrations as well as voltage.

These can be used to describe the dynamics of membrane potential in many varied preparations; all of the ion channels explicitly modelled in this thesis are consistent with the Hodgkin and Huxley formulation. Many of the channels that we have used are taken from a 19 compartment model of a CA3 hippocampal pyramidal neuron in the rat [98]. This model by Traub and co-workers features six different types of ion channel which are either consistent with, or extensions of the Hodgkin and Huxley scheme and is capable of reproducing the complex periodic and bursting firing patterns seen in these neurons.

Not all channels can be fitted to this scheme [47], notably currents in which the instantaneous current-voltage relationship is non-linear (one of the original assumptions of the formulation was this linearity). Moreover by being quantitatively accurate, the equations are largely intractable to mathematical analysis and so any study of such systems necessarily leads to extensive numerical solving.

1.2.3 Alternative Models of Ion Channels

Whilst Hodgkin and Huxley channels are sufficiently accurate for the modelling we shall do, we should mention the other ways in which ion channels may be modelled. In particular Hodgkin

and Huxley assumed that the instantaneous current-voltage relationship of open channel was linear. Here we shall consider an alternative formulation that leads to the Goldman-Hodgkin-Katz equation that can be a better approximation to ion channels in vertebrate axons [47].

First let us consider an ion species of concentration c, then its flux is given by Fick's Law

$$\mathbf{J} = -D\nabla c \tag{1.41}$$

where the scalar D is the diffusion coefficient. Similarly the flux due to an electric potential ϕ is given by Planck's equation

$$\mathbf{J} = -u\frac{z}{|z|}c\nabla\phi \tag{1.42}$$

where $u = D|z|F/RT$ is the mobility of the ion. z is the valency of the ion species, F Faraday's constant, R the universal gas constant and T the absolute temperature. Combining these and assuming that all flow is across a membrane of length L in the direction of the x-axis we can write down the one-dimensional Nernst-Planck relation

$$J = -D\left(\frac{dc}{dx} + \frac{zF}{RT}c\frac{d\phi}{dx}\right). \tag{1.43}$$

By setting $V = \phi(0) - \phi(L)$, that is the potential difference across the membrane due to the ion species, then integrating (1.43) for zero flux we obtain the Nernst equation

$$V = \frac{RT}{zF}\ln\left(\frac{c_o}{c_i}\right) \tag{1.44}$$

where c_o and c_i are the concentrations of the ion species inside ($x = 0$) and outside ($x = L$) the membrane respectively.

If we assume that the electric field in the membrane is constant (the so-called *constant field approximation*) then $dV/dx = -V/L$. At steady state, with no ion production, the flux J is constant and we obtain an ODE for the concentration c

$$\frac{dc}{dx} - \frac{zFV}{RTL}c + \frac{J}{D} = 0. \tag{1.45}$$

Integrating and satisfying $c(0) = c_i$ and $c(L) = c_o$ we get

$$J = \frac{D}{L}\frac{zFV}{RT}\frac{c_i - c_e\exp\left(\frac{-zVF}{RT}\right)}{1 - \exp\left(\frac{-zVF}{RT}\right)}. \tag{1.46}$$

The flux density J becomes a current density I when multiplied by zF and so we obtain

$$I = P\frac{z^2F^2}{RT}V\frac{c_i - c_e\exp\left(\frac{-zVF}{RT}\right)}{1 - \exp\left(\frac{-zVF}{RT}\right)}, \tag{1.47}$$

where $P = D/L$ is the permeability of the ion species, analogous to the conductance g in the Hodgkin and Huxley formulation. (1.47) is called the Goldman-Hodgkin-Katz equation.

1.2.4 The Fitzhugh-Nagumo Model

The Fitzhugh-Nagumo model [24] [66] [20] is an attempt to simplify the Hodgkin and Huxley equations into a model that allows mathematical analysis. Fitzhugh had already produced some elegant qualitative analysis of the original equations by considering the fast and slow phases of the Hodgkin and Huxley equations and it is by considering these different speeds that some progress can be made.

The m variable is much faster than n or h and so is assumed to be at steady state (the pseudo-steady state hypothesis introduced in section 1.2.1). The system still retains many of its features if $h = h_0$, a constant. The resulting two variable model can then be qualitatively approximated by the nondimensionalised system

$$\frac{dv}{dt} = v(a-v)(v-1) - w + I_a, \tag{1.48}$$

$$\frac{dw}{dt} = bv - \gamma w, \tag{1.49}$$

where $0 < a < 1$ and $b, \gamma > 0$. v acts like the membrane potential and w acts rather like a combined potassium activation and sodium inactivation. The dynamics of the system can be illustrated with phase plane analysis.

For certain values of a, b and γ it is possible for the system to have three steady states, two stable and one unstable. The model then displays bistability, with 'potential' resting at one of the stable steady states and suitably perturbing current injections shifting it from one to the other. For its particular relevance to the Hodgkin and Huxley model of the squid giant axon, we shall consider variable values for which there is only a single steady state.

For $I_a = 0$ the phase plane is then as in Figure 1.2 with a single stable steady state at zero. The excitability is clear, since any perturbation that pushes $v > a$ must pass through the right branch of the $\dot{v} = 0$ nullcline before it can return to 0.

For $I_a > 0$ the steady state can lie on the middle branch of the $\dot{v} = 0$ nullcline, as in Figure 1.3. For such current injections the steady state may be unstable and periodic oscillations are possible. For even greater values of I_a the steady state stabilises on the right branch.

The Fitzhugh-Nagumo is an example of a model *of* a model. Whilst it does not have the quantitatively accurate predictions of the original Hodgkin-Huxley equations it is open to mathematical analysis. With this simplified model we can explain important features like excitability. This is a technique we shall often use, where we take a complicated model that

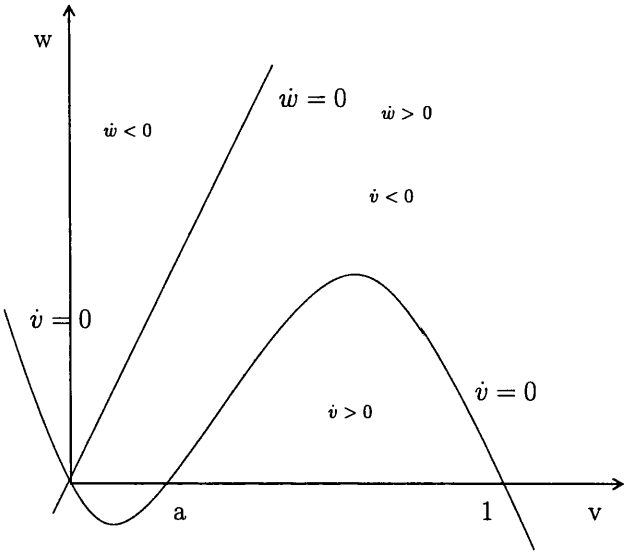

Figure 1.2: The phase plane for the Fitzhugh-Nagumo model for no applied current. The steady state at 0 is stable but excitable.

may only be solved numerically and produce a simplified model of this that we are able to analyse.

This model also shows how simplified a model may be, yet still retain many of the features of more complex systems. The Fitzhugh-Nagumo is only one of many 2-variable models of action potential firing in excitable membranes; others include the Morris-Lecar model [65] which may be considered to be a Hodgkin and Huxley / Fitzhugh-Nagumo hybrid. This model is based in the context of the electrical activity of the barnacle muscle fibre and incorporates a voltage-dependent calcium channel and a delayed-rectifying potassium channel. The equations are given by

$$\frac{dv}{dt} = -g\bar{C}a m_\infty(v)(v-1) - g\bar{K}w(v-v_K) - g\bar{L}(v-v_L) + I_{\text{app}} \tag{1.50}$$

$$\frac{dw}{dt} = \phi\frac{w_\infty(v) - w}{\tau_w(v)} \tag{1.51}$$

where

$$m_\infty(v) = \frac{1}{2}\left(1 + \tanh\left(\frac{v - v_1}{v_2}\right)\right), \tag{1.52}$$

$$w_\infty(v) = \frac{1}{2}\left(1 + \tanh\left(\frac{v - v_3}{v_4}\right)\right). \tag{1.53}$$

These equations are also amenable to phase plane analysis and provide explanations for such features as excitability and bifurcation to periodic solutions. For a full treatment see [49], [20] or [65].

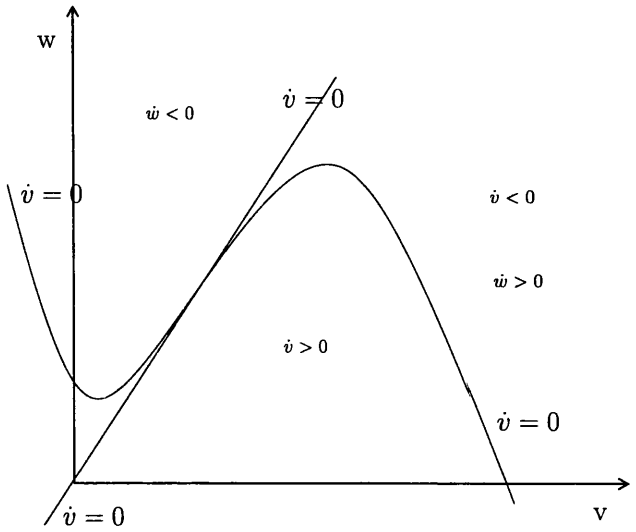

Figure 1.3: The phase plane for the Fitzhugh-Nagumo model for values of applied current that put the steady state on the middle branch. In this situation the steady state may become unstable and periodic oscillations are possible.

1.2.5 Models of Firing for Simulations

Whilst Hodgkin and Huxley provides a quantitatively accurate model of action potential firing its computational complexity makes it undesirable to use in models of coupled neurons, where we may only wish to know when a spike arrives rather than all the details of its shape and magnitude. Fitzhugh-Nagumo and Morris-Lecar, though much simpler, are largely engineered as qualitative models and may be difficult to fit to specific neurons. It is convenient in simulations to use the integrate and fire model.

The integrate and fire model [10] is perhaps the simplest model that generates discrete spikes. It depends on only two parameters; the spike threshold and the refractory period, both of which may be easily determined from experimental data. The model states that if the membrane potential is above the threshold and there has not been a spike in the previous refractory period, then one is generated. The output is then the time of the spike. This is clearly a simple and efficient procedure to implement in computer simulations.

When considering networks of coupled neurons it is then necessary to be able to interpret the effect on membrane potential of a train of spikes causing input to a neuron. A single stimulation of postsynaptic receptors causes a wave of depolarisation due to a time-dependent variation in the conductance. This variation can be approximated by a smooth function of

the form

$$g_{\text{syn}}(t) = \frac{Ag_{\max}}{\tau_1 - \tau_2}\left(\exp\left(\frac{-t}{\tau_1}\right) - \exp\left(\frac{-t}{\tau_2}\right)\right), \tag{1.54}$$

where A is a normalisation constant chosen such that g_{syn} reaches a maximum value of $g_{\max}$ [10]. τ_1 and τ_2 are of 'off' and 'on' times of the conductance respectively. For a sequence of spikes with arrival times given by $\{t_k\}$ incident on a synaptic connection with reversal potential E_{syn} the current input to the neuron, I_o, is given by

$$I_o = (E_{\text{syn}} - V_m)\sum_k H(t - t_k)\frac{Ag_{\max}}{\tau_1 - \tau_2}\left(\exp\left(-\frac{t - t_k}{\tau_1}\right) - \exp\left(-\frac{t - t_k}{\tau_2}\right)\right), \tag{1.55}$$

where $H(t)$ is the Heaviside step function, which again lends itself to computer simulation. The current input will serve to alter the membrane potential via a typical membrane as capacitor equation such as

$$C_m\frac{dV_m}{dt} = R(V_m, t) + I_o(t) \tag{1.56}$$

where $R(V_m, t)$ is an appropriate term that describes the currents due to the intrinsic ion channels of the cell.

1.2.6 Cable Theory

Thus far we have been regarding membrane potential to be a function of time only, considering that the preparation of study is a single electrical compartment and thus all points have the same potential. For an entire neuron, or even for parts, this cannot be expected to hold and we must consider how membrane potential changes over spatial scales.

The idealised picture of a neuron is of a central soma which is responsible for generating the action potentials, which it sends down excitable processes called axons (like the squid giant axon of section 1.2.2) which make chemical synapses with other neurons. The neuron receives signals on a series of branching processes called dendrites which are assumed to be passive (independent of membrane potential - no voltage dependent ion channels). The summation of all of these inputs at the soma is then considered to be the variable that determines whether an action potential is fired or not.

Of course this is not generally true; dendrites may be excitable; processes may act as both axons and dendrites; and there may be many areas of spike generation to name but three [45], but this description will be sufficient for our purposes. Neurons can be generally pieced together as thin tubes wrapped in membrane. This membrane is a good electrical insulator

compared to the intracellular fluid and so electrical current within the core tends to flow parallel to the cylinder axis. The spread of membrane potential may then be given by applying the one-dimensional cable equation [10] [49]:

Let us assume that the cylinder lies along the x-axis and that membrane potential V is a function of x and t only. We shall also assume that in this treatment that the membrane is passive. Then for longitudinal current I and cytoplasmic resistivity (resistance per unit length) r_i, Ohm's Law gives us

$$\frac{1}{r_i}\frac{\partial V}{\partial x} = -I, \tag{1.57}$$

taking current to be positive in the positive x direction.

Membrane current either crosses the membrane through passive pores, with resistance r_m, or charges the membrane, with capacitance per unit length c_m. Then the current change per unit length $(\partial I/\partial x)$ is the density of this membrane current and hence

$$\frac{\partial I}{\partial x} = -\left(\frac{V}{r_m} + c_m\frac{\partial V}{\partial t}\right). \tag{1.58}$$

Combining (1.57) and (1.58) we obtain the cable equation, a second order PDE in x and t

$$\frac{1}{r_i}\frac{\partial^2 V}{\partial x^2} = \frac{V}{r_m} + c_m\frac{\partial V}{\partial t}. \tag{1.59}$$

For a complete derivation of the cable equation, see Rall [80].

In practical models with spatial components the neuron is normally divided into many smaller compartments each of which is considered to be isopotential [98]. We then spatially discretise the membrane potential. If the potential of the kth compartment is V_k, which is connected to the $(k-1)$th and $(k+1)$th compartments then we may write

$$c_m\frac{dV_k}{dt} = \frac{1}{r_{k-1,k}}(V_{k-1} - V_k) + \frac{1}{r_{k+1,k}}(V_{k+1} - V_k) - I_{\text{ion},k}(V_k, t), \tag{1.60}$$

where $r_{i,j}$ is the resistance between the ith and jth compartments.

The cable equation (1.59) may be explicitly solved for various cases, particularly for assuming the steady state $(\partial V/\partial t) = 0$ and the variation of membrane potential with spatial distance derived. Note that in the case of a very small cylinder, $\partial V/\partial x \approx 0$ and (1.59) reduces to the isopotential case, as in (1.34).

It is this latter case that we are interested in; clearly any description of membrane potential in an excitable cell will become incredibly complicated and analytically intractable if we are required to consider spatial variation, whether this means evaluating (1.59) or (1.60). We can take a major step towards producing a simpler model with dynamics we can analyse if we can find good reason to neglect the spatial components.

1.2.7 Coupled Oscillators

Here we will introduce some of the work done on models that mimic the behaviour of two coupled oscillators, intended to study the ways in which biological oscillators may influence each other. For example the sinoatrial node in the heart has many oscillators of differing frequencies coupled together and their collective behaviour is largely responsible for the initiation of the cardiac action potential. We will be considering a model due to Rand et al [81] [10] where each component is taken to be a simple oscillator, ignoring any structure of the oscillation and the mechanisms that provoke it.

The behaviour of an oscillator will in reality be determined by a multitude of parameters. If we consider for a moment that the trajectory drawn in parameter space is a closed loop, then we may be able to describe our position around this loop by an angle θ, relative to some fixed angle θ_0. If we suppose as time progresses, θ moves uniformly around the closed loop with frequency ω then

$$\dot{\theta} = \omega \tag{1.61}$$

which implies, using modular arithmetic that

$$\theta(t) = (\omega t + \theta_0)(\text{mod}2\pi) \tag{1.62}$$

though for convenience we shall omit the (mod2π) from now on.

Suppose that we have two oscillators described by θ_1 and θ_2 and they are coupled (have an effect on each other). We will suppose that the coupling is as proposed by Rand et al [81] and given by $a_{ij}\sin(\theta_j - \theta_i)$, which is known as diffusive coupling. Hence

$$\dot{\theta_1}(t) = \omega_1 + a_{12}\sin(\theta_2 - \theta_1) \tag{1.63}$$

$$\dot{\theta_2}(t) = \omega_2 + a_{21}\sin(\theta_1 - \theta_2). \tag{1.64}$$

Defining the phase difference $\phi = \theta_1 - \theta_2$ we obtain

$$\dot{\phi}(t) = (\omega_1 - \omega_2) - (a_{12} + a_{21})\sin(\phi(t)) \tag{1.65}$$

which has steady states given by

$$\phi^* = \sin^{-1}\left(\frac{\omega_1 - \omega_2}{a_{12} + a_{21}}\right). \tag{1.66}$$

For small $a_{12} + a_{21}$ there are no solutions and the oscillators drift with respect to one another (the coupling is too weak). For steady state solutions the motion is *phase-locked* and one

oscillator will lead the other by an amount ϕ^*. Note that in the special case of the intrinsic frequencies being close together, $\omega_1 - \omega_2 \approx 0$ and the oscillators synchronise, either in phase or in anti-phase.

This model is not sufficient to describe all possible types of oscillatory behaviour, in particular the choice of diffusive coupling is restrictive. In Chapter 5 we adapt this phase equation idea to produce a specialised quantitatively accurate model of oscillating neurons coupled by gap junctions. Other workers, in particular Ermentrout and Kopell [22] [49] have extended the modelling of Rand with more realistic coupling. They prescribe

$$\dot{\theta_1}(t) = \omega_1 + p(\theta_2)r(\theta_1), \tag{1.67}$$

$$\dot{\theta_2}(t) = \omega_2 + p(\theta_1)r(\theta_1). \tag{1.68}$$

Here p is a periodic smooth pulse function, supposed to be a measure of the coupling effect from the incident oscillator. Strictly the arrival of a pulse should be modelled with a Dirac delta function but Ermentrout considered that since real stimuli are not instantaneous it is reasonable to replace the δ function with a smooth function p. r takes the form of a *phase response curve*. A phase response curve can be found experimentally by stimulating the oscillator and measuring the phase change when it settles back to periodic oscillations.

Ermentrout and Kopell show that for this type of coupling the phase equations display qualitative behaviour similar to more complex modelling efforts. Of particular interest is that for sufficiently strong coupling the system may exhibit *oscillator death* where the oscillator remains at a constant point in state space.

1.3 Modelling Techniques

This thesis contains a variety of attempts to mathematically model neuronal systems, with an emphasis on problems concerned with the purportedly addictive drug nicotine and Parkinson's disease. In this section we shall detail how we approach the task of developing, testing and analysing such a model.

1.3.1 Modelling Philosophy

We may first ask what it is we wish our modelling to achieve. Mathematical-biology is considered to be one of the fastest growing fields of interest in contemporary mathematics as both a source for new and interesting mathematical problems and for the insight that

mathematical analysis can bring to biology. For what may be considered the best approach to modelling biological systems I can do no better than quote from J.D. Murray, author of the seminal work Mathematical Biology [66]:

> *"The art of good modelling relies on: (i) a sound understanding and appreciation of the biological problem; (ii) a realistic mathematical representation of the important biological phenomena; (iii) finding useful solutions, preferably quantitative; and what is crucially important (iv) a biological interpretation of the results in terms of insights and predictions."*

This makes the important distinction that it is the biology that is the driving force. The modelling is designed to address biological problems and not to try and solve mathematical ones that have a tenuous link to something in biology.

A model will typically be based on a well defined biological system that will have, hopefully, been the subject of extensive experimental investigation. The processes built into this model will be (sub-)models of cellular functions that are known or believed to be present in this or similar preparations. It is natural to require that *all* experimental observations (qualitative and quantitative) are reproduced in the model; those that are not featured should be detailed, along with hypotheses on how the condition could be met and how this model fault affects its use as a viable representation of the biological system.

We accept that there will be occasions when too little is known of the mechanisms underlying a biological system to be able to model it correctly, to the extent we would wish. In such cases we shall propose our own processes, which shall be clearly stated with the reasons why we consider this to be a valid mechanism. This will typically be that a similar mechanism produces a similar response in other, relevant, systems. Where possible we should then use our model to design experiments that will test the viability of our proposal. This does not mean that we are going to include mechanisms purely on the grounds that they solve our problem.

In what may seem to be a conflicting aim, we also wish to produce models that describe cell function while being as simple as they can. In the course of this we may well produce a model that does not contain some cellular components we know to be present, typically because we can reproduce the system behaviour without it. Such omissions must be justified.

Producing a simple model has many advantages; we are often modelling to try to understand an otherwise horrendously complicated biological system and so a simpler model is easier to understand. Simplification also speeds model development and any quantitative fitting. In particular it eases model analysis; the mathematical procedures we wish to apply are often

limited in the systems that they may be applied to, for example the Poincare-Bendixson Theorem is only applicable to two-dimensional systems.

The simplification of the model in terms of including fewer, or simpler processes will be extended to the mathematics we shall use. There is no point in using complex mathematics in a model in an attempt to produce more accurate results if a simpler representation is sufficient, easier to understand and more amenable to analysis; to do so is to fly in the face of what we hope to achieve by modelling.

1.3.2 From Biological System to Model

Throughout our modelling we have used a fairly standard approach in deriving our models from the biological system of study. The model can be regarded initially as a black box with a series of inputs and outputs, which it is our first job to identify. The inputs are the set of experiments (wet, or suitably sound theoretical ideas in the absence of wet data) performed on the preparation and any other influences that we may wish the model to be subject to, which will often be stimulation with chemicals such as nicotine or changes in extracellular ion concentrations.

The outputs are any experimental observables combined with the results from the model with which we are primarily concerned. This may be anything from monitoring transmitter release and firing patterns to the abundance and location of nicotinic receptors.

With these so-called inputs and outputs determined, we then begin a process of identifying the mechanisms and processes that link the two together. This may require us to go to finer levels of detail until we can clearly define the steps that cause input to lead to output. Naturally the extent of detail that we feel is necessary is open to different interpretations and revisions. This should represent the model at its most complex, excepting any errors in the model results that lead to revisions. It may be possible at this time to discard some mechanisms that, although they help in development, may be superfluous for the uses we will put our model to.

Once such a theoretical model has been defined we will take each process or mechanism in turn and describe each in mathematical terms; either drawn from previous models of similar mechanisms or designing our own. The combination of all this process of course creates the mathematical model, which should then be amenable to any quantitative fitting that is required and to the analysis we wish to perform.

This approach may seem obvious, but is very useful in that we are immediately concerned with the inputs to and results of the system; that is what we know already and what we wish to. Only considering the links between the two means that we should never be dealing with cellular processes that are unnecessary and only serve to over-complicate our modelling.

1.3.3 Steady States and Periodic Orbits

For many of our models their behaviour may be characterised by the study of any steady states or periodic solutions they may possess. Our ODE models are generally non-autonomous and may be written as

$$\dot{\mathbf{u}}(t;\mathbf{u}_0) = \mathbf{F}(\mathbf{u}(t),t), \quad \mathbf{u}(0) = \mathbf{u}_0, \tag{1.69}$$

for state variable $\mathbf{u} \in \mathbb{R}^n$.

Definition 1.3.1 $\mathbf{u}^*$ *is a steady state for the system (1.69) if* $\mathbf{F}(\mathbf{u}^*,t) = \mathbf{0}\ \forall t \geq 0$.

Hence $\mathbf{u}^*$ represents a point in state space where the state remains constant.

Definition 1.3.2 *A steady state* $\mathbf{u}^*$ *of (1.69) is said to be stable if for a given* $\varepsilon > 0$ *there is* $\delta > 0$ *such that for each* $\mathbf{u}_0$ *satisfying* $||\mathbf{u}_0 - \mathbf{u}^*|| < \delta$ *then* $||\mathbf{u}(t;\mathbf{u}_0) - \mathbf{u}^*|| < \varepsilon$ *for all* $t \geq 0$.

A steady state is unstable if it is not stable. Stability implies that for small perturbations of the steady system, the solution for all future time remains close (in a mathematical sense) to the steady state. For an unstable steady state any small perturbation will cause the solution to diverge from the steady state.

This is important for biological models considering that such systems are generally subject to noise. Firstly for any solution of (1.69) at a steady state, the solution will effectively remain there for all time since the system is robust to the small perturbations caused by the noise. Conversely steady solutions at unstable steady states are generally not seen in biology, since the noise shifts the solution away from the steady state and it subsequently diverges.

Definition 1.3.3 *A steady state* $\mathbf{u}^*$ *of (1.69)is attractive (in a radius* $R > 0$*) if for any initial condition* $\mathbf{u}_0$ *such that* $||\mathbf{u}_0 - \mathbf{u}^*|| < R$ *then* $\mathbf{u}(t;\mathbf{u}_0) \to \mathbf{u}^*$ *as* $t \to \infty$. *If* $R = \infty$ *then* $\mathbf{u}^*$ *is globally attractive. The set of all points* $\mathbf{u}_0$ *such that* $\mathbf{u}(t;\mathbf{u}_0) \to \mathbf{u}^*$ *as* $t \to \infty$ *is called the basin of attraction (of* $\mathbf{u}^*$*).*

Note that the attractivity of a steady state does not imply stability. However:

Definition 1.3.4 *A steady state* $\mathbf{u}^*$ *of (1.69) is (globally) asymptotically stable if it is both (globally) attractive and stable.*

The asymptotic stability of a steady state implies that any solution within the basin attraction will tend to the steady state and remain there.

We now turn to period solutions.

Definition 1.3.5 $\mathbf{u}(t;\mathbf{u}_0)$ *is a* T*-periodic solution of (1.69) if* $\mathbf{u}(t;\mathbf{u}_0) = \mathbf{u}(t+T;\mathbf{u}_0)$ *for all* $t \geq 0$. T *is the minimum period if* $\mathbf{u}(t;\mathbf{u}_0) \neq \mathbf{u}(t+\tau;\mathbf{u}_0)$ *for* $0 < \tau < T$.

Hence the solution repeats every T time units. We can similarly define stability and attractivity.

Definition 1.3.6 *A* T*-periodic solution* $\mathbf{u}(t;\mathbf{u}_0)$ *of (1.69) is stable if for a given* $\varepsilon > 0$ *there is* $\delta > 0$ *such that for all initial conditions* $\mathbf{y}_0$ *with* $||\mathbf{y}_0 - \mathbf{u}_0|| < \delta$ *then* $||\mathbf{u}(t,;\mathbf{y}_0) - \mathbf{u}(t;\mathbf{u}_0)|| < \varepsilon$ *for all* $t \geq 0$.

Definition 1.3.7 *A* T*-periodic solution* $\mathbf{u}(t;\mathbf{u}_0)$ *of (1.69) is attractive (within a radius* $R > 0$*) if for an initial condition* $\mathbf{y}_0$ *such that* $||\mathbf{y}_0 - \mathbf{u}_0|| < R$ *then* $\mathbf{u}(t, by_0) \to \mathbf{u}(t,\mathbf{u}_0)$ *as* $t \to \infty$.

Global attractivity and (global) asymptotic stability may be defined analogously.

Although it is straightforward to find steady states, by solving $\mathbf{F}(\mathbf{u}^*, t) = 0,\ \ t \geq 0$ for $\mathbf{u}^*$, it is not so easy to find periodic solutions. For this we will try to appeal to the Poincare-Bendixson Theorem. First we define a positively invariant set:

Definition 1.3.8 *Consider the system (1.69) for* $\mathbf{F}$ *continuous. Then* $B \subset \mathbb{R}^n$ *is a positively invariant set of (1.69) if for all initial conditions* $\mathbf{u}_0 \in B$ *then* $\mathbf{u}(t,\mathbf{u}_0) \in B$ *for* $t \geq 0$.

Theorem 1.3.9 The Poincare-Bendixson Theorem *Consider the system (1.69) in* $\mathbb{R}^2$. *If* $B \subset \mathbb{R}^2$ *is a positively invariant set that contains no steady states then* B *possesses a stable periodic orbit.*

For a proof of this see, for example [38]. A corollary to this allows the set B to contain unstable steady states (not saddle points), since the set obtained from B by removing small

neighbourhoods of the steady states satisfies the conditions of the theorem. This can be very simple to apply; if our system only has one unstable steady state and the solution is bounded then we immediately know we have a periodic solution. In the case where we wish to show that a periodic solution does not exist we may apply Dulac's Criterion

Theorem 1.3.10 Dulac's Criterion *Consider the autonomous system* $\dot{\mathbf{x}} = \mathbf{f}(\mathbf{x})$ *in* $\mathbb{R}^2$, *let* $D \subset \mathbb{R}^2$ *be simply connected open set and* $B(x_1, x_2)$ *be a real valued continuously differentiable function in* D, *where* $\mathbf{x} = (x_1, x_2)$. *Then if*

$$\frac{\partial(Bf_1)}{\partial x_1} + \frac{\partial(Bf_2)}{\partial x_2} \tag{1.70}$$

is of constant sign and not identically zero in D, *then* $\dot{\mathbf{x}} = \mathbf{f}(\mathbf{x})$ *has no periodic orbits lying entirely within* D.

Much of our modelling involves the use of difference equations in which the determination of steady states and periodic orbits is particularly relevant. We will only have cause to consider autonomous systems and so will define such a general difference equation system by

$$\mathbf{N}_{t+1} = G(\mathbf{N}_t) \tag{1.71}$$

and proceed as before.

Definition 1.3.11 $\mathbf{N}^*$ *is a steady state of (1.71) if* $\mathbf{N}^* = \mathbf{G}(\mathbf{N}^*)$.

Definition 1.3.12 *A steady state* $\mathbf{N}^*$ *of (1.71) is stable if, given* $\varepsilon > 0$ *there is* $\delta > 0$ *such that for* $||\hat{\mathbf{N}}_0 - \mathbf{N}^*|| < \delta$ *with* $\hat{\mathbf{N}}_t$ *defined by* $\hat{\mathbf{N}}_{t+1} = G(\hat{\mathbf{N}}_t)$, $||\hat{\mathbf{N}}_t - \mathbf{N}_t|| < \varepsilon$ *for* $t \geq 0$.

Definition 1.3.13 *A steady state* $\mathbf{N}^*$ *of (1.71) is attractive (in a radius* R*) if for all* $\hat{\mathbf{N}}$ *such that* $||\hat{\mathbf{N}}_0 - \mathbf{N}^*|| < R$ *then* $\hat{\mathbf{N}}_t \to \mathbf{N}^*$ *as* $t \to \infty$.

The definitions for globally attractive and then (globally) asymptotically stable follow analogously to ODEs.

Definition 1.3.14 $\mathbf{N}_t$ *is a p-periodic solution of (1.71) if* $\mathbf{N}_{t+p} = \mathbf{N}_t$ *for all* $t \geq 0$.

Here $\mathbf{N}_t$ is a steady state of the system $\mathbf{N}_{t+p} = \mathbf{G}^p(\mathbf{N}_t)$ and it is then convenient, rather than in a form analogous to ODEs, to define the stability of a periodic solution by

Definition 1.3.15 *A p-periodic solution* $\mathbf{N}_t$ *is stable if all the p points of the periodic orbit are stable as steady states of* $\mathbf{N}_{t+p} = \mathbf{G}^p(\mathbf{N}_t)$.

There are no analogues of Poincare-Bendixson or Dulac's Criterion for difference equations.

The presence of globally (or over a sufficiently large set) asymptotically stable solutions (steady or periodic) is particularly important since they represent the actual behaviour of the model given a sufficiently long amount of time. The biological systems that we will be modelling can often be assumed to have been running for arbitrary long periods of time and so are displaying their ultimate behaviour. Hence to characterise the behaviour of our model and its relevance to the biological system it may only be necessary to study its asymptotic behaviour, which is often much simpler.

1.3.4 Dealing with Timescales

The modelling can be simplified greatly and the analysis and interpretation of results made much easier by considering the different timescales that are present in the model. We have already indicated that any transient behaviour may be ignored if the model has well characterised asymptotic behaviour.

Section 1.2.1 gives a rigorous basis for taking the fast processes to be at equilibrium. This is particular useful for reducing the order of a system. We can use this trick to simplify a model of the electrical properties of a cell membrane by assuming that the fast channels activate instantaneously. This is also used implicitly in many situations, such as assuming that nicotinic receptor activation and ion channel opening is fast (and so instantaneous) compared to the rate at which nicotine binds to the receptor in Chapter 2.

We also use the converse, that particularly slow timescales can be regarded as constants, such as considering the number of functional nicotinic receptors to be fixed when simulating experimental runs of 40 seconds when receptor inactivation takes days of chronic nicotine stimulation. This is again useful at reducing the number of differential equations in a system.

There is one other way in which the modelling may be simplified when we are considering a system where there are much faster timescales in operation. There may be situations where it is impractical to assume the pseudo-steady state, for example in the study of neuronal networks over longer periods of time where the firing pattern is generated by Hodgkin and Huxley ion channels. The timescales of the channel activation and inactivations are much

faster (ms) than the timescale of study (many seconds), but setting the activations to steady state destroys the ability of the model to fire action potentials.

In such cases it may be appropriate to reformulate the model so that instead of considering all of the fast mechanisms an appropriate average response is calculated and used. This would mean writing the model in our example in terms of average firing rates, rather than getting it to generate discrete spikes. Care should be taken with this technique since using an average necessarily destroys information.

1.3.5 Computer Simulations - GENESIS

It is very useful to be able to display the solutions of models in a numerical or graphical form. This can be an aid in interpreting results, or for getting a flavour of how the model behaves. One may be able to 'see' solutions tending to steady states, or tracing periodic orbits and provides illustrations that confirm the analytical results of the model. In some cases the visual identification of certain trajectories may be the most viable way of establishing a modelling result. This can arise in models where the equations do not give an adequate interpretation of some transient behaviour, such as in certain models of neuronal firing patterns. Certainly many models will give quantitative results and numerical simulation may be the easiest way that these may be obtained.

There are also many occasions where the complexity of the model precludes a lot of mathematical analysis and so numerical solution may be the only way that we can make any analysis of the model and its results. This is particularly true where we have developed models which make extensive use of Hodgkin and Huxley ion channels. The equations that describe the action of these channels are largely intractable to mathematical analysis and often the only way (and in many more cases the easiest way) that we can attempt to quantitatively fit such a model to experimental data, or determine the models output is by numerical solution. This is not an ideal situation but is our only option where the modelling necessitates the inclusion of such mathematically complicated equations.

The numerical solution of models involving ion channels is particularly important for the results of Chapters 2 and 3, and provides useful insights into the modelling of Chapter 4. These models were implemented and numerically solved using the General Neural Simulation System, or GENESIS, software designed and written at the California Institute of Technology [10]. As would be expected from the name, GENESIS is specifically designed for the numerical solution of models of neuronal systems and has specific routines dedicated to solving for;

membrane potential in compartments (equations of the form (1.34)); Hodgkin and Huxley ion channels (such as the solution of equations (1.36)-(1.37)); and synaptic input (1.54) with all the necessary links to combine them.

The code has been extensively tested, both in development and its use worldwide. This helps enormously since it means that our implementations are essentially bug free; there are no coding errors and the numerical schemes are stable. We are only required to input the appropriate parameters, such as the dimensions, membrane resistance resting potential for an implementation of an electrical compartment. We can therefore be confident that the results obtained are accurate approximations to the true solutions of our models.

GENESIS also provides a graphical interface (called Xodus) which allows interaction between the user and a running simulation. Graphs may be plotted as the simulation is running and 'dialog' boxes allow the user to arbitrarily change parameter values which makes for easy parameter searching. The graphical output from GENESIS is widely used in this thesis; all figures of the numerical solutions of models (even Figure 1.1) are produced by GENESIS.

We encountered one problem with GENESIS; there appear to be bugs with the allocation and freeing of computer memory that leave long simulation runs are prone to crashing. This was apparent with the long runs attempted in Chapter 4, but since they were only serving to illustrate a result that may be derived analytically we did not consider it a big problem.

1.4 Overview

This thesis is concerned with modelling some of the neuromodulatory effects of nicotine in Chapter 2 to 4, and the effects of the neurological disorder of Parkinson's disease on neuronal function in Chapter 5.

Nicotine is the major psychoactive ingredient in tobacco smoke [50] and is thought to underlie the apparent addictive effects of cigarette smoking in humans. Strong links have been established between smoking, heart disease and cancer, and have recently been acknowledged by the tobacco company Philip Morris Inc, makers of Marlboro and Benson & Hedges [1]. The study of nicotine and its analogs is therefore rightly the subject of intense study, although the causal links between smoking and disease do not themselves involve nicotine. We believe that this is, to date, the only attempt at mathematically modelling how nicotine may affect neuronal function in mammals.

Similarly we present the first mathematical modelling of the effects of Parkinson's disease. Parkinson's is a degenerative disease that affects 0.5% of the over-60s (with an interestingly much lower incidence in tobacco smokers)[96]. Symptoms of the disease, which is expressed in the progressive death of certain brain pathways, include various disorders of movement. Despite also being the subject of much medical investigation there is no cure and the cause of the disease remains unknown.

In Chapter 2 we study the effect of nicotine on nerve terminals by modelling the experimental preparation of synaptosomes, requiring us to consider not only the cellular functions but also how these are affected by the artificial nature of the experimental preparation. The quantitative nature of the experimental results leads to a very numerically orientated approach. The model is capable of explaining many of the experimental findings and the fitting to experimental data leads to sound hypotheses on the distribution and potency of nicotinic receptors within the synaptosomes.

The modelling of Chapter 3 produces a theory on the cellular functions underlying a particular type of firing pattern in a neuronal pathway, a pathway that is believed to mediate the rewarding effects of addictive drugs. We describe how stimulation by nicotine (and also by opiates) can lead to an increase in the incidence of this firing pattern which our model can reproduce. The conclusions of our hypothesis are supported by numerical results and from the analytical results of a simplified difference equation model. This demonstrates at a more fundamental level why smoking may be perceived as pleasurable.

The perceived addictive effects of nicotine are addressed in Chapter 4. We demonstrate how a sensitisation of nicotine may be induced in.synaptic connections with mechanisms known to be present is similar cells. A probabilistic model is presented of how the memory of this sensitisation may last indefinitely, which has important implications for nicotine addiction. The results are also relevant to opiate abuse.

We change to modelling a neuronal network that is attacked in Parkinson's disease in Chapter 5. We consider the change in the output of this network as the disease progresses and can demonstrate neuron-level substrates for many of the clinical symptoms of the disease, including how the standard treatments can reverse these effects. The modelling itself provides some interesting mathematical results on network dynamics and coupled oscillators.

Chapter 2

Nicotinic Agonist-Induced Release of Dopamine

2.1 Chapter Overview

The nicotinic agonist anatoxin-a (AnTx) has been shown to elicit the release of radio-labelled dopamine from rat striatal synaptosomes by acting on presynaptic nicotinic-acetylcholine receptors (nAChR) and hence present a potential target for therapeutic drugs. Regarding each synaptosome to be a single electrical compartment that has Hodgkin and Huxley descriptions of potassium, sodium and calcium ion channels, we build models that describe the membrane potential of individual synaptosomes on millisecond timescales. We calculate the transmitter release from a function of intracellular calcium concentration and the number of open calcium channels, allowing for the delay whilst these activate.

We find that AnTx prompts release by causing the cell to repetitively fire action potentials, as distinct from the release caused by a single step depolarisation caused by raised extracellular potassium concentrations. Combining our models in the appropriate proportions to represent the entire preparation and fitting this to the experimental data we deduce the existence of three major sub-types of synaptosome in that they are separated as to whether they have N- or P-type calcium channels and that a subset of those with N-type channels also have nAChR. This model of the preparation as a whole fits well to the experimental results for release prompted by KCl and the higher (1μM and above) doses of AnTx, but less well for the lower concentrations which we hypothesise can be remedied by taking into account the heterogeneity of nAChR in the preparation, to which the model may be easily extended.

2.2 The Presynaptic Actions of Nicotine

2.2.1 The Presynaptic Modulation of Transmitter Release

We are familiar with the classical picture of a neuron causing signal propagation by the generation and transmission of electrical impulses down the nerve axon to its terminals and the subsequent release of a chemical signal. The strength of the signal depends on many factors, not least the amount of chemical neurotransmitter released by the nerve terminal[45]. The amount of transmitter released in response to the arrival of an action potential is not constant, but is subject to modulation by the extracellular environment in the vicinity of the terminal. Terminals are affected not only by the variations in ion concentrations but also by the possible interaction of neurotransmitters and their agonists with presynaptic receptors.

The experimental stimulation of transmitter release by presynaptic nicotinic acetylcholine receptors (nAChR) in the brain has been widely documented and is considered to constitute a significant physiological role for ligand gated ion channels [85][104]. In particular the nicotinic stimulation of dopamine release from rat striatal synaptosomes has been the subject of extensive examination [21][32] [83][84]. The dopamine releasing neurons of the mesolimbic and nigrostriatal pathways terminate in the striatum, the former of which is widely implicated in the reinforcing effects of addictive drugs [50]. Therefore the nicotinic stimulation of presynaptic nAChR located on the terminals of these neurons could be a significant source of the reinforcing properties of nicotine. If we wish to investigate the neuromodulatory effects of nicotine we are certainly required to model these presynaptic effects.

2.2.2 Aims of the Model

Our primary aim is to understand how doses of nicotine may be able to enhance or prompt the release of dopamine from the terminals of the nigrostriatal pathway. As such we will be restricting our model to looking at terminal acting effects only, in which case the experimentation on rat striatal synaptosomes mentioned above provides a wealth of quantitative data. They are the data on which our model is created, quantitatively fitted to and tested against. Therefore our model will be essentially a model of the experimental preparation rather than a true nerve terminal. It will also be quantitative in flavour since we are forming and testing our model against quantitative data.

Our interest is in the effect of the presynaptic nAChR, an effect that is likely to be mediated by the activation of its ion channel that allows the influx of sodium and calcium ions[104].

Therefore our modelling efforts will be centred on the interaction of this ionic current with the other intrinsic currents of the terminal / synaptosome. This stipulates two major features of our model; firstly that it will be based on the millisecond timescale interactions of ion channels and membrane potential, which is starkly in contrast to the experimental preparation which has a time resolution of minutes[94]. This means that our model, if it describes the experimental results well, can provide a millisecond view of synaptosome action from which sound hypotheses on true nerve terminal action at physiologically relevant timescales can be derived. This could be considered a bonus, as well as being able to determine the effect of nicotine on dopamine release we may also be able to discover particulars about the terminals themselves.

Modelling the interaction of intrinsic ion channels and membrane potential leads us to our second major feature; accurate models of ion channel function (we will be using Hodgkin and Huxley-type models [41]) are notoriously intractable and hence our major tool for analysis of the system is likely to be the numerical solution of the model.

2.2.3 Synaptosomes and Terminals

The size of nerve terminals (1-2μm across) [45] currently precludes detailed examination of their individual release characteristics at physiologically relevant time scales. In its place we have the artificial preparation of synaptosomes which are used in many laboratories for the investigation of terminal effects. Detailed descriptions of the methodology in preparing and performing experiments upon synaptosomes can be found in [79] and papers such as [94] [95] [31] [60] [87] and so have no place here, but we shall present a short description of the parts of the procedures that are relevant to our modelling.

The experimental preparation is normally the rat (although we have taken some data from mouse synaptosomes), the relevant brain area (striatum) is dissected and then homogenised. The clearance of the homogeniser is such that the nerve terminals are 'snipped' off from the rest of the cell and will then reseal retaining their contents forming metabolically active packets, synaptosomes. These may be separated from the remainder of the homogenate by subcellular fractionation. The resulting preparation is therefore a composite of the dopamine releasing terminals with other terminals or bits of cell that have survived the process.

Prior to the experimental step, known as superfusion, the synaptosomes are loaded with [^{3}H]-labelled dopamine which will be released along with the unlabelled dopamine. The experimental observable is then the amount of labelled dopamine released, as counted by a

scintillation counter, in counts per minute (cpm). This is also quoted as release above baseline (unstimulated synaptosome experimental results have a total release curve that decays in an exponential fashion with time, this is taken to be the baseline). We therefore fit our model to this output parameter rather than an experimentally immeasurable true release. After the synaptosomes have been loaded, the uptake transporter is disabled by nomifensine, this prevents misleading results from released dopamine being taken back up before it can be counted. It also means that our model of a terminal is deprived of the fastest means of recycling transmitter which proves to be very important. We will be assuming that all other pumps and transporters, whether ion exchange or ATP (adenosine tri-phosphate) driven, are working as they would in the undisturbed brain.

The superfusion process consists of passing a buffer continuously over the synaptosome preparation and collecting the results in fractions (of two minute intervals typically [94]), which are then assessed for labelled dopamine by the scintillation counter. This means that the experimental results are of release collected over a two minute period. The buffer acts as the extracellular fluid for the preparations and will typically be of a similar composition to that of the brain. However this can easily be changed during superfusion to provide chemical pulses to the preparation. Of particular interest are the 40 second pulses of KCl and the nicotinic agonist anatoxin-a [94] [95] and the sustained application of nicotine [31].

2.2.4 The Experimental Results

The modelling is largely based on results using the nicotinic agonist anatoxin-a (AnTx) by virtue of its potency, stability and specificity [94][95]. It is pertinent to summarise these results before we attempt to describe the model. The other results we have used will be introduced as we need them.

AnTx evoked the release of [^{3}H]dopamine from striatal synaptosomes in a concentration dependent manner with an EC_{50} of $0.11\mu M$. Maximum release was achieved with concentrations of $1\mu M$ AnTx and above, but this response was only 20% of the maximum that could be produced by KCl depolarisation. KCl depolarisation also releases [^{3}H]dopamine in a dose dependent manner with an EC_{50} of $21\mu M$. There was no additivity between AnTx and submaximal concentrations of KCl.

Both KCl and AnTx evoked release is Ca^{2+} dependent. The stimulatory effect of AnTx was dependent on external Na^+, partially blocked by tetrodotoxin, and totally blocked by Cd^{2+}, consistent with depolarisation and the consequent opening of voltage-dependent Na^+

and Ca^{2+} channels. Further analysis implicated N-type calcium channels in AnTx-evoked responses since such release is blocked by the specific N-type blocker $\omega-$Conotoxin GVIA.

KCl evoked release was found to be increased under low external Na^{+} but independent of tetrodotoxin which suggests conflicting results regarding voltage-activated sodium channels. KCl evoked release was blocked equally and additively by $\omega-$Conotoxin GVIA and the P-type calcium channel blocker $\omega-$Agatoxin IVA. The lack of significant release in the presence of both toxins indicates that these are the only calcium channels involved in release and also that there is no contribution from calcium influx through nAChR.

2.3 The Model Cell

2.3.1 Reduction to an Electric Circuit

We model the synaptosomes by considering the interaction of membrane potential and intrinsic ion channels. The experimental results tell us that the release is dependent on calcium which flows in through voltage-activated calcium channels and so we wish to know such quantities as the membrane potential [94]. This immediately leads us to consider the membrane potential resulting from the interaction of all the other channels present. We therefore decided to follow the formulation of Hodgkin and Huxley [41], where the membrane of the synaptosomes is assumed to act as an electrical capacitor with capacitance C_m. If we denote the membrane potential relative to the cell exterior by V_m and the total electrical current due to the ion channels of the cell by $I(V_m, t)$, then by Kirchoff's conservation of current law

$$C_m \frac{dV_m}{dt} + I(V_m, t) = 0. \tag{2.1}$$

which we may solve to obtain the calcium influx and, by an appropriate model of this process, obtain the transmitter release. We therefore need formulations for the electrical properties of the membrane of a synaptosome and models of their ion channels.

2.3.2 Nernst or Reversal Potentials

The cell membrane of the synaptosomes serves to separate the differing ion concentrations of the interior and exterior of the cell and typically the opening of ion channels, that are selective for an ion species, will allow a flow of ions from one side to the other. There is a membrane potential that will prevent this flow and is capable of maintaining this imbalance

of ions, this is known as the Nernst or reversal potential of the ion species [45]. The difference between the reversal potential and the membrane potential is therefore the potential gradient (electro-motive force) that drives the ionic current.

For an ion species z with extracellular and intracellular concentrations $[z]_o$ and $[z]_i$ respectively and valency ν, the Nernst potential is given by the Nernst equation [45]:

$$E_z = \frac{RT}{F\nu} \ln\left(\frac{[z]_o}{[z]_i}\right) = \frac{25 \times 10^{-3}}{\nu} \ln\left(\frac{[z]_o}{[z]_i}\right), \tag{2.2}$$

R is the universal gas constant, T is the temperature in Kelvin and F is Faraday's constant.

2.3.3 The Basic Cell

Our experimental preparation is a collection of many individual synaptosomes, but to be able to study nerve terminal action and to be consistent with the formulation outlined above we will take the approach of producing models of single synaptosomes. A model of the total preparation may then be obtained by combining these models in the appropriate proportions.

Implicit in this is our realisation that the synaptosomes in the preparation are not identical. We are only going to consider the existence of dopaminergic cells in the preparation but accept that there are likely to be variations between these individuals too. However we will be assuming a large amount of homology between the cells and that they may only differ in such aspects as whether they have N-type or P-type calcium channels and such like. Not only is this simpler but we shall only impose different attributes on synaptosomes only when the combination of experimental data and modelling calls for it rather than in an attempt to obtain a better quantitative fit. With possibly thousands of independent synaptosomes we could fit to any release results we wished but such a model would be meaningless and no more informative than a curve fit.

We will regard each synaptosome to be a single electrical compartment 1 micron in diameter and length. Since this compartment is physiologically small we can consider it to be isopotential, that is the membrane potential is the voltage potential of the whole cell and hence there are no effects from the spatial distribution of ion channels or receptors. The compartment has a specific membrane resistance R_m and capacitance C_m which we will take to be those values used by Traub et al [98] in their model of rat hippocampal neurons, adjusted for cell size. Each cell can therefore be modelled by equation (2.1).

We have used four types of voltage-activated ion channels in the model, two selective for calcium (N-type and P-type) and one each for potassium or sodium. The ion flux (I) through

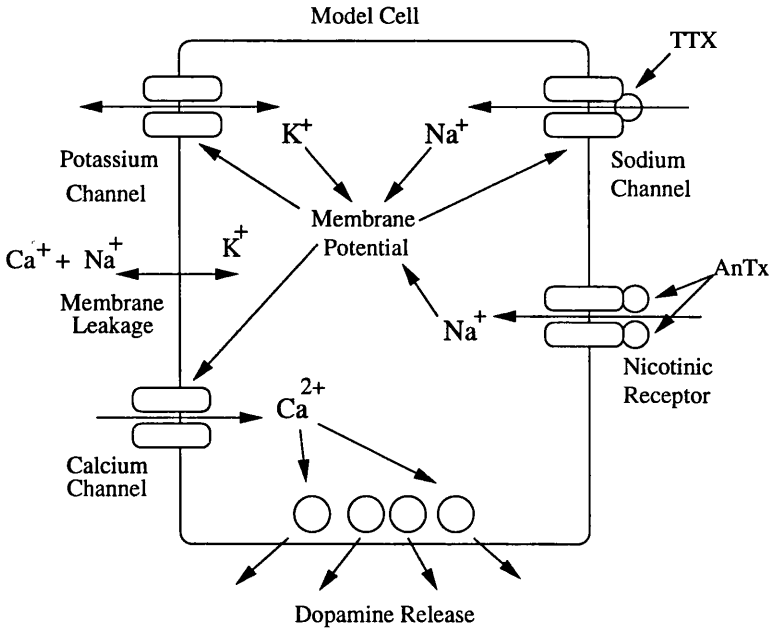

Figure 2.1: Schematic diagram of the model cell with the interactions between the components. The potassium, sodium, leakage and nicotinic receptor currents dictate the membrane potential of the cell, which then controls transmitter release via the activation of the calcium channels.

a set of channels is regarded as an electrical current and hence obeys Ohm's Law

$$I(V_m, t) = g(V_m, t)(E - V_m) \tag{2.3}$$

where g is the conductance of the channels (a function of total number of channels, channel activation and inactivation due to voltage and time) and will generally be a Hodgkin and Huxley model. $(E - V_m)$ is the difference between the membrane potential, V_m, and the reversal potential of the ion species, E, and represents the voltage gradient across the membrane. All values are given in SI units. Our conservation of current law (2.1) then becomes

$$C_m \frac{dV_m}{dt} + I_K + I_{Na} + I_{Ca} + I_R + I_{\text{leak}} = 0, \tag{2.4}$$

with

$$C_m = 1.57 \times 10^{-12}, \tag{2.5}$$

I_K and I_{Na} are the potassium and sodium currents respectively and I_{Ca} is the calcium current we prescribe for the terminal, we shall deduce later that the presence of the two types is mutually exclusive. I_R is the current due to the nicotinic receptor, not all synaptosomes will have this as we shall discuss later. I_{leak} is the leakage current described below.

2.3.4 Leakage Current and Ion Pumps

The membrane of a cell is not a perfect insulator and so there will be some leakage of current across it. Moreover there will be many forms of ion pumps, used to maintain the balance of ion concentrations across the cell membrane, that we do not explicitly model.

Due to this natural permeability of the cell membrane and the action of these ion pumps, there will be some ion flux across it aside from the ion channels we have explicitly included[10] [49]. We model this by assuming a leakage current given by

$$I_{\text{leak}} = \frac{E_m - V_m}{R_m} \tag{2.6}$$

$$E_m = -0.010 \tag{2.7}$$

$$R_m = 1.59 \times 10^{12} \tag{2.8}$$

where E_m is the reversal potential of this current, typically about 10mV [10], V_m the membrane potential and R_m the membrane electrical resistance. R_m is already fixed due to the cell dimensions and the specific resistance of [98]. We have used the estimation of the reversal potential for this current from a typical cell as used in other simulations [10].

2.3.5 Calcium Ion Channels

We implement models of N-type and P-type voltage-activated calcium channels, it having been shown that KCl-evoked release of [^{3}H]dopamine from striatal synaptosomes is blocked by the selective antagonists of N- and P-types, $\omega-$Conotoxin GVIA (ω-CgTx) and $\omega-$Agatoxin IVA (ω-Aga IVA) respectively [95]. This does not discriminate whether N- and P-types co-exist on terminals (and by some mechanism AnTx only causes the activation of N-types, although such a mechanism is not consistent with each cell being a single, isopotential electrical compartment) or terminals possess one type exclusively. We use the latter, simpler, hypothesis that a terminal contains either N- or P-type channels, but not both.

Voltage-dependent activation $x_\infty(V_m)$ and inactivation $y_\infty(V_m)$ curves for N-type channels were taken from McNaughton et al [61]. The time dependence of activation τ_x is taken from [82] and the inactivation τ_y then chosen to be consistent with the experimental data [61].

The current from N-type channels is then given by:

$$I_{\mathrm{N}} = \bar{g_{\mathrm{N}}} xy(E_{\mathrm{Ca}} - V_m) \tag{2.9}$$

$$\frac{dx}{dt} = \frac{x_\infty(V_m) - x}{\tau_x} \tag{2.10}$$

$$\frac{dy}{dt} = \frac{y_\infty(V_m) - y}{\tau_y} \tag{2.11}$$

$$x_\infty(V_m) = \frac{1}{1 + \exp(-\frac{V_m + 0.0045}{0.0052})} \tag{2.12}$$

$$\tau_x = 0.001 \tag{2.13}$$

$$y_\infty(V_m) = \frac{1}{1 + \exp(\frac{V_m + 0.074}{0.0065})} \tag{2.14}$$

$$\tau_y = 0.150. \tag{2.15}$$

The P-type calcium channel voltage-dependent activation curve $p_\infty(V_m)$ is taken from [101] and time constant of activation τ_p from [82]. P-type channels do not inactivate with voltage. The current due to P-type channels is then given by:

$$I_{\mathrm{P}} = \bar{g_{\mathrm{P}}} p(E_{\mathrm{Ca}} - V_m) \tag{2.16}$$

$$\frac{dp}{dt} = \frac{p_\infty(V_m) - p}{\tau_p} \tag{2.17}$$

$$p_\infty(V_m) = \frac{1}{1 + \exp(-\frac{V_m + 0.072}{0.0027})} \tag{2.18}$$

$$\tau_p = 0.0012. \tag{2.19}$$

We must then calculate the conductances of the channels, $\bar{g_{\mathrm{N}}}$ and $\bar{g_{\mathrm{P}}}$. Such data is not available for the rat striatum and so we have calculated values from the conductance densities used in another computer simulation for a general nerve terminal [93] and adjusted for cell size. This implies total conductances in our case of the order of 10^{-9}Siemens. This conductance leads to calcium currents which are much smaller (1000 times so) than the other currents used in our model and hence their contribution to the membrane potential is negligible as far as we are concerned. Hence for computational efficiency we do not include either of these channels in computing the membrane potential (solving equation (2.4)), however both are very important in calculating transmitter release, as we shall see later. Although it is not used; in such preparations $E_{Ca} \approx 0.095$V.

2.3.6 Potassium Ion Channels

In a classical view of neurotransmitter release from nerve terminals the cell is kept at a resting, hyperpolarised membrane potential by potassium channels. This seems to hold true in synaptosomes since they may be depolarised by increasing extracellular potassium levels.

There appear to be (at least) two types of potassium channel in synaptosomes. Stimulating synaptosomes with the A-type potassium channel blocker 4-aminopyridine (4-AP) produces oscillations in the membrane potential [14], this not only indicates that A-type potassium channels are present but also that another type, activated on depolarisation is present and responsible for the repolarising parts of the oscillation. This behaviour is consistent with the so-called delayed rectifying potassium channel.

We do not know the conductance of either the type of potassium channel in this preparation and hence, and for simplicity, it would be preferable to only include one type of channel, which would then have an increased conductance to compensate. We are interested in the release characteristics of the cell, which will occur when the cell is depolarised. In this range the delayed rectifier is dominant, since the A-type potassium channel inactivates if held at depolarised potentials [98] [49], as is typical for depolarisation induced by increased extracellular KCl. This is particularly relevant for later when we consider the action potential firing induced by AnTx. This requires the inclusion of the potassium channel to repolarise the cell in response to a spike and this is again the delayed rectifier.

We therefore include a potassium channel of the delayed-rectifying type only. The voltage dependent kinetics $\alpha(V_m)$ and $\beta(V_m)$ are taken from electrophysiological measurements on the rat hippocampus [89] [98]. At rest, only the potassium channels will be significantly activated and hence the resting potential is determined by the conductance of the delayed rectifying channel and the leakage current. The resting potential of rat nerve terminals has been measured at -78mV [88] and so we set the conductance $\bar{g_K}$ such that the cell rests here. The current is therefore given by:

$$I_K = \bar{g_K} m(E_K - V_m) \tag{2.20}$$

$$\frac{dm}{dt} = \alpha_m(V_m)(1-m) - \beta_m(V_m)m \tag{2.21}$$

$$\bar{g_K} = 1.0 \times 10^{-7} \tag{2.22}$$

$$E_K = -0.08 \tag{2.23}$$

$$\alpha_m(V_m) = \frac{16000(V_m + 0.0249)}{1 - \exp\left(-\frac{V_m + 0.0249}{0.005}\right)} \tag{2.24}$$

$$\beta_m(V_m) = 250 \exp\left(-\frac{V_m + 0.04}{0.04}\right). \tag{2.25}$$

We model stimulation by elevated extracellular potassium simply by changing the extracellular concentration of potassium in our model appropriately. This shifts the reversal potential E_K which results in potassium influx and so depolarises the cell [67].

2.3.7 Sodium Ion Channels

It has been observed that AnTx-evoked release is nearly halved if the synaptosomes are poisoned with the potent fast sodium channel blocker tetrodotoxin (TTX), indicating that these channels are present and in significant numbers.

We take fast sodium channel kinetics from the rat hippocampus as described by [88] [98]. Again we do not know the channel conductance $g_{\bar{\mathrm{Na}}}$ but can suppose that the conductance will be powerful enough to cause a sizeable action potential, that is one that forces the membrane potential to positive values. A cursory look at the AnTx-evoked release profile and the power of hindsight from the model results, suggests that AnTx doses of 1μM and above rapidly produce sodium channel-induced action potentials. We therefore set the conductance of the sodium channel such that, by numerical simulation, doses of 1μM initiate such an action potential. Since TTX is such a potent blocker of these sodium channels, we model the effect of its application by resetting the conductance of the channels to zero. Otherwise the current is given by:

$$I_{\mathrm{Na}} = g_{\bar{\mathrm{Na}}} r^2 s (E_{\mathrm{Na}} - V_m) \tag{2.26}$$

$$\frac{dr}{dt} = \alpha_r(V_m)(1-r) - \beta_r(V_m) r \tag{2.27}$$

$$\frac{ds}{dt} = \alpha_s(V_m)(1-s) - \beta_s(V_m) s \tag{2.28}$$

$$g_{\bar{Na}} = 1.0 \times 10^{-9} \tag{2.29}$$

$$E_{Na} = 0.085 \tag{2.30}$$

$$\alpha_r(V_m) = \frac{-3.2 \times 10^5 (0.0469 + V_m)}{\exp\left(\frac{V_m + 0.0469}{0.004}\right) - 1} \tag{2.31}$$

$$\beta_r(V_m) = \frac{2.8 \times 10^5 (0.0169 + V_m)}{\exp\left(\frac{V_m + 0.0199}{0.005}\right) - 1} \tag{2.32}$$

$$\alpha_s(V_m) = 128 \exp\left(-\frac{V_m + 0.028}{0.018}\right) \tag{2.33}$$

$$\beta_s(V_m) = \frac{4 \times 10^3}{1 + \exp\left(-\frac{V_m + 0.005}{0.005}\right)}. \tag{2.34}$$

2.3.8 The Nicotinic Acetylcholine Receptor

Neuronal presynaptic nicotinic receptors

Nicotinic acetylcholine receptors are membrane bound pentameric structures around a central ion channel [104] [79]. Ten receptor subunits have been identified so far ($\alpha 2 - \alpha 8$, $\beta 2 - \beta 4$).

The α subunits may be viewed as the 'functional' subunits and agonist binding to the α-β junctions (of which there are two per nAChR) causes the ion channel to open. The β subunits are therefore often designated to be structural, but in fact all subunits contribute to determining the binding properties and efficacies of nicotinic agonists.

The idealised construction of an nAChR is from two α subunits and three β subunits. Although we will assume this to be the case, and is so concerning nAChR on striatal dopamine terminals, it is not true in general. Indeed nAChR consist of a diverse array of subunits and present a range of pharmacological properties that is the study of many laboratories worldwide, see [104] for a review.

We have assumed only a single subtype of nAChR to be present in the synaptosome preparation. During the creation of this model and since its completion in this form significant evidence has accumulated that there are at least two subtypes, each with separate pharmacologies and efficacies to, amongst other things, AnTx [44][53]. Our model is still based on the assumption that there is only one type, with full efficacy for AnTx. The implications of this will be discussed later.

An important functional feature of nAChR is that receptors desensitise when exposed to agonist for prolonged periods of time (tens of seconds to minutes), recovery on removal of the agonist takes minutes [31]. While this is not of particular relevance to this model, since our results suggest that desensitisation during the 40 seconds for which we apply AnTx does not significantly affect our model, the phenomenon is present in the modelling of the receptor that we present and is of relevance in subsequent chapters.

Modelling a nicotinic receptor

The AnTx-evoked release of dopamine from synaptosomes is well established [94] [95] [44]. Such release is blocked by the nicotinic receptor antagonist mecamylamine, indicating that AnTx does act through nAChR. We do not model any non-specific (non-nAChR mediated) release. For simplicity we take the nACh receptors to be homogeneous.

Our model of the nicotinic receptor is taken to be consistent with the description given in Lippiello et al [57], who analysed the binding of [^{3}H]nicotine (which binds to the $\alpha4\beta2$ subtype of nAChR) to rat brain sites. Two binding rates are observed; an initial low affinity rate that is proposed to reflect binding to the active (sensitive) conformation of the receptor and a later, high affinity rate corresponding to binding to the desensitised conformation. Each

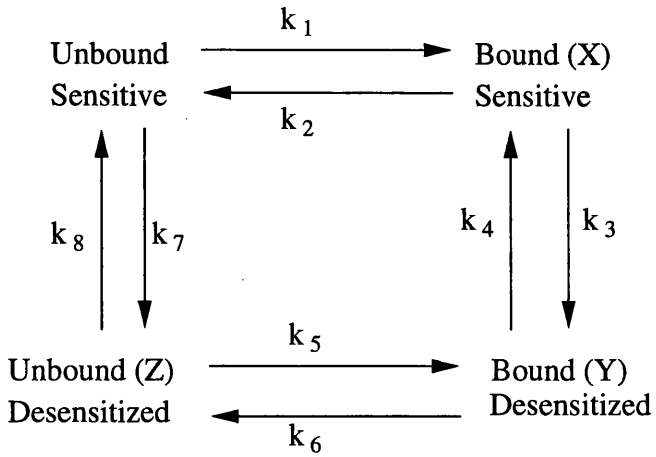

Figure 2.2: Receptor binding site state transition model [57]. For the receptor pore to open, both binding sites must be in the bound and sensitive state (X). The constants k_i are determined from experimentation.

binding site therefore has four states; unbound and sensitive; bound and sensitive (permissible for pore opening); bound and desensitized; unbound and desensitized. Consistent with our treatment of nAChR thus far each receptor has two such binding sites.

We let $X, Y, Z \in [0, 1]$ be the proportion of binding sites that are bound and sensitive; bound and desensitized; and unbound and desensitized respectively; as detailed in Figure 2.2. We will assume that the binding to one site is independent of the state of the other, in which case X^2 is the proportion of receptors that are gating ion flux. Noting that the proportion of sites in the unbound and sensitive state is then given by $(1 - X - Y - Z)$, the binding site state transition equations are:

$$\frac{dX}{dt} = k_1[\mathrm{n}](1 - X - Y - Z) + k_4 Y - k_2 X - k_3 X \tag{2.35}$$

$$\frac{dY}{dt} = k_3 X - k_4 Y + k_5[\mathrm{n}]Z - k_6 Y \tag{2.36}$$

$$\frac{dZ}{dt} = k_7(1 - X - Y - Z) - k_8 Z + k_6 Y - k_5[\mathrm{n}]Z \tag{2.37}$$

where [n] is the concentration of nicotine and the k_i's are experimentally derived constants [57] given by:

$$\begin{aligned} k_1 = 500 \quad & k_2 = 0.075 \quad k_3 = 0.00367 \\ k_4 = 0.00005 \quad & k_5 = 500 \quad k_6 = 0.00067 \\ k_7 = 0.0001 \quad & k_8 = 0.00015. \end{aligned} \tag{2.38}$$

Hence the channel conductance g is a function of agonist concentration instead of membrane potential as in equation (2.3). Explicitly $g = \bar{g_R} X^2$, where $\bar{g_R}$ is the total channel conduc-

tance. As detailed before, the conductance is set in combination with the conductance of the sodium channels $g_{\bar{Na}}$ such that AnTx doses of 1μM and above rapidly trigger action potentials in the model. The current from the receptor is therefore given by

$$I_R = g_{\bar{R}} X^2 (E_R - V_m) \tag{2.39}$$

$$E_R = 0.09 \tag{2.40}$$

$$g_{\bar{R}} = 1.5 \times 10^{-9}. \tag{2.41}$$

This contains three important assumptions that we shall now address. We have already assumed that we have only the single subtype of nAChR and have used the model described by Lippiello et al [57] and then taken these to be descriptive of the nAChR activation characteristics that we require. These measurements are taken from the entire rat brain using labelled nicotine and hence contain results from the $\alpha 4\beta 2$ subtype of nAChR and so may not be entirely representative of the subtype that we are including in our model, not that our inclusion of only one subtype is representative of the experimental preparation.

Moreover the figures quoted are for the binding of [^{3}H]nicotine and we will be modelling the application of AnTx for which the figures will almost certainly be different, if rather similar. However these are the best (only) figures available for the rates of transition between the states of the binding sites.

We do not consider this to be too much of a problem since the results of our model are largely dependent on the conductance levels, which we have effectively set ourselves by our condition on $g_{\bar{R}}$ and $g_{\bar{Na}}$. The experimentally determined rates then effectively set the 'on' and 'off' times of channel activation and desensitisation, which we will show do not affect the results from our model unduly.

The ion channels associated with nAChR are selective for sodium and calcium ions and the calcium component is thought to be very important given the ions capacity for producing intracellular signalling, such as via calcium-calmodulin kinase activation [104]. There is no experimental evidence that suggests that we should include such processes (so we do not), nor does the calcium influx seem able to cause transmitter release directly [94], this is probably due to the slow diffusion of calcium meaning that it is removed by pumps before it can interact with any transmitter release mechanisms. This has the bonus of making our treatment of transmitter release simpler. Therefore for our purposes the ion flux through the channel can be regarded as a simple electrical current. If the channel has (relative) permeabilities to sodium and calcium of g'_{Na} and g'_{Ca} respectively, then the combination of ions has reversal

potential E_R given by:

$$E_R = \frac{g'_{Na}E_{Na} + g'_{Ca}E_{Ca}}{g'_{Na} + g'_{Ca}}. \tag{2.42}$$

Calcium can make up 10-50% of the ionic flow and so $E_R \in [0.086, 0.09]$. We take $E_R = 0.09$.

2.3.9 Ion Concentrations

Table 2.1 contains the normal concentrations of ion species used for the model when the cell is resting. The extracellular concentrations are simply those concentrations present in the superfusion buffer, typically close to levels found in the mammalian brain. They are held constant since the superfusion process provides a constant stream of fresh buffer [94],[79].

The intracellular concentrations of potassium and sodium are taken to be typical mammalian ([45]), which is valid as we would expect a mammalian cell that has typical mammalian extracellular concentrations to have typical intracellular concentrations. These values are also held constant throughout the simulations. The intracellular potassium concentration is so high that changes are insignificant. The fast, powerful sodium influx does cause a noticeable increase in the intracellular concentration (1-2mM), such that repetitive firing could cause a sufficient intracellular build up and affect the current. We assume that the ion pumps (such as the K^+-Na^+ pump) present in the cell quickly remove these increases[45], this is precisely what they are there to do.

During the superfusion experiments the buffer will be modified to provide the chemical pulses that stimulate release from the synaptosomes. The concentration are then changed as follows:

- KCl stimulation: Potassium concentration set to the value of the KCl concentration. The osmolarity of the buffer is maintained by reducing the NaCl concentration and so we also reset the sodium concentration to the same amount. The reversal potentials E_K and E_{Na} are recalculated accordingly.

- Low Na^+ (10mM) buffer: Extracellular sodium is set to 10mM and E_{Na} recalculated ($E_{Na} \approx 0.017$). The osmolarity must be maintained and the 'missing' sodium is replaced by N-methyl-D-glucamine (NMDG).

- Calcium free buffer: Extracellular calcium set to 1pM, a small, non-zero value which is used simply to prevent a 'division by zero' error in our numerical computations.

	Intracellular (mM)	Extracellular (mM)
Potassium	120	5
Sodium	5	150
Calcium	0.001	2

Table 2.1: Default extra- and intracellular ion concentrations for the resting cell.

2.3.10 Membrane Potential Dynamics

Although we have yet to describe our model for transmitter release, we have been able to finalise the make-up of the ionic currents present in the cell and it is useful at this stage to review the behaviour of the cell when stimulated with KCl or AnTx. The model thus far is a system of seven coupled non-linear ordinary differential equations, a complexity that immediately leads us to a numerical solution. Computations have been performed using the neural simulator GENESIS [10]. We do not seek an analytical solution, however the qualitative features of the model solutions are quite simple.

The behaviour in the absence of any stimulation is particularly simple since the model rests at a steady voltage of -78mV. Small current injections will depolarise the cell and currents of 2pA or more will produce sodium mediated action potentials, as shown in Figure 2.3. This is a very small current to be able to produce such a depolarisation, intracellular currents of the order of 0.1nA being needed to prompt this response in whole neurons [41] [28]. This is due to the small size of the synaptosome being an electric compartment of large resistance meaning that current input has a large effect.

Increasing the extracellular potassium concentration increases the potassium reversal potential, causing a influx of current through the potassium channels. This depolarises the cell which will then settle to a new, steady, resting potential which is typically close to the revised potassium reversal potential. The depolarising dose of KCl is normally big enough to cause an action potential to occur before the cell rests at the new steady state, as in Figure 2.4. The cell does not fire repetitively since the raised potassium reversal potential prevents the cell hyperpolarising sufficiently to de-inactivate the sodium channels. If the synaptosomes have been treated with TTX, we get a simple step in current as shown in Figure 2.5. The experimental results [94] have shown that KCl-evoked release is independent of TTX, so from a release point of view these pictures are equivalent.

Stimulating the model with typical concentrations of AnTx does not create the instant re-

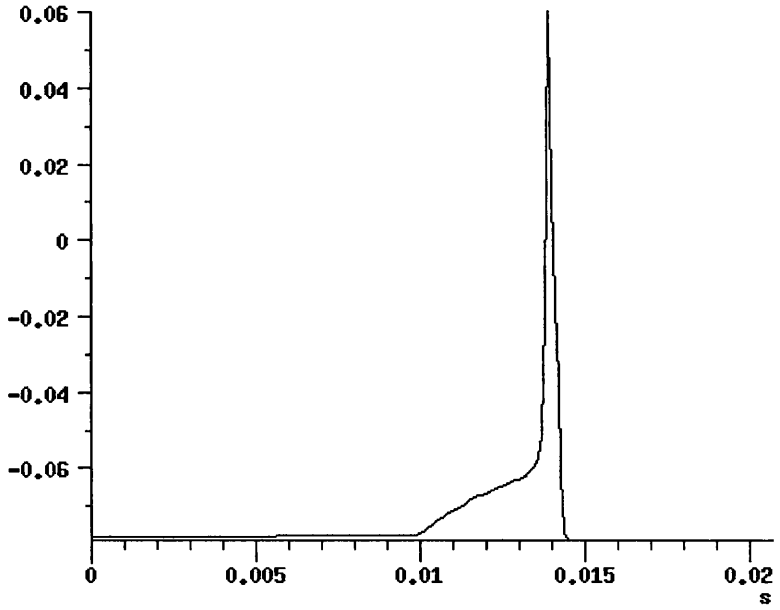

Figure 2.3: Plot of membrane potential in milli-volts against time in seconds for the simulation subject to an injection pulse of 2 picoamps applied at 0.01 seconds. This small current depolarises the cell past spike threshold, producing an action potential.

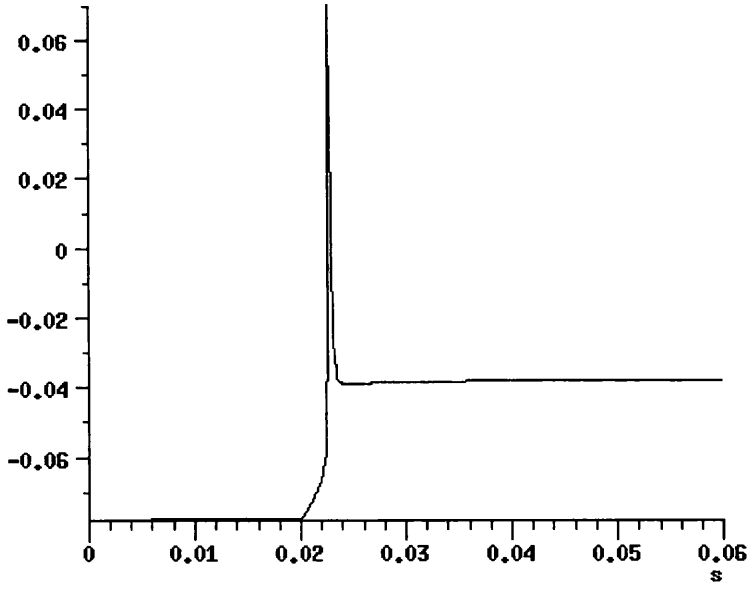

Figure 2.4: Plot of membrane potential in milli-volts against time in seconds for the simulation when the extracellular potassium concentration is stepped to 25mM at 0.02 seconds. The trace clearly shows the transient action potential and depolarized steady voltage typical of this form of stimulation [67].

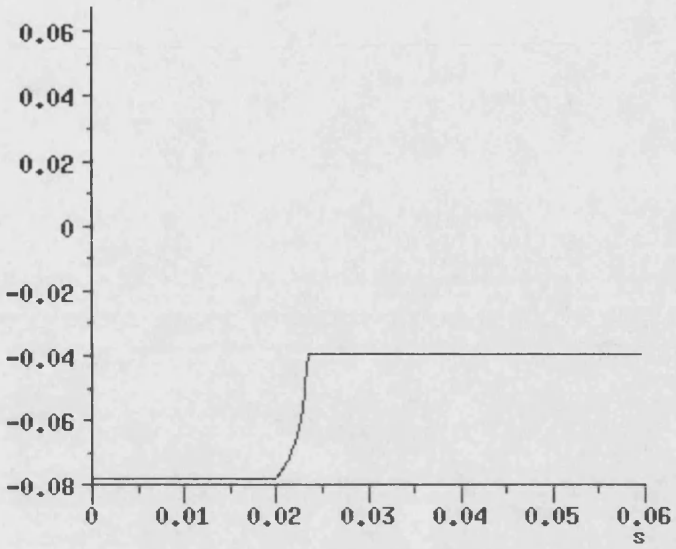

Figure 2.5: Plot of membrane potential in milli-volts against time in seconds for the simulation when the extracellular potassium concentration is stepped to 25mM at 0.02 seconds and the cell has also been treated with TTX. The trace shows the step change in membrane potential typical of this form of stimulation [67].

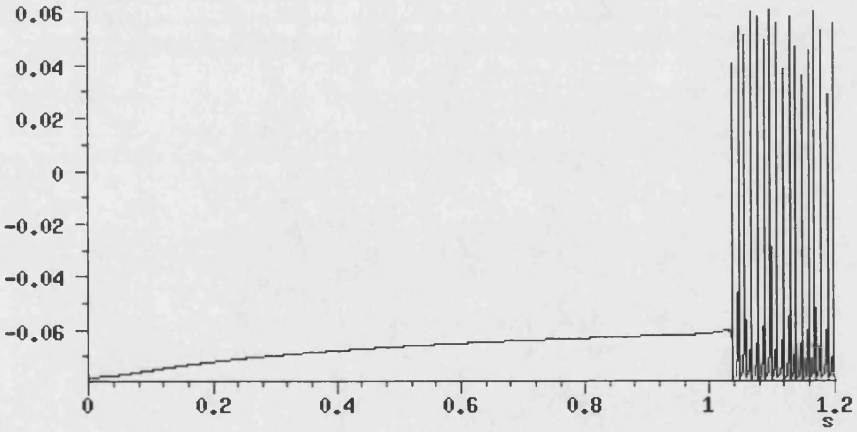

Figure 2.6: Plot of membrane potential in milli-volts against time in seconds for the simulation when 1μM AnTx is introduced at 0 seconds for the 1.2 seconds of this frame. The membrane potential rises slowly as the nAChR are activated, eventually causing repetitive firing.

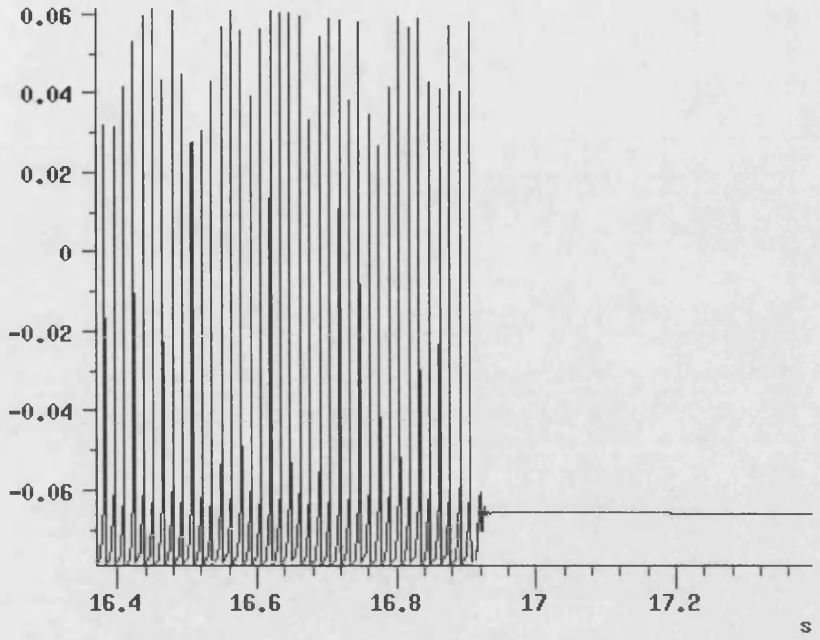

Figure 2.7: Plot of membrane potential in milli-volts against time in seconds for the simulation for the same cell as in Figure 2.6. The AnTx concentration is set to zero at 1.2 seconds, but the current takes a further 15.5 seconds to decay away sufficiently to stop the firing.

sponse that current injection or elevated potassium does since the nAChR require about a second to build up a level of activation, as may be seen in Figure 2.6. This illustrates also that the depolarisations achievable by some of the larger concentrations (here we have used 1μM) are capable of generating the repetitive firing of action potentials. Since the potassium reversal potential has not been shifted the depolarisation-activated potassium channels enable the de-inactivation of the sodium channels allowing them to fire again. Given that the nAChR are slow to activate, they are even slower to release the AnTx and de-activate when we reduce the concentration to 0mM. We remove the AnTx from the same cell in Figure 2.6 at 1.2 seconds and the cell is still firing some 15.5 seconds (Figure 2.7)later until the nAChR-mediated current has eventually decayed enough to stop it.

This 'off' time for the nicotinic current and repetitive firing is surprisingly long. This may simply be the result of the large membrane resistance allowing the small currents to still be effective since we would expect the (effective, or measurable) current from a receptor, such as fast nAChR, to decay quickly (< 1 second) after the removal of an efficacious agonist.

A striking feature of the repetitive firing that has been induced is the phenomenal firing rate of nearly 100Hz that is achieved, with typical nigrostriatal dopamine neurons firing at little over 9Hz, even in the presence of nicotine [28][33]. The small size of the cell means that is has a small electrical resistance and capacitance, giving it a small time constant. We would

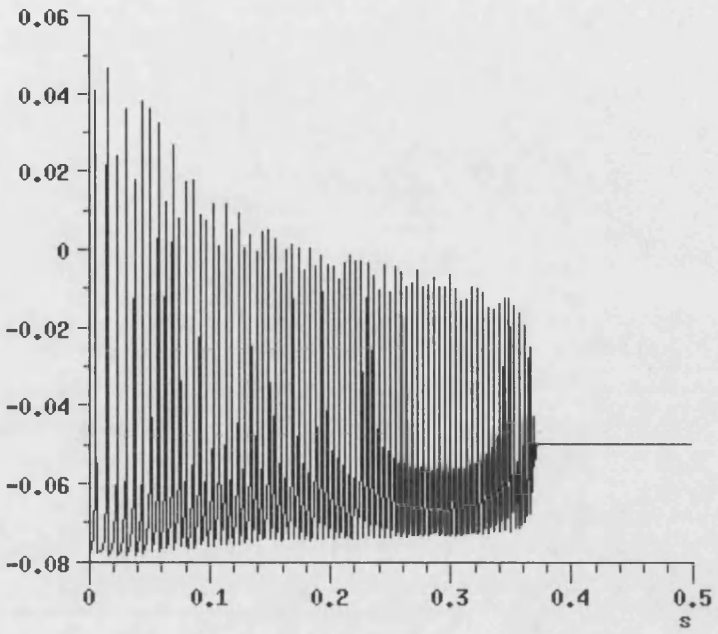

Figure 2.8: Plot of membrane potential in milli-volts against time in seconds for the simulation when 0.1mM AnTx is introduced at 0 seconds. The membrane potential rises quickly with such a high concentration of AnTx activating the nAChR. This depolarising current causes repetitive firing before it becomes to strong to allow the cell to hyperpolarise and de-inactivate the sodium channels between spikes.

expect that the extra capacitance of the whole cell membrane, the leakage of current through the axon and other potassium currents located elsewhere in the cell would slow this rate in the complete cell.

Receptor desensitisation is slower than the 'off' time of the current and therefore is not significant for the length of time we shall be required to apply AnTx for. So, within the range of the model, doses of around 1μM and above will cause the repetitive firing of action potentials for the entire length of time they are applied *plus* the further 15 seconds for the AnTx to wash out and the current to decay. Not all high concentrations do cause this though, concentrations of about 0.1mM and above produce nAChR mediated currents so large that they do not allow sufficient hyperpolarisation of the model cell after an action potential. This causes the firing to stall as the sodium channels remain inactivated in a similar way to elevated KCl, this process is illustrated in Figure 2.8 for a dose of 0.1mM. One can see the progressive inactivation of the sodium channels reducing the amplitude of the action potentials.

We may already be able to explain why stimulation with sub-maximal concentrations of KCl and AnTx are not additive. It seems that the two stimulants will prompt release in different ways; KCl producing a single step depolarisation and nicotinic agonists producing

repeated action potentials. The elevated potassium prevents action potentials by the progress inactivation of the sodium channels and so the AnTx will have little effect.

This covers the essential dynamics of the membrane potential with respect to chemical and electrical stimulation. KCl stimulation causes a step change in voltage to close to the revised potassium reversal potential, possibly with a transient action potential. AnTx causes a build up of depolarising current that can build up to cause the repetitive firing of action potentials.

2.4 Modelling the Transmitter Release

2.4.1 The Calcium Hypothesis of Transmitter Release

Given that the membrane potential dynamics have now been fixed we now present our model of transmitter release. Neurotransmitter is released slowly in small amounts by terminals all the time. The synaptosomes do this and this transmitter release is likely to make up a significant part of the baseline observed from synaptosomes superfused by a buffer without any stimulation from KCl or AnTx (the remainder is considered to be release from such things as damaged synaptosomes [79]). This baseline of release is subtracted from the results for when stimulatory pulses are applied and so does not feature in the experimental results.

We shall be studying that release which is calcium mediated. It has been observed that in such experimental preparations as the study of the neuromuscular junction *in-vitro* the omission of calcium from the bathing medium (analogous to a calcium-free buffer) blocks the transmission of the signal [19]. Supporting the role of calcium as a messenger rather than its influx acting as a depolarising current was the observation that the presynaptic cell's membrane potential was not changed by this omission. This also supports the exclusion of the calcium channels in our model from our calculations of membrane potential. A key observation was that the post-synaptic membrane potential, and hence the amount of neurotransmitter release, was proportional to the fourth power of the extracellular calcium concentration.

This has lead to the so-called calcium hypothesis of transmitter release, where the influx of calcium ions through voltage-sensitive calcium channels (such as the N- and P-types featured in our model) interacts with a putative release mechanism. This mechanism, that has not as yet been fully characterised, prompts the fusion of a vesicle with the cell membrane emptying its contents of transmitter into the synaptic cleft, known as exocytosis [45].

Once the calcium channels have opened there is a short (<1ms) gap before the transmitter is released[9], indicating that the site of interaction with the release mechanism is very close

to the cytoplasmic end of the channel. This supports the notion that calcium influx through the nAChR ion channel does not cause transmitter release directly. It also gives us a feature to study around which we build our model of transmitter release.

2.4.2 The Internal Calcium Concentration due to an Open Channel

Assuming that the release mechanism is close to the cytoplasmic end of the calcium channel we will regard transmitter release to be a function of (amongst other things) the concentration of calcium that is obtained at the end of such a channel when it opens.

In the model calcium flows in under a voltage potential difference V_{grad} given by:

$$V_{\text{grad}} = (E_{\text{Ca}} - V_m), \tag{2.43}$$

where

$$E_{\text{Ca}} = \frac{RT}{F\nu} \ln\left(\frac{[\text{Ca}]_{\text{o}}}{[\text{Ca}]_{\text{i}}}\right) \tag{2.44}$$

is the reversal potential for calcium as detailed in section 2.3.2, V_m is the membrane potential. Influx will continue until this gradient is reduced to zero. As we have regarded the terminal to be isopotential there are no local changes in membrane potential and so V_m is not altered. Instead the calcium influx will serve to increase the internal calcium concentration local to the channel end until it solves $V_{\text{grad}} = 0$, that is

$$[\text{Ca}]_{\text{i}} = c([\text{Ca}]_{\text{o}}, V_m) := [\text{Ca}]_{\text{o}} \exp\left(-\frac{V_m F\nu}{RT}\right) = [\text{Ca}]_{\text{o}} \exp\left(-80V_m\right) \tag{2.45}$$

where $[\text{Ca}]_{\text{o}}$ is the extracellular concentration of calcium.

2.4.3 Transmitter Release due to Change of Membrane Potential

We will be separating our model of transmitter release into two parts; one will be a simple model designed to reflect the calcium-dependent release of transmitter while the cell is resting at a steady membrane potential and will be described later; the other, which we describe now, is a more complicated design to take account of the release during fluctuations in membrane potential. The motivation for this comes from superfusion experimental set-ups with subsecond time resolution demonstrating that the majority of KCl-induced transmitter release occurs directly after the application of the stimulation [100]. This suggests that it is a step in membrane potential that causes the large amount of release rather than a prolonged,

steady release. This does make sense considering that release is normally prompted by action potential induced spikes in the membrane potential of the terminal.

We therefore make the following assumptions about our model,

1. The change in membrane potential causes the simultaneous opening of many channels around vesicle release sites, thus providing sufficient influx to cause significantly large amounts of transmitter release. This is the essential difference between this and the model for steady membrane potential release where we assume that the disparate opening leads to less release.

2. There is a delay between the change in potential and the opening of the channels, which we take to be the average time to open for a single channel. For a channel modelled using the formulation of Hodgkin and Huxley [41] with time constant of activation τ, the average time to open is $\ln(2)\tau$. This gives times to open for N- and P-type channels of about 0.7ms and 0.8ms respectively, which are consistent with experimentally observed delays between membrane depolarisation and calcium influx [9].

   As a consequence of this, should the depolarising influence behind a channel opening be removed before this delay has lapsed then we deem that the channel does not open. Hence for the depolarisation to be effective it must last for the period of the time lag.

   The motivation for this lag is the result that the application of the voltage-activated sodium channel antagonist TTX does not affect release evoked by 20mM KCl[94]. We hypothesise that this is because the action potential depolarisation is over too quickly to open significantly more calcium channels than will be opened without action potential (KCl dose with TTX). Hence the only part of the action potential depolarisation that is effective in terms of transmitter release is that which is maintained for the prescribed time lag and that, in these cases, this is little more than will be opened by the elevated potassium level without any sodium channel activation.

3. That channel inactivation is negligible for N-type calcium channels, since we are normally depolarising from largely negative potentials near rest where inactivation is small. We further assume that the rate of depolarisation to be fast in comparison to channel inactivation rate. This is valid since the time constant of N-type calcium channel inactivation is 150ms and the steps in membrane potential occur on the order of single milli-seconds. P-type calcium channels do not inactivate.

4. There is a finite pool of transmitter available for release. This pool is replenished at a constant rate, however we will show that this rate is slow in the sense that repetitive firing of action potentials cannot be supported for more than a few seconds. This is consistent with experimental observations [31] [94] and may be explained by the use of nomifensine in the superfusion experiments to disable the reuptake and recycling of transmitter by transporter. This is the fastest means of recycling transmitter and so the pool replenishment will slow.

5. We then assume that release is proportional to the number of channels that are opened by the depolarisation multiplied by (some power of) the internal calcium concentration achieved, provided of course that sufficient transmitter is available.

The proportion of the calcium channels that are open for a membrane potential $V(t)$ is given by the activation curve $x_\infty(V(t))$ (for N-type channels, we use the notation $p_\infty(V(t))$ for P-type channels). Hence the change in open channels for a small change in voltage is given by $\frac{d}{dV}x_\infty(V(t))$. We then have the expected release rate $\frac{dR}{dt}(t)$ from a terminal with channels that have a time lag of T to be:

$$\frac{dR}{dt}(t) = \begin{cases} 0 & \text{if } V_m(t-T) > \\ & \inf\{V_m(\tau) : t-T < \tau < t\}, \\ K\frac{d}{dt}V(t-T)\frac{d}{dV}x_\infty(V_m(t-T))c([\mathrm{Ca}]_o, V_m(t))^n & \text{otherwise.} \end{cases} \tag{2.46}$$

where n is the dependency of release on internal calcium concentration, which is to be determined by fitting the model to the experimental data. K is a suitable scaling constant chosen as to give the results in cpm for the entire experimental preparation (our modelled results of release are then the weighted sums of all the various types of terminal that we define). Note that the index to the number of channels opened is evaluated at time $(t-T)$, although the current would then flow under the voltage gradient at time t.

2.4.4 Steady-state Transmitter Release

We present a very simple model of this form of release and assume that is proportional to the number of open channels multiplied by (some power of) the internal calcium concentration achieved due to an open channel. Since we are dealing with the steady state we include the inactivation of the N-type calcium channels. We use the same power dependence on

intracellular calcium as for the transmitter release from a membrane depolarisation. Then for calcium influx through N-type channels

$$\frac{dR_{\mathrm{Ns}}}{dt}(t) = K_N x_\infty(V_m) y_\infty(V_m) c([\mathrm{Ca}]_\mathrm{o}, V_m)^n \tag{2.47}$$

where K_N is a constant, x_∞ and y_∞ the voltage dependent activation and inactivation curves for N-type channels and $c([\mathrm{Ca}]_\mathrm{o}, V)$ the internal calcium concentration. For P-type channels

$$\frac{dR_{\mathrm{Ps}}}{dt}(t) = K_P p_\infty(V_m) c([\mathrm{Ca}]_\mathrm{o}, V_m)^n \tag{2.48}$$

where K_P is a constant to be determined by fitting to experimental data and p_∞ is the voltage dependent activation of P-type channels (which have no voltage dependent inactivation). Again the quantitative fitting for this model of release is described in section 2.5.3.

2.4.5 Release from a Single Terminal

The total release from a single type of terminal is therefore the sum of the release due to changing membrane potential and that released at a steady state. If ν represents the amount of transmitter available from this terminal type then the release is given by

$$\frac{d}{dt}R_{\mathrm{term}}(t) = \begin{cases} \frac{dR_{-\mathrm{s}}}{dt}(t) + \frac{dR_{-\mathrm{p}}}{dt}(t) & \text{if } \nu > 0, \\ 0 & \text{if } \nu = 0. \end{cases} \tag{2.49}$$

2.4.6 The Neurotransmitter Pool

We are required to keep account of the amount of readily-releasable transmitter [31]. We assume that this has a fixed limit and rate of replenishment when it is depleted, and that this is the same for each terminal. For each type of terminal let ν be the amount of transmitter available in counts per minute (cpm) and $R_{\mathrm{term}}(t)$ as defined above, then for a constant rate of pool replenishment we have:

$$\frac{d\nu}{dt} = \begin{cases} -\frac{d}{dt}R_{\mathrm{term}}(t) & \text{if } \nu \geq 32000, \\ 533 - \frac{d}{dt}R_{\mathrm{term}}(t) & \text{otherwise.} \end{cases} \tag{2.50}$$

The quantitative fitting for this will be described in sections 2.5.3 and 2.5.4.

2.5 Fitting and Results

2.5.1 Estimation of Release from a Voltage Clamp

Fitting the model to the KCl-evoked release data is made easier by an approximation to the release evoked. This comes from the observation that applying elevated potassium with TTX

to block the sodium channels results in slow rise in potential from rest to close to the new potassium reversal potential, like the cell has been subject to a experimental voltage clamp.

Since this clamp produces a sustained depolarisation all the calcium channels will have sufficient time to open. Moreover, since the rate of depolarisation is slow in comparison to the time lag T, $V(t-T) \approx V(t)$ and we may dispense with the time lag altogether.

Hence, the total release R for such a clamp from v_1 to v_2 is given by

$$R = K \int_{v_1}^{v_2} \frac{d}{dV} x(V(t)) c([\mathrm{Ca}]_o, V(t))^n dV \tag{2.51}$$

where $x(V)$ is the activation curve of the appropriate calcium channel. A change of variables to x, where $x(V)$ is given by

$$x(V) = \frac{1}{1 + \exp\left(-\frac{V - V_h}{s}\right)} \tag{2.52}$$

for some constants V_h and s, yields

$$\begin{aligned} R &= K[\mathrm{Ca}]_o{}^n \int_{x(v_1)}^{x(v_2)} \exp\left(-80n\left(-V_h - s\ln\left(\frac{1}{x} - 1\right)\right)\right) dx \\ &= K[\mathrm{Ca}]_o{}^n \exp\left(80nV_h\right) \int_{x(v_1)}^{x(v_2)} \left(\frac{1}{x} - 1\right)^{80sn} dx. \end{aligned} \tag{2.53}$$

We are interested in elevated potassium doses of less than 35mM for the fitting which implies that the potassium reversal potential is never greater than -30mV. Up to this value we note that for both types of calcium channel the activation variable x is small and so

$$R \approx K[\mathrm{Ca}]_o{}^n \exp\left(80nV_h\right) \int_{x(v_1)}^{x(v_2)} \left(\frac{1}{x}\right)^{80sn} dx \tag{2.54}$$

$$\approx K[\mathrm{Ca}]_o{}^n \exp\left(80nV_h\right) \left[\frac{x^{(1-80sn)}}{(1-80sn)}\right]_{x(v_1)}^{x(v_2)} \tag{2.55}$$

from which we may then estimate the release.

2.5.2 Heterogeneity of Terminals

We expect there to be many types of terminal in the conglomerate of synaptosomes and that we have deduced the existence of three major sub-types. These follow from fitting the model to the experimental observations [94] [95] [31] and principally concern the distribution of the different calcium channels and the abundance of nicotinic receptors. While we shall be endowing all terminals with the same electrical properties and conductance of potassium

and sodium channels we shall only be allowing one type (N or P) of calcium channel on a terminal and furthermore that only some subset of those with N-types also have nAChR.

This is because the pharmacological blocking of N- and P-type channels has an approximately equal and additive effect on KCl-evoked release (at two different concentrations of KCl, 15 and 25mM). This implies that each set of channels activates discrete release mechanisms, but this is itself not a problem since these are supposed to be close to the cytoplasmic end of the channels. However AnTx-evokes release through N-type channels only, a result that is largely consistent with the co-existence of nAChR with N-types but not P-types. It is therefore simpler to assume that each terminal only has one type of calcium channel and that nAChR are only to be found co-existing with N-type channels.

2.5.3 Fitting to the KCl release data

The equal and additive inhibition of KCl-evoked release by N- and P-type blockers suggests that the release profiles are similar for the two types of channel; if they were different we would expect the blockers to have different efficacies at the two concentrations. We therefore assume that the release profile is identical for N- and P-types and so we can fit each independently.

The fitting is very simple, we calculate the expected release to a voltage clamp (equation (2.55) corresponding to a rest of $v_1 = -78\text{mV}$ and $v_2 = E_K$, the revised potassium reversal potential, for the two non-maximal doses of 15 and 25mM and set them equal to the observed release. Dividing one by the other removes the scaling constant K and we then solve for the power dependence of calcium concentration n. Because of the supposed correlation between n and the number of interaction sites needed for release [63] we will round n to the nearest integer. We obtain $n = 2$ for N-type calcium channels mediated release and $n = 4$ for P-type mediated. We note that these are typical values for n obtained experimentally for the cerebellum [63].

We impose this n on the model for steady state release. Summing the steady state and changing potential release for both concentrations then yields two simultaneous equations for the two unknown scaling constants, whose values we then obtain and are given in equations

Condition	[^{3}H]dopamine release (cpm)	
	Theoretical	Experimental Data from [94]
Control (25mM KCl)	18214	15558 ± 1247
25mM KCl + Low Na (10mM)	16281	25780 ± 607
25mM KCl + Ca-free	0	856 ± 31
Control (20mM KCl)	11532	7449 ± 1534
20mM KCl+1.5μM TTX	10398	7821 ± 156

Table 2.2: The effects of different buffer conditions on [^{3}H]dopamine release evoked by KCl, comparison between the experimental results [94] and those predicted by the model.

(2.56)-(2.61) below. For N-type mediated release

$$\frac{dR_{\mathrm{Np}}}{dt}(t)=\begin{cases} 0 & \text{if } V_m(t-T_N) > \\ & \inf\{V_m(\tau) : t-T_N < \tau < t\}, \\ 2.16\times 10^5 \frac{d}{dV}x_\infty(V_m(t-T_N))c([\mathrm{Ca}]_\mathrm{o}, V_m(t))^2 & \text{otherwise.} \end{cases} \tag{2.56}$$

$$T_N = 0.7 \tag{2.57}$$

and for P-type calcium channel mediated release

$$\frac{dR_{\mathrm{Pp}}}{dt}(t) = \begin{cases} 0 & \text{if } V_m(t-T_P) > \\ & \inf\{V_m(\tau) : t-T_P < \tau < t\}, \\ 7650 \frac{d}{dV}p_\infty(V_m(t-T_P))c([\mathrm{Ca}]_\mathrm{o}, V_m(t))^4 & \text{otherwise.} \end{cases} \tag{2.58}$$

$$T_P = 0.8 \tag{2.59}$$

And for steady state release; for N-type calcium channels we have

$$\frac{dR_{\mathrm{Ns}}}{dt}(t) = 101\, x_\infty(V_m)y_\infty(V_m)c([\mathrm{Ca}]_\mathrm{o}, V_m)^2 \tag{2.60}$$

and for P-type calcium channels

$$\frac{dR_{\mathrm{Ps}}}{dt}(t) = 0.5\, p_\infty(V_m)c([\mathrm{Ca}]_\mathrm{o}, V_m)^4. \tag{2.61}$$

A match to the maximum release is obtained by setting the upper limit of readily-releasable transmitter to be the maximum observed release, rounded to a convenient 32000cpm. Assuming the equal contributions of N- and P-types we may reproduce the KCl-evoked release

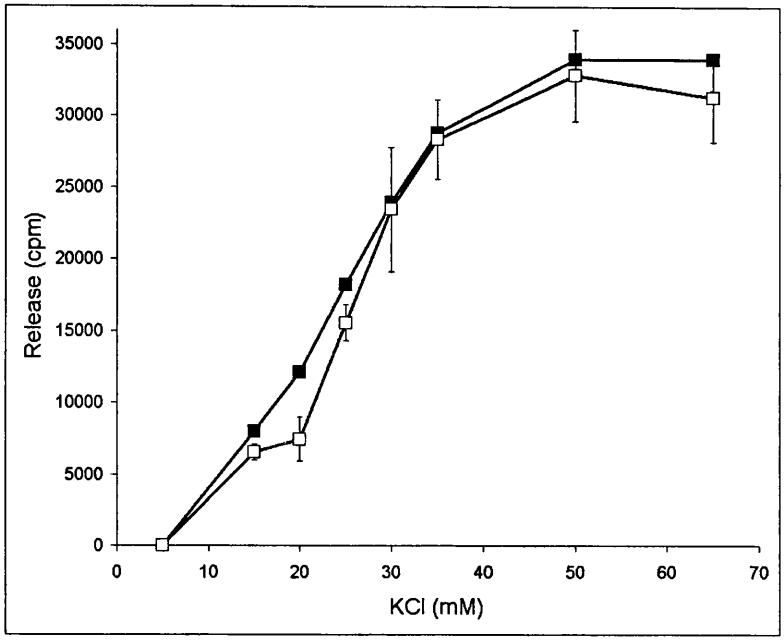

Figure 2.9: Dose-dependent KCl-evoked release of [^{3}H]dopamine from striatal synaptosomes: comparison of experimental (□) and the model (■) results. Experimental data points are taken from Soliakov et al [94], it is clear that a good fit is achieved.

profile and compare it to the experimental data [94] in Figure 2.9. The fit can be seen to be very good, but then it is the data we have specifically fitted to, with the slight over-estimation of the model largely due to numerical rounding of the scaling constants. The 'kink' in the experimental curve at 20mM KCl may as well be experimental error than error in our fit. The majority (approximately 90%) of the release is caused by the depolarisation as required.

Table 2.2 also shows the release figures for the model and the experimental results for the differing buffer conditions. We find a fault with regard to the buffer having a reduced concentration of sodium, with our model registering a slight decrease in release due to a weaker sodium current causing slightly less depolarisation, in contrast to the large increase observed experimentally.

Release for a calcium-free buffer is abolished, the trace level of extracellular calcium we used failing to register any significant release. We can also see that our model is largely independent of TTX when stimulated with KCl. The reason is simply that the most depolarised part of the action potential is ignored by the time-lag we built into the model.

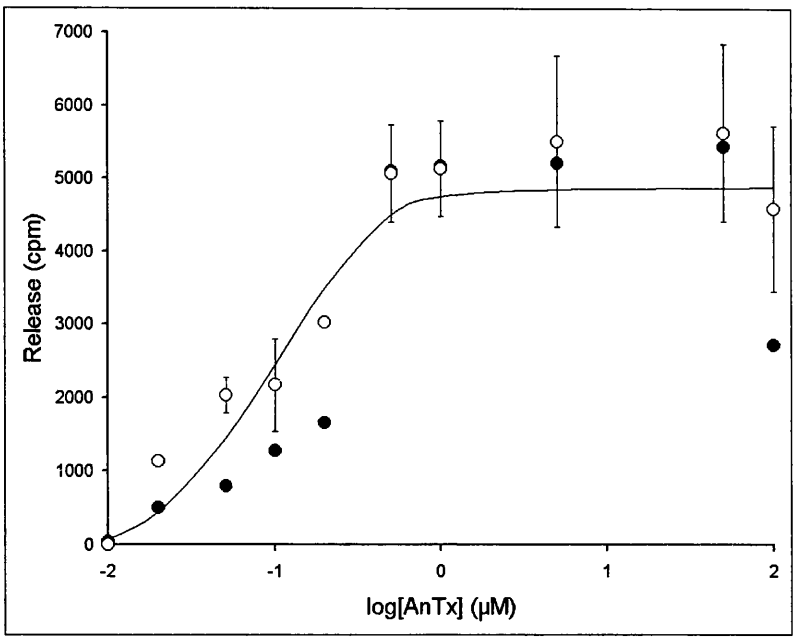

Figure 2.10: Dose-dependent AnTx-evoked release of [^{3}H]dopamine from striatal synaptosomes: comparison of experimental (○) and the model (●) results. Experimental data points and fitted curve are taken from Soliakov et al [94]. The model predicts the release for the higher concentrations well, but underestimates release for the lower doses where the nicotinic current does not causes action potential firing.

2.5.4 Fitting to the AnTx release data

We now regard the parameter values derived in the previous section as fixed and then study the effect of AnTx stimulation on the model. What we immediately notice with concentrations of 1μM AnTx, or above, is that the repetitive action potentials soon releases all of the readily-releasable transmitter. For a 40 second pulse of AnTx, as used experimentally [94], the model cell fires action potentials for a total of 55 seconds due to the slow 'off' time of the nAChR (section 2.3.10). Given that the pool replenishment is slow, the model cell will be releasing transmitter as soon as it is replaced. Hence the AnTx-evoked release is limited at such high doses by this rate of replenishment rather than the amplitude of membrane depolarisation.

We need to estimate the rate of readily-releasable transmitter replacement, for which we refer to the superfusion work of Grady et al [31] on mouse synaptosomes. Although this data does come from the mouse, we will assume that the same rate applies to our modelling.

Grady et al stimulated mouse synaptosomes with nicotine for periods of twenty minutes or more and collected fractions every minute to analyse for labelled dopamine content. Our model would suggest that the cell would still be firing action potentials at a pool-exhausting

Condition	[^{3}H]dopamine release (cpm)	
	Theoretical	Experimental Data from [94]
Control (1μM AnTx)	5165	5134 ± 654
1μM AnTx + 1.5μM TTX	1881	4213 ± 490
1μM AnTx + Low Na (10mM)	680	523 ± 93
1μM AnTx + Ca^{2+}-free	0	444 ± 199
Control (15mM KCl)	8080	6536 ± 568
15mM KCl + 1μM AnTx	8176	9273 ± 2068

Table 2.3: The effects of differing buffer conditions on [^{3}H]dopamine release evoked by AnTx, comparison between the experimental results [94] and those predicted by the model.

rate for the first few of these collected fractions. The first fraction would therefore represent the entire contents of the pool, assuming it was full to start with, and the amount replaced during one minute, assuming that the firing starts soon after the start of the fraction. The release in the second therefore is the amount replaced in one minute. This is approximately half the amount of release found in the first fraction, indicating that the entire pool is being refilled in about one minute. This corresponds to a replenishment rate of $32000/60 = 533$cpm per second in our model, we are assuming it is a constant rate.

Imposing this rate of replenishment in our model we may estimate the release from a terminal endowed with nAChR for a 40 second pulse of 1.5 μM AnTx. This is over twice the pool limit of a terminal and to fit to the experimental data we are therefore required to assume that only 8% of the population of synaptosomes have nAChR. This fitting to the experimental data has given us a methodology for estimating this proportion of terminals bearing nAChR.

We may now plot the modelled release of [H^3]dopamine release against the experimentally observed release for the various applied concentrations, this plot may be seen in Figure 2.10. The fit for the higher concentrations is very good, since we have fitted this release to the proportion of terminals. There is a consistent underestimation of the release for the lower concentrations of AnTx, and for AnTx with TTX (Table 2.3). However the model does predict the down turn in release for very large (0.1mM) concentrations of AnTx where the strong nAChR-mediated current soon inactivates the sodium channels. The lack of additivity is also reflected in the model of release, as is the calcium dependence of AnTx-evoked release.

2.5.5 The Combined Release

The release for the total preparation is the weighted sum of the release from the three types of terminal that we shall now define. Type 1 are those terminals with P-type calcium channels that we take to make up 50% of the synaptosome population; Type 2 terminals have N-type calcium channels and are 42% of the population; Type 3 terminals have N-type calcium channels and nAChR. Note that then there is a 50:50 split of N-type and P-type calcium channel bearing terminals. The total release is then simply given by

$$R_{\text{Total}}(t) = 0.5 \times R_1(t) + 0.42 \times R_2(t) + 0.08 \times R_3(t). \tag{2.62}$$

2.6 Review

We have derived a model that aims to represent the behaviour of rat striatal synaptosomes with respect to the evoked release of [^{3}H]dopamine in superfusion experiments [31] [94] [95]. This model fits much of the quantitative data well, with few qualitative faults, but the implications of the model and the nature of some of the modelling is worth discussion.

2.6.1 The Membrane Potential Dynamics

We have approached the modelling from the view of a single terminal subject to the buffer conditions found in synaptosome experiments. This causes us to study the electrical properties of the cell, with particular reference to the complement of ion channels present.

The inclusion of potassium and sodium channels are simple deductions from the effectiveness of elevated extracellular potassium and TTX on the cell, respectively [94]. Since the calcium channels present have an insignificant effect on membrane potential it is these two channels that decide how the model cell will behave, which is very typical for such a set up with depolarising current triggering action potentials. Although we think the choice of ion channel kinetics (from the rat hippocampus [88] [89] [98]) to be fair, the ability of small currents to produce the rapid firing of action potentials is concerning. This follows as a direct result of the high resistance and low capacitance of the cell from its small size, so this behaviour is to be expected. However these electrical properties would be expected to be significantly different in the intact cell; firing rates would be slower and it is likely that larger currents would be needed to evoke them. So while we can be confident that the behaviour of our

model cell is a good representation of the experimental behaviour, the results will not be directly applicable (quantitatively) to the intact whole-brain cell.

2.6.2 The Model of Transmitter Release

Firstly we have split release into two forms; steady state, where there is a general leakage of transmitter whilst the cell is at rest; and for a changing membrane potential. We consider that they are due to very slightly different mechanisms; whereas release is normally prompted by the coordinated opening of many calcium channels, the disparate flickering open and closed of channels whilst the cell is resting would also be capable of causing release, if somewhat less potently. It would therefore seem sensible to separate these ideas into two models.

Once we have done this, modelling release to be proportional to some power of the internal calcium concentration (a measure of the probability of calcium influx causing release from a site) and the number of open channels (number of sites) is sensible. We must consider is whether we are justified in including the time-lag which effectively ignores part of the action potential. We have used the average time to open for such channels, although some will open faster, some will of course open slower and so this seems to be the obvious value to take, moreover such a delay is consistent with experimentally observed delays [9]. A question that we may be prompted to ask is, why generate such an action potential if much of it is to be ignored? However we can hypothesise that the slower membrane time constant of the intact cell would produce wider action potentials that may negate the effect of this delay.

2.6.3 The Fit to the KCl-evoked Release Data

Fitting the model to KCl-evoked release data has required us to assume that release mediated by P-type calcium channels is proportional to the fourth power of intracellular calcium, whereas for N-type channel mediated release we have assumed a second power dependence. While the fourth power dependence is often quoted [19], different values for different calcium channels have also been reported in other preparations [63], here a fourth power dependence on N-type mediated release and a second to third power on P-types was reported.

It is hypothesized that the dependency on extracellular calcium reflected the number of sites for calcium binding needed to trigger release [63]. However this aspect is not present in the model, which only considers the concentration of calcium arising from the proportion of open channels. Indeed we can see where this power dependence arises in our model from

our approximation of release from a voltage clamp, equation 2.55. The relevant term is the product sn, s is the term that describes the slope of the transition from zero to full activation in the activation curves x_∞ and p_∞, appropriately this parameter is about twice the size for x_∞ as it is for p_∞. Hence these parameters ensure that release always depends on the same power (approximately 1/6) of the proportion of channels opened. Such similarities are expected when for a fixed concentration of calcium our estimate of release is purely a function of membrane potential and we are effectively fitting to the same voltage-release curve.

In our analysis, the n-th power of extracellular calcium appears as a scaling constant and so cancels in the quantitative fitting of the model. This means we cannot tell whether this dependence is actually correct with the experimental data we have. This dependence could be found experimentally by using superfusion buffers with a selective calcium channel blocker, two different concentrations of calcium and a depolarising source such as 25mM KCl.

This asks what does this mean for our model if we observe different dependencies experimentally? Our model is based on reasonable hypotheses on the dependence of release on the number of opened calcium channels and the internal calcium concentration and then gives sensible values for the dependencies. It is very difficult to predict on biological grounds why such differences in dependence on extracellular calcium could arise from the channel kinetics.

However the calcium channels are classified by their pharmacologies and it is therefore possible that the channels present in the synaptosomes may have slightly different kinetics (different s's) than those used in the model. Calcium channel parameters were taken from a human N-type channel expressed in HEK293 cells and claimed to resemble a presynaptic channel [61] and P-type channels in a rat motor-neuron [101]. Channel parameters from other preparations may yield different dependencies if used in the model, but we consider the channels chosen [61] [101] provide the most representative data available for nerve terminals.

The fits do match the experimental results well, as we should expect them to. Moreover our model does have the TTX independence of KCl-evoked release, simply by our use of the time lag whilst the calcium channels open. In fact the model has only one qualitative anomaly as KCl-evoked release is concerned; namely that it predicts little change in release for a concentration of 25mM KCl under conditions of low extracellular NaCl (10mM), when a large increase was reported [94]. Experimentally NaCl was replaced by N-methyl-D-glucamine (NMDG) to maintain the osmolarity, whereas the model only takes account of changes in the principal ions. NMDG has been shown to render the resting membrane potential of synaptosomes more negative [40], in which case depolarisation close to the potassium reversal

potential (achieved by the application of 25mM KCl) would represent a larger depolarisation and hence be expected to open more calcium channels than from the normal resting potential. This would then cause more transmitter release and so explain the experimental observation.

2.6.4 Heterogeneity of the Terminals

The distinction of three major sub-types of nerve terminal is the logical conclusion from the transmitter release data for synaptosomes stimulated in conjunction with various calcium channel blockers [95]. The blocking of N- and P-type calcium channels causing the equal and additive block of KCl-evoked release is consistent with there being distinct populations of terminals with exclusively N- or P-type channels and that there are roughly equal numbers of each. As AnTx-evoked release is significantly affected by N-type channel blockers only we deduce that nAChR only co-exist with N-type calcium channels in this preparation.

2.6.5 The Fit to the AnTx-evoked Release Data

Our fitting to the AnTx-evoked release data [94] [31] has enabled us to estimate the proportion of synaptosomes that bear nicotinic receptors. This estimate is derived from experimental studies of mouse synaptosomes under chronic exposure to nicotine. This assumes that the nicotine and anatoxin-a data is comparable and in our model we find that, for the higher concentrations of stimulating dose, release is largely dependent on whether or not the cell is firing action potentials and not so on specific dose and receptor activation times. We can be less sure how well data from the mouse can be applied directly to the rat, but we assume that the rate derived is comparable.

The figure of 8% so derived provides a good fit for the higher concentrations of anatoxin-a applied and the model has followed the down turn in release for doses of 0.1mM which we suppose is due to the inactivation of the sodium channels. The fit for the lower concentrations is not as good; we consistently underestimate release for these (values which do not produce action potentials) and for AnTx+TTX.

This suggests that we have too much emphasis on the ability of the AnTx to produce action potentials and our fit could be better if we had fewer sodium channels and more nAChR. However we have found that this is not the case since the difference in release for spike producing and non-spike producing concentrations is too great to be due to simple conditions such as nAChR conductance. The same result applies to the state transition rates (equations (2.35)-(2.38)) so is not a problem with the model of a nicotinic receptor that we have chosen.

Instead we consider that a better fit can be found if we assume a further type of terminal. This would have a different sub-type nAChR for which stimulation with AnTx does not activate sodium channels (either due to the numbers of receptors or agonist efficacy, or indeed the absence of sodium channels). Since this form of release would saturate at lower concentrations of agonist we would expect this sub-type of receptor to then have a higher affinity to AnTx than the sub-type we have used. Indeed the heterogeneity of nAChR in the synaptosome population has already been established [104] [44] [53].

Regarding the experimental data [94] it was originally hypothesised that the lower maximum release elicited by AnTx compared with KCl may be due to low numbers of nAChR uniformly distributed throughout the population, or sufficient receptors to have the same efficacy as KCl in releasing [^{3}H]dopamine but localized to a sub-population of terminals. The modelling suggests an alternative; that nAChR are restricted to a smaller proportion of terminals (8%) from which they are capable of releasing a *greater* amount of [^{3}H]dopamine than KCl acting on the same terminals. Preliminary electron microscopy results by the same laboratory intended to ascertain this abundance of nAChR in the synaptosome population suggest values of around 10% [personal communication from Ian Jones, Department of Biology and Biochemistry, University of Bath]. In particular our modelling has shown that the amount of AnTx-evoked release is largely dependent on the length of time the stimulus is applied for. In some preparations, such as adrenal chromaffin cells [64], AnTx has been shown to be more efficacious in releasing neurotransmitter than KCl and this property would explain why.

2.6.6 Heterogeneity of Nicotinic Receptors

The model assumes a homogeneous population of nAChR. However more recent studies than those on which our modelling was based provide evidence for the heterogeneity of nAChR on dopamine synaptosomes [44] [53]. The $\alpha 3\beta 2$-selective antagonist α-conotoxin MII partially blocks [^{3}H]dopamine release elicited by AnTx [44] or nicotine [53], consistent with the involvement of two or more subtypes of nAChR, one of which has an $\alpha 3\beta 2$ interface.

It is not known from this experimental data whether different nAChR reside on the same terminals or if they are segregated to separate terminals. It is notable that although it is straightforward to extend the model to accommodate these results by including further terminal types with appropriate sub-types of nAChR, any such description would require the different sub-types of nAChR to be segregated to separate terminals. This is because at the higher concentrations of nicotinic agonists used release has been shown to be dependent

on the transmitter availability following the activation of sodium channels. In the case of coexistence, large scale blocking of one sub-type of nAChR would either not effect release significantly as the others would be sufficient to generate action potentials, or release would be largely abolished if action potentials are not generated. Here our model may be a useful tool in discerning the segregation and abundance of these sub-types and terminal types.

2.6.7 Other Nicotinic Agonists

The model has been based on studies using AnTx as an agonist. The estimate of 8% of dopamine terminals having nAChR assumes that all these receptors are fully sensitive to AnTx. Other nicotinic agonists elicit [^{3}H]dopamine release from striatal synaptosomes with varying efficacies [42] [44]. To include these results we require the binding kinetics of the agonist to the receptor sub-type and the ensuing efficacy of the agonist on the ion channel conductance (relative to AnTx). Such parameters could be radically different between agonists and would indeed lead to the different release profiles observed experimentally. Inverting the problem, we may use the release data and the model to estimate these parameters.

2.6.8 Summary

We have produced a sub-cellular and sub-second time resolution mathematical model of the nicotinic stimulation of [^{3}H]dopamine release from striatal synaptosomes that reproduces the experimental data well. It provides sound reasons for some of the experimental observations made, such as the lack of additivity between submaximal concentrations of KCl and AnTx. This arises from the clamped depolarisation achieved with KCl causing the persistent inactivation of sodium channels, whose activation is necessary for significant AnTx-evoked release. The description of elevated KCl-evoked release is quantitatively accurate with the exception of failing to predict an increase in release for low extracellular sodium concentrations, the increase is likely to be caused by the membrane potential shift caused by its replacement in the buffer, NMDG, which we do not take account of.

Where the description from the model is inaccurate, such as for the smaller concentrations of AnTx, we are able to use our model as a qualitative or quantitative tool to provide sound suggestions for what is wrong. It suggests that a better fit could be achieved with at least two types of terminal possessing different sub-types of nAChR. Where it is insufficient, in this heterogeneity of nAChR, the model provides a basis for the subsequent addition and fitting

of these experimental results. The model therefore provides a solid theoretical basis for the description of synaptosome preparations. It also provides a foundation for investigation of more holistic preparations, such as slices.

Chapter 3

Bursting in Mesolimbic Dopamine Neurons

3.1 Chapter Overview

The firing pattern known as bursting found in mesolimbic dopamine neurons has been shown to significantly potentiate the release of transmitter from nerve terminals, a burst consisting of a period of faster firing of action potentials, each (on average) progressively shorter and wider and occurring after an increasing interspike interval. Since nicotine increases the amount of bursting in these cells, which are implicated in the rewarding effects of addictive drugs, the mechanism underlying this firing pattern may be of great importance.

Given the hypothesis, based on extensive experimental results, that a burst is caused by the calcium-dependent inactivation of a potassium channel we build a model of the electrical properties of a dopamine neuron incorporating this mechanism. The cell contains; a fast sodium / calcium channel responsible for the action potential; a GABAergic current from neurons of the substantia-nigra pars reticula; a slow depolarisation that brings the cell from a hyperpolarised state to spike threshold; a slow after-hyperpolarisation current that suppresses action potential firing; and a delayed rectifying potassium channel that repolarises the cell following an action potential, and by our hypothesis partially inactivates in the presence of calcium. We demonstrate that the numerical solution of this model can reproduce the burst firing pattern observed *in-vivo* if we allow an external (glutamatergic) stimulus to cause an action potential, thus raising the calcium levels and inactivating the potassium channel.

A mathematical analysis of a generalisation of this model, that is independent of parameter

choices and the form of the calcium-dependent inactivation, proves that the external stimulus is a necessary component and that in its absence the neuron fires in a rigid pacemaker fashion. We also highlight that bursting may also be caused by the relief of the GABAergic current and so the opiates may promote bursting in a similar way.

3.2 The Mesolimbic Pathway

3.2.1 The Reward Pathway

The mesolimbic dopamine pathway is widely believed to be involved in the reinforcing effects of addictive drugs, which have been shown to potentiate the release of dopamine from these neurons [18][50]. Cocaine has been shown to block the dopamine re-uptake transporter and so increase the concentration of dopamine in the synaptic cleft. Amphetamine has been shown to evoke dopamine release from nerve terminals. Nicotine and the opiates, acting on nicotinic or opioid receptors respectively, have been shown to increase excitatory influences on the mesolimbic neurons, which one would then expect to increase dopamine release.

Our particular interest lies in the effects of nicotine on this pathway. It has already been shown experimentally that challenging mesolimbic dopamine neurons in the rat with doses of nicotine (0.5 mg/kg) causes significant increases in the phenomenon of 'bursting' [33] [70]. This is a firing pattern that can strongly facilitate dopamine release and will be described below. This is of particular relevance for smoking in humans since this increased release of dopamine from mesolimbic neurons may underlie the reinforcing effects of nicotine as an addictive drug. Therefore the mechanism of bursting and how nicotine potentiates this represents an important subject of study.

3.2.2 Firing Patterns

There have been three distinctive firing patterns observed in mesolimbic dopamine neurons. For *in-vitro* preparations, such as slices, the neurons fire in a regular pacemaker pattern [30] only, that is the cell fires identical action potentials at equal intervals in time. The pattern is not changed by the injection of depolarising current injection, this merely increases the firing rate of the cell by increasing the rate of rise of the membrane potential in between spikes. Sufficiently strong hyperpolarising intracellular current injection can cause firing to cease altogether.

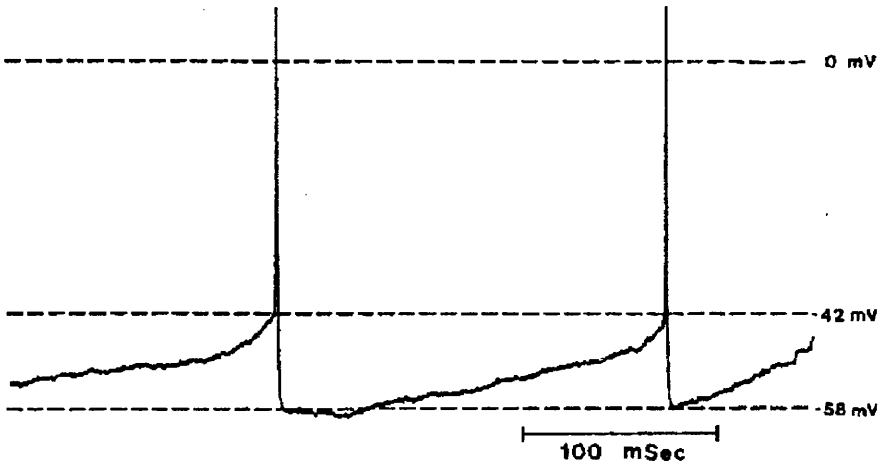

Figure 3.1: Trace from an intracellular recording of a mesolimbic dopamine neuron, reproduced from Grace and Bunney [28]. This neuron was firing in an irregular pattern and so the action potentials can be seen to be identical, in contrast to those in a burst as seen in Figure 3.2.

Instead *in-vivo* we can observe two patterns, which have been termed irregular firing and bursting. The neurons typically fire in the irregular firing pattern, but under excitatory influences the pattern can become interspersed with occasional bursts [27] [33] [35]. The irregular firing pattern is one in which the cell fires action potentials of variable heights and inter-spike intervals. A histogram of these inter-spike intervals for a cell firing in such an irregular pattern has the appearance of a normal distribution.

A burst consists of a period of faster firing of progressively shorter, wider action potentials with longer interspike intervals followed by a long afterhyperpolarisation. A histogram of interspike intervals for bursting cells has a bi- or tri- modal appearance, with the peaks corresponding to the intervals between spikes in a burst, those between spikes during irregular firing and a smaller, less distinct peak for the intervals corresponding to the long afterhyperpolarisation following the end of a burst.

This burst pattern is physiologically relevant; a bursting neuron releases many times more dopamine (measured in terms of DOPAC turnover) than a non-bursting neuron with a similar firing rate [70]. This facilitation in release is probably due to the summation of the action potentials in the nerve terminal [27].

The naming of this facilitatory pattern as bursting was coined by the many experimentalists involved in the study of this firing pattern [27] [35]. It is not to be confused with the firing pattern of cells which alternate between periods of activity and quiet. This is generally

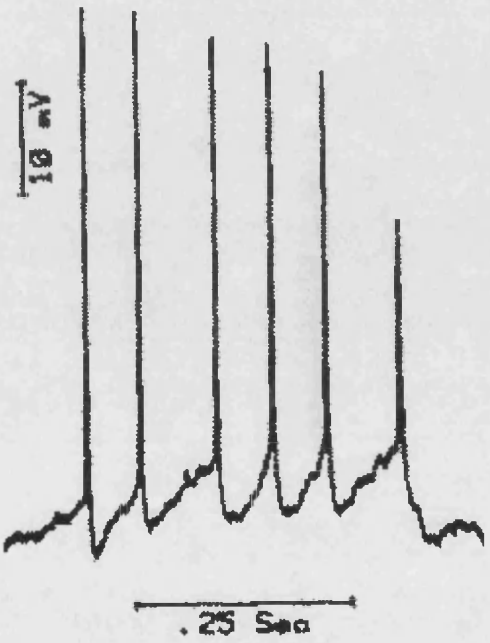

Figure 3.2: Another trace from the intracellular recording of a mesolimbic dopamine neuron, reproduced from Grace and Bunney [27]. In this case the neuron is firing a burst. The faster firing rate and progressive shortening of action potentials are apparent. The tendency for interspike intervals to increase can be seen from the third spike on.

termed 'bursting' and cells of this class are the subject of much study by other mathematical modellers such as Bertram et al [56] and Miura and de Vries [17]. There are many similarities between the two phenomena, as we shall see later on, but they are essentially separate patterns that arise from different actions. Our pattern of interest is indeed never quiet, but varies in the rate of firing and shape of action potentials. Throughout this chapter we shall persist with the term bursting.

3.2.3 Aims of the Model

These are rather simple, by appropriate modelling of mesolimbic dopamine neurons (or otherwise) we wish to find out how nicotine can cause these neurons to fire, or increase their firing, in bursts. This does reduce to two more fundamental questions, the foremost being what cellular mechanisms cause bursting? Then, why is this mechanism potentiated by nicotine?

Modelling provides an ideal platform for the addressing this problem. There have been quite intensive experimental investigations into the phenomenon of bursting in mesolimbic dopamine neurons, which we shall detail below, that also produces a hypothesis on bursting. This splits our modelling into two parts; we shall first build a computer model based on the hypotheses on bursting derived both experimentally and from our own ideas, which will be solved numerically to try and find a burst-like pattern. Analysis of this model will then allow us to make more general conclusions for the mechanisms involved in bursting.

3.2.4 The Experimental Data

We are fortunate in that the bursting of mesolimbic dopamine neurons (in rats) has been extensively studied. Grace and Bunney investigated the burst firing *in-vivo* [27][28]. Additional data, such as the effect of nicotine, comes from Svensson and co-workers [15][33][34]. The neurons and their ion channels have been studied *in-vitro* by Grace and Onn [30].

Bursting was first classified by Grace and Bunney in an *in-vivo* study of the rat brain. A burst was defined to start when the interval between two spikes drops to < 80ms and end when the interval grows to > 160ms. Although this quantitative measure may seem a rather haphazard method of counting bursts it proves to be effective since for a cell firing in what is viewed to be an irregular pattern the average firing rate is rarely higher than 8Hz and bursts tend to finish (with the afterhyperpolarisation) if they do not fire again within 160ms.

It was observed that the two modes of firing; irregular and irregular with bursts; seem to be quite separate. The two modes could be distinguished by the cells' response to 100-200ms pulses of depolarising current (0.5-1.5nA); non-bursting cells showed a typical increase in firing rate of identical spikes with accommodation, whereas those in burst-firing mode consistently responded with a burst. Shorter (25ms) pulses could not elicit bursts in any cells. However it was found that non-bursting cells would become burst firing by the longer term (order of minutes) depolarising current injection of 0.3-0.5nA.

It was discovered that the production of an action potential was caused by the decay of a so-called afterhyperpolarisation current and the rise of a slow depolarisation current. The afterhyperpolarisation current is considered to be a slowly activating calcium-activated potassium channel and hence will become activated by the influx of calcium during an action potential and will suppress further spiking until it decays away. As this current decayed the membrane potential was also caused to rise by a slow influx of sodium and calcium which activates when the cell is hyperpolarised and depolarises it to spike threshold, the so-called slow depolarisation.

In the light of this one might expect that the intracellular injection of calcium would suppress the firing of cells. Instead this was found to be the most potent inducement to bursting found [27]. Other powerful incentives for a cell to burst were a combination of glutamate and intracellular current and the injection of barium and TEA (tetraethylammonium). The latter two treatments are potassium channel blockers.

These results of calcium-induction and potassium channel blocking enabled Grace and Bunney [27] to advance a hypothesis; that a burst was initiated by a calcium induced inactivation of the delayed-rectifier potassium channels of the cell (the channels responsible for the repolarisation of the cell following an action potential). The input resistance of the cell was seen to increase prior to the onset of a burst and this suggests that the relevant action involves the inactivation of outward currents, rather than the activation of an inward current such as the I-CAN [75].

Such an injection of calcium will cause the (slower) rise of the afterhyperpolarisation potassium channel and the activation of this channel may then lead to the ending of the burst. This would suggest that it is the level and time course of intracellular calcium that underlies the ability of mesolimbic dopamine cells to burst. Whether the delayed-rectifying channels do inactivate with calcium has not been established.

This calcium-mediated hypothesis is lent further support by the eradication of bursting by the

progressive injection of the calcium buffer EGTA (ethylene glycol **bis**(β-aminoethylether)-*N*,*N'*-tetraacetic acid). As EGTA is injected the cells cease to burst and then tend to fire in a more rigid pacemaker fashion, more typical of the firing pattern seen in slice preparations. An investigation of mesolimbic neurons *in-vitro* found that bursting could not be elicited in these cells with any of the treatments that were effective *in-vivo*. These investigations did reveal that the currents responsible for the slow depolarisation and the fast spiking are mediated by both sodium and calcium and hence the firing of action potentials is likely to be a potent source of calcium influx.

The reason for our investigation is the observation by Grenhoff and Svensson that the systemic injection of nicotine (0.5mg/kg) caused a significant 165% increase of bursting in mesolimbic neurons [33]. However it was also demonstrated [15] [34] that the naturally occurring bursting of these neurons was eradicated if the neurons were bathed in kynurenate, the excitatory amino-acid (i.e. glutamate) antagonist. While one may expect that this simply removes an excitatory input that is needed to keep calcium levels high, it would also be expected to reduce the firing rate of the cell, which it did not. The unchanged firing rate would be expected to maintain the calcium levels and so the apparently necessary external input does not seem to have a calcium component; while this is essentially true, there is a hole in this argument which will be closed later, in section 3.4.2.

This requirement for the afferent input has particular relevance for the treatment of the neurons with nicotine. Typically nicotine acts through nicotinic acetylcholine receptors (nAChR) which are thought to be located on the cell bodies and terminals (Chapter 2). However more recent evidence [26] [69] suggests that nicotine acts preferentially by acting on nAChR in the ventral tegmental area located presynaptically on the glutamatergic terminals that innervate the dopamine neurons. Therefore nicotinic challenge will potentiate the (necessary) excitatory input to these cells.

3.3 The Irregular Firing Pattern

EGTA injection switched the cells from bursting, to irregularity to pacemaker firing, and excitatory current input could shift the cell from irregularity back to bursting [27]. This observation caused us to suspect that the irregular firing pattern represents an intermediate state between pacemaker and bursting and so characterising the irregularity could give a useful insight into true bursting. This suspicion is not entirely correct but has led us to some

interesting conclusions on what may cause bursting.

It was our initial opinion that some form of external input would be needed, an opinion supported by the results with kynurenate. The irregularity of the firing pattern, the amount of bursting and the occurrence of a burst appears to be quite random [35], which is behaviour we would not associate with characteristics that are intrinsic. We would consider it to be more reminiscent of interference by some essentially independent external stimulus.

We considered that while the induction of bursting by the calcium-dependent inactivation of the rectifying channel seems a reasonable hypothesis, that this would require a quick rise in calcium to cause sufficient inactivation before the rise of the calcium-activated potassium channel could counteract it. It is not clear from where within the cell such a rise could come from; although there is the well known process of calcium-activated calcium release from internal stores this still needs an initial rise from somewhere. The influx of calcium through external input forcing an action potential, for example, could provide such a mechanism.

It has been observed that *in-vitro* cells fire in a purely pacemaker fashion. If we consider the *in-vivo* cell, then following an action potential when will the next spike occur? We have every reason to suspect that it to will fire like the *in-vitro* pacemaker unless it experiences some outside interference.

Suppose that there is an externally driven excitatory stimulus that forces an action potential slightly earlier than one would arise allowing for the intrinsic properties of the cell. This action potential will cause an influx of calcium. If we suppose that the afterhyperpolarisation current I_{ahp} is already activated and therefore capable of suppressing further action potentials then the cell will not burst according to any hypothesis of ours. Instead the elevated calcium level will further increase the activation of the I_{ahp} and slow its decay, hence delaying the rise of the next, intrinsically prompted, action potential.

Let us suppose that the neuron would have a pacemaker firing pattern period of T *in-vivo* in the absence of the excitatory stimulus. When this excitatory stimulus arrives we suppose that it prompts an action potential immediately at a time $t < T$ after a 'normal' spike (we shall refer to action potentials arising from the intrinsic behaviour of the cell and those prompted by external stimuli as 'normal' and 'forced' respectively). An action potential has thus appeared $T - t$ earlier than expected.

Assuming a simple calcium extrusion pump, the elevated calcium levels will decay exponentially and we will assume a similarly exponential decay, with decay rate λ, in the I_{ahp}. The

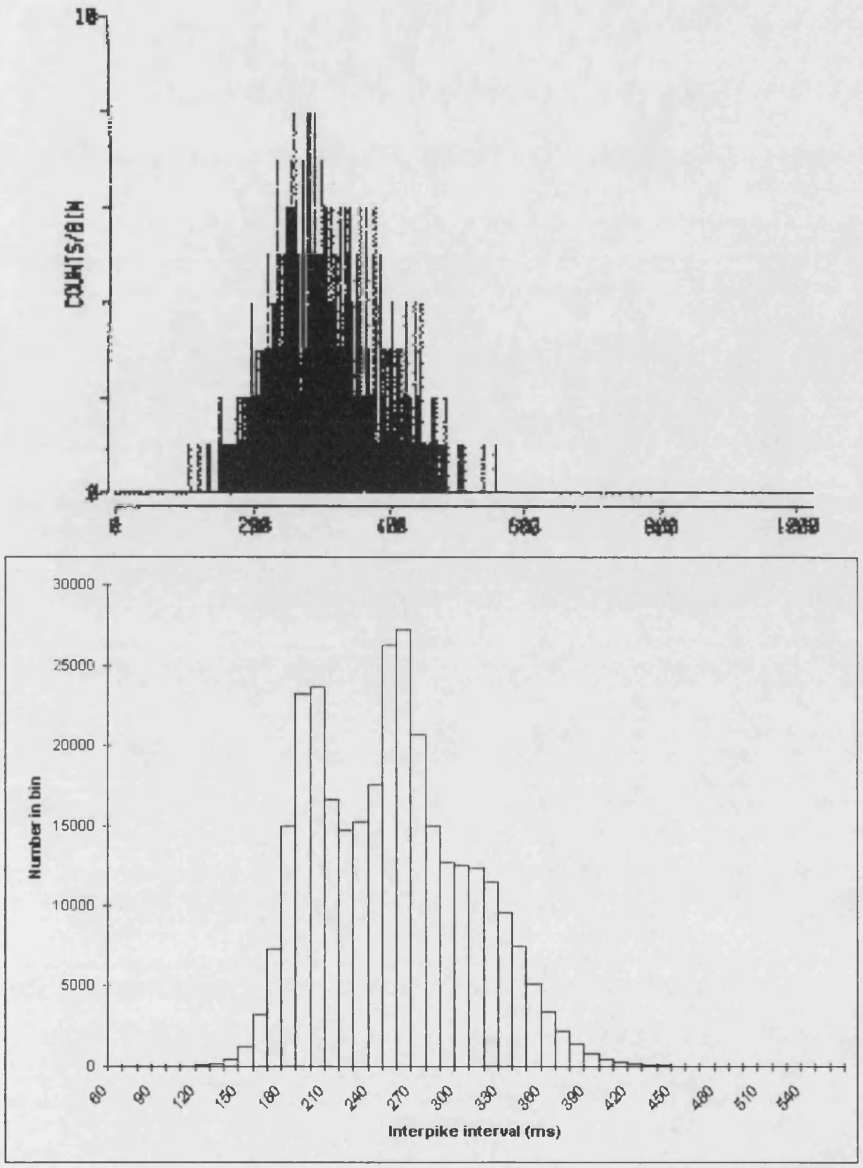

Figure 3.3: Comparison of histograms of interspike intervals. Top: recordings taken from a mesolimbic dopamine neuron firing in an irregular fashion, reproduced from Grace and Bunney [27]. Bottom: the irregular firing model (3.5), for an excitatory stimulus of 1.5Hz incident on a cell firing at 4Hz and allowing for 5% Gaussian noise, is similar in appearance.

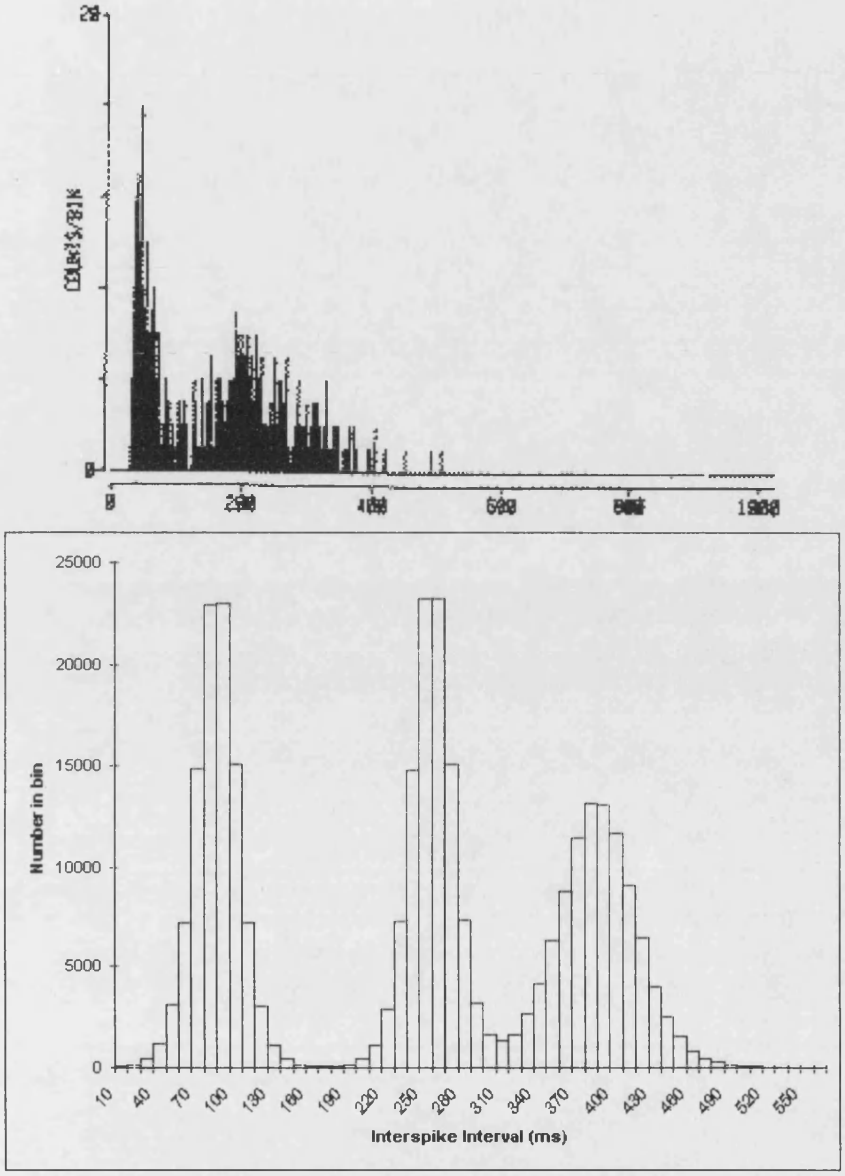

Figure 3.4: Comparison of histograms of interspike intervals. Top: recordings taken from a mesolimbic dopamine neuron firing in bursts, reproduced from Grace and Bunney [27], displaying the bi-modal nature of this mode of firing. Bottom: the irregular firing model (3.5), for an excitatory stimulus of 2.5Hz incident on a cell firing at 4Hz and allowing for 5% Gaussian noise. This would have a similar appearance if the left hand spike were bigger (including the interspike intervals from within the generated bursts) and the righthand one smaller and more spread out (the resulting afterhyperpolarisations).

delay caused by an early, forced, action potential can then be qualitatively approximated by

$$f(t) = \frac{1}{\lambda}\ln\left(1 + \frac{T-t}{T}\right) = \frac{1}{\lambda}\ln\left(2 - \frac{t}{T}\right). \tag{3.1}$$

This has the essential qualities; $\lim_{t\to 0+} f(t) = \frac{1}{\lambda}\ln 2$, i.e. a near 'double' action potential doubles the calcium level and so it takes $\frac{1}{\lambda}\ln 2$ longer to decay to the same level. $f(T) = 0$ and so a forced action potential that coincides with a normal one will not cause any delay, since the firing pattern has not essentially been interfered with.

The 'phase' of the firing cycle has been shifted an amount $T - t - f(t)$ by this forced spike.

Let us suppose for the moment that the external stimulus is periodic, with period S and that the arrival of this stimulus forces an action potential instantly (and furthermore that, as regards calcium influx, this spike is identical to normal spikes). To prevent this stimulus simply driving the firing of the cell we will assume that

$$MT < S \leq (M+1)T \tag{3.2}$$

for some $M \in \mathbb{N}$ and hence define the period difference (modulo T), k, to be

$$k := (M+1)T - S, \tag{3.3}$$

note that $k \in [0, T)$. If we define t_n to be the interspike interval between a normal spike and the nth forced spike, then the next such interval, t_{n+1} is given by

$$t_{n+1} = jT - k - f(t_n). \tag{3.4}$$

Here $j \in \mathbb{N}$ is the lowest integer such that $t_{n+1} > 0$. It is possible that for appropriate k (obviously larger values) that $k + f(t_n) > T$, which merely implies that the forced spike appears after the $M-1$th normal spike or earlier.

For simplicity and the illustration of our idea we shall restrict $k \in [0, \frac{1}{\lambda}(1 - \ln 2))$ and then our system is given explicitly by

$$t_{n+1} = T - k - f(t_n). \tag{3.5}$$

The difference equation (3.4) has some interesting dynamics in its own right. It can be shown that for various ranges of k there are steady states and n-periodic orbits where $n \in \mathbb{N}$, aperiodic solutions are also possible for larger values of k. Before we consider that the irregularity of the pattern is solved by reference to these solutions (particularly the aperiodic ones), there are many reasons why this is not a valid description of the firing in the cell.

Firstly we have assumed the external stimulus is periodic and instantly produces an action potential. The function we have used to approximate the delay is not necessarily accurate, while it may describe the delayed decay of the elevated calcium well, one may consider that the activation (whatever function of calcium this may be) of the I_{ahp} is better approximated by a double exponential decay. We also know that such cells are capable of bursting and we have made no provision for the shift in phase associated with such a firing pattern.

We persist with this description because of the idea that it will be shown to illustrate. For each $k \in [0, \frac{1}{\lambda}(1 - \ln 2))$ there exists a steady state $t^* \in (0, T)$, the solution of the equation

$$t^* = T - k - f(t^*). \tag{3.6}$$

By writing $t_{n+1} = g(t_n)$ we observe that $\frac{d}{dt}g(t) = \frac{1}{\lambda T}\frac{1}{2-t/T} \in (0,1)$ for all $t \in (0,T)$ if we assume $\lambda T \geq 1$. This then gives stability. In our modelling of the I_{ahp} in the later sections we took $\lambda = 1/150$ $(\text{ms})^{-1}$.

Consider the histogram of interspike intervals for such a cell where the interaction between the intrinsic firing and the external stimulus is given by equation (3.5) at steady state. Then the distribution has three peaks, at t^*, T and $T + f(t^*)$. For $T = 250$ms (a typical firing rate of 4Hz), $\lambda = 1/150$ $(\text{ms})^{-1}$, $S = 740$ms, then $k = 10$ms is comparatively small and the three peaks are close together. As illustrated in Figure 3.3, allowing for 5% gaussian noise the histogram has a rather uni-modal appearance very similar to the distribution of interspike intervals for the real irregular firing.

[As an aside it is worth observing that this model has the correct response to EGTA. This would be expected to buffer most intracellular calcium and thereby prevent activation of the I_{ahp}. This has the effect of setting $f(t) \equiv 0$ and so our three peaks would appear at $T - k$, T and T again, respectively, giving a histogram resembling that of a pacemaker.]

For the not too dissimilar $T = 200$ms, $S = 550$ms and hence $k = 50$ms we have a clear separation between the peaks as in Figure 3.4. This is reminiscent of the histogram for a bursting neuron if the first peak where higher, and strictly if the third peak were flatter. Now consider the following idea; the irregular firing neuron does not burst because the I_{ahp} is already activated and suppressing any subsequent spiking until it decays (an assumption of our flawed model). For this latter cell the forced spike comes much earlier, and we may suppose that in this case the I_{ahp} has not had time to activate (sufficiently). If we allow the calcium influx caused by the action potential to cause an inactivation of the delayed-rectifying potassium channels sufficient to prompt another action potential we have created a burst.

From the point of view of the histogram, this flurry of spikes will add to the frequency of short interspike intervals and the subsequent afterhyperpolarisation will create a flatter, wider third (delay) peak and turn it into one that looks precisely like that of a recording bursting neuron. While a match of histograms is not conclusive it has proposed the following idea; the forcing of action potentials by an external stimulus and the subsequent delaying of normal firing seems to fit with the irregular firing pattern. If the same external stimulus forces two action potentials close together, the sharp rise in calcium above normal levels could produce an inactivation of one form of calcium channel before the I_{ahp} can activate to compensate. This imbalance may be sufficient to cause additional action potentials, i.e. a burst.

This proposed additional mechanism involved in bursting can explain certain aspects well, as well as standard irregular firing. The cessation of bursting when the cells are bathed in kynurenate, blocking this external stimulus, is a case in point. It also solves our problem of where an initial rise in calcium can come from.

3.4 The Theoretical Hypothesis

3.4.1 The Combined Calcium and Forced-Spike Hypothesis

We propose our own hypothesis for the cause of bursting in mesolimbic dopamine neurons, that is essentially the combination of Grace and Bunney's [27] and what the need for input [15] [34] we have considered so far. We will suppose that bursting is caused by the calcium-induced inactivation of the delayed-rectifying potassium channels (I_{dr}) present in the cell increasing cell excitability, but that this initial rise is prompted by the forcing of an action potential by an external excitatory stimulus.

The hypothesis can be described as follows:

1. at 'low' intracellular calcium levels, the neuron fires in a pacemaker fashion, the spike threshold is reached due to the rise of a slow depolarisation. The spike is generated by a fast calcium channel and repolarised by a rectifying potassium channel. The incident external stimulus may (or may not if the lack of inactivation of the I_{dr} makes this current sufficiently strong) prompt additional action potentials. Where these spikes are generated, they will cause a simple shift in the phase of the cell, the I_{ahp} will fail to activate at such low calcium levels.

2. sufficiently 'high' calcium levels can cause an inactivation of the I_{dr} (which we assume to be fast). The (comparatively late) forcing of action potentials may cause over-activation of I_{ahp} to compensate, inducing a delay in the onset of the next normal spike and hence give an irregular firing pattern.

3. at 'high' calcium levels, if an action potential is forced soon after a normal spike then the inactivation of the I_{dr} may be sufficiently greater than the activation of the I_{ahp} to induce a period of faster firing in the cell. This will then be attenuated by the slow rise of the I_{ahp}. This is 'bursting'.

4. the increasing inter-spike intervals found in bursts will be due to the progressive rise of the I_{ahp}, which will also be responsible for the long afterhyperpolarisation following a burst.

5. the decreasing spike height in a burst will be caused by a combination of the higher levels of calcium reducing the calcium gradient across the cell membrane (and hence the strength of the fast calcium channel component of the action potential) and the voltage-dependent inactivation of the fast, spiking channels at the higher firing rates.

6. the increasing spike width will be caused by the reduced rectification of spikes by the I_{dr} (caused by the increasingly high calcium levels). Less rectification will slow the repolarising of the cell and hence increase the width of the action potential.

7. excitatory intracellular current input (or persistent excitatory input caused by prolonged exposure to glutamate) may act to increase firing rate and hence increase calcium levels. This will increase the probability of inactivating the I_{dr} sufficiently and thereby promote bursting. Similarly injection of the calcium buffer EGTA would reduce calcium levels so that the cell fires as a pacemaker. Calcium injection will promote bursting for the obvious reasons.

The hypothesis can provide an explanation for the observed weak correlation between the amount of bursting in a cell and its average firing rate [27]. Here bursting arises from the locally short time interval following of a normal spike by a forced one and so is disassociated from the global firing rate. A weak correlation does arise since one would expect a faster firing cell to maintain higher average calcium concentrations which would then increase the probability of the cell bursting.

We can be less sure why short current injections (pulses of 25ms) cannot produce bursts but can suppose that the injections used are not sufficiently strong to force action potentials early enough. Recall that bursts are recognised by an interspike interval of $<$ 80ms and we may expect that such a time period still lies in the relative refractory period of the cell, from which we would expect larger current inputs to be needed. In contrast the longer injection times of 100-200ms may be sufficient and would also enhance the effect of the inactivation of the I_{dr} and so increase the probability of a burst. For a non-bursting cell the calcium concentration is unlikely to be able to rise to a burst-friendly level in this time.

Our hypothesis therefore provides a sound theoretical explanation of all aspects of bursting in mesolimbic dopamine neurons.

3.4.2 A Direct Calcium Influx Hypothesis

The need for a forced action potential is the only consistent hypothesis that we have been able to come up with. Whilst it is able to explain this firing pattern in the cells one may be tempted to reject this notion of a forced action potential for the following idea; could the external stimulus simply be a calcium influx that causes the inactivation. That is rather than affecting the cell by raising membrane potential to spike threshold, could the calcium influx directly inactivate the I_{dr}?

This has the advantage of being a slightly more direct method of inactivating the I_{dr} and there is experimental evidence for the presence of NMDA receptors (a form of glutamate receptor that gates a high proportion of calcium) on dopamine neuron dendrites. However this explanation cannot explain the ability of a 100-200ms pulse of current to reliably produce bursts unless this also works by producing action potentials, an action which therefore favours our original hypothesis.

3.4.3 The Effect of Nicotine

Our hypothesis on bursting ties in very neatly with the observed ability of nicotine to increase bursting significantly in mesolimbic dopamine neurons [33]. It relies on the ability of the excitatory input to force action potentials in the cell. Nicotine potentiates the glutamatergic input and naturally a more potent input will have a better ability to do this. As we suggested earlier the ability of nicotine to enhance bursting is much easier to explain than the reasons for bursting. This explanation also means that we will not need to model any nicotinic input explicitly, but simply take account of more powerful excitatory input as we desire.

3.5 The Computer Model

3.5.1 Aims of the Computer Model

It is our intention to build a simplified computer model of the membrane properties, ion channels and calcium dynamics of a mesolimbic dopamine neuron. We shall then use this model to investigate whether this is capable of producing bursts. This provides a way to test whether our theoretically sound hypothesis actually works.

Mesolimbic dopamine neurons have been shown to contain the following types of ion channel [30]; fast sodium and fast calcium for spike generation; sodium and calcium dependent slow depolarisation for the depolarisation of the cell to threshold; rectifying potassium; calcium-activated potassium channel and an anomalous rectifier has also been identified. The kinetics for these intrinsic channels have not been explicitly measured and so we have taken activation and inactivation curves from other preparations, or in the case of no available analogs, assumed a form ourselves. This immediately leaves us the problem that we cannot claim that our model is an accurate quantitative description of the neuron, however it is only intended to test the viability of our calcium-dependent and forced action potential bursting hypothesis.

There are many parameters of the model that we do not know. In particular we do not know the intracellular calcium concentration, or how this varies with the influx through fast calcium channels and then what inactivation of the delayed-rectifying channels this may have, an action that has not been established experimentally in this preparation. The voltage dependencies of ion channels are taken from other experimental preparations and so are specified in millivolts. Similarly we take the values of the ion reversal potentials to be the numerical values of the true reversal potentials expressed in milli-volts. The model is then fitted, in milli-volts, to the membrane potential characteristics of dopamine neurons as regards resting potential, spike threshold and spike height; this aids the fitting of parameters to the model since we know what behaviour we can expect and so judge whether the results we obtain are sensible. For similar reasons time is expressed in milliseconds, all other units are in SI unless otherwise stated.

3.5.2 Electrical Compartments

It is not clear from our model whether there are any effects from the spatial arrangement of the neuron and its ion channels. For example our hypothesis does rely on what comes

out as a temporal difference between the calcium inactivation of one sort of channel and the compensatory calcium activation of another; it is likely that this may involve, significantly or not, the diffusion of calcium ions throughout the cell and therefore we would have a spatial component. As this appears as a temporal characteristic, we may as well assume it is purely this. By neglecting spatial components we also reduce the complexity of our model from a system of partial to one of ordinary differential equations.

The neuron is therefore regarded to be a single electrical and spatial compartment. We will use Hodgkin and Huxley models for the ion channels [41] and a standard calculation for the internal calcium concentration. Hence the ion channels are considered to be electrical currents in parallel with an electrical capacitance representing the cell membrane and we can solve for membrane potential by solving Kirchoff's Law for this system, that is

$$C_m \frac{dV_m}{dt} = I_{\text{leak}} + I_{\text{dr}} + I_{\text{sd}} + I_{\text{sp}} + I_{\text{ahp}} + I_{\text{ga}} + I_{\text{ext}}, \tag{3.7}$$

$$C_m = 1.0 \times 10^{-8}, \tag{3.8}$$

where C_m is the capacitance of the membrane in F, V_m is the membrane potential in mV, I_{leak} is the leakage conductance (which is then in mA). I_{ext} is the excitatory input from the external source that we propose is a requirement in bursting and the other $I_{\_}$ are the currents due to the ion channels, which will be discussed in the following sections.

3.5.3 Leakage Current

The cell will typically have a leakage of current through the membrane due to its natural permeability and the action of other ion channels or ion pumps that we do not explicitly model [41]. However we have the problem that we do not know the conductance of this current; while the true membrane resistance could be estimated to perhaps within an order of magnitude by reference to values obtained for other preparations or model we do not know how this value may compare to the conductances of the other ion channels in the model. We may only estimate the comparative conductance if we can find a specific use for this type of current. We therefore assume that it has an effect similar to the GABAergic input to the cell (section 3.5.11) in keeping the membrane potential low and obtain

$$I_{\text{leak}} = \frac{E_m - V_m}{R_m}, \tag{3.9}$$

$$E_m = -75, \tag{3.10}$$

$$R_m = 1.0 \times 10^{13}, \tag{3.11}$$

where E_m is the reversal potential of this current and R_m is the membrane resistance in Ω. The value of R_m is chosen such that removal of the powerful GABAergic current will increase the firing without causing a depolarisation block.

3.5.4 Calcium Accumulation

We calculate the intracellular calcium level, which is then used to calculate the activation and inactivation of the calcium-activated potassium channels and calcium-inactivation of the rectifying channels respectively. For simplicity we assume that only the spike generating channel gates calcium and that the ion is removed by a simple pump. The concentration of calcium is then described by the equation [10]:

$$\frac{dc}{dt} = B(I_{\text{sp}} + I_{\text{sd}}) - \frac{c - c_{\text{base}}}{\tau_c}, \tag{3.12}$$

$$B = 1.0 \times 10^4 \tag{3.13}$$

$$c_{\text{base}} = 290, \tag{3.14}$$

$$\tau_c = 300, \tag{3.15}$$

where c is the intracellular calcium concentration expressed in μM, I_{sp} and I_{sd} are the currents due to the spiking and slow depolarisation channels and τ_c is the time constant of the extrusion pump. In practice it turns out that the I_{sd} is small in comparison to the I_{sp}.

Strictly the currents I_{sp} and I_{sd} gate both calcium and sodium and we should take account of this. The calcium influx will not be a fixed proportion of these currents due to the fluctuations in the individual reversal potentials of the two ions, but these variations are typically small (we estimate it to be of the order of 5%) and we consider this extra complication unnecessary.

3.5.5 The Calcium Reversal Potential

The changes in the calcium reversal potential plays an important role in our hypothesis where it is supposed to restrict the height of the burst spikes. The reversal potential is given by

$$E_{Ca} = 12.5 \ln\left(\frac{[\text{Ca}]_o}{c}\right) \tag{3.16}$$

where c is the intracellular calcium concentration given by equation (3.12) and $[\text{Ca}]_o$ is the extracellular calcium concentration which we assume is fixed at

$$[\text{Ca}]_o = 1.5 \times 10^5. \tag{3.17}$$

This value is derived from the fitting of the model as described later (section 3.6.1). The factor of 12.5 is the numerical value derived from the physical constants, see Chapter 2, section 2.3.2 and [45] [47] for an explanation of what these are.

3.5.6 The General Form of Ion Channels

All ion channels are assumed to gate current (I) according to Ohm's Law, $I = gV$, where g is the conductance of the channel and generally a function of time, membrane potential and calcium concentration and V is the voltage gradient. Of all the ion channels that have been identified in the preparation thus far the only one we do not include any model of is the anomalous rectifier current. This current only arises as a weak hyperpolarising influence when the cell is clamped at hyperpolarised membrane potentials and may even be a slow voltage-dependent inactivation of the delayed-rectifying potassium channels. Its weak actions do not seem to be particularly relevant to the cell function within our range of interest given the current data.

3.5.7 The Rectifying Potassium Channel

We have taken the voltage activation curve from a guinea-pig potassium channel [89] [98] and assumed for simplicity and computational efficiency that it activates instantaneously. The current is given by

$$I_{\mathrm{dr}} = \bar{g_{\mathrm{dr}}} m_\infty(V_m) h_\infty(c)(E_{\mathrm{dr}} - V_m) \tag{3.18}$$

$$m_\infty(V_m) = \frac{1}{1 + \exp\left(-\frac{V_m - V_{mh}}{V_{ms}}\right)} \tag{3.19}$$

$$V_{mh} = -5 \tag{3.20}$$

$$V_{ms} = 14.2 \tag{3.21}$$

$$\bar{g_{\mathrm{dr}}} = 3.85 \times 10^{-7} \tag{3.22}$$

$$E_{\mathrm{dr}} = -75 \tag{3.23}$$

where $\bar{g_{\mathrm{dr}}}$ is the total conductance of the channels, $m_\infty(V_m)$ is the steady state (instantaneous) voltage-dependent activation curve. E_{dr} is the reversal potential of this current, taken to be the reversal potential for a potassium current.

$h_\infty(c)$ is the calcium-dependent inactivation of the channel. No form is known for this since the effect has not been established, but it will typically be a decreasing function of intracellular

calcium, c. We have assumed a partial inactivation involving a Boltzmann curve because such a form saturates at low and high values allowing us to tweak the function for sensitivity to calcium easily without having to worry about causing negative conductance values. We used the explicit form:

$$h_\infty(c) = 0.6 + \frac{0.4}{1 + \exp\left(\frac{c - c_h}{c_s}\right)} \tag{3.24}$$

$$c_h = 920 \tag{3.25}$$

$$c_s = 1 \tag{3.26}$$

where the half inactivation, c_h, and slope, c_s, constants are estimated from typical calcium concentrations observed when running the simulation for $h_\infty(c) = 1$. We will be assuming that the inactivation is fast in comparison to the calcium-dependent activation of the afterhyperpolarisation current and therefore take it to be instantaneous for simplicity.

3.5.8 The Slow Depolarisation Current

The rise in membrane potential from the hyperpolarised state following an action potential to spike threshold is mediated by a slow depolarisation current [30]. The membrane potential rises at a fairly constant rate, which gives the appearance of a leakage conductance if it were not for the inactivation of the current if it does cause an action potential. Although it is described as a slow current, because of the slow rise in membrane potential it causes, it is not apparent whether this slowness arises from the time taken for the current to activate to a perhaps strong conductance level, or whether the current activates quickly but is weak. For our purposes it does not particularly matter which (or what combination of the two) since we only require its effect, rather than a true model of the current (for which there is insufficient experimental data). We use the latter description since it omits the need to bring in extra parameters to describe the time dependence.

We therefore assume that the current is fairly constant at hyperpolarised potentials and that

it inactivates quickly at above threshold potentials. We take it to have the form

$$I_{\text{sd}} = \bar{g_{\text{sd}}} u_\infty(V_m)(E_{\text{sd}} - V_m) \tag{3.27}$$

$$u_\infty(V_m) = \frac{1}{1 + \exp\left(\frac{V_m - V_{uh}}{V_{us}}\right)} \tag{3.28}$$

$$V_{uh} = -40 \tag{3.29}$$

$$V_{us} = 1 \tag{3.30}$$

$$\bar{g_{\text{sd}}} = 4.0 \times 10^{-10} \tag{3.31}$$

$$E_{\text{sd}} = E_{Ca} \tag{3.32}$$

where u_∞ is a voltage-dependent inactivation curve of our own design that acts to switch off the current at above threshold potentials (hence the sharpness of the slope V_{us}). While this form is for an ionic current is non-standard, it fits with the experimental observations on the channels behaviour and in practice works well. The current is mediated by sodium and calcium ion flow and hence has a high reversal potential (of around about 100). This will be a combination of the sodium and calcium reversal potentials, E_{Na} and E_{Ca} respectively and would be given by

$$E_{\text{sd}} = \frac{g_{Na}E_{Na} + g_{Ca}E_{Ca}}{g_{Na} + g_{Ca}} \tag{3.33}$$

where g_{Na} and g_{Ca} are the relative conductances of the channel for sodium and calcium. Since we do not know what these figures are and observing that the sodium and calcium reversal potentials are typically close together we take $E_{\text{sd}} = E_{Ca}$. In practice the variation in E_{Ca} for calcium influx makes little impact on this current, representing a change of 10-20 in a voltage gradient of 160.

3.5.9 The Spiking Channel

This is a fast activating channel that generates the action potential. Dopamine neurons have been observed to have two types of such a fast channel, selective for calcium and sodium. Since both forms of channel perform similar functions and cannot be differentiated by there observed voltage dependencies we only include a single form of fast channel which we assume gates both calcium and sodium. For the same reasons as for the slow depolarisation channel discussed above (section 3.5.8) we use the calcium reversal potential only.

The voltage-dependent activation and inactivation curves are taken from a fast sodium channel in the guinea pig hippocampus [88] [98]. For the sake of simplicity and a little computational efficiency we assume that activation is so fast as to be instantaneous. The time

constant of channel inactivation is put in this form to reflect the fast inactivation at depolarised potentials and a slower action at resting and hyperpolarised potentials. The chosen values are fairly typical [88] [98] [49], if a little slow for the more polarised potentials, with the specific ones chosen simply because they worked well. The channel current is then given by

$$I_{\text{sp}} = \bar{g_{\text{sp}}} r_\infty(V_m)^2 s(E_{\text{sp}} - V_m) \tag{3.34}$$

$$\frac{ds}{dt} = \frac{s_\infty(V_m) - s}{\tau_s} \tag{3.35}$$

$$r_\infty(V_m) = \frac{1}{1 + \exp\left(-\frac{V_m - V_{rh}}{V_{rs}}\right)} \tag{3.36}$$

$$s_\infty(V_m) = \frac{1}{1 + \exp\left(\frac{V_m - V_{sh}}{V_{ss}}\right)} \tag{3.37}$$

$$V_{rh} = -29 \tag{3.38}$$

$$V_{rs} = 5.7 \tag{3.39}$$

$$V_{sh} = -67.6 \tag{3.40}$$

$$V_{ss} = 7.4 \tag{3.41}$$

$$\bar{g_{\text{sp}}} = 1.05 \times 10^{-5} \tag{3.42}$$

$$E_{\text{sp}} = E_{Ca} \tag{3.43}$$

$$\tau_s = \begin{cases} 50 & \text{for } V_m < -40 \\ 1 & \text{for } V_m \geq -40 \end{cases} \tag{3.44}$$

where r_∞ and s_∞ are the steady-state voltage-dependent activation and inactivation curves respectively.

3.5.10 Afterhyperpolarisation Current

It has been observed in mesolimbic dopamine neurons that trains of action potentials give rise to a slowly activating, afterhyperpolarisation current (I_{ahp}) [30]. This is putatively a calcium-activated potassium channel, that is its activation is a function of the intracellular calcium concentration c rather than membrane potential. It was experimentally estimated that the activation of this I_{ahp} was proportional to the number of action potentials elicited by a depolarising intracellular injection. Since each action potential will gate slightly less calcium than the one before, and from a non-zero base, it suggests that in this range the dependence is supra-linear. This calcium influx through action potentials activation of the I_{ahp} also supports our modelling result that the I_{sp} is the main source of intracellular calcium

over the I_{sd}.

We have therefore assumed that the steady state activation of the channel is equal to the internal calcium concentration squared (c^2). It was found that this value gave a suitably strong afterhyperpolarisation and it is consistent with the calcium-dependent potassium currents found and used in other preparations and models [49]. In accordance with experimental observations we take the time constant of activation to be slow. This potassium current is then given by

$$I_{\text{ahp}} = \bar{g_{\text{ahp}}} a^2 (E_{\text{ahp}} - V_m) \tag{3.45}$$

$$\frac{da}{dt} = \frac{c - a}{\tau_a}, \tag{3.46}$$

$$\bar{g_{\text{ahp}}} = 8.0 \times 10^{-16}, \tag{3.47}$$

$$E_{\text{ahp}} = -75 \tag{3.48}$$

$$\tau_a = 150. \tag{3.49}$$

This description is non-standard in that the activation of the channel is typically greater than 1 and we have included the correction factor in $\bar{g_{\text{ahp}}}$. Strictly we should write the activation in a scalar Michaelis-Menten form, but for the ease of fitting have left it as above. Writing it in the form where a calcium level equal to the extracellular concentration (150mM) has an activation of 1 (which would seem reasonable) corresponds to a sensible maximum channel conductance of 8.0×10^{-6}S.

3.5.11 GABAergic Input

Mesolimbic dopamine neurons *in-vivo* are observed to be under intense external stimulation from GABAergic neurons [29] which serves to keep the cell hyperpolarised. Since removal of this input can cause significant changes in firing rate an approximation to this input was included. The stimulation is of such a high frequency (about 20Hz [29]) that it can be well approximated by a simple channel of constant conductance rather than many temporally-discrete inputs. The current is a flux of chloride ions and therefore has a typical reversal potential of around -75(mV). Hence it may be written

$$I_{\text{ga}} = \bar{g_{\text{ga}}} (E_{\text{ga}} - V_m), \tag{3.50}$$

$$\bar{g_{\text{ga}}} = 5.0 \times 10^{-8}, \tag{3.51}$$

$$E_{\text{ga}} = -75. \tag{3.52}$$

3.6 Results of the Computer Model

3.6.1 The Quantitative Fitting of the Model

We have already quoted the numerical values of the parameters used in the model in the sections above. The derivation of these values comes from fitting the model together to produce a description of a mesolimbic dopamine neuron. However combining all the models of ion channels and calcium accumulation together into such a model is not going to be straightforward. We must first consider what sort of fit we would wish to achieve, our ultimate aim is to demonstrate bursting in these cells but this may not be practical given the many different mechanisms that we propose are involved.

Our first step will be to create a model of a cell that fires periodically, the so-called pacemaker firing, since this represents a slightly simpler system, being devoid of the external excitatory input. Given that we are then only interested in a regular firing pattern we do not (for the moment) need to consider the calcium-dependent inactivation of the I_{dr} and so can temporarily set $h_\infty(c) \equiv 1$. For similar reasons we temporarily ignore the calcium-activated current, the I_{ahp}, and set the calcium reversal potential to a constant value of 100.

We first choose typical time constants for inactivation for the I_{sp}, fast at 1ms for depolarised values and slow (50ms) at resting and lower potentials. We take a conductance of 1μS for the I_{sp} [88]. The conductance of the I_{dr} is then set so that induced action potentials have a height of more than 90mV and a duration of around 2ms, as observed in [28]. We then add in the I_{sd} with the conductance set so that the cell fires at about the observed rate of 4Hz. To avoid interference in this fitting from the leakage current the membrane resistance is set to a large value so that it has a very low (negligibly so) conductance. This results in a combination of three channels that produces pacemaker firing at a rate of 4Hz and running this model simulation allows us to monitor the variations in intracellular calcium levels from its nadir just before an action potential, to its peak just after one.

Based on these observed calcium levels we then add in the I_{ahp} current such that it hyperpolarises the cell and suppresses further action potentials for approximately another 250ms (the current natural period of the cell) when two action potentials are induced close together ($<$ 10ms apart). The longer interspike intervals that are thus possible meant that intracellular calcium levels could decay to close to zero. Identifying that this could cause unwanted interference regarding the calcium reversal potential we raised the base calcium level (effectively the reversal concentration of the calcium pump) to prevent this.

The activation of the I_{ahp} at the lower calcium levels hence produces an additional hyperpolarising influence on the cell and so we reset the conductances of the I_{sp}, I_{dr} and I_{sd} as above to return the cell to a firing rate of 4Hz. We then perform a similar action when adding in the I_{ga}, assuming that subsequent removal of this current can cause the cell to reach threshold in 10-20ms (as observed in [29]). The restriction of a constant calcium reversal potential was then lifted.

The most difficult part of the model to fit is the calcium-dependent inactivation of the I_{dr} since we have no indication of form or the results of this mechanism, save for our hypothesis that it could prompt bursting. Firstly we note that the increased firing rate found during a burst, typically 2-3 times the normal firing rate, can be produced in the model by reducing the conductance of the I_{dr} by a factor of about 0.85. This gives the range of calcium-inactivation that we require and we can keep within these limits by assuming the inactivation is described by a Boltzmann curve.

We are then required to fit the two parameters for this Boltzmann function. It will be easier to attempt to reproduce a significant level of calcium inactivation for an action potentials worth of calcium influx if the slope of the curve is steep, giving it a step like appearance. For that reason we set the slope parameter to be 1, small (implying steep) when compared to typical calcium ranges of around 1mM. The half-inactivation parameter is therefore a marker for where the channel inactivates. If we are investigating the possibility of the cell bursting *without* the need for an external excitatory input then we will set this parameter to cause inactivation in the upper range of intracellular calcium concentrations reached during the fitted pacemaker firing. Alternatively when we look into the possibility of the input forcing action potentials that lead to bursts it is set in the higher range of concentrations reached when two action potentials are forced close together, as in the fitting of the calcium-activation of the I_{ahp}.

This method; of starting with a few channels that have simple, independent actions and building the rest of the model from there; was thought to be the most sound and easiest way of producing a system involving all the channels that fired in the observed way.

3.6.2 Pacemaker Firing

Our fit of the computational model fired in a pacemaker fashion of about 4Hz as we designed it to. The cell fires action potentials of 90mV in height, but from a more hyperpolarised spike threshold of -55mV, hyperpolarising to a comparatively depolarised -65mV, in comparison to

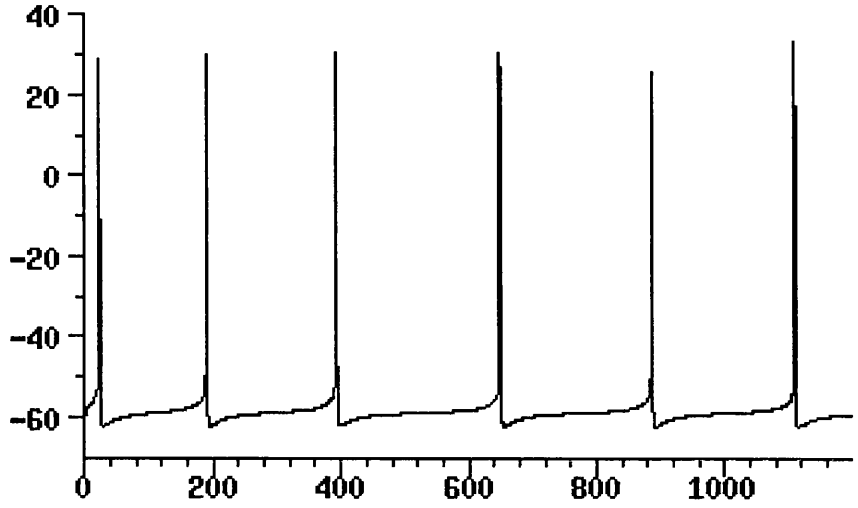

Figure 3.5: The pacemaker firing, at a rate of 5Hz, of the computer simulation that is left unperturbed. The slight variation at the beginning is due to the simulations initial conditions, but from the third spike on the interspike interval is regular.

experimental observations [28]. The firing rate could easily be altered by shifts in the model parameters. Typically this involved changing the conductance of the slow depolarisation, reductions in this parameter reducing the firing rate to a minimum of about 2Hz. For slow depolarisation conductance values below this minimum the membrane potential remained at a steady, hyperpolarised potential. It is notable that mesolimbic dopamine neurons do have an observed minimum firing rate of about 2Hz.

Conversely, increases in slow depolarisation conductance produces a faster firing cell and rates of over 10Hz can be generated. The pacemaker firing pattern of the cell firing at a rate of about 5Hz can be seen in Figure 3.5. Altering the other conductances of the ion channels affects the cell as one would expect; reducing the conductance of the I_{dr} makes the cell fire faster with less hyperpolarisation (2-3mV less) in between spikes, although the spike threshold is relatively unchanged due to a slight inactivation of the I_{sp}. Increasing the conductance of the I_{sp} increases the firing rate by reducing the spike threshold by 2-3mV but retains the original level of hyperpolarisation.

Increasing the conductance of the I_{ga} slows the firing of the cell, increasing both the hyperpolarisation and spike threshold. A similar effect can be obtained by increasing the strength of the I_{ahp}, although the activation of this channel can cause an initial oscillation in the firing rate when the simulation is started as the calcium concentration is not synchronised. This soon (within three or four spikes) settles down to pacemaker firing.

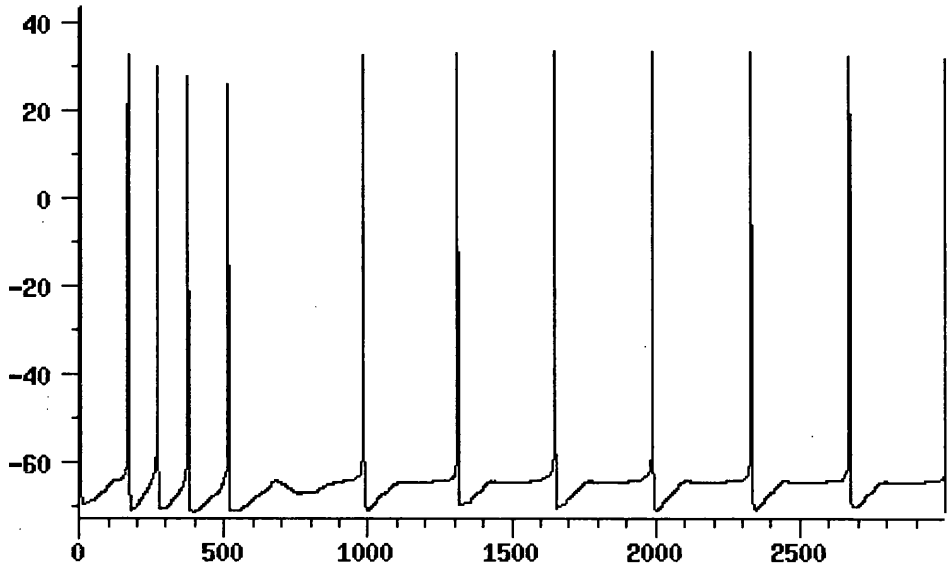

Figure 3.6: The initial conditions of the simulation can cause transient behaviour before settling down to pacemaker firing. Here a cell follows an initial spike with a burst-like pattern of four spikes and a putative afterhyperpolarisation which cuts off a possible fifth.

Significantly, excitatory influence such as increases in the I_{sd} or I_{sp} conductance, continuous injection of depolarising current, or decreasing in I_{dr}, I_{ga} or I_{ahp} conductance cannot induce sustained bursting, or any burst-like pattern. Small, or slowly building currents purely increase the firing rate; larger, or quickly arising, currents produce faster firing with some accommodation (and a possible small oscillation in firing rate due to the activation of the I_{ahp}).

The key word here is sustained. All the simulations run eventually settle down to pacemaker firing, within what is observed to be no more than six spikes. Typically the initial conditions of the simulation will not correspond to the ultimate periodic solution and so there is some transient behaviour. This can be a slight oscillation in the interspike interval, which is due to the membrane potential and calcium concentration being out of synchronisation leading to alternate over- or under-activation of the I_{ahp}.

Where there is a large imbalance in the initial conditions, as regards the ultimate pacemaker firing of the cell, the model can display transient behaviour that does appear to contain a burst. Figure 3.6 is a prime example of this; after an initial spike there follows another in the comparatively short (regarding the period of the pacemaker firing of the cell) interval of 150ms, which creates three further spikes very quickly. Each successive spike has a slightly greater interspike interval and is slightly shorter in height. There then follows a long (500ms)

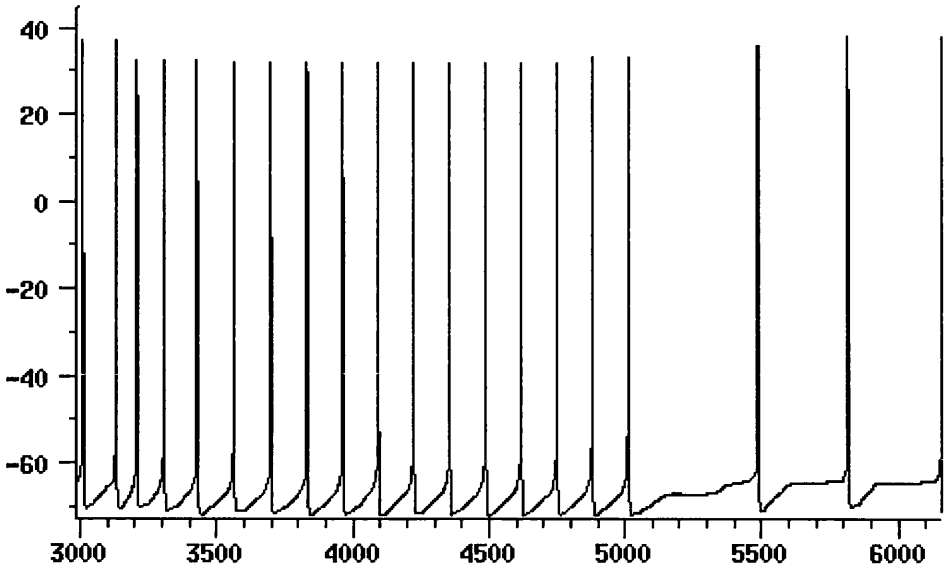

Figure 3.7: For the same cell as in Figure 3.6, the injection of a depolarising current (from 3050ms) can cause a burst-like pattern but the cell soon settles to a higher frequency of pacemaker firing. When the depolarising current is removed (at 5000ms) the cell returns to firing at the original 3Hz.

interval without firing, although the cell does appear to nearly break threshold at 700ms absolute it is prevented by the activation of the I_{ahp} which then hyperpolarises the cell. Once this is over the cell fires with a steady period at 3Hz.

As one would then expect, sufficiently large step changes in depolarising current can trigger some burst like phenomena if the change in firing rate causes the intracellular calcium levels to rise from a region of low inactivation of the rectifying current to one of high inactivation. The increase in depolarising current causes a period of rapid firing which can raise calcium levels sufficiently high and the cell may then produce a similar burst firing pattern. This 'burst' is also attenuated by the rise of the I_{ahp}, whereupon the cell fires once more as a pacemaker, although at a higher firing rate due to the increased depolarising influence.

Figure 3.7 shows how a cell that is firing as a pacemaker responds to a prolonged depolarisation. The pattern is not a typical burst, but the cell does fire faster with increasing interspike intervals. There is no apparent long afterhyperpolarisation due to continued presence the depolarising current which then makes the cell fire at a pacemaker 7Hz. Removing the depolarising current causes the cell to return to its original firing rate of 3Hz, the long interspike interval is caused by the high calcium concentration sustained by the high firing rate strongly activating the I_{ahp}.

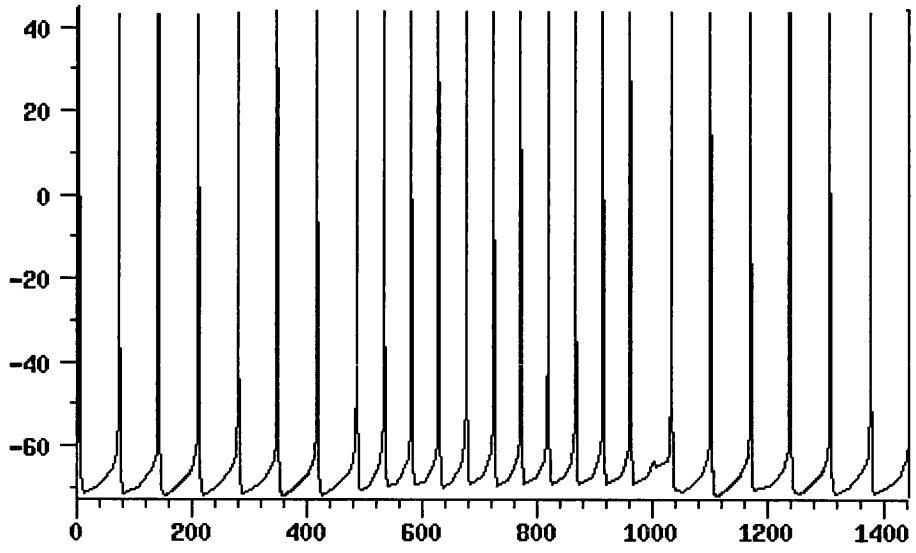

Figure 3.8: For a cell injected with EGTA, thereby mopping up the intracellular free calcium that would activate the I_{ahp}, the injection of depolarising current between 500 and 1000ms simply increases the firing rate.

In contrast we may simulate the effect of injection of the calcium buffer EGTA into the cell by reducing the time constant of the calcium pump, reflecting a quick removal of intracellular free calcium. For such a cell, the injection of depolarising current causes a switch between two rates of pacemaker firing with no noticeable transients, see Figure 3.8. This is consistent with the experimentally observed response to depolarising current in EGTA-treated cells [27].

3.6.3 Induced Burst Firing

The computer model has supported our hypothesis thus far. The undisturbed cell merely fires as a pacemaker and it will not be perturbed from this, simply because there is no mechanism that would cause this. However we can see that sufficient disturbance of the cell, either by an imbalance of initial conditions for the simulation or injections of depolarised current, can create burst-like phenomena although these are only transient occurrences.

It is apparent that regular discrete stimulation of the cell may then create the combination of irregular firing and bursting that we seek. We therefore examined the response of the simulation to discrete depolarising stimuli. Using a depolarising current to force an action potential at some point in a simulation run produced two different responses depending on the levels of intracellular calcium reached by the forced influx. A forced spike that produced little calcium-induced inactivation of the rectifying channel responded with a longer following

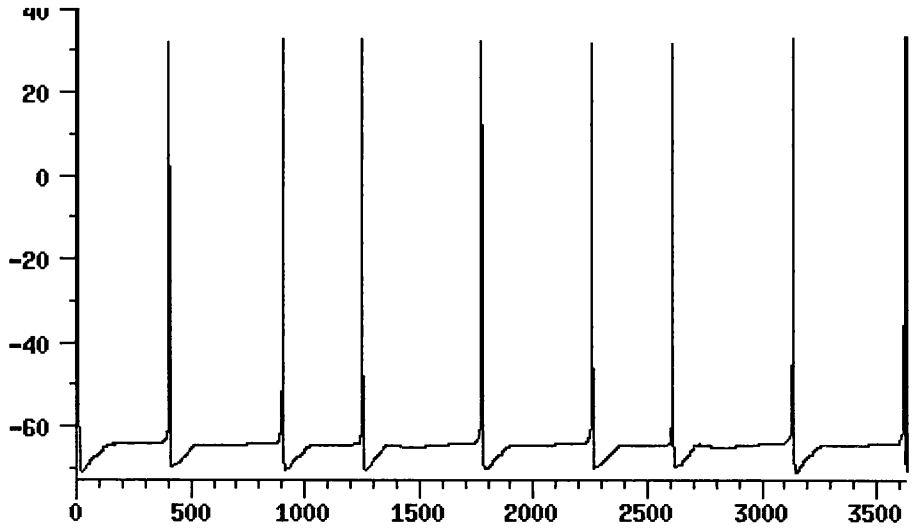

Figure 3.9: The irregular firing that the simulation is capable of, the third and seventh spikes have been forced by depolarising current. This does not change to firing rate of the cell since the shortening of an interspike interval produced by forcing a spike is compensated for by the ensuing delay caused by increased activation of the I_{ahp}.

interspike interval, simply caused by the elevated calcium concentrations activation of the I_{ahp}. The cell then returns to pacemaker firing. However, the shortened interspike interval caused by forcing a spike followed by a longer one is similar to the irregular firing that is seen in cells *in-vivo* [35] and one can produce such a pattern consistently by forcing spikes at arbitrary times in the simulation run. This is illustrated in Figure 3.9 where the third and seventh spikes were forced by the application of depolarising current. We also note that the forcing of spikes occasionally in this manner does not significantly affect the firing rate of the cell as the increased interspike interval following a forced spike approximately makes up for the shortened interval caused by prematurely generating an action potential. The cell in Figure 3.9 fires at a rate of about 2.33Hz for the irregular firing pictured and for undisturbed pacemaker firing.

A different effect may be produced if the forced spike causes a large amount of inactivation of the rectifying channel. In such circumstances, the cell can produce a startlingly good representation of a burst [27]. Examples may be seen in Figures 3.10 and 3.11, where the forcing of a spike causes a further three or four to be generated before a long afterhyperpolarisation. Interspike intervals do increase as the burst progresses and as hypothesised this is due to an increasing level of activation of the I_{ahp}. Spike width also increases from about 3.0 to 3.2ms in the burst in Figure 3.10 and the spike height does progressively decrease by a few

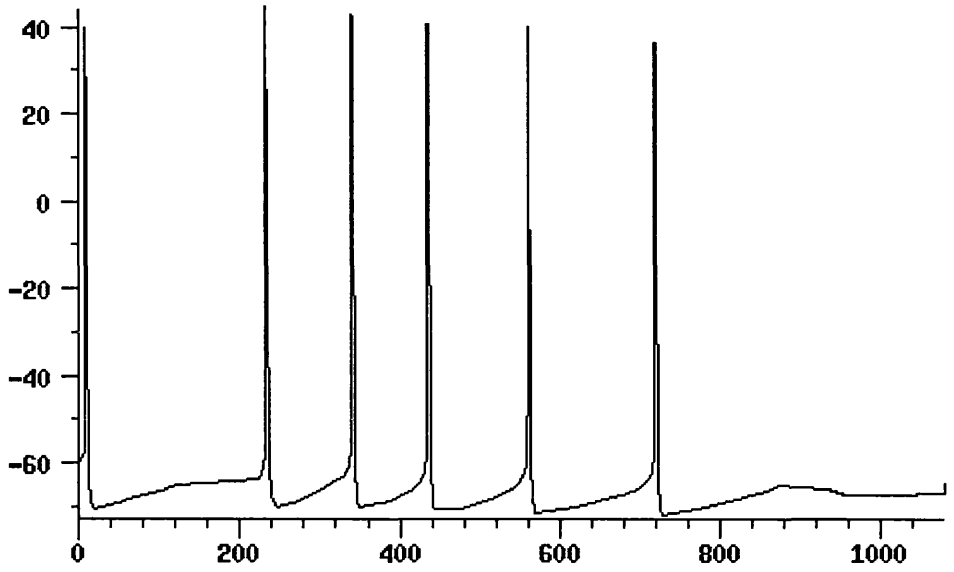

Figure 3.10: The simulation can generate a realistic burst of five spikes when an action potential is forced 200ms after a normal spike. The burst has the increasing interspike interval, spike width and decreasing spike height of experimentally observed burst. The burst is followed by an afterhyperpolarisation of about 400ms duration.

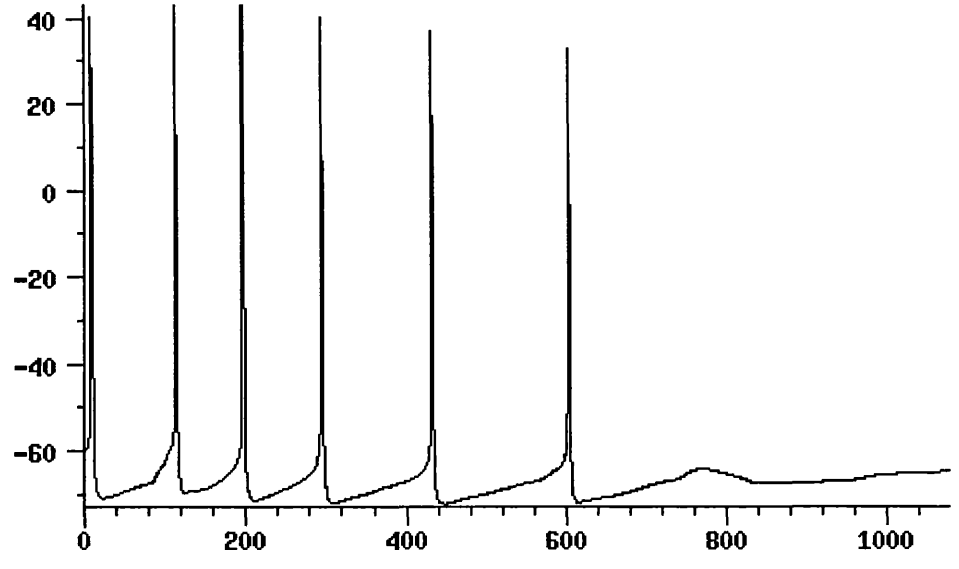

Figure 3.11: The simulation can generate a realistic burst of six spikes when an action potential is forced about 50ms after a normal spike. The burst has the increasing interspike interval, spike width and decreasing spike height of experimentally observed burst. The burst is followed by a long (500ms) afterhyperpolarisation.

millivolts. After the afterhyperpolarisation, the cell returns to pacemaker firing. However, one can see from this that a regular forcing of spikes could cause a realistic and sustained burst / irregular firing pattern.

The distance between a normal, unforced spike and the forced spike provides an index to the number of spikes in a burst as illustrated by Figures 3.10 and 3.11 where a gap of 200ms produces a 5-burst and a gap of 50ms produces a 6-burst respectively. This is quite reasonable since the closer together the spikes, the higher the level of calcium and the lower the I_{ahp} activation at the start of the burst, thus giving the burst more opportunity to fire many spikes. This would support the consideration of irregular firing to be a burst of one spike. Such a mechanism provides a neat explanation of how a single cell may produce a mixture of irregular firing and bursts of varying numbers of spikes, it merely depends on the interval between a normal spike and a forced one.

Imposing a fast calcium pump, which reflects the fast (in comparison to the period of the cell) buffering of free intracellular calcium wipes out the ability of the cell to burst. The reason is simple, the calcium level is never at a sufficiently high concentration to cause inactivation of the I_{dr}. Similarly the I_{ahp} is maintained at a low level of activation by the small calcium concentration and so the cell fires like a pacemaker, as is observed experimentally [27]. Forcing an action potential does not cause any change in pattern save for the shortened interspike interval that immediately precedes it.

3.6.4 Conclusions

The computer simulation has demonstrated that the hypothesis of a calcium-inactivation rectifying channel can lead to very realistic bursting effects if the cell is suitably perturbed by an excitatory stimulus. We can produce bursts consisting of varying numbers of spikes which is dictated by the length of the interval between the normal and forced spikes. The burst spikes get shorter and fatter as the burst progresses, with increasing interspike intervals and a following afterhyperpolarisation caused by the activation of the I_{ahp}.

In this sense we can see that the elevated calcium hypothesis is a robust one. However it is also clear that in this simulation sustained bursting or irregular firing needs the excitatory stimulus. Even by slight variations in the parameters we have used for the simulation we have not been able to sustain burst firing with any level of depolarising current injection. The requirement for external stimuli does agree with our initial opinion and the experimental observations under the blocking of EAA input with kynurenate [15] [34]. One can see from

the computer simulation that our reasoning behind this is also correct; for a burst to occur we need the calcium concentration to be elevated way above the activation of the I_{ahp} and there is no other mechanism present that could cause this perturbation.

In the simulation of an unperturbed system the I_{ahp} activation always rises to match the calcium level and so prevent any attempt at an intrinsically generated 'early' spike that could produce a burst. We could suppose that whatever combination of calcium-dependent inactivation or activation we used, that such a system would always find a 'happy medium' between the calcium activation and inactivation mechanisms and so pacemaker fire. Of course the computer model only produces a realisation of one set of parameters that happen to give qualitatively (and to some extent quantitatively) similar firing patterns.

3.7 Difference Equation Model of Bursting

3.7.1 Simplification of the Computer Model

The system of non-linear ordinary differential equations that forms the computer model requires numerical solution and hence is restricted to the quantitative results for a specific set of parameters. Although we may freely change these parameters to any values we wish, we still require a simplification of this model that enables us to analyse the results for a class of parameters.

Our major simplification comes from the observation that we do not need to follow the change of membrane potential with respect to time, it is the tracing of the potential through action potentials and other non-linear phenomena that makes the model analytically intractable. Instead we can deduce the firing pattern of a cell entirely by knowing the interspike intervals. If we assume that there are no (discrete) external stimuli, then given the state of the system immediately after an action potential and that we know all the influences on the cell, we may be able to estimate the time taken for the membrane potential to rise to spike threshold. Continuing this we may then be able to calculate the state after this action potential and so iteratively derive the entire firing pattern of the cell.

Hence we wish to solve for the time taken for the cell to rise from the hyperpolarised membrane potential following an action potential (v_L) to the threshold voltage (v_U). For a cell with membrane capacitance C_m, the total charge transfer required is given by

$$Q = C_m(v_U - v_L). \tag{3.53}$$

Hence by integrating equation (3.7), we wish to solve

$$Q = \int_0^T I_{\text{tot}}(c(t), V_m(t), t)dt \tag{3.54}$$

for T, where I_{tot} is the sum of all the channel currents in the cell.

This is still a non-linear problem, with the currents being non-linear functions of membrane potential and calcium concentration, each a function of time themselves. The calcium concentration is easily obtainable if we assume that there is only significant calcium influx during a spike, with the implication that during the interspike interval there is negligible influx from the I_{sd} and I_{sp}. Hence the calcium will decay exponentially. Realising that due to the base firing rate of the cell, there may be some base level of calcium c_b, we are then just required to solve

$$\frac{dc}{dt} = \frac{c_b - c}{\tau_c} \quad c(0) = c_0 \tag{3.55}$$

which has the simple solution

$$c(t) = c_b + (c_0 - c_b)\exp\left(-\frac{t}{\tau_c}\right). \tag{3.56}$$

Using this solution we can then solve for the I_{ahp} activation, a

$$\frac{da}{dt} = \frac{c(t) - a}{\tau_a} \qquad a(0) = a_0 \tag{3.57}$$

which has the solution

$$a(t) = c_b + \alpha_0 \exp\left(-\frac{t}{\tau_a}\right) + (a_0 - \alpha_0 - c_b)\exp\left(-\frac{t}{\tau_c}\right) \tag{3.58}$$

$$\alpha_0 = (c_0 - c_b)\frac{\tau_c}{(\tau_c - \tau_a)}. \tag{3.59}$$

Hence we may substitute these into equation (3.54). In this situation we need to use a simpler function for calcium-induced inactivation of the rectifying current, $h(c)$. We may use a piecewise linear approximation of the Boltzmann curve used (equation (3.24)) in the computer simulation.

The dependencies of the channels on membrane potential are not so straightforward, in particular the time course of membrane potential is not known *a-priori*. However we can approximate these as follows. We are only examining a small voltage range (see, for example, Figure 3.5 where the interspike interval covers only a small range of membrane potentials) and so we may approximate the non-linear steady state voltage dependencies of the channels with a linear function of voltage. Many of the channels, such as the I_{ahp} and I_{ga} are linear

function of membrane potential anyway, the other voltage dependencies are approximately linear over the small potential range, although if desired we could use a piecewise linear description.

We then assume that the voltage may be approximated by a piecewise linear function with n pieces, where between voltages v_{L_i} and $v_{L_{i+1}}$ it has the form

$$v(t) = v_{L_i} + r_i t \tag{3.60}$$

$$r_i = \frac{(v_{L_{i+1}} - v_{L_i})}{T_i} \tag{3.61}$$

noting that

$$v_{L_0} = v_L, \quad v_{L_{n+1}} = v_U, \quad \sum_{i=0}^{n} T_i = T. \tag{3.62}$$

Assuming this form for the path of the membrane potential and the linear approximation of $s_\infty(V_m)$ allows us solve for the I_{sp} inactivation parameter $s(t)$ (given an initial value s_0, the inactivation of the channels immediately following an action potential). We may then write the channel currents purely as integrable functions of t. Hence on any interval $(v_{L_i}, v_{L_{i+1}})$ we can perform the integration on the RHS of equation (3.54) and given the initial values for calcium (c_0), I_{ahp} activation (a_0) and the hyperpolarised and threshold voltages (v_L and v_U), with an appropriate mesh of v_{L_i}'s we may solve for each T_i and hence for T. It follows that if our estimation of the function $v(t)$ and associated mesh accurately models the time dependent change in voltage, then the estimate of T will be accurate to the interval calculated by the simulation.

Suppose we take the voltage mesh to be the same for each interval, this merely assumes it is fine enough to give a good approximation of any of the voltage paths we could encounter. If our cell is pacemaker firing, then each spike is identical and the inactivation of the I_{sp}, $s(t)$ is identical at each of the first points in the mesh (each v_L). If the cell is bursting then the spikes are by definition different and this will not hold, although the amount of variation is quite small according to our model.

Let us assume for the moment that the cell is firing as a pacemaker, in which case s_0 is identical for each interspike interval. Then T may be regarded solely as a function of the initial calcium concentration c_0 and I_{ahp} activation a_0 since all other variables are now fixed. Once T is calculated for a given c_0 and a_0, we may then calculate the next interval given the 'next initial' conditions, c_1 and a_1 say. We know how these amounts vary with time and so

we may calculate what these values will be, namely:

$$c_1 = c(T) + c_{\text{sp}} \tag{3.63}$$

$$a_1 = a(T) \tag{3.64}$$

that is the new calcium concentration is the amount that was present as the cell reached spike threshold (clearly $c(T)$) and the amount the calcium concentration is increased by a single action potential, c_{sp}, which we will assume to be constant. Since the action potential is very fast compared to the time constant of activation of the I_{ahp} the activation will be unchanged by the action potential.

It is therefore clear that given a starting calcium concentration c_0 and I_{ahp} activation a_0 we may calculate the corresponding interspike interval T_0 and thus c_1 and a_1. Hence we may iteratively calculate all of the subsequent interspike intervals and so derive the entire firing pattern of the neuron.

We compared the predictions of this model to the results from the simulation, using a simple mesh in which the voltage was approximated by two linear functions. This model did accurately predict the interspike intervals of the simulation for a range of parameter choices. Inaccuracies would occur at parameter choices far from those that have previously been used in the simulation. At such parameter choices it was apparent that the membrane potential was not well approximated by the mesh used. Improving the mesh consistently improved the accuracy of the results. This is not surprising, since equation (3.54) is exact and so the better we may approximate $I_{\text{tot}}(t)$ (by better piecewise linear approximation) the better our predictions of T.

Hence we have reduced the system of non-linear ordinary differential equations requiring numerical solution to a system of algebraic equations that can calculate the interspike intervals and therefore the firing pattern of the cell to any desired accuracy.

3.7.2 Generality of the Algebraic Model

It may not be particularly clear why this algebraic model is an improvement on the computer model since we cannot write down an explicit form for T, the comparisons briefly described above still required a computer to solve for it. However, the computer model is highly dependent on the specification of the ion channels and their non-linear dependence on voltage. Here we are only considering a small range of voltage where these currents can be approximated

by linear functions of the form $I_j = g_j(e_j - v(t))$ and for those channels that are functions of membrane potential only (all those apart from the I_{dr} and I_{ahp}) g_j and e_j are constant.

For a collection of N such channels, they can be expressed in the form of a single channel I_o, where

$$\begin{aligned} I_o &= G(E - v(t)), && (3.65)\\ G &= \sum_{j=1}^{N} g_j, && (3.66)\\ E &= \frac{1}{G}\sum_{j=1}^{N} g_j e_j. && (3.67) \end{aligned}$$

Hence in our algebraic model we may combine all channels that do not involve calcium into this channel I_o and we then wish to solve

$$Q = \int_0^T I_{\text{ahp}}(t) + I_{\text{dr}}(t) + I_o(t)dt \tag{3.68}$$

The only restriction we place on G and E is that they give a solution for T, that is that the cell will fire at sometime in the future. As long as this is true then our analysis below will hold. Therefore any combination of (voltage-dependent) channels that we may wish to endow our model of a dopamine neuron with can be combined to form this single channel without any difference to the analytical results of our model.

Such a class of channels naturally includes the actual combination that a dopamine neuron will have, with regard to both the types of channels present and the parameters used. Hence, with correct assumptions on the behaviour of the I_{dr} and I_{ahp} which shall be covered later, our results are directly applicable to the firing pattern behaviour of mesolimbic dopamine neurons.

3.7.3 Difference Model and Analysis

Firstly we shall express our algebraic model (3.68) as a system of difference equations. That is for calcium concentration c_n and I_{ahp} activation a_n after a spike and previous interspike interval T_n;

$$\begin{aligned} a_{n+1} &= \hat{A}(a_n, c_n, T_{n+1}),\\ c_{n+1} &= \hat{C}(c_n, T_{n+1}), && (3.69)\\ T_{n+1} &= \hat{T}(a_n, c_n), \end{aligned}$$

for appropriate functions $\hat{A}$, $\hat{C}$ and $\hat{T}$. The functions $\hat{A}$ and $\hat{C}$ are known; $\hat{A}(a_n, c_n, T) = a(T)$ with the initial condition $a = a_n$ and $\hat{C}(c_n, T) = c(T) + c_{\text{sp}}$ with the initial condition $c = c_n$, equations (3.64) and (3.63) respectively. The function $\hat{T}$ cannot be written down explicitly but a solution exists and may be numerically solved for if required. The surface $T = \hat{T}(a, c)$ defines a surface in $\mathbf{R}^3$, which we will call the T-surface.

Despite the inability to write down $\hat{T}$ explicitly we may make two assumptions:

1. $\frac{\partial \hat{T}}{\partial c}(a, c) < 0$, that is that elevations in initial calcium concentration will shorten the interspike interval. This is precisely the condition that we hypothesise initiates a burst and hence is a perfectly valid assumption within the range we are interested in. It is possible that for very high levels of calcium (big c) the inactivation of the I_{dr} may have saturated and so the unboundedness of the activation of the I_{ahp} may lead to a contradictory lengthening of the interspike interval. For such a range of c and a bursting is clearly not possible and so this possibility need not concern us.

2. $\frac{\partial \hat{T}}{\partial a}(a, c) > 0$, that is that a raised activation level for the I_{ahp} will tend to lengthen the interspike interval. This is quite apparent since it causes an increased amount of hyperpolarising current.

Existence of a Steady State

We claim that there is a steady state of the system (3.69) on the T-surface. We first observe that for every initial calcium concentration $c^* \in (c_b + c_{\text{sp}}, \infty)$, there exists a time T^* such that $\hat{C}(c^*, T^*) = c^*$. This merely states that for any (above baseline) initial concentration of calcium, the calcium level will decay to $c^* - c_{\text{sp}}$ within a finite amount of time T and be returned to initial levels by an instantaneous action potential.

Moreover for a combination of c^* and T^*, there then exists $a^* \in (c_b, \infty)$ s.t. $\hat{A}(a^*, c^*, T^*) = a^*$. That is there is an initial level of activation of the I_{ahp} that, when combined with the calcium concentration of initial value c^* has the same activation after time T^*. Note that we can refine the legitimate range of a^* to $a^* \in (c^* - c_{\text{sp}}, c^*)$. If this point (a^*, c^*, T^*) lies on the T-surface, then it represents a steady state of the system of non-linear difference equations (3.69).

Let $\mathbf{T}$ be the line in $\mathbb{R}^3$ defined by (a^*, c^*, T) where for a chosen c^*, there is a corresponding T^* and hence an a^*, but T is then chosen to ensure that the point lies on the T-surface.

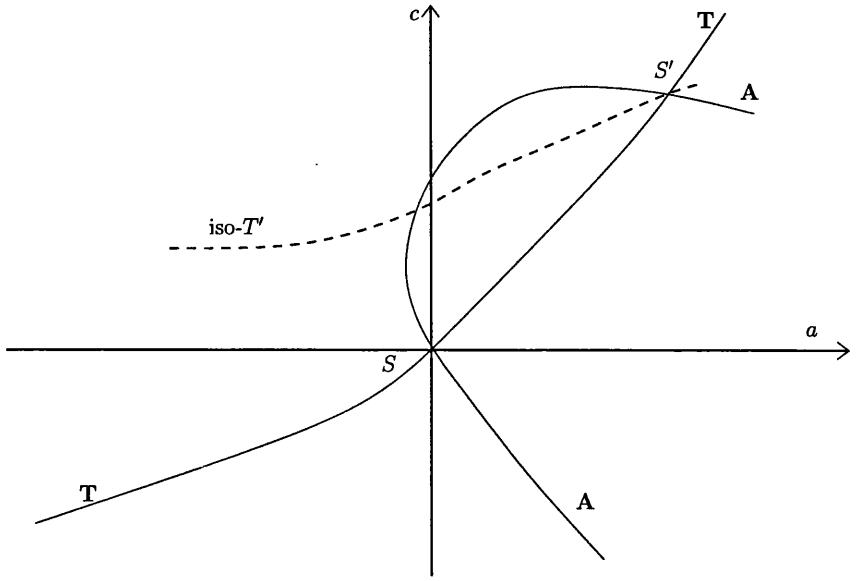

Figure 3.12: Projection onto the (a, c)-plane of the T-surface for the system of equations 3.69. This diagram shows that assuming the existence of two steady states S and S' leads to a contradictory crossing of **A** by the same time line, iso-T'.

Similarly define the line **A** (a variable). Then any crossing of these two lines identifies a steady state on the T-surface and therefore a steady state for the system (3.69).

Note that the 'graph' function for **T**; $\mathbf{T}(c^*) \mapsto (a^*, c^*, T)$ is continuous by the continuity of $\hat{A}(\cdot)$, $\hat{C}(\cdot)$ and $\hat{T}(\cdot)$ and hence the line **T** has no discontinuities. And moreover that $\mathbf{T}(c^*)$ defines a unique point on the T-surface. Similar conclusions apply to the line **A**.

Consider a steady value for the initial calcium concentration c^* and corresponding steady time T^*. Then $\hat{C}(c^*, T) \in (c^* - c_{\text{sp}}, c^*)$ for all $T \in (0, T^*)$. Hence for any corresponding a^*, $a^* \in (c^* - c_{\text{sp}}, c^*)$. Hence **T** is bounded in the (a, c)-plane and on the T-surface by the lines $a = c$ and $a = c - c_{\text{sp}}$.

The smallest theoretical value for c^* is clearly $c_b + c_{\text{sp}}$ with corresponding steady time $T^* = \infty$. Noting that $\frac{\partial \hat{T}}{\partial a}(a, c) > 0$ we see that for small c^* values the line **A** must lie at high a values on the T-surface. In fact we can assume that there exists c^* sufficiently small such that $(a, c^*, T^*) \in \mathbf{A}$ and $a > c^*$.

We now claim that **A** also lies arbitrarily close to the line $a = c_b$. Suppose not and that the point (a_0, c^*, T^*) is the point of **A** closest to $a = c_b$. Then the point on the T-surface (c_b, c^*, T_0) has the property that $T_0 < T^*$ because $\frac{\partial \hat{T}}{\partial a}(a, c) > 0$. Hence there exists $c_1 = c^* + \varepsilon$, for some $\varepsilon > 0$ and $T_1 \in (T_0, T^*)$ such that there exists a_1 with $(a_1, c_1, T_1) \in \mathbf{A}$ and $a_1 < a_0$. This establishes the contradiction.

This then establishes that the line **A** extends arbitrarily close to the line $a = c_b$ for values of c greater than $c_b + c_{\text{sp}}$. Therefore there is a point of **A** on the T-surface for all $a \in (c_b, \infty)$ and so it crosses the lines $a = c$ and $a = c - c_{\text{sp}}$. Hence it must also cross **T** at some point, establishing the existence of at least one steady state.

Uniqueness of the Steady State

We claim furthermore that the steady state is unique. Take a steady state of the system (3.69), letting it be denoted by the point $S^* = (a^*, c^*, T^*)$. By definition the lines **A** and **T** go through this point.

At the steady state; let us assume that **A** crosses **T** from right (positive a) to left (negative a). For the existence of another steady state (denoted S') **A** must 'curve back round' to meet **T** again, as in Figure 3.12. This will have steady time $T' < T^*$. The line of equal times, iso-T' must then exit the closed loop of **A** and **T** through **A** since $T' < T^*$, that is it must cross **A** twice. This is a contradiction since the combination of steady c and T is unique by equation (3.63).

If **A** and **T** cross in the opposite direction then the same argument applies by observing that the iso-T^* line must cross **A**. We have therefore shown that the lines **A** and **T** can cross at most once. Hence the steady state is unique.

Attractivity and Stability of the Steady State

Our proof of attractivity and stability of the unique steady state can be summarised as follows, with reference to Figure 3.13. The line **W** on the T-surface extends from low a and c values, through the steady state and on to high values of a and c. If **W** presents a wall to the trajectory, in the sense that initial points above **W** in the upper-right quadrant from the steady state cannot cross it and those below **W** in the lower-left cannot cross into the upper-left, then all trajectories must (ultimately) tend to the steady state. Since perturbations from the steady state are bounded this attractivity also implies stability. We shall make one simplification, that without loss of generality we take $c_b = 0$ since is merely a translational shift in the calcium and I_{ahp} activation values.

We shall first consider a point (a_0, c_0, T_0) in the upper-right quadrant from (a^*, c^*, T^*) in the (a, c)-plane that is on this **W** and gives rise to the next point (a_1, c_1, T_1). We will suppose for the moment that this point also lies in the upper-right quadrant. If **W** is such that for

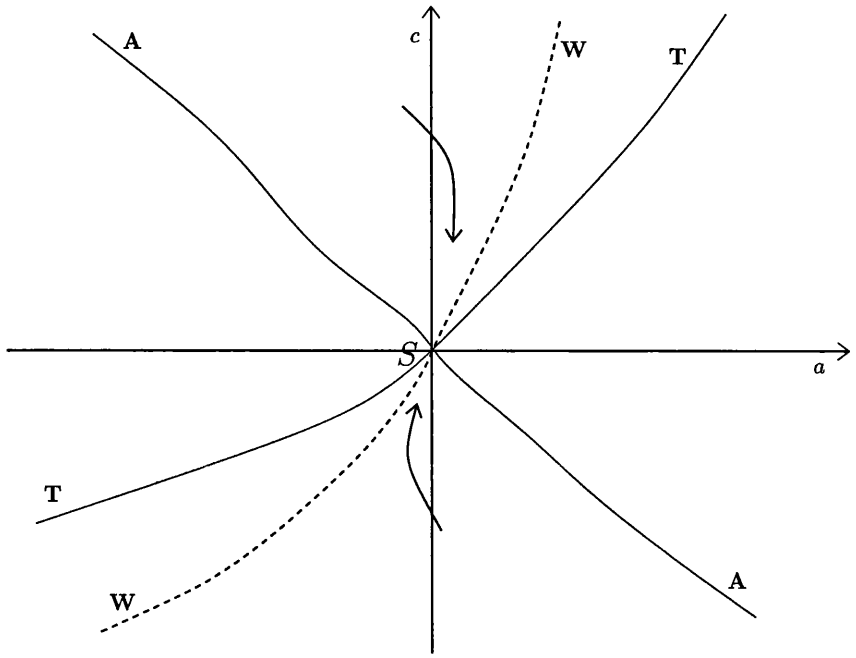

Figure 3.13: Projection onto the (a, c)-plane of the T-surface for the system of equations 3.69, showing the presence of the wall **W** that forces all trajectories to the steady state S.

all points $c > c^*$ it lies to the right of **A**, then the interspike interval T_0 is too large to be steady with a_0 and c_0, by an over shoot of t_a and t_c respectively. Hence we may ignore the first $T_0 - t_a$ and $T_0 - t_c$ of their respective trajectories as these leave a and c at their original values. Hence c_1 and a_1 may be given by

$$c_1 = c_0 \exp\left(-\frac{t_c}{\tau_c}\right) \tag{3.70}$$

$$a_1 = a_0 \exp\left(-\frac{t_a}{\tau_c}\right) + \alpha_0 \left(\exp\left(-\frac{t_a}{\tau_a}\right) - \exp\left(-\frac{t_a}{\tau_c}\right)\right). \tag{3.71}$$

If we denote the equation of the line **W** in the (a, c)-plane by

$$a = W(c) \tag{3.72}$$

then $a_0 = W(c_0)$ and the new point (a_1, c_1, T_1) lies above **W** if

$$W(c_1) - W(c_0) \exp\left(-\frac{t_a}{\tau_c}\right) - \alpha_0 \left(\exp\left(-\frac{t_a}{\tau_a}\right) - \exp\left(-\frac{t_a}{\tau_c}\right)\right) > 0 \tag{3.73}$$

which may be written purely in terms of c_0 as

$$W\left(c_0 \exp\left(-\frac{t_c}{\tau_c}\right)\right) - W(c_0) \exp\left(-\frac{t_a}{\tau_c}\right) - c_0 \frac{\tau_c}{\tau_a - \tau_c} \left(\exp\left(-\frac{t_a}{\tau_a}\right) - \exp\left(-\frac{t_a}{\tau_c}\right)\right) > 0. \tag{3.74}$$

If, in the upper-right (a, c) quadrant, $\mathbf{W}$ lies to the left of $\mathbf{T}$, then

$$t_c < t_a \tag{3.75}$$

and so we may write

$$\begin{aligned} &W\left(c_0 \exp\left(-\frac{t_c}{\tau_c}\right)\right) - W(c_0)\exp\left(-\frac{t_a}{\tau_c}\right) - c_0\frac{\tau_c}{\tau_a - \tau_c}\left(\exp\left(-\frac{t_a}{\tau_a}\right) - \exp\left(-\frac{t_a}{\tau_c}\right)\right) \\ &> W\left(c_0 \exp\left(-\frac{t_a}{\tau_c}\right)\right) - W(c_0)\exp\left(-\frac{t_a}{\tau_c}\right) - c_0\frac{\tau_c}{\tau_a - \tau_c}\left(\exp\left(-\frac{t_a}{\tau_a}\right) - \exp\left(-\frac{t_a}{\tau_c}\right)\right) \end{aligned} \tag{3.76}$$

eliminating the two different times t_a and t_c and giving us a sufficient condition for (a_1, c_1, T_1) to lie above $\mathbf{W}$ of

$$W\left(c_0 \exp\left(-\frac{t_a}{\tau_c}\right)\right) - W(c_0)\exp\left(-\frac{t_a}{\tau_c}\right) - c_0\frac{\tau_c}{\tau_a - \tau_c}\left(\exp\left(-\frac{t_a}{\tau_a}\right) - \exp\left(-\frac{t_a}{\tau_c}\right)\right) > 0 \tag{3.77}$$

Noting that this has zeros at $t_a = 0$ and $t_a = \infty$, the sign of the expression (3.77) is determined by the sign of the derivative with respect to time evaluated at $t_a = 0$. That is, for the positivity of (3.77) we require

$$\begin{aligned} -\frac{dW}{dc}(c(t_a))\frac{c(t_a)}{\tau_c}\exp\left(-\frac{t_a}{\tau_c}\right) + \frac{W(c(t_a))}{\tau_c}\exp\left(-\frac{t_a}{\tau_c}\right) - \\ c_0\frac{\tau_c}{\tau_a - \tau_c}\left(\frac{1}{\tau_c}\exp\left(-\frac{t_a}{\tau_c}\right) - \frac{1}{\tau_a}\exp\left(-\frac{t_a}{\tau_a}\right)\right) > 0, \end{aligned} \tag{3.78}$$

which, with $c(t_a) = c_0$ at $t_a = 0$, fortunately reduces to

$$W(c) > c\left(\frac{\tau_c}{\tau_a} + \frac{dW}{dc}(c)\right). \tag{3.79}$$

This gives a condition on the wall $\mathbf{W}$. If we solve (3.79) for equality and add a small amount $\varepsilon > 0$ to force the correct inequality, along with the condition $a^* = W(c^*)$ we obtain

$$W(c) = \left(\frac{\tau_c}{\tau_a}c + 1 + \varepsilon\right) + k(\varepsilon)\exp(-c) \tag{3.80}$$

$$k(\varepsilon) = \exp(c^*)\left(a^* - \frac{\tau_c}{\tau_a}c - 1 - \varepsilon\right). \tag{3.81}$$

We observe that $W(c)$ is an increasing function of c with maximum gradient $(\tau_c/\tau_a) < 1$ and the projection of $\mathbf{T}$ onto the (a, c)-plane has minimum gradient 1, so $\mathbf{W}$ does indeed lie between $\mathbf{A}$ (which with respect to the (a, c)-plane has a negative gradient) and $\mathbf{T}$ as required. Moreover, by the definition of $\mathbf{W}$ (and $W(c)$), the point (a_1, c_1, T_1) does indeed lie in the upper-right quadrant.

We now consider any point above $\mathbf{W}$ in the upper-right quadrant (a, c, T). Consider the point obtained by projecting (a, c, T) along the a-axis onto $(a_W, c, T_W) \in \mathbf{W}$. Since $T_W > T$

and $a_W > a$ the next point in the trajectory with initial conditions (a, c, T) lies at a smaller a and larger c than that with initial conditions (a_W, c, T_W), by equations (3.63)-(3.64), and hence stays above **W**.

Hence we have shown that there exists a line, denoted **W**, in the quadrant $a > a^*$ and $c > c^*$ that prevents trajectories crossing it. All trajectories that pass through this region must therefore tend to the steady state.

We must now establish the existence of a similar wall in the lower-left quadrant of the (a, c)-plane that prevents trajectories passing through the region below to cross it. We may follow a similar analysis to the above to establish the presence of this line, it is not surprising to discover it is also described by $a = W(c)$, for $c < c^*$. This necessarily requires the establishing of conditions similar to (3.77), (3.78) and (3.79) but with the inequality reversed. This follows simply from observing that in this region $t_c < t_a < 0$, since the interspike interval is too small to be steady for the initial conditions.

This line **W** cannot guarantee a complete block of trajectories at low a values where the interspike interval can be small. This is because our analysis has assumed that

$$\frac{\partial \hat{A}}{\partial T}(a, c, T) < 0 \tag{3.82}$$

as regards steady values of a. This is on the basis that bigger values of T than are required to be steady will cause further decay of the activation, a. This is not true for sufficiently small values of T, where a can be on its initial climb towards the calcium level c. In this case the sign is reversed and our analysis no longer applies.

This possible problem need not concern us, since this situation cannot arise for points sufficiently close to the steady state. This is all we need to establish the attractivity and stability of the steady state, any trajectories that can escape **W** in the lower left quadrant by having sufficiently small interspike intervals T are still bounded and will then be 'caught' by the portion of **W** in the upper-right quadrant.

We have mentioned that perturbations from the steady state are bounded but have not indicated why. This can be seen by considering the initial point (a_0, c_0, T_0) in the lower-right quadrant of the (a, c)-plane, as Figure 3.14. The interspike interval T_0 is too small for a steady a and c and hence both of these values increase. Consider the point obtained by the projection of this along the c-axis to $(a_0, c_A, T_A) \in \mathbf{A}$. This point has a higher initial c since $c_A > c_0$ and a smaller interspike interval, $T_A < T_0$ and so it must lead to a higher subsequent c value. However, by the definition of **A**, c is steady on this line and so c_A represents an

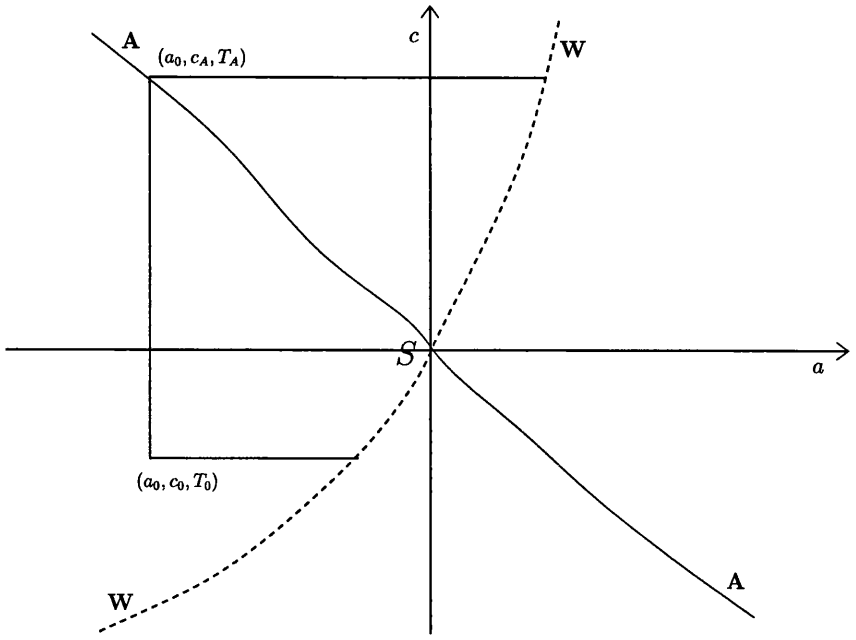

Figure 3.14: Projection onto the (a, c)-plane of the T-surface for the system of equations 3.69, showing how the trajectory for an initial point (a_0, c_0, T_0) is bounded by its projection to the line **A**, (a_0, c_A, T_A) and the line **W**.

upper bound for c. The trajectory for the point (a_0, c_0, T_0) is then bounded within the region $c < c_A$ and **W**.

This boundedness of trajectories gives us the asymptotic stability of the steady state when combined with the attractivity. Therefore, whatever the initial conditions, all trajectories will tend to the steady state and stay there unless the system is regularly perturbed. Hence the only possible firing pattern for an undisturbed cell is one with a constant interspike interval, that is pacemaker firing.

3.8 Review

We have been able to produce a mathematical model of a dopamine neuron that displays a burst-like pattern in accordance with the experimental observations. This modelling was based both on experimentally derived hypotheses and ideas of our own, principally a requirement for an external stimulus. We have shown further that this perturbation to the model is necessary for any pattern other than a regular one to be obtained. The results that we have thus derived are based on many assumptions that we should now discuss.

3.8.1 The Irregular Firing Pattern

We have been fortunate with the extent of the experiments performed by Grace and Bunney [28] [27]. This has provided a wealth of (largely qualitative) information on the nature of bursting in mesolimbic dopamine neurons and they have even advanced their own hypothesis on what causes bursting. We can use this as a starting point for our own investigation.

We have shown that the calcium-inactivation of the I_{dr} hypothesis that Grace and Bunney propose leads to good bursting patterns when combined with a suitable perturbation. This idea for a perturbation is largely based on our model of the irregular firing (section 3.3); a model in which we consider the pattern obtained by the interaction of a periodically firing cell with a calcium-dependent potassium channel and an external stimulus. We first considered the inclusion of an external driving force because we could not see any particular reason why the irregular firing cell may generate action potentials unexpectedly early and so this model was developed. This is backed up by the experimental evidence of Charlety et al [15] and Grenhoff et al [34], demonstrating that bursting is attenuated by the blocking of glutamatergic input to the cells, without significantly affecting the overall firing rate.

The model is interesting because, despite its simplicity it provides many of the ideas that we use later in the computer simulation. It assumes a periodic external stimulus that causes an immediate action potential with nice exponential decay of calcium and a fixed amount of delay, an oversimplification of the true system. However, the model does provide the following fundamental idea; that a burst can be caused by a normal action potential and a forced one occurring sufficiently close together.

Such an idea can be consistent with the hypothesis of Grace and Bunney; if a burst is caused by a calcium-inactivation of the I_{dr} (assumed fast), then any mechanism that quickly causes increased calcium levels will enhance the ability of a cell to burst. We then continue our modelling with the realisation of how a burst may, truly, be caused.

3.8.2 The Computer Model

We have now been able to derive what appears to be a fully working hypothesis on the ability of dopamine neurons to burst. The details are given in section 3.4.1 and we consider that we can address every aspect of the firing patterns of mesolimbic dopamine neurons.

We are then required to test this hypothesis and see whether it is genuinely capable of generating bursts and the most straightforward approach is to implement this in a computer

model. This necessarily means modelling the electrical potential of the cell membrane and its constituent ion channels. We do not know the correct voltage-dependencies of the channels, nor the spatial and electrical characteristics of the cell and so clearly cannot attempt a quantitatively accurate model. Instead we must draw from models of ion channels similar to those identified in the experimental preparation and make assumptions on the nature of such mechanisms as the calcium-dependent inactivation of the I_{dr}.

The calcium-dependent inactivation of the I_{dr} is fundamental to the hypothesis on bursting but we do not know what form it may take, the existence of this mechanism has never actually been demonstrated. We have had to assume this and the action of such currents as the slow-depolarisation. The ion channels that we have drawn together are fitted in what we consider to be the most methodical way, endowing us with a simulation in which all the channels influence the qualitative behaviour of the cell as we would expect.

We have thus produced a model consistent with our hypothesis on bursting that produces quantitatively accurate bursting patterns. In the absence of an external stimulus the cell fires in a regular pattern; in its presence the cell can fire irregularly or irregularly in bursts depending on the calcium concentration and the activation of the I_{ahp}. The burst is caused by the calcium inactivating the I_{dr}, progressive activation of the I_{ahp} widens the interspike intervals and causes the afterhyperpolarisation. The reduction in the calcium gradient across the cell membrane does cause a slight shortening of the spike heights and the spikes do get moderately wider.

It is noticeable from our simulation that the closer the forced spike is to the normal one, the more spikes occur in a burst. This is because a sooner spike will lead to a higher level of calcium and hence prompt a faster rate of firing within the burst. This correlation between a shorter initial interspike interval and increasing numbers in a burst is observed experimentally [27]. Indeed our computer model is qualitatively consistent with *all* of the experimental observations made by Grace and Bunney, we have not found any faults with it at all save for slight quantitative errors. This even extends to the ability of depolarising intracellular current injections of >100ms producing bursts, but not those of around 25ms for intracellular current injections of around 1nA.

3.8.3 The Difference Equation Model

The only problem with the computer model is that we have been forced to use specific parameters and forms for the activation of the I_{ahp} and inactivation of I_{dr} and so we cannot

be sure that some variation of the parameters may lead to a spontaneously bursting model cell. We have therefore derived the more general difference equation model.

This model has little dependence on the non-calcium dependent ion channels in the cell, we only require that this combination ensures that there is another action potential at some later time. Our analysis from there on is the same, so the exact make up of the channels used, or that we may have missed some channels out altogether does not actually matter. Moreover we only stipulate that the interspike interval increases with initial calcium concentration and decrease with initial I_{ahp} activation level. This means that we are not making any unsubstantiated claims on the form of these mechanisms.

We write the system as a set of difference equations describing the interspike intervals and initial calcium and I_{ahp} activation levels. We then present a proof that this system has a unique, asymptotically stable steady state. This demonstrates that our computer model is, in general, correct and that the undisturbed cell will only fire in a pacemaker like fashion. Hence the bursting or irregular firing must be generated by a perturbation to the system, such as by a forced action potential.

This rather general result may seem to contradict the ability of cells to produce the other type of 'bursting' described in section 3.2.2 and [56] [17] . Here cells fire a series of spikes followed by a period of quiet and then repeat. This alternating between firing and non-firing states is typically caused by the slow cycle of activation of a calcium dependent potassium channel. This does not seem consistent with our description, which includes a slow activating calcium-dependent potassium channel and one might think suggests that this pattern could not arise. Fortunately it does not suggest this; one of the assumptions of our difference equation model was that the cell is firing repetitively, hence the assumption on the other channels I_o in equation (3.68) that they give a solution for T. Our proof states that when such a cell is firing repetitively, that it will tend to pacemaker fire and says nothing on the behaviour of the cell at levels of excitation that leave it in a non-firing state. We may note that for such 'quiet-active' bursting cells the active phase has a tendency to pacemaker fire, as seen in the models of Miura and de Vries [17] and Bertram et al [56].

3.8.4 Consequences for Nicotine

Although we have covered the ability of a dopamine cell to burst in great detail, we have neglected one of our original aims in examining how nicotine may potentiate bursting (as has been experimentally observed [33]). We have no specific to model the action of nicotine

explicitly as we have clearly established the requirement for the external stimulus forcing an action potential in the dopamine neuron. It is such a stimulus that nicotine potentiates.

Our modelling illustrates that the chance of a cell producing a burst depends on the ability of the stimulus to produce an action potential sufficiently close to a preceding normal spike. A more powerful stimulus (nicotine-enhanced) will lead to more forced, and closer, action potentials which will then lead to more bursts with more spikes in each. Hence nicotine may increase bursting in these cells.

It is an interesting aside to consider the action of opiates on mesolimbic dopamine cells. The opiates (such as heroin) are rewarding drugs that have also been shown to potentiate the release of dopamine [50] [18]. Opiates act pre-synaptically to inhibit the release of the inhibitory neurotransmitter GABA and therefore have an excitatory effect on the dopamine neurons [58]. This poses the question of whether the opiates may potentiate dopamine release from mesolimbic cells by also promoting bursting with their excitatory influence.

The computer model does feature the GABAergic current and the relief from this current can cause action potentials (as it was designed to do) and hence may cause bursting. In fact the bursts seen in Figures 3.10 and 3.11 were actually caused by action potentials produced from a temporary cessation of this current. We can therefore propose that opiates increase bursting in mesolimbic dopamine neurons by a similar method to nicotine.

3.8.5 Summary

Based on one already proposed from extensive experimental observations we have derived a hypothesis for the cause of bursting in mesolimbic dopamine cells. This is that an external excitatory influence forces action potentials within the cell, raising calcium levels sufficiently to partially inactivate a potassium conductance.

A computer model built according to this hypothesis demonstrates bursting patterns that satisfy *all* of the experimentally observed phenomena qualitatively and is in general quantitatively accurate. The need for an external stimulus is verified by a more general difference equation model.

Chapter 4

Sensitisation and Tolerance to Nicotine

4.1 Chapter Overview

Under differing experimental conditions nicotine has been shown to induce both a tolerance and a sensitisation to its effects in laboratory animals. We first consider a model describing the turnover of nicotinic acetylcholine receptors (nAChR) and their transformations, when exposed to nicotine, from active to desensitised and then a slower shift to an inactivated state. By assuming that degradation of the inactivated conformation is reduced, perhaps due to an internalisation of the receptor, we demonstrate that the chronic application of nicotine increases nAChR numbers. However functionality is always reduced and hence a tolerance to the effects of nicotine is developed.

Identifying that the pharmacological aspects of the observed sensitisation to daily injections of acute nicotine have much in common with the phenomenon of long-term-potentiation (LTP), we build a model of a synaptic connection. The glutamate-releasing presynaptic terminal has nAChR, fast sodium and rectifying potassium channels for action potential production and subsequent cell repolarisation and a simple integrate and fire model of transmitter release. The post-synaptic process has both receptors of the NMDA and non-NMDA (AMPA) type. Nicotinic stimulation potentiates the glutamate release causing sufficient post-synaptic depolarisation to release the magnesium block of the NMDAR. The resultant calcium influx leads on to upregulate the AMPAR numbers, potentiating the post-synaptic response. We find that this potentiation can be self-sustaining since the enhanced post-synaptic response

can cause NMDAR activation in the absence of nicotine. We introduce a probabilistic model that aims to quantify the persistence of this sensitised response and demonstrate that it may be maintained indefinitely, which has important implications for nicotine and other addictive drug seeking behaviour.

4.2 Sensitisation and Tolerance

Many researchers have observed that the repeated exposure of laboratory animals to nicotine can produce two conflicting effects. Some experiments demonstrate the development of a tolerance in rats to doses of nicotine [16][60][86], whilst others report a sensitisation to its effects [3][5].

Given the observed desensitisation of nicotinic-acetylcholine receptors (nAChR) in response to prolonged exposure to nicotine [31], the development of a tolerance to its effects may not be that surprising. However the chronic exposure of rats to nicotine leads to a paradoxical upregulation in the number of nicotinic receptors [16][60][102], yet it is suspected that these increased numbers of nAChR are not functional. Although it is not clear, it would appear that such mechanisms would lead to an overall downregulation of nicotinic function and hence lead to a tolerance to nicotine and its effects.

Against these processes that may cause a tolerance to nicotine, there are reports of a contradictory sensitisation to nicotine developing under certain experimental conditions. In particular, daily injections of nicotine have been shown to sensitise mesolimbic dopamine neurons to future challenges [3]. This may be particularly important since the mesolimbic dopamine pathway is supposed to mediate basic drives such as food or sex in mammals and has been widely implicated in drug reinforcement [50]. Drugs of abuse such as nicotine, cocaine, amphetamine and heroin have all been shown to increase the release of dopamine from these neurons [18] and nicotine has been shown to mediate this effect by increasing the firing of bursts by the neurons (as modelled in Chapter 3 with reference to [33]). Therefore the development of a sensitisation to nicotine expressed through the mesolimbic pathway may partially underlie its perceived addictive effects.

The possible importance of tolerance and particularly sensitisation to the neuromodulatory effects of nicotine mean that this is a phenomenon that would be of great interest to model. We shall first investigate the upregulation of nAChR reported in some experimental preparations which we propose may underlie the tolerance to nicotine. We then turn our attention to

modelling a mechanism that may cause a sensitisation to nicotine and this model's relevance to nicotine's apparent addictive effects.

4.3 The Upregulation of Nicotine Receptors

4.3.1 The Experimental Background

In Chapter 2 we modelled the comparatively short-term (10s of seconds) effects of the nicotinic agonist anatoxin-a (AnTx) on rat striatal synaptosomes. Other laboratories have also studied the effects of the prolonged exposure of similar preparations to nicotine. In particular Marks et al [60] exposed mice chronically to nicotine over periods of 3-6 days and observed that, using [H^3]-nicotine to label the $\alpha 4\beta 2$ sub-type of nAChR, the receptor numbers increased.

This increase may seem to be a paradox, since it is largely thought that the over-exposure of a receptor to an agonist will lead to a compensatory decrease in receptor numbers [45]. Marks and others have proposed that the observed upregulation was indeed a compensatory mechanism, but to the shorter-term desensitisation of nAChR [60][86]. nAChR have been observed to desensitise when exposed to nicotine over timescales as short as seconds, and recovery takes place over 10s of seconds to minutes on removal of the agonist. This leads to a temporary downregulation of normal receptor function and it would appear that receptor numbers increase to compensate for this downregulation.

Once the agonist is removed, the nAChR would be expected to re-sensitise faster than the receptor numbers downregulate, which may be expected to lead to an overall increase in the numbers of active $\alpha 4\beta 2$ nAChR. This would lead to a sensitisation of nicotine, however further investigation suggests that these 'new' receptors are not functional, but appear to be in an inactivated form [60] [86]. This is since the overall effect of nicotine appears to be downregulated, indicating that, whatever the individual actions of all these mechanisms and the participation of other nAChR sub-types, they summate to less nicotinic effect.

4.3.2 Modelling the States of Nicotinic Receptors

We have already featured a model of a nicotinic receptor in Chapter 2 (from Lippiello et al [57]). This model allowed each agonist binding site of nAChR to be in one of four states depending on whether it was bound to nicotine or not; and whether the site was in a low-affinity (active) or high-affinity (desensitised) conformation. This model is illustrated in

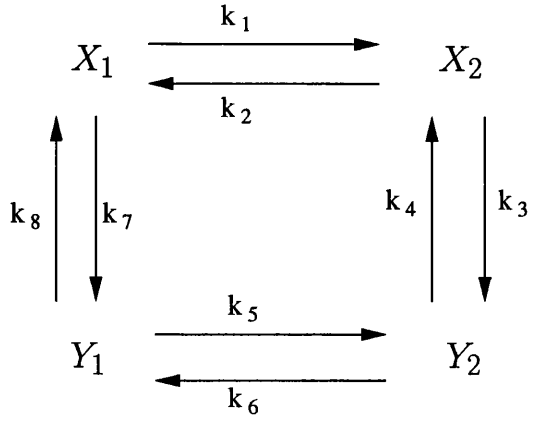

Figure 4.1: Receptor binding site state transition model as proposed by [57]. The sensitised state, unbound and bound is designated by X_1 and X_2 and the desensitised, unbound and bound by Y_1 and Y_2 respectively. For the receptor pore to open, both binding sites must be in the bound and sensitive state (X_2). The constants k_i are determined from experimentation.

Figure 4.1 where, with a view to the modelling we shall be performing, we re-designate the active conformation, unbound or bound, by X_1 and X_2 respectively. Similarly we denote the desensitised conformation, unbound and bound, by Y_1 and Y_2 respectively.

The experimental results of Rowell and Duggan [86] suggest that there is another form of the nAChR, the inactivated form that becomes apparent under chronic exposure to nicotine. This conformation of the receptor does not appear to de-inactivate, or so slowly it is negligible when compared to receptor turnover rates. We therefore propose to extend the model of Lippiello et al [57]to include this possible new state of binding site. We will denote this inactivated conformation, unbound or bound, as Z_1 and Z_2, as illustrated in Figure 4.2.

Since the inactivated state arises from chronic exposure to nicotine we have made the assumption that this form can be obtained from the desensitised conformation only. Clearly there are no experimentally derived values for the additional state transition rates $\{k_i : 9 \leq i \leq 14\}$ but it would seem fair to assume (similar to Lippiello et al did [57]) that $k_5 = k_{11}$ and $k_6 = k_{12}$. This should not particularly concern us since neither of these states is active.

Our interest lies in the rates of change between the desensitised conformation and the inactivated one. The inactivated form is identified because it does not appear to return to an active conformation during timescales (hours) that would be expected to re-activate those in the desensitised conformations. This suggests that the transition rates k_{10} and k_{14} are very small in comparison to the others, indeed we shall assume that $k_{10} = k_{14} = 0$. Since the inactivated form is only noticeable after a few days of chronic nicotine it is apparent that the transition

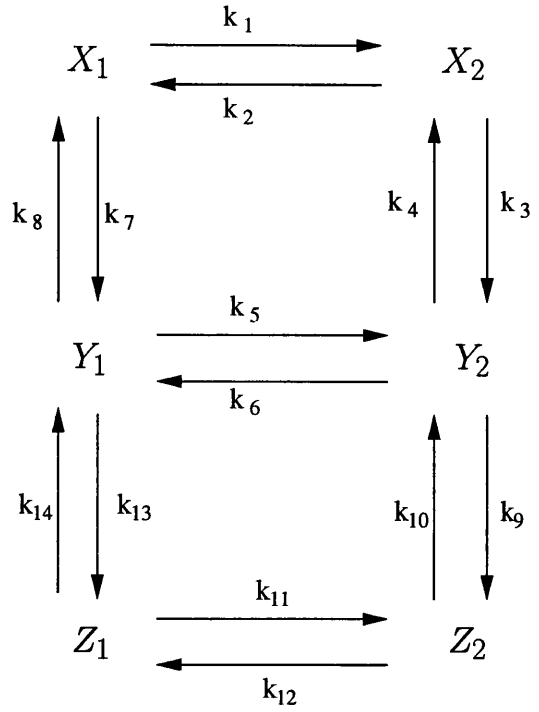

Figure 4.2: Our proposed extension of the Lippiello model from Figure 4.1, the additional inactivated form is denoted by Z_1 (unbound) and Z_2 (bound). The additional k_is are defined in section 4.3.2.

rates from the desensitised to the inactivated conformations are small in comparison to the forward rates k_5 and k_7, but they are significant over timescales of days.

For our purposes we are not particularly interested in whether a receptor binding site is bound or not, but what the total number of binding sites (hence the number of receptors) is. We can therefore define the total number of binding sites in the active conformation X by

$$X = X_1 + X_2 \tag{4.1}$$

and similarly we define

$$Y = Y_1 + Y_2, \tag{4.2}$$

$$Z = Z_1 + Z_2. \tag{4.3}$$

We now consider transitions purely between these conformations. As this will mean studying the proportions of these over timescales of several days we must also consider the production and degradation of receptors, actions that have previously been considered too slow to significantly affect the function of a collection of nAChR.

The binding of nicotine to the binding sites is fast (k_1, k_6 large) in comparison to the transitions to the inactivated form (and to a lesser extent transitions to the desensitised form).

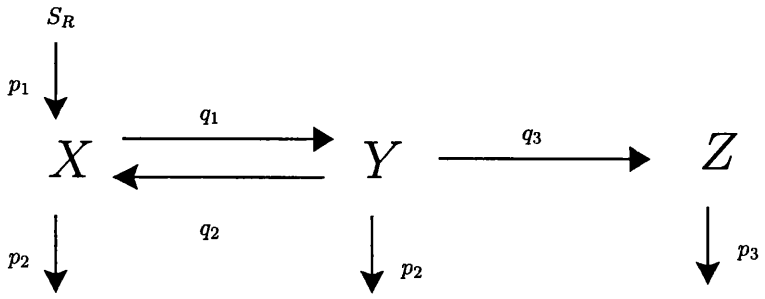

Figure 4.3: Our proposed model for the shifts between binding site forms, combining the unbound and bound states and including receptor production and degradation.

Hence we will assume that the nicotine binding reaches steady state instantaneously, for all conformations, this is the pseudo-steady state hypothesis discussed in Chapter 1. We will further assume that the transitions from X to Y to Z are from the bound states of each conformation at fixed rates q_1 and q_3 and that there is a fixed rate transition q_2 from Y back to X is from the unbound state. We are assuming that transitions out of the Z are impossible, save for receptor degradation. From the above assumptions it can be implied that $q_1 = k_3$ and $q_2 = k_8$.

We suppose that receptors are produced at a rate p_1 from an abundant substrate S_R and that this produces receptors in an active conformation. We assume that the active and desensitised receptors decay with rate p_2 and the inactivated receptors decay with rate p_3. The system is shown schematically in Figure 4.3 and the state transitions are then described by

$$\frac{dX}{dt} = p_1 S_R - p_2 X - q_1 f([n])X + p_2(1 - g([n]))Y, \tag{4.4}$$

$$\frac{dY}{dt} = -p_2 Y + q_1 f([n])X - p_2(1 - g([n]))Y - q_3 g([n])Y, \tag{4.5}$$

$$\frac{dZ}{dt} = -p_3 Z + q_3 g([n])Y. \tag{4.6}$$

where $[n]$ is the concentration of nicotine. The functions $f(\cdot)$ and $g(\cdot)$ are the steady state fractions of the active and desensitised conformations (respectively) bound with nicotine. For the formulation of Lippiello et al described in Chapter 2 and Figure 4.1 these are given by

$$f([n]) = \frac{k_1[n]}{k_1[n] + k_2}, \tag{4.7}$$

$$g([n]) = \frac{k_5[n]}{k_5[n] + k_6}. \tag{4.8}$$

For the synaptosome experiments of Marks et al [60], where a fixed nicotine dose is applied

chronically for days, the steady states of these are relevant. These are given by

$$X^* = \frac{p_1 S_R + q_2 Y^*}{q_1 f([n]) + q_2}, \tag{4.9}$$

$$Y^* = \frac{q_1 f([n])}{q_3 g([n]) + q_2(1 - g([n])) + p_2} X^*, \tag{4.10}$$

$$Z^* = \frac{q_3}{p_3} g([n]) Y^*. \tag{4.11}$$

These may be solved to give X^*, Y^* and Z^* explicitly in terms of the rate constants and nicotine concentration, but the resulting expressions are complicated and we consider that those above give a better picture of the behaviour of the system.

The introduction of a dose of nicotine causes a shift from X to Y and then a slower shift from Y to Z and hence both Y and Z increase with $[n]$. Of particular relevance are the quantities $(X+Y)$ and $(X+Y+Z)$. $(X+Y)$ is the total number of binding sites that are potentially in an activatable state, they are either active or desensitised, in which case they may return to an active state given a sufficient amount of time in the absence of agonist. $(X+Y+Z)$ is the total number of binding sites (and hence $\frac{1}{2}(X+Y+Z)$ is the total number of receptors). We may write

$$\frac{d}{dt}(X+Y) = p_1 S_R - p_2(X+Y) - p_3 Z, \tag{4.12}$$

$$\frac{d}{dt}(X+Y+Z) = p_1 S_R - p_2(X+Y+Z) + (p_2 - p_3) Z, \tag{4.13}$$

with steady states (partial solutions again) given by

$$(X+Y)^* = \frac{p_1 S_R - q_1 g([n]) Y^*}{p_2}, \tag{4.14}$$

$$(X+Y+Z)^* = \frac{p_1 S_R + (p_2 - p_3) Z^*}{p_2}. \tag{4.15}$$

The inactivated conformation (Z) has been hypothesised to be inactive because it may have undergone a structural change or become internalised [86], quite why this may occur is beyond the scope of our model. However if this is so, suppose that the agent that causes the degradation of the X and Y forms is, as a consequence, less effective at degrading the inactivated form. This would seem reasonable if this proposed internalisation causes a separation of degradant from its normal site of action on the cell membrane.

This would imply that X and Y degrade faster than Z and hence $p_2 > p_3$. This in turn implies the following two results; firstly that the total number of binding sites (hence receptors) increases with nicotine concentration $[n]$. This implies that the chronic application of nicotine

will lead to the upregulation of binding site numbers, and on a timescale of around $p_2 - p_3$, less than the decay rate of active receptors and hence taking days to be apparent.

This demonstrates that the simple hypothesis of the inactivated receptor conformation leads to a slow upregulation of receptor numbers, consistent with the experimental observations. We have already assumed that the inactivated variant is not functional. This leads to our second observation; that the number of potentially activatable binding sites $(X+Y)$, hence the number of potentially functional receptors, is a decreasing function of nicotine concentration $[n]$. This follows from Y being an increasing function of $[n]$.

This means that the system displays a functional tolerance to nicotine; not only does the inactivated conformation provide dummy binding sites for nicotine (though we would expect this effect to be small), but the number of functioning receptors is reduced. This suggests that nAChR do display a downregulation in response to chronic agonist after all.

Since the numbers of functional nAChR is monotonic decreasing as a function of nicotine, any concentration will serve to decrease the number of functional receptors and only complete abstinence can restore pre-dosing functionality. This demonstrates that any sensitisation to nicotine that arises does not come from an upregulation in receptor numbers and so the cause of such a phenomenon must lie elsewhere.

4.4 The Experimental Background to Sensitisation

4.4.1 Identifying the Site of Action

Our work thus far has demonstrated that whatever may be the cause of the experimentally observed sensitisation to nicotine it does not appear to be from an upregulation of nAChR numbers, indeed there is evidently a development of a tolerance to nicotinic effects. This rules out a direct upregulation of nicotinic function and so we must look downstream, at the effects that the activation of nAChR have on the cell.

As identified in Chapter 3 and the experimental support referenced therein, the rewarding effect of nicotine is speculated to act through potentiating the release of glutamate, an excitatory neurotransmitter, from terminals making synapses with mesolimbic dopamine neurons [69]. These neurons have been observed to become sensitised to nicotine [3] [5] and hence we can expect to find the sensitising mechanism by studying the effect of nicotine here.

The nicotinic sensitisation results after a protocol of pre-exposure. Pre-exposure to opiates has also been shown to cause a smaller, but significant sensitisation (called a cross-sensitisation) [39]. Opiates have been shown to act pre-synaptically too, activating opiate receptors that inhibit the release of GABA on to the mesolimbic neurons [58]. However pre-exposure to other rewarding drugs such as cocaine and amphetamine does not induce this sensitivity to nicotine [7].

Cocaine and amphetamine act in the terminal field of the dopamine neurons [50], whilst nicotine and opiates act mainly through increasing the firing of bursts (c.f. Chapter 3 and the references therein) in these neurons. This would suggest that the sensitisation induced may be comparatively local to its site of action. In particular, with reference to the phenomenon of long-term potentiation (LTP) in cells, we consider that it may be the synaptic connection itself that mediates the sensitivity.

4.4.2 Long-Term Potentiation

The phenomenon of long-term potentiation [45] [67] [48], or LTP, has been subject of extensive investigation with the typical preparation being glutamatergic synaptic connections in the (rat) hippocampus. In these preparations it has been observed that the strength of the connection may be potentiated experimentally by applying a high frequency stimulus to the pre-synaptic cell local to the connection for a few seconds. After this stimulus the excitatory post-synaptic potentials (EPSPs) in response to the normal signalling of the cell are observed to be significantly larger. This effect has been observed to last from minutes and hours to weeks and months under experimental conditions.

This sensitises the connection to future stimuli and so provides a memory of the potentiating stimulus. LTP has been proposed as a model of memory in the mammalian brain. The induction, but not expression, of LTP is blocked by the *N*-methyl-D-aspartate (NMDA) receptor antagonist dizocilpine (MK801) [90] [36]. NMDA receptors (NMDAR) are ligand-gated ion channels with glutamate as their endogenous agonist [45]. The channels are blocked at resting membrane potentials by magnesium ions but depolarisation of the cell membrane frees them from this magnesium block and allows the influx of sodium and calcium ions. Hence they serve to detect the coincidence of glutamate release and postsynaptic depolarisation.

Although this means that the receptors are excitatory in nature, the calcium ions are also thought to act as a second messenger. In the post-synaptic cell free calcium can bind to the buffer calmodulin and the compound can then activate calcium / calmodulin kinase

(CaM kinase) [45] [59]. This enzyme can then promote phosphorylation of such things as AMPA receptors [36]. AMPA (α-amino-3-hydroxy-5-methyl-4-isoxazolepropionate) receptors are activated by glutamate and open an ion channel selective for sodium and calcium. This excitatory effect is proposed to mediate the EPSPs and phosphorylation is thought to increase the efficacy of the AMPA receptors (AMPAR).

Hence the LTP is proposed to be caused in the post-synaptic cell by the high frequency stimulus relieving the magnesium block of the NMDA receptors by depolarisation via AMPAR, the resulting calcium influx ultimately leading to phosphorylation and an increase in AMPAR mediated EPSPs. Hence the blocking of NMDAR will prevent the induction of LTP, but the expression is unaffected since it is AMPAR mediated. The LTP will decay as endogenous phosphotases break down the phosphate bonds. However, a longer lasting LTP can be caused by the kinase. It has been proposed that the CaM kinase may be able to alter gene expression and by this means cause the upregulation of AMPAR numbers, a change that occurs on a timescale of days rather than the fractions of seconds associated with phosphorylation. Hence a repeated exposure to the stimulus could lead to a semi-permanent memory.

LTP may also be expressed pre-synaptically, by releasing more glutamate for the same stimulus [45] [48]. It is thought that the post-synaptic calcium influx can induce the production of a retrograde messenger (putatively NO) which diffuses to the pre-synaptic cell and then, by some mechanism, upregulates glutamate release.

This suggests that a potentiation of the synaptic connection can be achieved if the pre- and post-synaptic cells are sufficiently excited. Such a stimulation may come from exposing the terminal to sufficiently high doses of nicotine and thus creating the sensitisation we seek. This is supported by the experimental observation that like LTP the induction, but not expression, of the sensitisation to nicotine is blocked by MK801 [90].

4.5 The Sensitisation Model

4.5.1 General Layout and Aims of the Model

It would be expected that one of the major aims of our modelling would be to see if nicotine is capable of inducing a sensitisation through the proposed mechanism of NMDAR activation and so on. Unfortunately there is a lack of quantitative data at a cellular level for our preparation of study. To make a reasonable attempt at answer this question we would need to

know, amongst other things; the conductance of the nAChR with their locations; conductance of NMDA and AMPA receptors and their binding kinetics to glutamate; the action of calcium pumps; the amount of calmodulin; the rate of conversion of free calcium and calmodulin to active kinase and then how this affects AMPAR action and expression. Very little of this is known or can be accurately estimated.

We shall assume that the presynaptic nicotinic receptor stimulated release of glutamate is sufficient to cause significant activation of post-synaptic NMDAR, then that the resulting calcium influx causes (ultimately) significant activation of the appropriate kinases. We suppose that these active kinases may lead to an upregulation of AMPAR function in the post-synaptic cell but we will not include the possibility of a retrograde NO messenger to the presynaptic terminal. The mechanisms involved have not been well characterised and there is little help our modelling may be, given that we have already assumed the presence of upregulating mechanisms in the post-synaptic cell. Assuming a presynaptic mechanism in a similar way to the processes in the post-synaptic cell would then represent an unnecessary complication.

It is apparent that we do not need to model the entire dopamine neuron, but just a single synaptic connection. We will assume that only a single glutamate releasing terminal forms a connection with a single post-synaptic structure. Our model is therefore a relatively simple one of nicotine potentiating the release of glutamate which can cause sensitising effects in the post-synaptic structure.

A requirement of any such model is that it agrees with the observed experimental data which, as we have already said, there is very little of. Indeed the main observation is that MK801 blocks the induction of the sensitisation to nicotine and this is already built directly into the model. We shall therefore be addressing the nature of this sensitisation; what protocols of stimulation (nicotinic or otherwise) are necessary to induce it and then, more importantly, the ability of the sensitisation to decay away. Since such a sensitisation may be implicated as one substrate of addiction it would be interesting to describe how, if it can be, it may be lost and how long this will take. SI units are used with the exception of time, which is scaled in milliseconds.

4.5.2 The Pre-Synaptic Cell

The presynaptic cell should be a model of a (glutamate releasing) terminal that can be potentiated by doses of nicotine. Naturally our model is based largely on the model of

a dopaminergic terminal derived in Chapter 2. The parameter values are taken from this chapter.

Hence we consider the spatially small terminal to be a single electrical compartment of membrane resistance R_a, capacitance C_a and potential V_a described by a conservation of current law given by

$$C_a \frac{dV_a}{dt} = I_{\text{leak}} + I_{\text{Na}} + I_{\text{KDR}} + I_{\text{R}} + I_{\text{O}} \tag{4.16}$$

$$C_a = 1.57 \times 10^{-9} \tag{4.17}$$

where

$$I_{\text{leak}} = (E_{\text{leak}} - V_a)/R_a \tag{4.18}$$

$$E_{\text{leak}} = -0.010 \tag{4.19}$$

$$R_a = 1.59 \times 10^{12} \tag{4.20}$$

is the membrane leakage.

We have only included a (spike-generating) fast sodium channel and a delayed rectifying potassium channel. We regard each action potential as identical and shall not be concerned with the calcium influx as we were in Chapter 2. The membrane leakage is then set such that the cell rests at -70mV and the capacitance is set so that time appears in milliseconds.

The I_{Na} is the current due to a Hodgkin-Huxley model of a fast sodium channel taken from measurements on the guinea-pig hippocampus [88] given by

$$I_{Na} = g_{\bar{N}a} r^2 s (E_{Na} - V_m) \tag{4.21}$$

$$E_{Na} = 0.085 \tag{4.22}$$

$$g_{\bar{N}a} = 1.0 \times 10^{-9} \tag{4.23}$$

$$\frac{dr}{dt} = \alpha_r(V_m)(1-r) - \beta_r(V_m) r \tag{4.24}$$

$$\alpha_r(V_m) = \frac{-3.2 \times 10^5 (0.0469 + V_m)}{\exp\left(\frac{V_m + 0.0469}{0.004}\right) - 1} \tag{4.25}$$

$$\beta_r(V_m) = \frac{2.8 \times 10^5 (0.0169 + V_m)}{\exp\left(\frac{V_m + 0.0199}{0.005}\right) - 1} \tag{4.26}$$

$$\frac{ds}{dt} = \alpha_s(V_m)(1-s) - \beta_s(V_m) s \tag{4.27}$$

$$\alpha_s(V_m) = 128 \exp\left(-\frac{V_m + 0.028}{0.018}\right) \tag{4.28}$$

$$\beta_s(V_m) = \frac{4 \times 10^3}{1 + \exp\left(-\frac{V_m + 0.005}{0.005}\right)}. \tag{4.29}$$

The I_{KDR} is the current due to a delayed-rectifying potassium channel from data also from the guinea-pig [88] given by

$$
\begin{aligned}
I_K &= \bar{g_K} m(E_K - V_m) && (4.30)\\
E_K &= -0.079 && (4.31)\\
\bar{g_K} &= 1.0 \times 10^{-7} && (4.32)\\
\frac{dm}{dt} &= \alpha_m(V_m)(1-m) - \beta_m(V_m)m && (4.33)\\
\alpha_m(V_m) &= \frac{16000(V_m + 0.0249)}{1 - \exp\left(-\frac{V_m + 0.0249}{0.005}\right)} && (4.34)\\
\beta_m(V_m) &= 250 \exp\left(-\frac{V_m + 0.04}{0.04}\right). && (4.35)
\end{aligned}
$$

The I_{R} represents the current from the nAChR (Chapter 2) given by

$$
\begin{aligned}
I_R &= \bar{g_R} X_2^2 (E_R - V_m) && (4.36)\\
E_R &= E_{Na} && (4.37)\\
\bar{g_R} &= 1.5 \times 10^{-9}. && (4.38)
\end{aligned}
$$

where

$$
\begin{aligned}
\frac{dX_2}{dt} &= k_1[\mathrm{n}](1 - X_2 - Y_1 - Y_2) + k_4 Y_1 - k_2 X_2 - k_3 X_2 && (4.39)\\
\frac{dY_1}{dt} &= k_3 X_2 - k_4 Y_1 + k_5[\mathrm{n}] Y_2 - k_6 Y_1 && (4.40)\\
\frac{dY_2}{dt} &= k_7(1 - X_2 - Y_1 - Y_2) - k_8 Y_2 + k_6 Y_1 - k_5[\mathrm{n}] Y_2. && (4.41)
\end{aligned}
$$

With the parameters given as in Lippiello et al [57]

$$
\begin{array}{lll}
k_1 = 0.5 & k_2 = 7.5 \times 10^{-5} & k_3 = 3.67 \times 10^{-6} \\
k_4 = 5.0 \times 10^{-8} & k_5 = 0.5 & k_6 = 6.7 \times 10^{-7} \\
k_7 = 1.0 \times 10^{-7} & k_8 = 1.5 \times 10^{-7} &
\end{array} \qquad (4.42)
$$

This is the original model of Lippiello et al [57] that we have included. However in an earlier section (4.3) we proposed an extension to this model featuring an inactivated form of the nicotinic receptor that led to a functional downregulation. This form arose over a timescale of days, a similar timescale over which the sensitisation has been observed to develop and hence is relevant. Although we are unable to estimate the parameters involved in this model the experimental results of Rowell and Duggan [86] suggest that this downregulation is significant. However we have already assumed that nicotinic stimulation causes sufficient (additional) excitation to cause the relief from magnesium block of the post-synaptic NMDAR and so

shall consider that this extends to the downregulated nicotinic effect that may be induced by chronic nicotine. We shall still take into account the temporary desensitisation produced by prolonged (seconds to minutes) exposure to nicotine, but assume that the total number of activatable (active+desensitised) receptors remains high.

The additional current, denoted I_O, represents the arrival of pre-terminally generated action potentials. The spatial separation of the terminal from the site of generation of the action potential will mean that this wave of depolarisation has a much flatter appearance than a sharp spike. We will approximate this wave with an equation of the form

$$H(t-t')\left(\exp\left(-\frac{t-t'}{\tau_1}\right)-\exp\left(-\frac{t-t'}{\tau_2}\right)\right) \tag{4.43}$$

for a wave that arrives at time t' with a rise time of τ_2 and decay time of τ_1 [10] [49]. $H(\cdot)$ is the Heaviside step function.

If these spikes arrive in a sequence of times given by $\{t_k : k = 1 \ldots \infty\}$ then I_O is given by

$$I_O = (E_a - V_a)\sum_{k=1}^{\infty} G_k \tag{4.44}$$

$$E_a = E_{Na} \tag{4.45}$$

assuming that the wave acts against the sodium reversal potential. The G_k is then given by

$$G_k = H(t-t_k)\frac{g_{\max}}{\tau_1-\tau_2}\left(\exp\left(-\frac{t-t_k}{\tau_1}\right)-\exp\left(-\frac{t-t_k}{\tau_2}\right)\right) \tag{4.46}$$

with

$$g_{\max} = 1.0 \times 10{-}11, \tag{4.47}$$

$$\tau_1 = 5, \tag{4.48}$$

$$\tau_1 = 0.67, \tag{4.49}$$

where $g_{\max}$ describes the conductance of this axonal current. τ_1 and τ_2 are the off and on time constants respectively. We use this mechanism to convert the time-discrete arrival of an action potential into a change in membrane potential. We will assume that the transmission of an action potential to the nerve terminal always causes an action potential (and hence transmitter release) in the terminal and so we shall set $g_{\max}$ such that a temporally isolated action potential causes the membrane potential to break spike threshold.

For the computer simulations the sequence of input spikes to the terminal $\{t_k\}$ is generated from a Poisson process, typically with an average firing rate of 4Hz.

For simplicity and computational efficiency we use an integrate and fire model for transmitter release [10], in that our model releases a fixed amount of transmitter at a fixed firing rate whenever the membrane potential V_a is above a set threshold. This means that the output from the presynaptic cell is essentially a sequence of spikes (of glutamate) with times of generation t'_k, $k = 1 \ldots \infty$ hence

$$t'_k = t \qquad \text{if } V_a(t) > V_{\text{thold}} \text{ and } t - t'_{k-1} > t_{\text{refrac}} \tag{4.50}$$

$$V_{\text{thold}} = -0.02 \tag{4.51}$$

$$t_{\text{refrac}} = 15 \tag{4.52}$$

where t is time, V_{thold} is the action potential threshold, chosen to be a depolarised value that is normally only reached by an action potential. t_{refrac} is the absolute refractory period and corresponds to the maximum firing rate of the terminal, large current inputs to our model of Chapter 2 could generate rates of over 50Hz. The sequence then serves as an input to the model of the post-synaptic cell. In the absence of nicotinic stimulation the terminal transmits the sequence of spikes input to it, except at high rates of incident spikes where the membrane potential can remain above threshold for long enough to generate additional action potentials. Nicotinic stimulation leads to a depolarising current that increases the firing rate of the terminal.

4.5.3 The Post-Synaptic Cell

LTP in experimental preparations is observed to be an increase in the height of the excitatory post-synaptic potentials produced in the cell [45]. Therefore we again need to consider the electrical properties of the cell, which is in this case a post-synaptic structure. We denote the membrane potential in the postsynaptic cell by V_b, with membrane resistance R_b and capacitance C_b, is governed by

$$C_b \frac{dV_b}{dt} = I_{\text{leak}} + I_{\text{NMDA}} + I_{\text{AMPA}} \tag{4.53}$$

where the membrane leakage and electrical constants are given by

$$I_{\text{leak}} = (E_{\text{leak}} - V_b)/R_b \tag{4.54}$$

$$E_{\text{leak}} = -0.07 \tag{4.55}$$

$$R_b = 1.0 \times 10^{10} \tag{4.56}$$

$$C_b = 1.57 \times 10^{-9}. \tag{4.57}$$

We have assumed that since synaptic structures are so small (we estimate them to be similar in size to a terminal, that is 1μm across [45]) that it constitutes a single electrical compartment. We further assume that this (electrical) compartment of the cell does not generate action potentials and so we do not include voltage-activated sodium or rectifying potassium channels. This is consistent with the classical view of post-synaptic potentials propagating to a central point (such as the axon hillock) were they summate and produce an action potential if a particular threshold is reached. As might be expected, this is not generally true, with calcium and potassium channels having been identified in what are then called 'active' dendrites [49]. We shall make the assumption that any such channels are located sufficiently downstream from the structure and that any of their effects do not propagate back and affect the structure significantly.

Excitatory input to the cell is provided by the two types of glutamate receptors, NMDA and non-NMDA, which we assume to be the AMPA type. The current due to the AMPA receptors, I_{AMPA} is given by

$$I_{\text{AMPA}} = (E_{\text{AMPA}} - V_b)G_{\text{AMPA}}(t) \tag{4.58}$$

$$E_{\text{AMPA}} = E_{Na} = 0.085 \tag{4.59}$$

where $G_{\text{AMPA}}(t)$ is given by

$$G_{\text{AMPA}}(t) = \sum_{k=1}^{\infty} H(t - t'_k)\frac{Ag_{\text{AMPA}}}{\tilde{\tau}_1 - \tilde{\tau}_2}\left(\exp\left(-\frac{t - t'_k}{\tilde{\tau}_1}\right) - \exp\left(-\frac{t - t'_k}{\tilde{\tau}_2}\right)\right) \tag{4.60}$$

with

$$g_{\text{AMPA}} = 2.0 \times 10^{-13} \tag{4.61}$$

$$\tilde{\tau}_1 = 80 \tag{4.62}$$

$$\tilde{\tau}_2 = 0.67 \tag{4.63}$$

where $H(\cdot)$ is the Heaviside step function [10]. A is a measure of the 'number' of AMPAR and g_{AMPA} their associated individual conductance. With an non-upregulated value of $A = 100$, this gives an AMPAR conductance of 2.0×10^{-11}S, which gives typical postsynaptic potentials of 30-40mV [19].

$\tilde{\tau}_1$ and $\tilde{\tau}_2$ are the off and on time constants of the current respectively. The input to the AMPAR is the spike train sequence $\{t'_k : k = 1 \ldots \infty\}$ from the pre-synaptic terminal. We assume that the receptors only allow the flow of sodium ions, hence the reversal potential for the current $E_{\text{AMPA}} = E_{\text{Na}}$.

NMDAR are blocked at low membrane potentials by magnesium ions, hence for them to gate current, the cell must also be depolarised (such as by activation of AMPAR, as in our model) [45]. The current I_{NMDA} is given by

$$I_{\text{NMDA}} = (E_{\text{NMDA}} - V_b)G_{\text{NMDA}}(t) \tag{4.64}$$

$$E_{\text{NMDA}} = E_{\text{Ca}} = 0.120 \tag{4.65}$$

where $G_{\text{NMDA}}(t)$ is given by

$$G_{\text{NMDA}}(t) = \sum_{k=1}^{\infty} H(t - t'_k) g_{\text{NMDA}} \left(\frac{\exp\left(-\frac{t-t'_k}{\tilde{\tau}_1}\right) - \exp\left(-\frac{t-t'_k}{\tilde{\tau}_2}\right)}{1 + \eta[\text{Mg}^{2+}]\exp(-\gamma V_b)} \right). \tag{4.66}$$

with

$$g_{\text{NMDA}} = 2.0 \times 10^{-10}. \tag{4.67}$$

We assume the same on and off time constants $\tilde{\tau}_1 = \tau_1$ and $\tilde{\tau}_2 = \tau_2$ as for the AMPAR. Typically, $[\text{Mg}^{2+}] = 2\text{mM}$, $\eta = 0.33/\text{mM}$, $\gamma = 0.06/\text{mV}$ and the conductance is 0.2nS [10]. For simplicity we assume that the NMDAR only gate calcium, so $E_{\text{NMDA}} = E_{\text{Ca}}$. This is not considered to be a problem given that our only use of the NMDAR is to provide a voltage dependent calcium influx. Again the input is the spike train sequence from the pre-synaptic channel.

Calcium influx through NMDAR serves to increase intracellular calcium levels. We assume that NMDAR are the only source of calcium influx and that calcium is removed by a simple pump with a slow time constant $\tau_c = 150\text{ms}$ (which will assume represents the binding to other proteins or sequestration by mitochondria). The intracellular calcium concentration c in mM is then given by

$$\frac{dc}{dt} = BI_{\text{NMDA}}(t) - \frac{c}{\tau_c} + \tilde{B}(k_{p2}p - k_{p1}c^4 M), \tag{4.68}$$

$$B = 5.0 \times 10^5, \tag{4.69}$$

$$\tau_c = 150, \tag{4.70}$$

$$\tilde{B} = 5.0 \times 10^4, \tag{4.71}$$

where the $\tilde{B}$ term adjusts for the calcium lost to calmodulin binding. The calcium interacts with the buffer calmodulin and thence activate a CaM kinase (and we are assuming that there is sufficient influx through NMDAR when they are activated by membrane depolarisation)

[36][59][68]. We will assume that whatever the changes in calcium concentration, they are too small to significantly affect E_{Ca}.

Calmodulin binds free intracellular calcium at a rate comparative to the calcium pump (otherwise the calcium would be removed before it had chance to bind)[49]. Hence $\tilde{B}$ is adjusted so that the removal by calmodulin binding is comparable to extrusion by pump at the typical intracellular free calcium concentrations that arise in the computer simulations.

Intracellular calcium can bind with the protein calmodulin (with a stoichiometry of four), a compound that can activate a substrate to form a protein kinase (CaM kinase) [36][68]. Such kinases have been shown to be able to alter gene expression and therefore cause long lasting changes in cells and we assume that in our case it increases the rate of production of AMPAR. If c is the intracellular calcium concentration and M is the concentration of unbound calmodulin, the concentration of the compound protein p is given by

$$\frac{dp}{dt} = k_{p1}c^4M - k_{p2}p - k_{a1}pS_a + k_{a2}a, \tag{4.72}$$

where the production rate and rate of conversion to the active kinase is given by the law of mass action. From results on the bullfrog sympathetic ganglion cells [49] we obtain that the on rate of calcium / calmodulin binding is $10^5\mathrm{mM}^{-1}\mathrm{s}^{-1}$ and the off rate is $100\mathrm{s}^{-1}$. Hence $k_{p1} = 100$ and $k_{p2} = 0.1$ as we are working in milliseconds. The change in calmodulin concentration is then simply given by

$$\frac{dM}{dt} = -k_{p1}c^4M + k_{p2}p. \tag{4.73}$$

The active kinase concentration a is then given by

$$\frac{da}{dt} = k_{a1}pS_a - k_{a2}a, \tag{4.74}$$

where we assume there is an abundance of substrate S_a for the active kinase which is produced according to the law of mass action. We will arbitrarily assume that $S_a = 1\mathrm{mM}$. The total concentration of calmodulin, C, is then

$$C = M + p + a \tag{4.75}$$

and we observe that $\frac{dC}{dt} = 0$, hence C is a constant and the total concentration of calmodulin is conserved.

We have been unable to find any experimental data for the timescales of production and decay of the kinase a, although the binding of calcium to calmodulin rate (k_{p1}) is fast and

disassociation (k_{p2}) slow [49] and the calcium pump (time constant of 150ms) will quickly remove any free calcium. Active kinase levels have been shown to be significant up to two hours after being activated by calcium influx [12][74]. We do not know the rates k_{a1} and k_{a2}, however, setting

$$k_{a1} = 1.0 \times 10^{-5}, \tag{4.76}$$

$$k_{a2} = 1.0 \times 10^{-6}. \tag{4.77}$$

This gives a resting concentration of $< 10^{-4}$mM (suitably small) and a significant level of presence two hours after it has been activated.

Our model of sensitisation assumes that the presence of active kinase upregulates the production of AMPAR, A [12][91]. We suppose that this takes place by the kinase altering gene expression, although we have little idea how such a complex mechanism may be modelled [45] [68]. Given that we only require the active kinase to (ultimately) cause the upregulation of AMPAR we will suppose that we can model this as a simple production and decay process, with the production augmented by a reaction between the kinase and a supposed AMPAR substrate. Hence upregulation can only take place whilst the kinase is activated. We take

$$\frac{dA}{dt} = k_{A1} S_A (1 + h(a)) - k_{A2} A \tag{4.78}$$

where S_A is the concentration of AMPAR substrate (in abundance, and taking the value $S_A = 1$ for the computer simulations) and k_{A1} and k_{A2} are the regular rates of production and decay. Assuming that upregulation takes place over a time scale of days we take

$$k_{A1} = 5.0 \times 10^{-7} \tag{4.79}$$

which follows this timescale in the computer simulations. Taking receptor degradation to also be a slow process we set

$$k_{A1} = 5.0 \times 10^{-9} \tag{4.80}$$

which then gives a steady state measure of AMPAR numbers in the absence of active kinase of 100.

The function $h(a)$ describes the increase in production rate in the presence of active kinase, which we assume is achieved instantaneously and we consider a reasonable assumption when considering the upregulation process takes place over a timescale of days. We set $\bar{u} = 1.5$ to be the maximum upregulation rate. This value is chosen such that at full upregulation

the depolarisation achieved by an EPSP (according to our computer simulations) is comparable to that seen in studies of LTP. In the absence of experimental data on the qualitative nature of this upregulation, we have used a Michaelis-Menten form for h, assuming that the upregulation will be linear for small a but saturate at high values. We set

$$h(a) = \bar{u}\frac{a}{K_g + a} \tag{4.81}$$

where K_g is a suitably chosen constant. To make future analysis simpler, we assumed that K_g was small in comparison to the levels of active kinase we achieved and so typical calcium influx and kinase activation essentially caused a switch to a higher AMPAR production rate. We set

$$K_g = 0.01. \tag{4.82}$$

The value of A then provides a quantitative measure of the sensitivity of the model. For the computer simulation the post-synaptic membrane depolarisation achieved by a single pre-synaptic spike provides a good visual cue of sensitisation analogous to that observed experimentally for LTP.

4.6 Sensitisation Model Results

4.6.1 The Computer Simulation

The millisecond resolution of portions of the model with real time processing of individual spikes lends itself to computer simulation. The model described in the previous few sections was implemented on the neural simulator GENESIS [10]. Indeed many of the numerical values of the parameters are drawn from searches made by running this simulation.

The input train of spikes for the pre-synaptic cell $\{t_k\}$ is generated by a Poisson process that gives an average firing rate of 4Hz. The threshold for transmitter release is set to be -20mV, a depolarised voltage normally reached only by an action potential, we then use our integrate and fire model (equation (4.50)) to detect this spike. Figure 4.4 illustrates the membrane potential of the pre- and post-synaptic cells when subject to such a train of spikes.

Introducing a concentration of 1μM nicotine to the pre-synaptic terminal causes the cell to start firing at a much faster rate (see Figure 4.5), in this simulation at over 50Hz. Over the time course of tens of seconds, the receptors will begin to desensitise. This effect is difficult

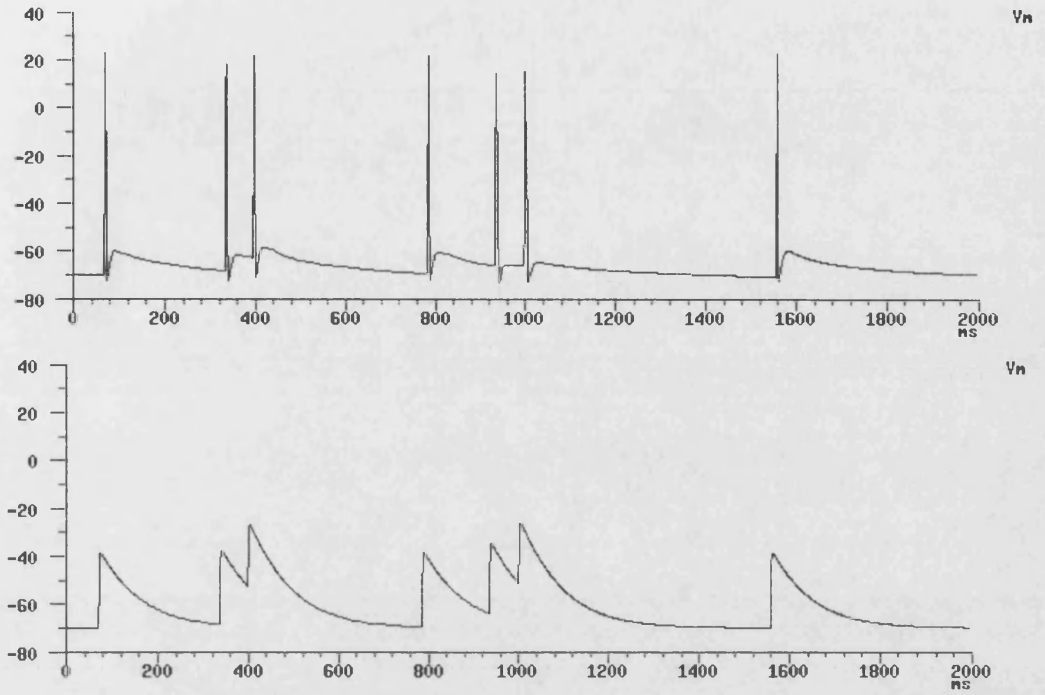

Figure 4.4: Plots of the membrane potential in millivolts of the presynaptic (upper) and postsynaptic (lower) cells against time in milliseconds when the presynaptic cell has an average firing rate of 4Hz. One can see that the presynaptic action potentials cause transmitter release, giving rise to the post-synaptic potentials.

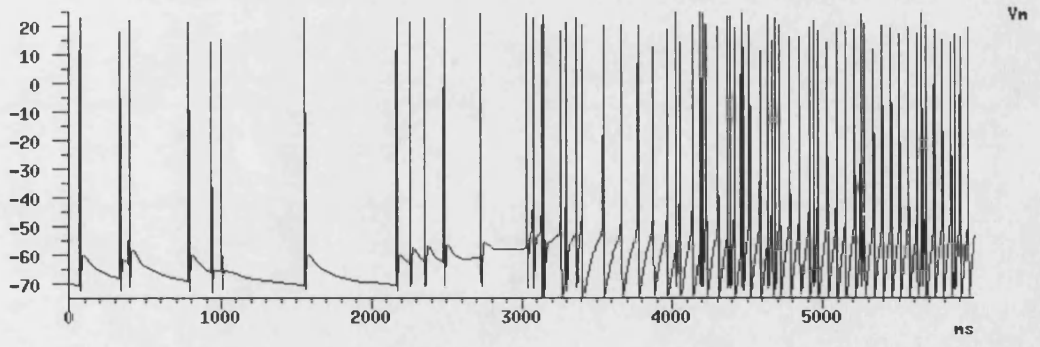

Figure 4.5: Plot of the presynaptic cell membrane potential against time when subject to a firing rate of 4Hz with 1μM nicotine applied at 2000ms. It is clear that the extra excitatory current input causes a large increase in the firing rate of the cell.

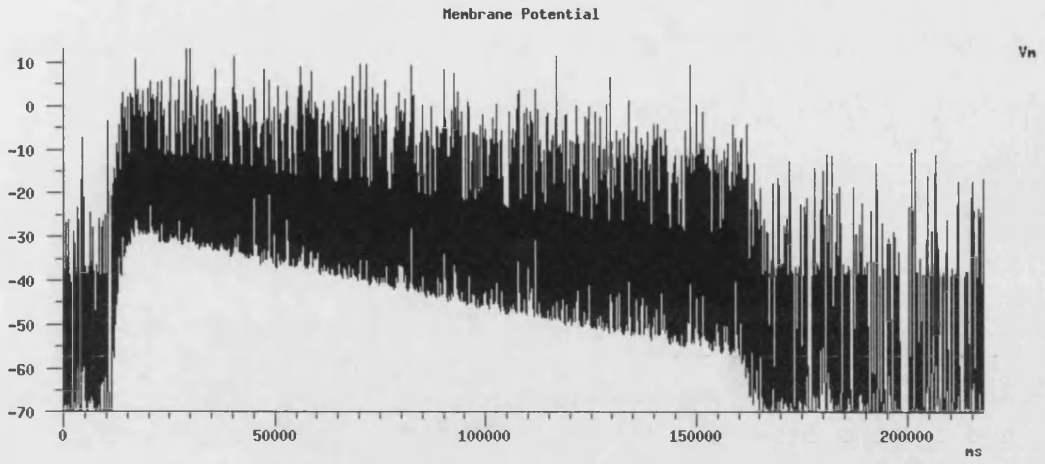

Figure 4.6: Membrane potential against time of the post-synaptic cell when the presynaptic cell is subject to an intrinsic stimulus of 4Hz and 1μM nicotine is applied at 2 seconds and removed at 92 seconds. Note the decay in potential as the nAChR desensitise. The slow 'on' and 'off' times of nicotinic stimulation are apparent, with an initial pause of 10 seconds before there is a noticeable effect, which then continues for another 60s after the nicotine is removed.

to see in the pre-synaptic cell where it is masked by the high firing rate, but is well illustrated in the post-synaptic cell as seen in Figure 4.6. This shows the membrane potential for the post-synaptic cell when 1μM nicotine is applied for ninety seconds, from two seconds in. Within a matter of seconds of its introduction the postsynaptic cell is at its most depolarised and it then decays slowly until at 92 seconds (absolute) the nicotine is removed and the postsynaptic potential returns to base levels of stimulation.

The extra stimulus provided by the nicotine-induced current causes the activation of the NMDAR, signified by calcium influx, which then goes on to cause the production of the active kinase. This can be in Figure 4.7, where the brief pulses of calcium lead to a maintained active kinase level (concentration in Molar). Note that prior to the build up of the nicotine-induced current (nicotine is only introduced after 2000 milli-seconds) there is insignificant calcium influx and hence kinase activation. We assume that kinase activation to such concentrations is sufficient to promote significant upregulation of the AMPAR, note that this calcium influx has produced kinase concentrations from close to 0 (compared to the scale of the graph) to above the half-upregulation concentration $K_g = 0.001$.

Since the upregulation of the AMPAR is a slow process compared to the other biological mechanisms, the simulation needs to be run for large amounts of simulated time, days when

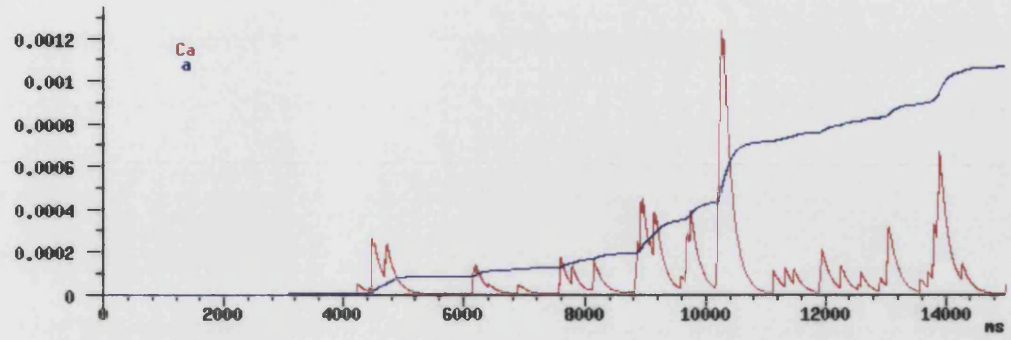

Figure 4.7: The calcium concentration (red) and active kinase level (blue) in Molar in the postsynaptic cell from Figure 4.6. When 1μM nicotine is applied (at 2000ms), the nicotine-mediated stimulation is sufficient to open NMDA channels and allow the influx of calcium. The binding of calcium and calmodulin ultimately leads to kinase activation.

the model covers milli-second time-scale phenomena. This necessarily demands a lot of computing power and we have made attempts to run a simulation where the cells are given a protocol of 40 doses of nicotine over 16 hours ('daytime') followed by an 8 hour gap ('night time'), intended to model the habit of a 40-a-day smoker. These have been unsuccessful due to computer memory problems and the unreliability of the computers and software.

As a result of this we have only been able to run the simulation for two hours of simulated time, during which the four doses of nicotine applied led to an upregulation of about 4% out of a maximum of 250% we allow, an upregulation that tends to double the height of excitatory postsynaptic potentials, typical of observations of LTP [48]. This sensitisation is largely independent of the number of doses applied since active kinase levels can persist for over an hour (hence across a number of doses) and therefore active kinase levels are typically maintained throughout the day. As detailed in the section on model analysis (section 4.7) we can estimate from this that regular smoking could approach maximum sensitisation in fourteen days.

4.6.2 Demonstration Simulations

It is inconvenient that we have been unable to generate upregulation with the computer simulation from unsensitised states. We would like to be able to use the simulation to investigate, in particular, the loss of sensitisation in the absence of nicotinic simulation. What we decide to do is tweak our computer simulation so that the upregulation of AMPA receptors is set immediately to its steady state value with the concentration of active kinase. Thus the upregulation is then given by the instantaneous value of the active kinase concentration

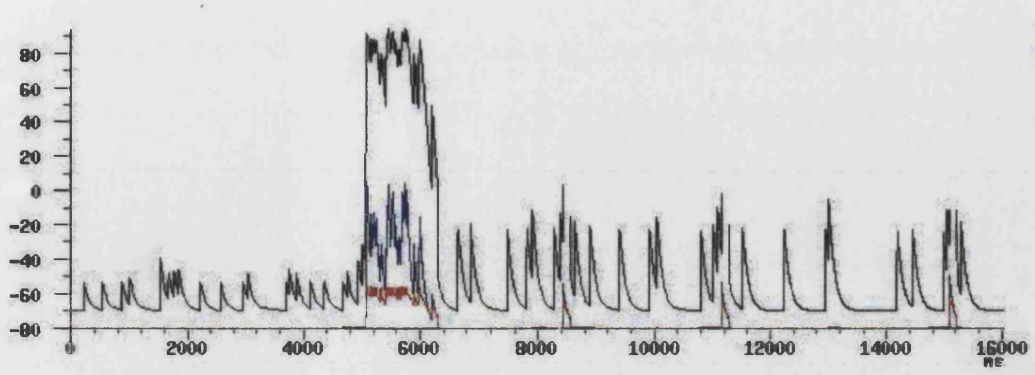

Figure 4.8: Plot of membrane potential (black trace) against time for a demonstration of the induction of sensitisation in the postsynaptic cell. So that we may see the effect of the sensitisation on this timescale we have applied the steady state level of upregulation appropriate to the active kinase concentration. The cell is initially subject to a stimulus of 4Hz, but a 1 second pulse of 65Hz causes activation of the NMDAR on a large scale, causing a large membrane depolarisation and a correspondingly large calcium influx (red) and kinase activation (blue), whose values have been scaled to appear on this graph. The calcium leads ultimately to AMPAR upregulation and so the cell gives a bigger response per spike when we return to a 4Hz stimulus.

and so the sensitisation develops in a matter of seconds. To enable us to examine the loss of sensitisation we have also increased the decay rate of the active kinase, such that it has an effective span of about 10 seconds. We accept that this is then obviously not a model of sensitisation on the timescales that have been experimentally observed, but it does serve to illustrate the sensitisation principles.

Figure 4.8 is an example of this 'speeded-up' sensitisation. The pre-synaptic cell is initially firing according to a Poisson process with an average firing rate of 4Hz. We then give a pulse of 65Hz for one second, causing massive NMDAR activation. Returning to 4Hz the sensitisation is plain to see, with individual excitatory post-synaptic potentials doubling in height. This also demonstrates that the model does fit the experimental observation of MK801 blocking the induction but not the expression of the sensitisation; our sensitisation is caused by calcium influx through NMDAR, but mediated by increased AMPAR numbers.

It is also clear that the base firing rate of the cell when in a sensitised state is capable of activating the NMDAR and hence reinforcing the levels of active kinase, the effect is maintained way past the 10 seconds in which it would have otherwise inactivated, providing a semi-permanent memory of the event. The trace of membrane potential for the same cell is

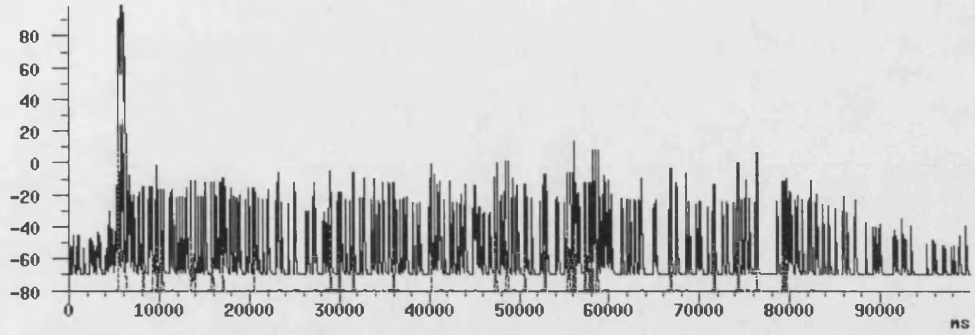

Figure 4.9: Plot of membrane potential against time for the same cell as in Figure 4.8, but for a longer period of time. This demonstrates that the sensitisation continues past the time (about 10 seconds) when the kinase should have been inactivated. The stimulus is reduced to 2.5Hz at 60 seconds and takes a further 30 seconds to forget the sensitisation and the post-synaptic response to return to the original level.

illustrated in Figure 4.9. The sensitisation is present up until 60 seconds (although we notice that it nearly "forgets" near 27 and 47 seconds). At 60 seconds we reduce the firing rate to 2.5Hz, but this lower rate is still able to retain the sensitisation for a further 30 seconds until the active kinase has decayed away to a sufficiently low concentration.

Clearly these must be significant levels of active kinase present in the cell after it is supposed to have decayed. The cell has been returned to its normal stimulation rate of 4Hz and so it must be that this low firing rate is capable of activating NMDAR when the cell is in a sensitised state. The sensitisation only decays at close to the rate it is supposed to when we take the applied stimulus down to an average rate of 2.5Hz.

This demonstration has highlighted an important aspect of these synaptic connection level memories, in that the time taken to forget can be much greater than the normal decay time of the sensitised component. For example, in the absence of active kinases our sensitised post-synaptic terminal would be expected to have desensitised to pre-stimulus EPSP spike heights in about four days. However, the base firing rate of the cell can, in the sensitised state, cause calcium influx and activate the kinase and so prolong the memory. This suggests that the memory of nicotine provided by the sensitisation may last indefinitely.

4.7 Sensitisation Model Analysis

4.7.1 Induction of Sensitisation

It is reasonable to assume that the induction of sensitisation will be subject to two opposing effects; firstly a period of prolonged kinase activation while the subject is dosed with nicotine (either a daily injection protocol or daytime smoking in humans) which will tend to increase AMPAR production. This will be followed by a rest period (night, sleeping) when we will assume there is no kinase activation and the AMPAR production is at a minimum, leading to downregulation from any sensitised state. We are aware that kinase may remain activated way into the night if initial levels are high and we have already seen that for a sensitised cell, the base firing rate can cause calcium influx by itself, but as we wish to look at induction from an unsensitised state we will assume that neither of these happen.

For simplicity, let us assume that the day lasts for time t_1, during which levels of active kinase are sufficient to induce full upregulation of AMPAR production. (Alternatively we could consider t_1 to be the period over which there is full upregulation of AMPAR production.) Then the number of AMPAR, $A(t)$ is described by

$$\frac{dA(t)}{dt} = k_{A1}S_A(1+\bar{h}) - k_{A2}A(t), \qquad A(0) = A_0 \tag{4.83}$$

where $\bar{h} = \sup\{h(a) : a \geq 0\}$. In the computer simulations h has a supremum of $\bar{u}$. Hence at the end of the day the AMPAR number, $A(t_1)$, is given by

$$A(t_1) = \left(A_0 - \frac{k_{A1}}{k_{A2}}S_A(1+\bar{h})\right)\exp\left(-k_{A2}t_1\right) + \frac{k_{A1}}{k_{A2}}S_A(1+\bar{h}). \tag{4.84}$$

For a night (period of no upregulated production) of length t_2 the receptor numbers at the end of the night (in the morning), $A(t_1+t_2)$, is given by

$$\begin{aligned} A(t_1+t_2) &= \left(A(t_1) - \frac{k_{A1}}{k_{A2}}S_A\right)\exp\left(k_{A2}t_2\right) + \frac{k_{A1}}{k_{A2}}S_A, \\ &= \frac{k_{A1}}{k_{A2}}S_A\left(1+\bar{h}\exp(-k_{A2}t_2)\right) \\ &+ \left(A_0 - \frac{k_{A1}}{k_{A2}}S_A(1+\bar{h})\right)\exp\left(-k_{A2}(t_1+t_2)\right). \end{aligned} \tag{4.85}$$

Naturally at the end of the night, the daytime upregulation of AMPAR production starts again and we may this determine $A(t)$ for all time.

It is clear that $A(t)$ tends to a stable periodic orbit, by virtue of the globally stable steady states for the separate day and night-cycle equations (4.84)-(4.85). We may then use these

to write down a difference equation for the number of AMPAR first thing in the morning (this is clearly the lowest value of $A(t)$ during the periodic orbit). Assuming t_1 and t_2 to be constants, this is simply

$$\begin{aligned} A_{n+1} &= \frac{k_{A1}}{k_{A2}} S_A \left(1 + \bar{h} \exp(-k_{A2} t_2)\right) \\ &\quad + \left(A(n) - \frac{k_{A1}}{k_{A2}} S_A (1 + \bar{h})\right) \exp\left(-k_{A2}(t_1 + t_2)\right), \end{aligned} \tag{4.86}$$

which has a stable steady state given by

$$\begin{aligned} A^* &= \frac{\frac{k_{A1}}{k_{A2}} S_A}{1 - \exp\left(-k_{A2}(t_1 + t_2)\right)} \\ &\quad \times \left\{1 + \bar{h} \exp\left(-k_{A2} t_2\right) - \exp\left(-k_{A2}(t_1 + t_2)\right) - \bar{h} \exp\left(-k_{A2}(t_1 + t_2)\right)\right\}. \end{aligned} \tag{4.87}$$

This is an increasing function of S_A, t_1, k_{A1} and $\bar{h}$ and a decreasing function of t_2 and k_{A2}. The minimum value of A^* is $A^*_{\text{Min}} = \frac{k_{A1}}{k_{A2}} S_A$, the steady value in the complete absence of active kinase. Hence for any regular dosing of nicotine, each of which ultimately leads to kinase activation, $A^* > A^*_{\text{Min}}$. Hence the nicotine induces a sensitisation.

4.7.2 Persistence of Sensitisation

The results from our computer simulation have demonstrated that the base firing rate of a pre-synaptic terminal may be sufficient to maintain the sensitised state of the post-synaptic cell. It is apparent that this arises from a period of faster firing locally in time which provides sufficient excitation to activate NMDAR. The interval, x, between presynaptic spikes is not fixed but subject to a probability distribution $p(x)$, which will have zero probability for intervals less than the absolute refractory period of the cell, endowing it with a theoretical maximum firing rate of $\bar{\nu}$. In this model the persistence of the sensitisation depends on the finite probability that the cell can, locally in time, fire at a sufficiently high rate to activate the NMDAR; conversely, the cell will "forget" the sensitisation if the rate is not achieved. Naturally we wish to estimate the time until the cell forgets the sensitisation.

The problem is complicated by many factors; firstly the firing rate may be encoded over many spikes, for example the excitation produced by two spikes very close together could be equivalent to three slightly further apart. We choose to concentrate solely on the interval between two spikes, which would tend for us to underestimate the time to forgetting although we expect any such difference to be small. Secondly the stimulus required to activate the NMDAR is increasing with time, since in the absence of a reinforcing stimulus the number of AMPAR is decaying. Thirdly, activation of NMDAR leading on to the re-activation of the

kinase may not necessarily produce complete re-sensitisation. We will assume that it does, this is valid for small amounts of desensitisation but may not be when the cell has nearly forgotten. We must also come up with a definition of what this 'forgotten' means, as the receptor numbers are decaying exponentially the value will never return to the minimum.

It turns out to be quite easy to give a definition for forgotten; we shall say that a cell has forgotten its sensitisation when the local firing rate required for reinforcement is greater than the maximum firing rate of the cell, in which case the necessary local firing rate cannot be achieved. The sensitisation cannot then be reinforced and will simply decay away.

If the post-synaptic cell is at its resting membrane potential (we assume it is), then we suppose it needs a finite charge transfer Q to depolarise the cell to a potential sufficient to cause sizable calcium influx. We suppose that this corresponds to a local firing rate of ν, that is an interspike interval of ν^{-1}. If we further assume that the repolarising leakage current is small in comparison to the influx through AMPAR and that the influx through the receptors is the same for each spike, valid for membrane potentials close to resting, then the influx is proportional to the number of AMPAR A. In the absence of active kinases, A decays exponentially with time constant k_{A2}, hence a time t later, the flux through AMPAR will have decreased by a factor $\exp(-k_{A2}t)$.

For membrane potentials away from the sodium reversal potential we can assume that any two spikes cause equal excitatory current influx and so the decrease in flux through the receptors can be compensated for by an increase in the local firing rate by a factor of $\exp(k_{A2}t)$. Hence the required firing rate increases exponentially, or the required interspike interval decreases exponentially, with time. Since k_{A2} is typically a very long time-scale (days) in comparison to inter-spike intervals (order of 500ms), we can assume that this required firing rate changes little over the interval.

We will normalise the initial required firing rate to be 1, hence the firing rate required at time t is $\exp(\lambda t)$ for suitable time constant λ. We may now calculate a finite time in which the sensitisation must be reinforced otherwise the cell will have forgotten. This will be the time T at which the required firing rate is equal to the maximum firing rate, that is

$$\exp(\lambda T) = \bar{\nu} \;\Rightarrow\; T = \frac{1}{\lambda}\ln(\bar{\nu}) \tag{4.88}$$

recalling that $\bar{\nu}$ is the maximum firing rate of the cell. We are therefore required to find the probability that the cell fires fast enough during this time. If the effect is reinforced, we reset the cell to full sensitisation and start again, otherwise the cell has forgotten.

The input to the post-synaptic cell is a sequence of spikes $\{t_k\}$, where t_k is the time of arrival of the kth spike. The probability that the next inter-spike interval is sufficiently short is therefore

$$\int_0^{\exp(-\lambda t_k)} p(x)dx \tag{4.89}$$

where $p(x)$ is the probability distribution of the interspike intervals for the firing pattern of the cell. Hence the probability that the sensitisation is reinforced on the lth spike (and not on any of the previous ones) is given by

$$\prod_{k=1}^{l-1}\left(1-\int_0^{\exp(-\lambda t_k)} p(x)dx\right)\int_0^{\exp(-\lambda t_l)} p(y)dy \tag{4.90}$$

from which we may calculate the actual probability that the sensitisation is reinforced, which we denote by P. The finite time to forget T is typically large, since λ is small, and so the total number of spikes N is an integer such that $N \approx T\nu$, where ν is the average firing rate. Hence

$$P=\sum_{l=1}^{N}\left\{\prod_{k=1}^{l-1}\left(1-\int_0^{\exp(-\lambda t_k)} p(x)dx\right)\int_0^{\exp(-\lambda t_l)} p(y)dy\right\}. \tag{4.91}$$

We may use this to calculate two expectation values, $E(T_R)$, the expected time into the interval T that the sensitisation is reinforced, and $E(N_R)$, the expected number of times the effect is reinforced. The expected time to forget the sensitisation, $\mathbf{E}$, is then

$$\mathbf{E} = E(T_R) \times E(N_R) + T. \tag{4.92}$$

We have

$$E(T_R) = \sum_{l=1}^{N} t_l\left\{\prod_{k=1}^{l-1}\left(1-\int_0^{\exp(-\lambda t_k)} p(x)dx\right)\int_0^{\exp(-\lambda t_l)} p(y)dy\right\} \tag{4.93}$$

$$E(N_R) = \sum_{n=1}^{\infty} nP^n = \frac{P}{(1-P)^2} \tag{4.94}$$

We can then observe the following:

1. $P > 0$ for $\bar{\nu} > 1$; there is a non-zero probability of reinforcement if the cell can theoretically fire faster than the initial required rate. If $\bar{\nu} < 1$ then $P = 0$.

2. for $P = 0$ the time to forget is 0; the sensitisation cannot be reinforced.

3. $\mathbf{E} > T$ for $P > 0$; for such situations the expected time to forget is greater than T and so the memory of the sensitisation is expected to be extended by the base firing rate of the cell.

4. **E** is finite for $P < 1$; the cell will forget given enough time.

5. **E** is an increasing function of mean firing rate ν, the maximum firing rate $\bar{\nu}$ and the time window for reinforcement T; the faster a cell does or can fire and the longer the period of time in which a sufficient rate may be produced, the more the memory will persist.

6. **E** is a decreasing function of the AMPAR decay rate λ; this will reduce T and require higher reinforcement firing rates during a shorter time.

This demonstrates that the base spike firing of the cell can sustain a sensitisation induced in it. This may have important implications for the proposed addictive qualities of nicotine.

4.8 Review

In this chapter we have addressed two of the longer term effects of nicotine, the apparently conflicting developments of a tolerance and a sensitisation to its effects. The modelling of these phenomena at the sub-cellular level has forced us to make many simplifications and to propose our own mechanisms that cause their development. We must now review our model with a particular view to justifying the mechanisms we introduce and how our hypotheses may be tested experimentally.

4.8.1 The Upregulation of Receptors

The upregulation in $\alpha 4\beta 2$ nicotinic binding sites in mouse striatal synaptosomes chronically exposed to nicotine has been well established by Marks et al [60] and others [102]. In particular Rowell and Duggan [86] provides the observation that chronic nicotine treatment seems to give rise to an inactivated conformation of nAChR.

We have extended the model of Lippiello et al [57] in the obvious way, assuming that this inactivated form presents another state that the receptor may shift to once it has desensitised. We have assumed that this inactivation is permanent, since nicotinic function was not fully restored after 5 hours relief from the nicotine, which would be expected to re-sensitise receptors in the desensitised conformation [86]. It is possible that the inactivated form can return to a functional conformation, but at a much longer timescale. We consider that at such timescales it may be indistinguishable from normal receptor turnover.

The inactivated form in the model leads to an overall downregulation of nicotinic function when nicotine is applied by shifting active conformations into desensitised or inactive states. This means that a functional downregulation, or tolerance, develops. This is of course consistent with the experimental results of Marks et al [60], and of Rowell and Duggan [86] whose observation of an increase in binding and decrease in function led them to the hypothesise the existence of an inactivated form of nAChR. This overall reduction in nicotinic function also suggests that, while our model relates primarily to the $\alpha 4\beta 2$ sub-type of nAChR, any sensitisation is not produced by an increase in the numbers of other sub-types of nAChR.

Our key hypothesis is that the inactive conformation is degraded at a slower rate than either the active or desensitised forms. It is this condition that causes chronic nicotine to bring about an increase in binding site numbers by shifting the nAChR into this slower decaying form. It is not apparent why this inactivated conformation may degrade at a slower rate. However it has been proposed that the apparently 'new' binding sites are located internally, suggesting that this inactivated form may correspond to an internalisation of the nAChR which could be considered a natural reaction to an over exposure to agonist. It would seem reasonable that such an internal pool may be segregated from the receptor degrading agents and thus reduce their degradation.

The proposed existence of an internal pool can suggest a slightly different model; that rather than degrading, the receptors in the internal pool are simply slow at returning to the cell membrane. This would mean a direct rate of transition between the inactive and (say) active forms instead of going via a process of decay and production from a substrate as we do already. It is apparent that this would make little difference to the results.

It may be possible to determine turnover rates if two different labels could be used; one applied chronically that would bind and cause a shift to the inactivated state and a second applied acutely to bind to the non-inactivated forms; and then monitoring the progress of each. We do not know whether such an experiment would be feasible.

4.8.2 The Sensitisation Model

Our initial aim was to produce a model that described the sensitisation effects on prolonged nicotine exposure. We have done this by hypothesising that the sites of induction are the nicotine-potentiated synaptic connections incident to the mesolimbic dopamine neurons. The proposed mechanism then follows from drawing analogies with the phenomena of long term

potentiation and noting that NMDAR are implicated in the establishment of both nicotine sensitisation and LTP [90] [92].

We have not included the fast acting upregulation of AMPAR function by phosphorylation [45]. There is no evidence that, if present, this mechanism of upregulation is significant since no sensitisation is reported soon after a single injection of nicotine, it may be that any sensitisation induced may be masked by the desensitised nAChR producing a temporary functional downregulation. It is also undesirable to include phosphorylation as we do not know the parameters involved in such a mechanism, particularly its interaction with the longer term increase in AMPAR numbers which is our primary interest.

It has been proposed that nicotinic receptors may also be present on the cell bodies of mesolimbic dopamine neurons, though we have assumed there are none. Balfour and Fagerstrom [4] propose that the sensitising effects of nicotine are mediated by more than one sub-type of nicotinic receptor (and hence nicotine, by activating both potently, may be uniquely addictive amongst nicotinic drugs). Our work in Chapter 2 suggests that any heterogeneity of nAChR should be segregated to separate terminals. Assuming that the same holds here raises the possibility of sufficient postsynaptic depolarisation being caused by two terminals incident on the same structure, or one sub-type being located on the structure directly depolarising the postsynaptic cell.

This suggests that we have over-simplified the model. It is apparent that we have already had to express many variables of the system in arbitrary units and therefore had to assume that nicotine can cause sufficient excitation that leads (via potentiated glutamate release and AMPAR activation) to the activation of the NMDAR. In turn we have assumed that this calcium influx ultimately activates a CaM kinase which goes on to cause upregulation of AMPAR. Although we are justified in choosing this mechanism for upregulation ([36] [91]) we do not know the numbers involved and so have no choice but to assume that all components have the potency that we desire. There is then no point in further complicating the system by specifying different nAChR in varying locations and such like.

We have experienced many hardware and software problems associated with running the computer simulation for long periods of time. An alternative would be to write our own numerical scheme but we have already been able to show that the model does start an upregulation of the AMPAR. It is then much simpler, and robust, to introduce the difference equation that approximates the AMPAR numbers (the true measure of upregulation) at the lowest point in their 'daily' cycle. This set the upregulation of production to be $\bar{h}$, the

supremum of equation (4.81), yet it is clear we need not be so precise and $\bar{h}$ may be an appropriate average of upregulation over the daytime. $\bar{h} > 0$ ensures that the model does develop a sensitisation to the excitatory effects of nicotine.

We have, more interestingly in our opinion, also shown that the sensitisation can remain in the absence of nicotinic stimulation for a longer period of time than the AMPAR would be expected to decay in. The reason for this is clear, that the upregulated AMPAR response can be sufficient to activate the NMDAR and thus set in motion the chain of events that leads to kinase activation. We have been able to provide a robust definition of the time to forget the sensitisation as the period of time in which it can be reinforced without the need to present the sensitising (nicotinic) stimulus.

We have estimated the time for which the sensitisation persists and have shown that this does extend past the time in which the AMPAR would be otherwise expected to decay. It would be highly desirable to calculate the expected length of time explicitly but unfortunately we do not know the firing pattern of the incident neuron (hence $p(x)$), nor the firing rate needed from a state of full sensitisation. Each of these is likely to be different for each different synaptic connection too.

The development of a sensitisation to nicotine may be expected to form one substrate of its perceived addictive qualities [3]. The sensitisation means that even the non-nicotinic base firing rate produces an enhanced response. This persistent increase in excitation may lead to a downregulation in dopamine function downstream from the connection, such as the desensitisation of postsynaptic dopamine receptors, whilst retaining a potent response to nicotine. The possible persistence of the sensitisation long after the sensitising stimulus has been removed could have serious implications for such an addiction relapse.

It would seem that the human smoker / laboratory animal will be free of this substrate of addiction once they have forgotten the sensitisation. Our analysis has shown that this is no simple matter of ceasing nicotine doses and allowing for the decay of the AMPAR, for memories of the drug can be kept for many times longer. This provides an interesting slant on the known tendency for ex-addicts (to smoking and also to opiates such as heroin, given the parallels discussed below) to lapse back into use even after months of abstinence.

Our model also suggests a cure for this; the anti-addiction qualities of NMDAR antagonists such as ibogaine have already been reported [6][78][77] and dosing the subject with it for the 'time to forget' period immediately following addictive drug abstinence will prevent sensitisation reinforcement. This would allow the upregulation of AMPAR to decay away sooner

and free the subject from this substrate of addiction. Interestingly this would also suggest that any (acute) exposure to a like sensitising stimulus, such as the replacement therapy of using methadone on heroin addicts, is counterproductive.

The dependence on NMDAR activation and the speculated site of action of nicotine pre-synaptic to the dopamine neurons (on glutamate terminals) has led us to this sensitisation of a synaptic connection picture. There may be many thousands of such connections, each may sensitise to different degrees and persist to different extents. This would be consistent with the experimental observations that there is no cross-sensitisation to amphetamine or cocaine, which act in the dopamine terminal field inducing dopamine release and blocking or reversing dopamine transporters. However a cross-sensitisation with opiates has been reported and we can suggest a reason for this. Opiates act on dopamine neurons by pre-synaptically blocking (inhibitory) GABAergic input, excitation by the block of inhibition. If such an input is local to the nicotine / glutamate connection it may be able to produce the extra post-synaptic depolarisation required to activate the NMDAR (the expression of sensitisation to the opiates can be blocked by AMPAR antagonists [13] and the induction prevented by NMDAR antagonists [39]). This could then lead to the sensitisation of the cell much like it would if the excitation where nicotine mediated. The limitations of the cross-sensitisation would arise from the lack of local co-incidence of both types of terminal at the same structure. This suggests that opiate sensitisation may act in a similar way to nicotinic, indeed the induction of opiate sensitisation is blocked by NMDAR antagonists [99] and the expression features an upregulation of AMPAR [23].

4.8.3 Summary

We have produced two essentially separate models. The first is a fairly simple model that demonstrates how chronic nicotine can prompt the co-development of a contradictory upregulation in nicotinic binding sites and a functional downregulation. This model is based on the experimentally proposed existence of an inactivated form of nAChR.

The second model is much more complex and describes a mechanism whereby a sensitisation to stimulation may be induced. The mechanism is probably over-simplified but is a result of the lack of subcellular level quantitative data available on the phenomenon. This model demonstrates that the sensitisation can persist indefinitely, which draws parallels with, and has serious implications for, addiction to nicotine and the opiates.

Chapter 5

Modelling Parkinson's Disease

5.1 Chapter Overview

The clinical symptoms of Parkinson's disease are mainly disorders of movement such as a tremor in limbs at rest and a slowness or rigidity of movement. The disease may be traced to the degeneration of the dopamine cells of the nigrostriatal pathway. We consider this pathway and, using a formulation in terms of averaged neuron firing rates and responses, model the feedback loop of dopamine neurons and striatal GABAergic neurons such that we reduce this network of thousands of neurons to a system that essentially describes a simple loop of two neurons. The inputs from other neurons are assumed to be proportional to the firing rates of the incident neurons, which are in turn proportional to their membrane potentials. We assume that the dopamine neurons have a simple linear current-voltage relationship whereas the striatal neurons have a relationship described by a cubic, which gives rise to the interesting dynamics of the system.

We demonstrate that the model output can be robust to large losses in dopamine input reflecting that seen in Parkinson's disease where there can be a 50% loss of neurons before the sufferer becomes symptomatic. Moreover the model develops an oscillatory component analogous to the resting tremor when the dopamine loss becomes too great. This also allows us to advance hypotheses on the causes of the rigidity and bradykinesia complaints. The symptomatic output of the model may be reversed when the modelled effects of common Parkinson's treatments are imposed. Interestingly the D2 receptor agonist ropinirole removes the oscillatory component, leading us to suggest that this may be involved with the known side effect of dyskinesia in high dose L-DOPA patients.

5.2 The Neuroscience of Parkinson's Disease

5.2.1 The Symptoms and Causes of Parkinson's Disease

Named after James Parkinson who first described the disease in detail in 1817 in his *Essay on the shaking palsy*, Parkinson's disease affects 0.5% of the over 50's. The underlying cause is unknown but it is generally assumed that is does have a clearly defined cause. There is no evidence for dietary or infectious influences. In a minority of cases the disease is inherited. Whilst increased incidence has been linked at various times to both industrialised and rural areas, decreased incidence has been observed in cigarette smokers (this is probably due to nicotine's neuroprotective effects)[96].

The classical symptoms are disturbances in movement[45][96]. There is a resting tremor in limbs that disappears on movement or sleep; a muscle rigidity that offers a resistance to movement and often makes such movement jerky or have a cogwheel feel. There is a difficulty in initiating movement, which is generally slow. This typically results in the shuffling gait of sufferers and they often grind to a halt, unable to move. Making them step over an obstacle frees them from this paralysis. There are other symptoms typical of sufferers; stooped posture, speech problems, excessive sweating and micrographia (small writing). Dementia has also been recorded, though infrequently, in Parkinson's sufferers.

Post-mortem examination of the brains of Parkinson's disease sufferers reveals a specific degeneration of the substantia nigra pars compacta region, a dense projection of principally dopaminergic neurons to the striatum. Indeed a greater than 50% depletion in dopamine and its metabolite homovanillic acid has been observed in the striatum of Parkinson's patients. It is this loss of dopaminergic function in the striatum, with its involvement in motor control, that is thought to account for many of the symptoms of the disease. There is less pronounced cell loss in the locus coeruleus and the nucleus basalis of Meynert [96].

The remaining neurons of the nigrostriatal pathway increase dopamine metabolism and there is also a postsynaptic upregulation in dopamine receptors. Such compensatory mechanisms will, in part, be responsible for the absence of clinical signs for the disease until there is some 80% depletion of dopamine cells [45][96].

Since the symptoms of Parkinson's are thought to be largely due to the depletion of striatal dopamine, treatments for it have centred on dopamine replacement. Dopamine taken orally is not useful since it does not pass the blood-brain barrier, however its precursor, L-3,4-dihydroxyphenylalanine (L-DOPA) does. L-DOPA then is metabolised to dopamine in the

brain and has been shown to alleviate symptoms if given in a high enough dose. When given with benserazide or carbidopa, to prevent peripheral metabolism to dopamine, L-DOPA is a successful therapy for the symptoms of Parkinson's. The treatment does have side effects such as a decreased efficacy with time; dyskinesia (involuntary, jerky movements) and psychiatric disturbances, probably by over-activation of the neighbouring mesolimbic pathway.

A lower incidence of dyskinesia has been seen in the treatment of Parkinson's patients with dopamine D2 receptor agonists such as apomorphine, bromocriptine, or more recently, ropinirole. These tend to be less potent than L-DOPA, but a combination of dopamine agonist and low doses of L-DOPA has been shown to be effective. The efficacy of dopamine agonists, which will provide a constant stimulation of dopamine receptors, supports the idea that the striatonigral neurons provide a tonic level of synaptic dopamine.

Monoamine oxidase B (MAO-B) inhibitors, such as selegiline, have been used in treatment therapies to reduce the breakdown of synaptic dopamine. Whilst it does not appear to have an effect on its own, it does seem to potentiate L-DOPA treatment. A more advanced attempt at treatment has been the transplanting of dopaminergic cells into the diseased brain. Results have been mixed and the technique is still experimental.

Whatever the causes of the disease, it is generally expressed by the progressive death of the sufferer's dopaminergic neurons, principally in the nigrostriatal pathway. There is a reciprocal (striatonigral) GABAergic pathway and so the two units form a feedback loop. It would seem to be that the symptoms of Parkinson's arise as a result of the changes that the degeneration of dopamine cells induces on this loop.

5.2.2 The Microcircuitry of the Striatum

All communication between the striatum and other cell nuclei is associated with one type of striatal neuron, the so-called medium spiny neuron [8] [37] [76]. With a soma some 15-20μm in diameter and a profusion of dendrites with many dendritic spines (hence the name), they release the neurotransmitter GABA and are hence inhibitory in action. A large amount of dye-coupling has been observed between these spiny neurons, indicating the cells are linked by gap junctions [73].

Major projections are sent to the substantia-nigra pars reticula, which we shall cover in the next section, and to the thalamus. It is through this connection that the spiny neurons exert an excitatory (by inhibiting other inhibitory inputs) influence on the motor cortex and hence

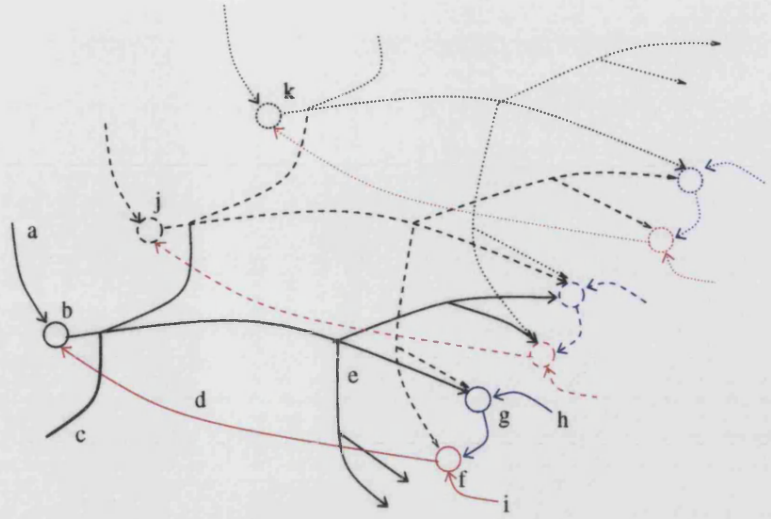

Figure 5.1: Schematic diagram of the connections between the striatum (black) and the substantia-nigra pars reticula (blue) and pars compacta (red). The parts are: (a) cortical input to the (b) striatal projection neuron; (c) gap junction connections between projection neurons; (d) dopaminergic input from the substantia-nigra pars compacta; (e) arborisation of the GABAergic striatal projection to the substantia-nigra neurons; (f) dopaminergic substantia-nigra neuron; (g) GABAergic input from the pars reticula; (h) and (i) cortical excitation (glutamate) to the substantia-nigra. (j) and (k) are the neighbouring neurons.

the firing of the medium spiny neurons (which we shall refer to as striatal projection neurons) is positively correlated with movement. This correlation allows us to model our output as the firing of the striatal projection neurons and removes the need to model the propagation of signals through other nuclei such as the thalamus, this would be immensely complicated.

The spiny neurons receive excitatory (glutamatergic) input from the cortex. This input to the cells has been observed to be an extremely powerful and coordinated current that if it were not for strong potassium channels intrinsic to the cells would drive them to over-excitation. The coordination of the input endows the neuron with a switch-like on/off quality, either resting at a low membrane potential or depolarised to a action potential firing state [103].

The other major input that the striatum receives is the dopamine input from the substantia-nigra. This input is inhibitory in overall effect but has both excitatory and inhibitory components [52][54]. Dopamine receptors of the D1 type mediate the excitatory component by activating the second messenger adenylyl cyclase. The inhibitory component is mediated by receptors of the D2 variety which open ion channels selective for potassium. A dopamine D2 receptor supersensitivity has been observed in animal models of Parkinson's disease, the

lower levels of synaptic dopamine cause the upregulation in the number of D2 receptors and a downregulation in D1's [96].

Projections to the substantia-nigra and the reciprocal connections are topographically organised in that closely originating projections from the striatum terminate close together in the substantia-nigra and the returning fibres terminate close to the source of the striatal output [76]. The circuitry of the striatum and the substantia-nigra is summarised in Figure 5.1

There are other (less abundant) types of neuron within the striatum; these include large aspiny GABA releasing neurons, Substance-P releasing neurons [8] and small cholinergic neurons [46]. Little work has been done on the arrangement of the connections for these neurons, but what has been done can be neatly summarised in the following statement; each type of neuron makes connections with all other types in the striatum. Naturally this will lead to problems in modelling this region, but the anatomical work does reveal that these inter-neurons make only local connections even within the striatum and so their effects are likely to involve the modulation of only small numbers of discrete projection neurons.

5.2.3 The Microcircuitry of the Substantia-Nigra

The substantia-nigra, divided into pars compacta and pars reticula regions, is much simpler in that there are only two abundant types of neurons [71]. The major neuron is the dopaminergic, the cells that are killed off in Parkinson's disease. These cells arise in the pars compacta and are arranged in a sheet 4-6 neurons thick. They project predominantly to the striatum and to the cortex, although it is the nigrostriatal projection that is most affected by Parkinson's. Labelling both pathways has revealed a small number of noradrenergic cells.

The dopaminergic cells receive an excitatory input from the cortex, an inhibitory input from the striatum and an inhibitory GABAergic input from the other major type of neuron in the substantia-nigra, the GABAergic interneuron. Located in the pars reticula, these fast firing neurons receive a GABAergic input from the striatal projection neurons. The interneurons are much more sensitive to GABA than the dopamine neurons and so, despite the direct striatal connection, striatal excitation has an overall excitatory effect on the dopamine neurons by preferentially inhibiting the inhibitory input from the interneurons [29].

The dopamine cells also have a self and near neighbour inhibition since they release dopamine from their dendrites which are also endowed with D2-type receptors [54] [71].

5.2.4 Aims of the Model

It is clear from the above descriptions of the circuits involved that we can, at best, model the striatonigral feedback loop and so study how the output from the striatum changes as dopamine cells are killed off. There are certain aspects of Parkinson's disease that we would hope to model. The first of these is the apparent redundancy involved in the system, the classical symptoms (tremor, etc) are not observed until there has been about an 50% depletion of dopamine cells. It implies that either large parts of the system are redundant, or that it has a large array of compensatory mechanisms.

Implicit in this is a more fundamental question, what is it that goes wrong? The death of the dopaminergic cells undoubtably has an effect, the effective treatment of Parkinson's by dopamine replacement and fetal transplants [96] indicates that it is the degeneration of these cells that is responsible for the symptoms. Since the major target of these cells is the striatum the symptoms must be traceable to changes in these neurons. What change is this?

If we are then able to identify what changes are induced by the onset of Parkinson's then we may be able to identify the roots of sufferer's symptoms. We would aim to define under what conditions, or at least advance hypotheses, as to how such things as a tremor at rest arise and why advanced Parkinson's may induce muscle rigidity. Moreover, by knowing how the onset of Parkinson's disease causes disruptions in the striatum we may also be able to characterise the action of Parkinson's treatments, specifically the widely used L-DOPA.

With the complex nature of the system under study, possibly thousands of neurons with thousands of connections, means that an accurate quantitative model is unlikely to be possible. We must therefore concentrate our efforts on producing a model that provides a good qualitative description of the action of the striatal output.

5.3 The Model

5.3.1 The Reduced Circuit

The massively complicated microcircuitries of the striatum [8] and, to a less complicated extent, the substantia-nigra [71] described above essentially preclude detailed modelling of all the neuron types and connections involved. Since the precise internal and external circuit connections cannot be known in their entirety any modelling attempt is clearly doomed to

failure. We must therefore make assumptions on the nature of the circuits involved and hence reduce the system to a more manageable size that we can model.

We are going to include both the sheet of striatal projection neurons and the dopaminergic neurons of the substantia-nigra since our principal aim is to study the effect of the former due to the degradation of the control imposed by the latter. Since these two types of neuron form the majority of connections between the striatum and substantia-nigra, we make the assumption that these are the only connections between the two and then may function as discrete units.

Dopamine neurons directly innervate the striatal projection neurons and have a principally inhibitory effect mediated by D2-like receptors and hence we include this in our model. We do not include the excitatory influence of the less abundant D1-like receptors. This is particularly valid for the latter stages of Parkinson's disease, where the lower levels of extracellular dopamine leads to the upregulation of D2 receptors and the downregulation of D1's [96]. We prescribe an external, excitatory input to the striatal projection neurons to model the dense glutamatergic innervation from the cortex. We are then able to describe the main features of the striatal innervation; excitation by glutamate and inhibition by dopamine. We assume that the contribution from the complex internal microcircuitry of the striatum is negligible and only include the coupling of the projection neurons via gap junctions, and then only nearest neighbour coupling. Hence the only efferent output of the striatum comes from the projection neurons.

Since the GABAergic input to the substantia-nigra has an (ultimately) excitatory influence on the dopamine neurons we actually suppose that the striatal neurons make direct excitatory connections with these neurons. This precludes the need to model the GABAergic interneurons responsible for this excitation by relief of inhibition and therefore greatly simplifies the circuitry. Indeed this reduces the substantia-nigra circuitry to excitatory inputs to the dopamine neurons from the striatum and the cortex.

We make further assumptions on the connections between the striatum and substantia-nigra, principally that many dopamine neurons project to a selection of striatal neurons and only this selection. Each striatal neuron is known to receive inputs from many dopamine neurons [8], moreover single dopamine neurons send many afferent fibres into the striatum with many destinations [71]. It is likely that the same dopamine neuron will innervate many striatal neurons but we make the assumption that it only innervates, significantly, the neurons that it receives inputs from. This simplifies our circuitry again. In turn each of these striatal

neurons sends afferent fibres to these dopamine neurons and as the output (to the thalamus).

Our circuit has then been reduced to individual "packets" of striatal neurons exciting another collection of dopamine neurons, which produce inhibitory feedback. The packets are connected to their neighbours via the gap junctions between adjacent striatal neurons.

5.3.2 Modelling the Dopamine Neurons

Since we are interested in the longer term implications of the death of dopamine neurons we have no need for complex integrate and fire models of single neurons. We are not interested in individual spikes, but more the changes in average firing rate. The firing rate of a cell is typically proportional to the current input to that cell, which over long timescales is proportional to average membrane potential (measured from a resting potential defined to be 0mV) of that cell, except at high levels of excitation where the firing rate tends to saturate [49]. We shall assume that this level of excitation is not reached in the range of our model and therefore, for a dopamine neuron with (average) membrane potential u relative to rest, its average firing rate is βu for some $\beta > 0$. We will ensure that the reversal potentials for all currents will be ≥ 0, so that $u \geq 0$. This averaging out of current input and membrane potential will also be used to take account of the spatial variations in the cells and allow us to regard each cell as a single electrical compartment.

Typically the firing pattern of cells, as well as the pure firing rate, has a significant effect on the terminal release of neurotransmitter. This is true for striatonigral dopamine cells which, like the neighbouring mesolimbic dopamine cells modelled in Chapter 4, can display a bursting pattern that augments dopamine release [35]. However, we are considering dopamine action averaged over minutes and hours and so the variation between the release caused by individual spikes is averaged out in the parameter β.

For a dopamine neuron, we define the membrane potential u by

$$C_D \frac{du}{dt} = R_D(u) + I_D(u, \nu), \tag{5.1}$$

where C_D is the capacitance of the cell membrane [49]. $R_D(\cdot)$ represents the current flow in the cell due to the intrinsic ion channels and pumps and the external input from regions other than the striatum. The external input is modelled as a simple fixed conductance, representing the average synaptic conductance, with a fixed reversal potential derived from the weighted average of the afferent input reversal potentials, that is an equation of the form $g_I(E_I - u)$. Since this is mainly the excitatory glutamate input then $E_I \approx E_{Na/Ca} \approx 90$mV,

the reversal potential of the current of sodium, potassium and calcium ions gated by glutamate receptors [45]. The membrane of dopamine cells shows an approximately linear current-voltage relationship [28] and so may be similarly modelled as $g_m(E_m - u)$, where g_m and E_m are the conductance and reversal potential of this current respectively. These may be combined to form the single term

$$R_D(u) = g_D(E_D - u). \tag{5.2}$$

We model the input from the striatum in a similar way. We suppose that the striatal neurons activate a synaptic connection with the dopamine neurons that has reversal potential E_ν; since this will relieve inhibition of the excitatory glutamatergic neuron it could be regarded as having an additional glutamatergic input (hence E_ν is typically around 90mV). The current gated by each connection is (approximately) proportional to the firing rate of the incident neuron and so the current gated by all striatal connections will be proportional to the average firing rates of the incident neurons ν. For constant of proportionality g_ν, the conductance of all striatal synaptic connections per spike in unit time, the input term is given by

$$I_D(u, \nu) = g_\nu \nu(E_\nu - u). \tag{5.3}$$

We assume the proportionality of firing rate and membrane potential for the striatal neurons. If $\bar{v}$ is the average membrane potential, then $\nu = \gamma\bar{v}$ is the average firing rate for an appropriate $\gamma > 0$. Hence the membrane potential u for a dopamine neuron is given by

$$C_D \frac{du}{dt} = g_D(E_D - u) + g_\nu \gamma \bar{v}(E_\nu - u), \tag{5.4}$$

5.3.3 Modelling the Striatal Projections Neurons

We model the striatal neurons in a similar way, deriving equations for the average membrane potential v. This is of a similar form to the dopamine neurons, described by

$$C_S \frac{dv}{dt} = R_S(v) + A_S(v, \mathbf{u}) + I_S(v, \beta u). \tag{5.5}$$

Again C_S is the capacitance of the membrane, R_S is the regulatory term that describes the combination of currents intrinsic to the cell and the other external inputs, and I_S is the input from the dopamine neurons. We have a new term, A_S, that describes the coupling between striatal neurons through gap junctions.

The simplest of these to describe is the coupling via gap junctions. Gap junctions consist of large macromolecules that extend through the membranes of the coupled cells [45]. Pores

in these molecules allow the exchange of ions and hence the flow of ionic currents between them. The lower resistance of the gap junction compared to the surrounding membrane and extracellular space allows inter-cellular communication leads it to be modelled as a low conductance 'short-circuit' between the cells. We assume there is no leakage from the gap junctions and hence for two coupled neurons of with membrane potentials v_1 and v_2, the current input to the first due to the gap junction is given by

$$I_1 = g_a(v_2 - v_1) \tag{5.6}$$

where g_a is the electrical conductance of the gap junction [10]. The current input to the second is naturally given by

$$I_2 = g_a(v_1 - v_2). \tag{5.7}$$

Note that $I_1 + I_2 = 0$, as no leakage implies conservation of current. This essentially describes the coupling between cells in our model. If the components of the vector $\mathbf{u}$, u_i hold the membrane potentials of the coupling neurons, then the coupling term is given by

$$A_S(v, \mathbf{u}) = g_a \sum_i (u_i - v), \tag{5.8}$$

assuming that all gap junction connections have the same conductance.

The input from the dopamine neurons is modelled like the reciprocal connection from the striatum and is given by

$$I_S(v, \beta\bar{u}) = g_u(c)(m - l)\ \beta\bar{u}\ (E_u - v), \tag{5.9}$$

where E_u is the reversal potential of the current and we put in the explicit term $\beta\bar{u}$ for the (averaged) dopamine neuron firing rate. Here we state the conductance as conductance per synaptic connection per spike in unit time, $g_u(c)$, multiplied by the explicit number of connections $(m - l)$, where m is the original number of connections and l represents those lost due to the onset of Parkinson's disease.

Here the conductance of the each synaptic connection $(g(c))$ is not constant, but instead depends on the synaptic concentration of dopamine c. This comes from the observation by Fornaguera et al [25], amongst others (for example [51]), of dopamine receptor supersensitivity in 6-OHDA-lesioned rats, that is the receptors upregulate in response to low concentrations of synaptic dopamine. The conductance is given simply by the number of receptors $(R(c))$ multiplied by the single receptor channel conductance g_R

$$g_u(c) = g_R R(c). \tag{5.10}$$

We lack a good characterisation of the processes underlying this dopamine receptor supersensitivity. However we only require a model that behaves correctly qualitatively, i.e. it has increased receptor numbers in response to lower averages of synaptic dopamine and so we use the simplest model with this property. We assume that the dopamine receptors are produced at a constant rate k_1 from an abundant substrate S_R, but that their rate of decay, proportional to the number of receptors, increases with the concentration of dopamine. We assume a decay term of the form $(k_2 + k_3 c)R$. The number of receptors is then given by

$$\frac{dR(c)}{dt} = k_1 S_R - (k_2 + k_3 c)R. \tag{5.11}$$

Of particular relevance is the steady state number of receptors R^*, given by

$$R^*(c) = \frac{k_1 S_R}{k_2 + k_3 c}. \tag{5.12}$$

The rates of production and decay of receptors will be fast (hours to days) in comparison to that of cell death due to Parkinson's (years) [67] [96], and so when studying the dynamics of the model with respect to the progressive death of cells we assume that the receptor numbers are at an averaged steady state. These rates are still slower than any dynamic changes in the firing rates of the dopamine neurons which we would expect to be more of the order of seconds, such that the receptor number can be regarded as constant. In this case the receptor number is taken to be $R^*(c) = R^*(\bar{c})$, where $\bar{c}$ is the dopamine concentration averaged over a sufficiently long period of time. Note that in our formulation $\bar{c} \propto \beta \bar{u}$ and hence

$$\bar{c} = k_c \beta \bar{u} \tag{5.13}$$

for an appropriate choice of k_c. Regarding R as a constant makes our analysis much simpler.

We must now derive the regulatory term for the striatal neurons, $R_S(v)$, which is considerably more complex than the corresponding term for the dopamine neurons. This complexity lies in the nonlinearity of the cell membranes own current-voltage relationship, as observed by Wilson and Kawaguchi [103].

Wilson and Kawaguchi observed that the spontaneous membrane potential of striatal projection neurons tends to oscillate between two levels, from a Down state (-61 to -94 mV) to an Up state (-71 to -40 mV), with little time spent inbetween. This reveals what one may be tempted to refer to as a bistability in the current-voltage relationship, although this is not quite true, since the Up state only exists in the presence of the enormous synaptic excitation that these cells receive. Although they found they could not abolish these fluctuations by alteration of the membrane potential, intracellular injection of current did alter the time

spent in each state. As one would expect, the injection of depolarising current increased the tendency of the neuron to be in the Up state.

Experimentation involving the pharmacological blocking of intrinsic ion channels, particularly the results regarding the caesium-poisoning of potassium channels, led to the following explanation. The experimental results suggest that the Up and Down states are determined by the interaction of intrinsic potassium channels with the synaptic excitation. There are two types of potassium channel (of significance), one is activated at hyperpolarised membrane potentials and is responsible for the maintenance of the Down state, attained in the absence of the synaptic excitation. This channel inactivates if held at depolarised membrane potentials and hence has steady-state current characteristics that resemble the A-type potassium channel. In the presence of the synaptic excitation, a powerful and coordinated input, the cell depolarises. This inactivates the A-type-like channels and the cell is then constrained from hyper-excitation in the Up state by the repolarising influence of another form of (caesium-sensitive) potassium channels. This depolarisation-induced activation would suggest that these channels are similar to the so-called delayed-rectifying potassium channels.

Traub et al [98] used Hodgkin and Huxley-type models of A-type and rectifying potassium channels in their model of hippocampal pyramidal neurons. The steady state current in the soma for these channels can be seen in Figure 5.2. From this it is quite clear how such a two-state membrane potential could arise; with the absence or presence of the synaptic excitation shifting the steady-state voltage to the left or right branch of the steady state current curve respectively. The middle (unstable) branch would serve to separate these two stable branches and 'flick' the potential from one to the other as the synaptic current dictates.

Wilson and Kawaguchi's experimental findings [103] suggest that the striatal projection neurons have a steady-state current-voltage relationship like that found in Traub's model. Obviously we do not wish to model to the depth of ion channel kinetics and so, noting the cubic-like appearance of the steady state current curve, we choose

$$R_S(v) = g_s(a - v)(v^2 + b) + I_{syn}(t) \tag{5.14}$$

for $g_S, a, b > 0$, the simplest representation of a cubic with a single real zero (at $v = a$). Taking a large and b small gives us the correct cubic appearance, as we shall see later on (strictly $b < a^2/27$). The $I_{syn}(t)$ term is simply the synaptic excitation current which we take to be either 0 or I_{max}, a positive constant.

Our modelling of the striatal projection neurons is essentially complete, for such a neuron,

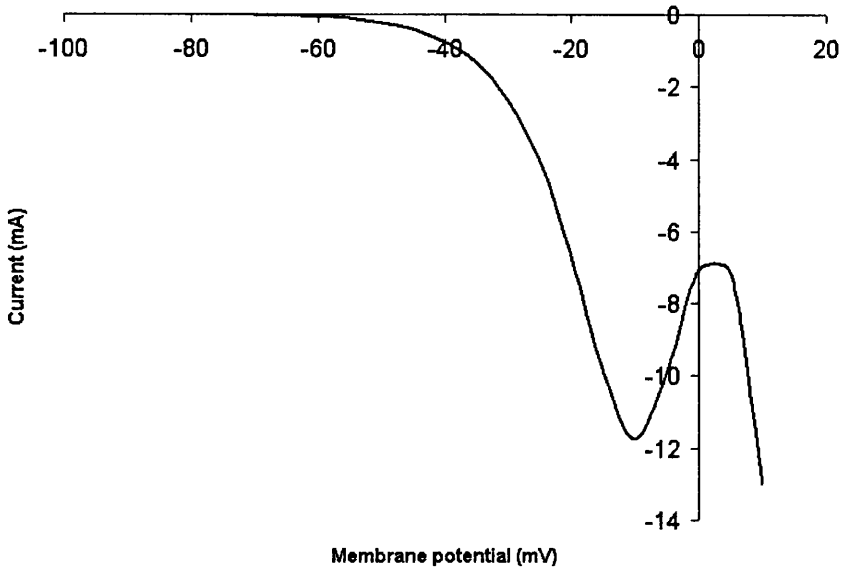

Figure 5.2: The steady-state current in milli-amps against clamped membrane potential for the somatic A-type and delayed-rectifying potassium channels, for the channel parameters taken from Traub et al [98]. The curve has a cubic appearance, reflecting the alternation between the inactivation of the A-type channels and activation of the delayed-rectifier (and hence we use a cubic form for our model). The cell rests at around -70mV where the steady current is zero, however powerful excitatory current input would shift the curve upwards and the steady state would lie at more depolarised potentials, possibly such that it lies on the right branch of the $I - V$ curve.

the membrane potential v is given by

$$C_S\frac{dv}{dt} = g_S(a-v)(v^2+b) + I_{syn}(t) \; + \; g_a\sum_i(u_i - v) \; + \; g_u(c)(m-l)\;\beta\bar{u}\;(E_u - v). \quad (5.15)$$

5.3.4 The Model Packet Network

Sections 5.3.2 and 5.3.3 describe how we have chosen to model the two types of neuron that our model features. Our analysis can be simplified further by a few observations on the nature of this modelling. One such simplification has already been mentioned in that, by analysis of the timescales, we regard the number of dopamine receptors as constant, i.e. $g_u(c) = g_u$ is constant. Also, since the inhibitory dopaminergic input to the striatum will tend to prevent the cell from firing, it is sensible to take $E_u \approx 0$. As the striatal input to the dopamine neurons is supposed to be excitatory, we shall also assume that $E_D < E_\nu$.

Whilst the gap junctions modelled allow communication directly between striatal neurons, the conductance of gap junctions (which we called g_a) is small in comparison to the conductance of the intrinsic channels of cells and their (chemical) synaptic connections [45] [48]. Hence we shall regard the influence of these gap junctions to be negligible in comparison to the regulatory (R_S) and synaptic (I_S) currents. We shall only have cause to consider them when we study coupling between packets in section 5.3.7.

A simple observation of the model reveals the following; we have regarded each striatal neuron and each dopamine neuron to be identical. Moreover each receives exactly the same input and hence *each striatal neuron and each dopamine neuron behaves exactly the same.* Hence the averaged firing rates $\bar{v}$ and $\bar{u}$ are the actual firing rates v and u of these neurons and so, when considering a single packet, we can regard it as a simple loop of one striatal neuron and one dopamine neuron. This reduces our system to being able to study isolated packets that have only two independent variables v and u. Then a packet is described by:

$$C_S\frac{dv}{dt} = g_S(a-v)(v^2+b) + I_{syn}(t) \; - \; g_u(m-l)\beta uv, \quad (5.16)$$

$$C_D\frac{du}{dt} = g_D(E_D - u) + g_\nu\gamma v(E_\nu - u). \quad (5.17)$$

For notational convenience we substitute $C'_S = C_S/g_S$, $I_{syn}(t) = I'_{syn}(t)$ and $g'_u = g_u(m-l)\beta/g_S$ into equation (5.16) and $C'_D = C_D/g_D$ and $g'_\nu = g_\nu\gamma/g_D$ into equation (5.17) to obtain the slightly simpler

$$C'_S\frac{dv}{dt} = (a-v)(v^2+b) \; - \; g'_uuv \; + \; I'_{syn}(t), \quad (5.18)$$

$$C'_D\frac{du}{dt} = (E_D - u) + g'_\nu v(E_\nu - u). \quad (5.19)$$

Before we lose sight of it altogether, we should reiterate that the onset of Parkinson's will, by killing off dopamine neurons, gradually decrease the parameter g'_u.

5.3.5 Projection Neuron Dynamics

We have made many assumptions on the circuitry involved in the striatum and substantia-nigra and then again in attempting to model the behaviour of individual neurons. Before studying the effect that the onset of Parkinson's disease has on our system (5.18)-(5.19) we shall take a moment to demonstrate that the striatal neurons do have the two-state membrane potential that is observed experimentally [103]. As we have managed to reduce our model to a two variable system this is most easily done by phase plane analysis.

For the $\dot{v} = 0$ nullcline we obtain

$$u = \frac{1}{g'_u v}\left((a-v)(v^2+b) + I'_{syn}(t)\right) \tag{5.20}$$

and for the $\dot{u} = 0$ nullcline

$$u = \frac{E_D + E_\nu g'_\nu v}{1 + g'_\nu v}. \tag{5.21}$$

The Jacobian for the system (5.18)-(5.19) is given by

$$J = \begin{pmatrix} -3v^2 + 2av - b - g'_u u & g'_\nu(E_\nu - u) \\ -g'_u v & -(1 + g'_\nu v) \end{pmatrix} \tag{5.22}$$

from which we may write the trace of the Jacobian as

$$\mathrm{tr}J = -3v^2 + 2av - b - g'_u u - (1 + g'_\nu v) \tag{5.23}$$

which is negative except for a sub-interval of $\left(\frac{a}{3} - \frac{1}{3}\sqrt{a^2 - 3b}, \frac{a}{3} + \frac{1}{3}\sqrt{a^2 - 3b}\right)$ if a is sufficiently large and b sufficiently small. The determinant is given by

$$|J| = (3v^2 - 2av + b)(1 + g'_\nu v) + g'_u(u + g'_\nu v E_\nu) \tag{5.24}$$

which is large and positive for E_ν sufficiently large.

For $I'_{syn}(t) = 0$ a typical phase plane could look like Figure 5.3, which corresponds to the Down state of the neuron. The left branch of the $\dot{v} = 0$ nullcline grows like $(g'_u v)^{-1}$ and so for this state to exist, g'_u must be large (the dopaminergic input is strong) and the gradient of the $\dot{u} = 0$ nullcline must be steep for small v. We therefore assume that $E_\nu g'_\nu$ is large, we shall show later with some parameter estimation that g'_ν is 'not particularly big' and so we

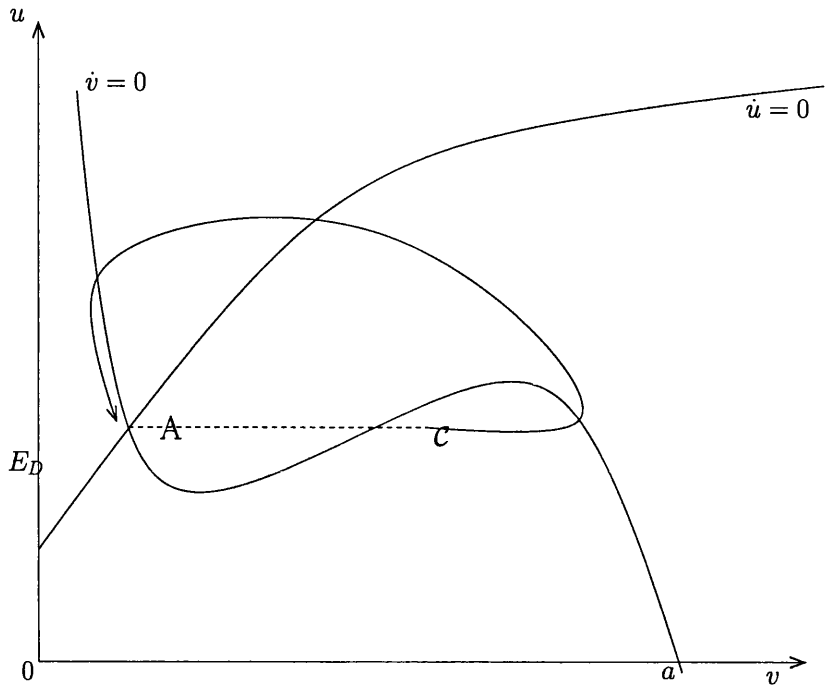

Figure 5.3: The phase plane diagram for $I'_{syn}(t) = 0$ corresponds to the Down state of the neuron, with the point A marking a stable node or focus.

take our condition to be that E_ν is large; which section 5.3.2 suggests and we shall assume this is large enough.

This also ensures that the point A is a globally stable node or focus, the steady membrane potential in this hyperpolarised state. However the system is excitable, in the sense that any deviation of v past the middle branch of the $\dot{v} = 0$ nullcline causes the system to go on a large deviation along the curve C before it can return to the steady state A. Hence a sufficiently large current input can cause the striatal membrane potential to 'flip' up to a more depolarised membrane potential and, if the current is too small or not maintained, drop back to the hyperpolarised state. This illustrates the quick transitions between the Up and Down states seen by Wilson and Kawaguchi [103].

If the current $I'_{syn}(t) = I'_{max}$ is sufficiently big, the steady state will shift from the left to the right branch and the membrane potential will stay at this more depolarised state. Naturally this corresponds to the Up state, as illustrated in Figure 5.4. The steady state B is also excitable in that hyperpolarisations in the striatal membrane potential cause a similar large deviation before returning.

The effective separation of the Up and Down membrane potentials is caused by the $\dot{v} = 0$ nullcline having two positive (in terms of v) turning points. This is ensured by the condition

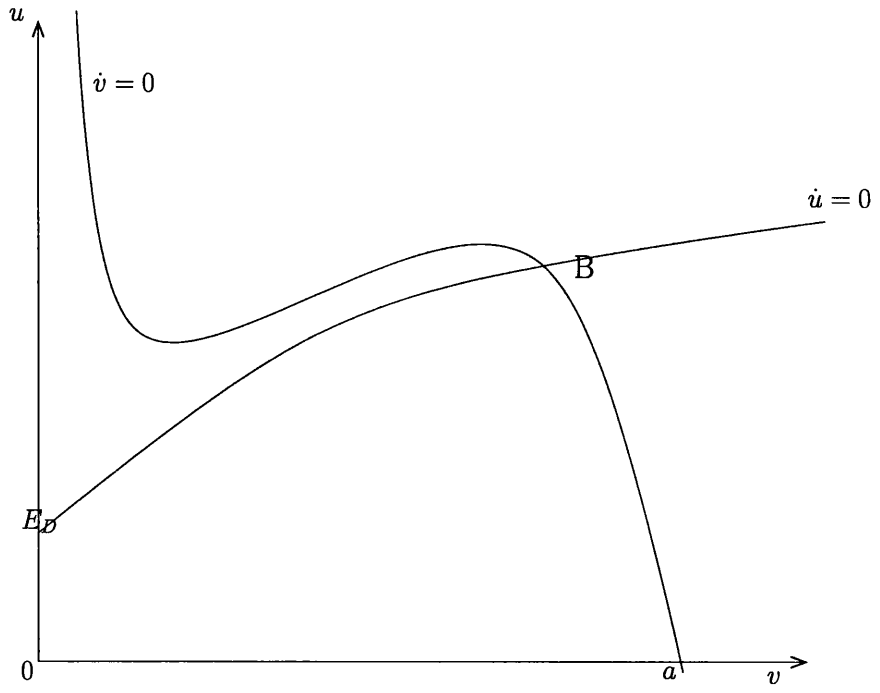

Figure 5.4: The phase plane diagram for $I'_{syn}(t) = I'_{max}$ corresponds to the Up state of the neuron, the point B is a stable node or focus.

$b < a^2/27$ and may be obtained by differentiating the $\dot{v} = 0$ nullcline equation (5.20) with respect to v and considering the zeros and turning points of this function.

We have so far considered $I'_{syn}(t)$ for sufficiently small and large values, such that the phase plane has stable spirals corresponding to the Down and Up states respectively. From the work of Wilson and Kawaguchi it is clear that the synaptic input is extremely powerful and has a switch-like on and off capability that may well preclude intermediate currents where there is a steady state on the middle branch (where instability can occur). However, we need to study this possibility as it not only serves to reinforce our modelling, but also has very important implications later on when we consider the effects of the onset of Parkinson's disease.

There are two possibilities when our model has a steady state on the unstable branch. Figure 5.5 shows the case where we have three steady states, C, D and E, of which C and E and stable and D is unstable. Hence for this range of parameters the Down (C) and Up (E) states co-exist and perturbations in the striatal membrane potential can cause shifts between them.

The other, which proves to be more interesting, possibility is illustrated in Figure 5.6, that of a single unstable steady state, labelled F. The steady state is unstable if $\mathrm{tr}J > 0$ which can occur around $v^* = a/3$ if a is sufficiently big. Taking b and $1 + g'_\nu$ to be negligibly small

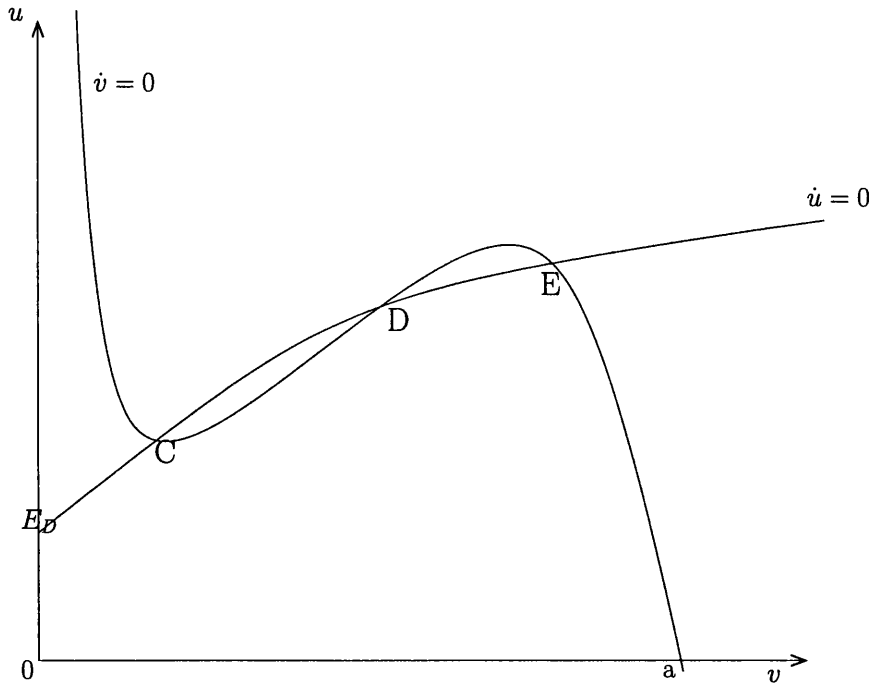

Figure 5.5: A possible phase plane diagram for intermediate values of $I'_{syn}(t)$ that produces two stable (C and E) and one stable (D) steady states and therefore exhibits bistability.

(O(1)) in comparison, $a = O(10)$, then we have instability at $v^* = a/3$ for

$$\frac{a^2}{3} > g'_u u^* = \frac{g_u}{g_S}(m - l)\beta u^*. \tag{5.25}$$

It is difficult to accurately estimate these parameters, but we can indicate whether these conditions could be met. Since a marks the upper limit of the membrane potential for the Up state we can estimate it, from Wilson and Kawaguchi [103], to be equivalent to 30-40mV (relative to the hyperpolarised rest potential of 0mV).

Hence we expect there is instability for $g'_u u^* < 300$, indicating that the dopaminergic conductance needs to be 100 times more powerful than the intrinsic current of the striatal neuron for stability. It seems fair to assume that even though the dopamine does have a potent effect this is not the case, especially when this input is decimated by Parkinson's disease.

Sufficient conditions for the uniqueness of the steady state are

$$a < (g'_v)^{-1}, \qquad a < E_v g'_u \tag{5.26}$$

The latter is met by both E_v and g'_u being large. The former condition corresponds to $a < g_D/(g_v\gamma)$. Wilson and Kawaguchi allow us to estimate γ, with an increase in striatal membrane potential from 0mV to 40mv (relative) only increasing firing to about 5Hz, suggesting $\gamma \approx 0.125\text{mV}^{-1}$. Additional, the work of Grace and Bunney in studying the effects of

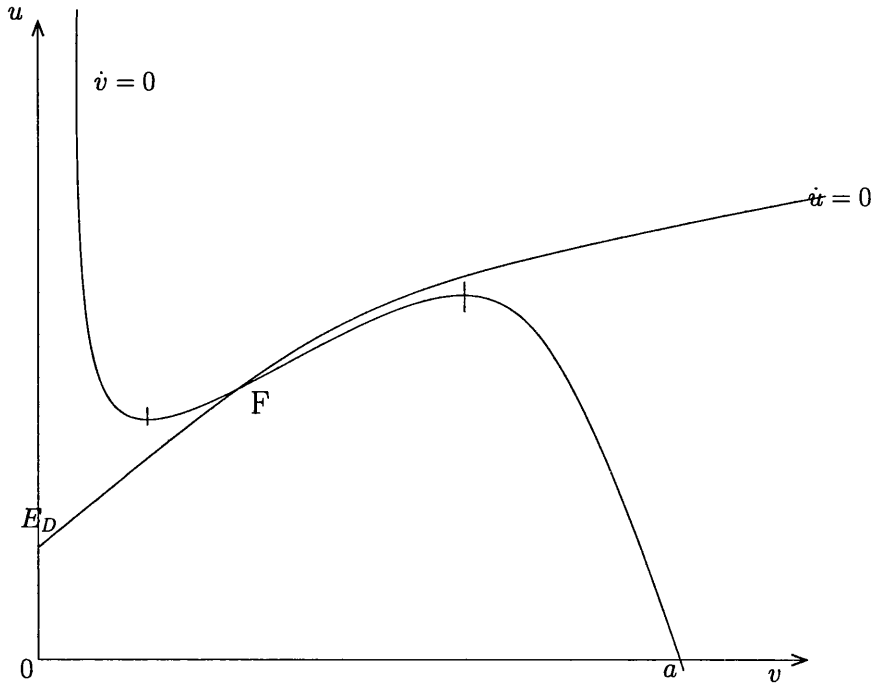

Figure 5.6: A possible phase plane diagram for intermediate values of $I'_{syn}(t)$ that a single, unstable steady state, F. Periodic orbits are possible.

striatal firing on the firing rate of dopamine neurons [29]always to estimate the ratio g_D/g_ν and we obtain $g_D/g_\nu \approx 10$. Since this implies that we require $a < 80mV$, we can demonstrate that the conditions can be, indeed are likely to be, met.

We suppose that these conditions are met and that we have a single, unstable steady state located on the middle branch of the $\dot{v} = 0$ nullcline. Then we have a stable periodic orbit; since this is the only positive steady state, and the set $(v, u) \in [0, a] \times [0, E_u]$ is positively invariant, a straightforward application of the Poincare-Bendixson theorem gives us the result.

We are then forced to ask that, if such periodic orbits exist, why they were not observed by Wilson and Kawaguchi [103]. This is purely the rate of rise of the synaptic current, which goes from (effectively) 0 to full inside 100ms, the approximate time taken for the membrane potential to go from Down to Up. This is much faster than the period of oscillation, which is initially very long and so the Up state is established before any oscillations are apparent.

The time spent in the Up and Down states could be altered by the injection of intracellular current, a feature which our model retains. Intracellular current injection will serve to move the Down steady state along the left hand branch and accordingly alter the amount of current required to cause the jump to the Up state. This will cause the jump to be sooner or later, depending on the current injection, as the synaptic current builds up. A similar argument

applies for the transition from Up to Down.

5.3.6 The Onset of Parkinson's

Whatever may be the root cause of Parkinson's disease, it is clearly expressed in the progressive death of nigrostriatal dopamine neurons, as found in post-mortem examination and modelled in the 6-OHDA lesioning of rat brains[96][45] or as found in MPTP (1-methyl-4-phenyl-1,2,3,6-tetrahydropyridine)-poisoned humans. Our primary objective now is to study the effects that this progressive cell death will have on our model.

For no cell death, the phase plane (for $I_{syn}(t) = 0$) is the same as Figure 5.3, the phase plane for the Down state of the neuron and so the steady state corresponds to a low membrane potential and hence a low firing rate on average. The cell can still easily be controlled by the synaptic current, with this input causing the cell to switch between the Up and Down states as before.

We now suppose that some of the dopamine neurons die. We assume that this does not affect the nigrostriatal connection at all, only the dopaminergic innervation of the striatal neurons. We model this by reducing the strength of this synaptic connection, directly implemented by the $(m - l)$ term, describing m original connections of which l have been lost. While this will tend to reduce the synaptic strength, this shall be partially compensated for by the subsequent upregulation of dopamine receptors, i.e. an increase in $R^*(c)$. However the overall effect will be a gradual reduction in the model parameter g'_u, an effect that would take place over a timescale of years.

The reduction of g'_u causes an appropriate scaling up of the $\dot{v} = 0$ nullcline. This will cause the stable steady state (A) to move down the left branch as shown in Figure 5.7, until it loses stability somewhere on the middle branch after B. Up until the steady state reaches this it retains its stability. Moreover the cell is still controllable in the sense that the presence or absence of the synaptic excitation causes the selection of the Down or Up states respectively.

The above situation describes the model state in the early stages of Parkinson's disease. Although the cells are dying off, the cell is still controllable as long as the steady state stays on the left branch and under these conditions the model shows little change. For an initial steady state far up the left branch and allowing for the appropriate upregulation of dopamine receptors, many cells may have to die before the steady state reaches B. One of the characteristics of Parkinson's disease is that the symptoms do not appear until the disease is

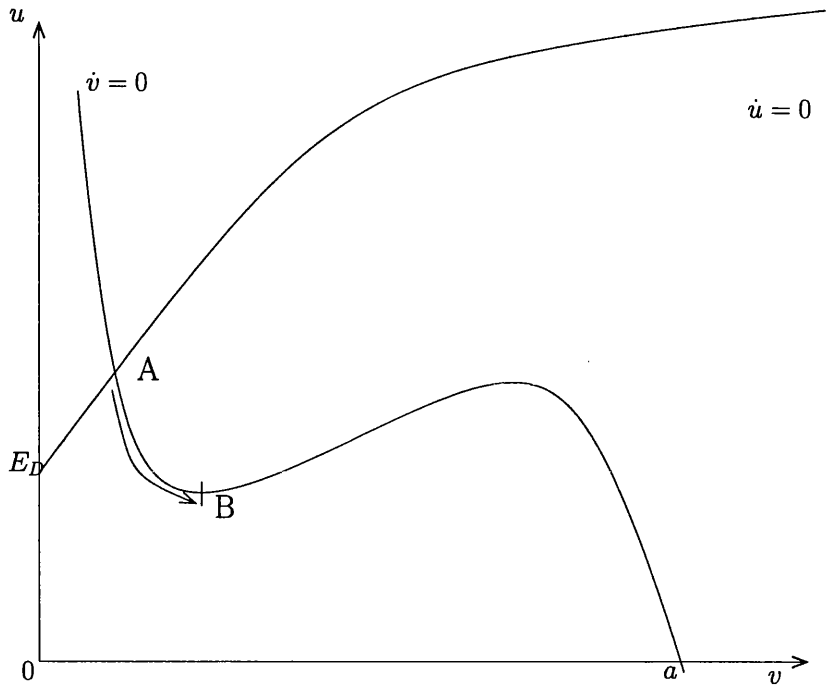

Figure 5.7: The phase plane diagram for the early stages of Parkinson's disease. The steady state A moves down the left branch until it loses stability at the point B.

well progressed, in the sense that up to 50% of the nigrostriatal pathway cells can die before the patient is aware of any problems such as tremors or rigidity [96]. This characteristic of our model provides an interesting hypothesis as to why this is so, with the length of the left branch combined with the compensating upregulation of dopamine receptors [51] allowing the neuron to still function properly as the dopamine input decays.

This situation does change as the steady state passes B and becomes unstable. As illustrated in Figure 5.8, for the steady state between B and C it may be unstable in which case we have a periodic orbit by an application of the Poincare-Bendixson Theorem. We have lost the Down state of the neuron completely; whilst the synaptic excitation can again propel us to the stability of the Up state, in its absence the neuron oscillates between Up and Down. This suggests that at rest, the striatum will still be sending a periodic input to the thalamus, which one would expect to be present in the thalamic output such as motor control. Again we can relate this to the symptoms of Parkinson's disease as one of the earliest signs of its progression is a physical tremor at rest [96].

For more advanced stages of Parkinson's disease the parameter g'_u will become so small that the steady state will move over to the right branch of the $\dot{v} = 0$ nullcline, as illustrated in Figure 5.9. The steady state regains stability here and our neuron is clamped in the Up state,

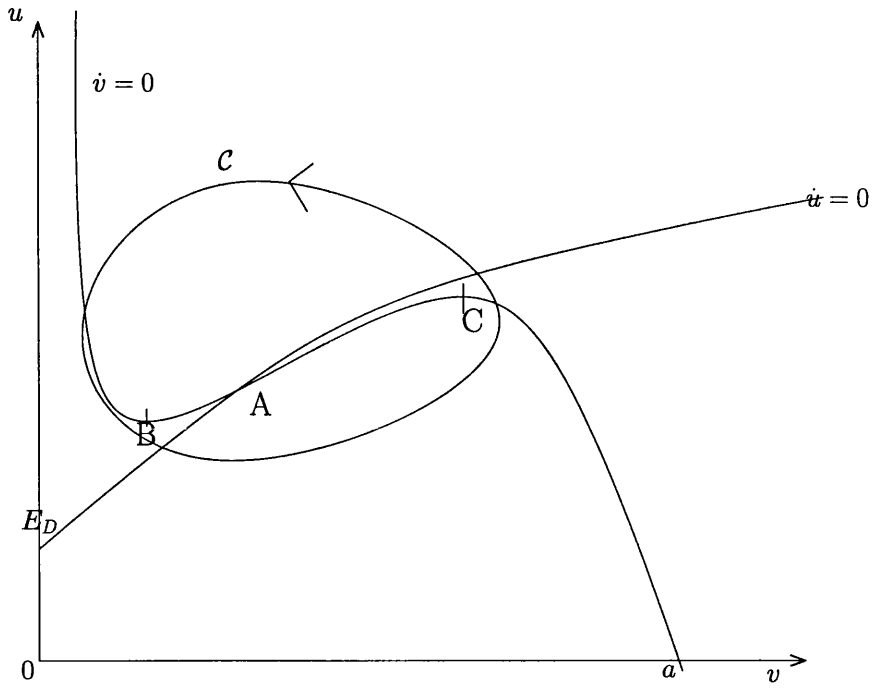

Figure 5.8: The phase plane diagram for later stages of Parkinson's disease. The steady state A is now on the unstable branch and the model admits a periodic solution in the curve $\mathcal{C}$.

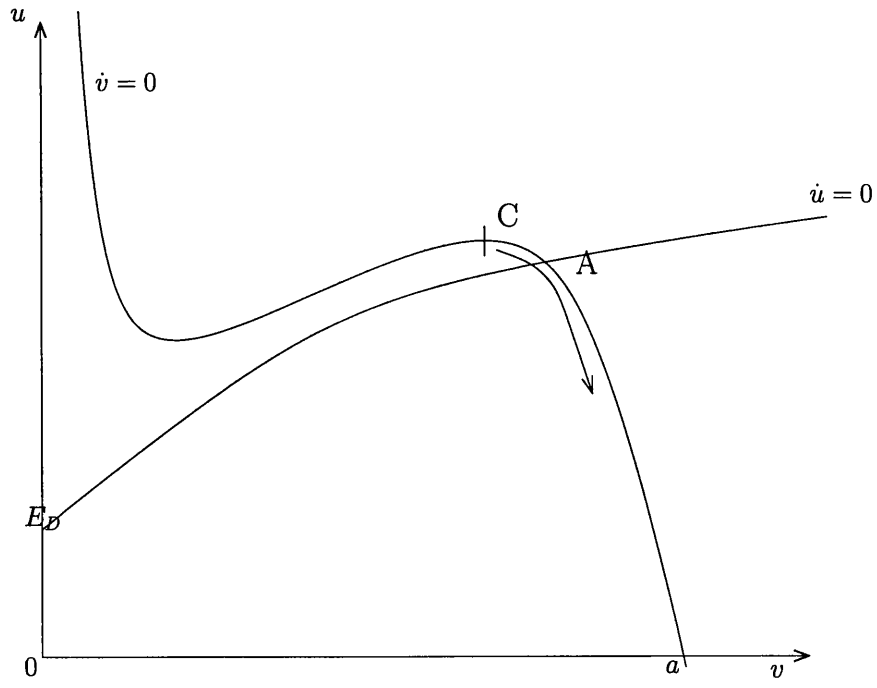

Figure 5.9: The phase plane diagram for the advanced stages of Parkinson's disease. The steady state A has regained stability on the right branch.

even in the absence of the synaptic current. The rise of the synaptic current serves only to shift the steady state further along the right branch and we have effectively lost control of the neuron. Since the neuron is clamped in the Up state, it will be persistently firing at a high rate even in the absence of the synaptic current, in the presence of this powerful current the neuron will be firing at an abnormally high rate. This will cause persistent activation of the thalamus, which may lead to the persistent activation of the motor control output. This may in turn lead to a paralysis of the sufferer as their muscles lock up and is analogous to the rigidity that more advanced Parkinson's sufferers experience.

Our model can also provide some theoretical backing for another problem and solution of Parkinson's disease sufferers. Advanced Parkinson's disease sufferers walk with a shuffling gait and often come to a complete halt, no longer able to move [96]. They can be freed from this paralysis by placing an object in front of them which they need to step over. They are still able to perform this action and find that then they are free to walk again.

To perform the action of walking, the synaptic current to the striatal neurons which maps, via the thalamus, to the muscles associated with walking, will be activated. In advanced sufferers this will cause the striatal neurons, already clamped in their Up state, to fire at abnormally high rates and possibly bring the sufferer to a stop if this over-activates the pathway and forces the muscles to lock. They will not be able to carry on, since such a desire to keeps the synaptic current activated that is causing this rigidity. Distracting the sufferer, such as by making them perform a different action, will switch this off, free the pathway from its over-excitation and thus enable it again.

5.3.7 Network Dynamics

The previous two sections have detailed how individual packets of striatal and dopaminergic neurons behave, both in terms of parameter values and then viewed as the subject of progressive Parkinson's disease. We may now address the question of what happens to the entire collection of packets as a whole. This has a fairly straightforward answer; as the coupling between the packets is weak each behaves independently. However as dopaminergic cells are killed off by Parkinson's disease we would expect that the death of cells is uniformly distributed and therefore that each packet is depleted equally. This in turn implies that each packet (synaptic excitation of the striatal neurons aside) is doing the same thing, they are either all still controllable in the Down state; suffering from oscillations; or clamped in the Up state.

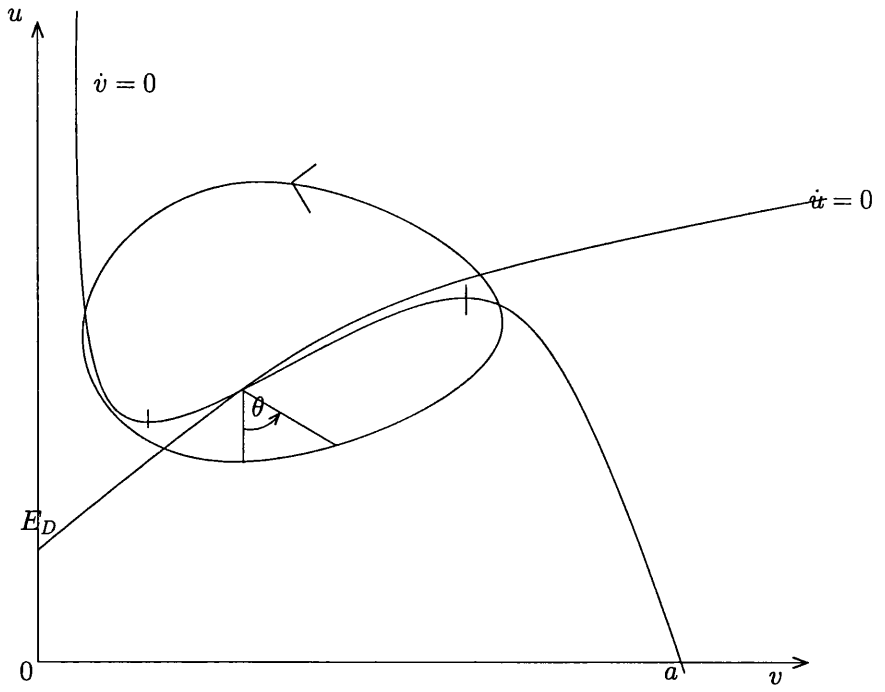

Figure 5.10: For an oscillating neuron the membrane potential can be uniquely determined by the phase angle, θ, see section 5.3.7

If packets are resting in the Down state or clamped in the Up state then the coupling between the packets is zero and each packet is behaving in exactly the same way. We may then deduce the striatal neurons action by reference to sections 5.3.5 and 5.3.6. This is not quite so true if the packets are oscillating. In particular two adjacent packets could be oscillating but whilst one is in the Up state, the other could be in the Down state and vice-versa and in this case the coupling between the cells via the gap junctions is non-zero. We have already considered the case of an oscillatory output from the striatum, but if the oscillating packets are not synchronised (suppose they are uniformly distributed around their cycles) then one would expect the output to actually be approximately constant. We are therefore required to study the cycles of these oscillators with regard to the weak coupling between them.

First, consider an oscillating neuron as in Figure 5.10. The membrane potential v follows a complex course but we can makes things much simpler by thinking of the phase, θ, of the oscillation. θ can simply be regarded as the angle, from some fixed reference (here we choose it to with respect to the line from the steady state, straight down), around the closed curve of the periodic orbit. We can completely characterise the oscillation in terms of θ as for appropriate functions $v = a(\theta)$ and $u = \eta(\theta)$ it uniquely determines the membrane potentials of the striatal and dopaminergic neurons. Note that a possible $a(\theta)$ would be of the form

$a(\theta) = v_d + r(\theta)\sin\theta$, where v_d is the membrane potential of the steady state and $r(\theta)$ is the radial distance of the steady state from the position of the orbit that makes the angle θ.

Now consider two striatal neurons of membrane potentials v_1 and v_2 which we shall assume for the moment are uncoupled. For notational convenience we shall normalise C'_S and C'_D to 1. Then for a suitably chosen $a(\theta)$,

$$v_1(t) = a(\theta_1(t)), \tag{5.27}$$

$$v_2(t) = a(\theta_2(t)), \tag{5.28}$$

where θ_1 and θ_2 are the appropriate phases. Since we have assumed the uniform distribution of cell deaths, each striatal neuron, whether in the same packet or a different one, is oscillating with identical periodic orbits and hence may be described by the same $a(\cdot)$.

Differentiating with respect to time we obtain

$$\frac{dv_1}{dt} = \frac{da}{d\theta}(\theta_1)\frac{d\theta}{dt}(t), \tag{5.29}$$

$$\frac{dv_2}{dt} = \frac{da}{d\theta}(\theta_2)\frac{d\theta}{dt}(t). \tag{5.30}$$

We may choose $a(\theta)$ such that $v = a(\omega t)$ for a constant $\omega > 0$, hence $\frac{d\theta}{dt}(\theta) \equiv \omega$ and obtain

$$\frac{dv_1}{dt} = \frac{da}{d\theta}(\theta_1)\omega, \tag{5.31}$$

$$\frac{dv_2}{dt} = \frac{da}{d\theta}(\theta_2)\omega. \tag{5.32}$$

The periodic orbit of the striatal neurons has a unique minimum and maximum membrane potential, located where the orbit crosses the $\dot{v} = 0$ nullcline. Hence define θ_m and θ_M by

$$\frac{da}{d\theta}(\theta_m) = \frac{da}{d\theta}(\theta_M) = 0, \quad a(\theta_m) < a(\theta_M). \tag{5.33}$$

Let us now consider our striatal neurons to be coupled through gap junctions, as detailed in section 5.3.3. Then we may write

$$\frac{dv_1}{dt} = \frac{da}{d\theta}(\theta_1)\omega + g_A(v_2 - v_1), \tag{5.34}$$

$$\frac{dv_2}{dt} = \frac{da}{d\theta}(\theta_2)\omega + g_A(v_1 - v_2). \tag{5.35}$$

Substituting θ_1 and θ_2 for v_1 and v_2, away from θ_m and θ_M, we obtain

$$\frac{d\theta_1}{dt} = \begin{cases} \omega + g'_A(\theta_1)(a(\theta_2) - a(\theta_1)), & \theta_1 \in (\theta_m, 0] \cup [0, \theta_M), \\ \omega + g'_A(\theta_1)(a(\theta_1) - a(\theta_2)), & \theta_1 \in (\theta_M, \theta_m). \end{cases} \tag{5.36}$$

$$\frac{d\theta_2}{dt} = \begin{cases} \omega + g'_A(\theta_2)(a(\theta_1) - a(\theta_2)), & \theta_2 \in (\theta_m, 0] \cup [0, \theta_M), \\ \omega + g'_A(\theta_2)(a(\theta_2) - a(\theta_1)), & \theta_2 \in (\theta_M, \theta_m). \end{cases} \tag{5.37}$$

Where we have written

$$g'_A(\theta) = g_A / \frac{da}{d\theta}(\theta). \tag{5.38}$$

The asymmetry arises from describing the oscillations of v with the increasing (modulo 2π) variable θ. At the singularities θ_m and θ_M the phase is increasing in a purely u direction, perpendicular to the v component, hence the coupling has no effect and

$$\left.\frac{d\theta_i}{dt}\right|_{\theta=\theta_m,\theta_M} = \omega \quad \text{for } i = 1, 2. \tag{5.39}$$

We are interested in the possible synchronisation of oscillations and so define the phase difference, ϕ by

$$\phi := \theta_1 - \theta_2. \tag{5.40}$$

By writing, where a dot denotes differentiation with respect to time, $\dot{\phi} = \dot{\theta_1} - \dot{\theta_2}$, we may write down a single differential equation for ϕ in terms of θ_1 and θ_2. We notice immediately that such a system has a steady state at $\phi = 0$, that is $\theta_1 = \theta_2$ and the oscillators are synchronised (in phase).

We claim that this is the only steady state of the system. If the periodic orbit describes a perfect ellipse in phase space with axes parallel to the v and u axes and θ traces the phase with a constant angular speed then there is a steady state for the oscillators being in anti-phase ($\phi = \pm\pi$). We assume our periodic orbit is not of this form.

We are then only required to study the dynamics of this system for θ_1 close to θ_2 and we shall only deal with the case $\theta_1, \theta_2 \in (\theta_m, 0] \cup [0, \theta_M)$. The calculations are identical for the case $\theta_1, \theta_2 \in (\theta_M, \theta_m)$ since the change of sign is cancelled out by the change of sign of $\frac{da}{d\theta}(\theta)$. The case when either θ_1 or $\theta_2 = \theta_m$ or θ_M can be calculated in a similar fashion and the same result follows since $\frac{d^2a}{d\theta^2}(\theta) > 0$ close to θ_m and $\frac{d^2a}{d\theta^2}(\theta) < 0$ close to θ_M, by the definitions of θ_m and θ_M.

If, for notational convenience, we set $b(\theta) = \frac{da}{d\theta}(\theta)$ we then have

$$\dot{\phi} = g_A(a(\theta_2) - a(\theta_1)) \left(\frac{1}{b(\theta_1)} + \frac{1}{b(\theta_2)}\right) =: f(\theta_1, \theta_2). \tag{5.41}$$

The steady state at $\phi = 0$ is apparent. Its stability is determined by the sign of

$$\left.\frac{d}{d\phi} f(\theta_1, \theta_2)\right|_{\phi=0} \tag{5.42}$$

Observing that $\frac{d}{d\phi} = \frac{\partial}{\partial\theta_1} - \frac{\partial}{\partial\theta_2}$ we obtain

$$\frac{d}{d\phi} f(\theta_1, \theta_2)\Big|_{\phi=0} = -4g_A, \tag{5.43}$$

which is negative and hence the steady state is stable.

This shows that an isolated pair of coupled packets will synchronise their oscillations. We must now extend this result to any number of packets coupled to their nearest neighbours. Suppose we have $n+1$ such packets with associated phases θ_j then we have

$$\begin{aligned}
\dot{\theta}_1 &= \omega + g_A(a(\theta_2) - a(\theta_1))\left(\frac{1}{b(\theta_1)} + \frac{1}{b(\theta_2)}\right) && (5.44)\\
\dot{\theta}_j &= \omega + g_A(a(\theta_{j-1}) - a(\theta_j))\left(\frac{1}{b(\theta_{j-1})} + \frac{1}{b(\theta_j)}\right) && (5.45)\\
&\quad + g_A(a(\theta_{j+1}) - a(\theta_j))\left(\frac{1}{b(\theta_{j+1})} + \frac{1}{b(\theta_j)}\right) \quad \text{for } j = 2\ldots n. && (5.46)\\
\dot{\theta}_{n+1} &= \omega + g_A(a(\theta_n) - a(\theta_{n+1}))\left(\frac{1}{b(\theta_{n+1})} + \frac{1}{b(\theta_n)}\right). && (5.47)
\end{aligned}$$

Analogously we define $\phi_j := \theta_j - \theta_{j+1}$ for $j = 1\ldots n$ and obtain

$$\begin{aligned}
\dot{\phi}_1 &= -2g_A(a(\theta_2) - a(\theta_1))\left(\frac{1}{b(\theta_2)} + \frac{1}{b(\theta_1)}\right) && (5.48)\\
&\quad + g_A(a(\theta_2) - a(\theta_3))\left(\frac{1}{b(\theta_2)} + \frac{1}{b(\theta_3)}\right), && (5.49)\\
\dot{\phi}_j &= g_A(a(\theta_{j-1}) - a(\theta_j))\left(\frac{1}{b(\theta_{j-1})} + \frac{1}{b(\theta_j)}\right) && (5.50)\\
&\quad - 2g_A(a(\theta_j) - a(\theta_{j+1}))\left(\frac{1}{b(\theta_j)} + \frac{1}{b(\theta_{j+1})}\right) && (5.51)\\
&\quad + g_A(a(\theta_{j+1}) - a(\theta_{j+2}))\left(\frac{1}{b(\theta_{j+1})} + \frac{1}{b(\theta_{j+2})}\right), \text{ for } j = 2\ldots n-1, && (5.52)\\
\dot{\phi}_n &= g_A(a(\theta_{n-1}) - a(\theta_n))\left(\frac{1}{b(\theta_{n-1})} + \frac{1}{b(\theta_n)}\right) && (5.53)\\
&\quad - 2g_A(a(\theta_n) - a(\theta_{n+1}))\left(\frac{1}{b(\theta_n)} + \frac{1}{b(\theta_{n+1})}\right). && (5.54)
\end{aligned}$$

Again we assume that the only steady state is $\phi_j = 0$, $j = 1\ldots n$. Define $\boldsymbol{\phi}$ to be the vector whose components are the ϕ_j's, the steady state is $\boldsymbol{\phi} = \mathbf{0}$. For a small perturbation $\boldsymbol{\eta}$ from this steady state the dynamics are defined locally by

$$\dot{\boldsymbol{\eta}} = J(\boldsymbol{\phi})|_{\boldsymbol{\phi}=\mathbf{0}}\, \boldsymbol{\eta}, \tag{5.55}$$

where $J(\boldsymbol{\phi})$ is the matrix with components $J_{kl} = \frac{\partial f_k}{\partial \phi_l}$, $k, l = 1\ldots n$ where $\dot{\phi}_k = f_k$, i.e. the

Jacobian matrix. Given $\frac{d}{d\phi_l} = \frac{\partial}{\partial\theta_l} - \frac{\partial}{\partial\theta_{l+1}}$ we may calculate this matrix and we obtain that

$$J(\phi)|_{\phi=\mathbf{0}} = -g_A \begin{pmatrix} 4 & 1 & 0 & \ldots\ldots\ldots\ldots & & & 0 \\ 1 & 4 & 1 & 0 & \ldots\ldots\ldots & & 0 \\ 0 & 1 & 4 & 1 & 0 & \ldots & 0 \\ 0 & \ddots & \ddots & \ddots & \ddots & \ddots & 0 \\ 0 & \ldots & 0 & 1 & 4 & 1 & 0 \\ 0 & \ldots\ldots\ldots & 0 & 1 & 4 & 1 & \\ 0 & \ldots\ldots\ldots\ldots & & 0 & 1 & 4 & \end{pmatrix} =: -g_A A. \tag{5.56}$$

The stability of the steady state $\phi = \mathbf{0}$ is determined by the eigenvalues of $J(\phi)|_{\phi=\mathbf{0}}$, if they are all negative then they are stable. This is true if and only if the eigenvalues of the matrix A are positive. Since every principal minor of A has a positive determinant then A is a positive definite matrix, in the sense that $\mathbf{x}^{\mathrm{T}}A\mathbf{x} > 0$ for all $\mathbf{x} \in \mathbb{R}^n$. It then follows that A has positive eigenvalues and so the steady state $\phi = \mathbf{0}$ is stable [55].

We have therefore shown that when neighbouring packets are displaying oscillatory behaviour the gap junctions between them causes the oscillations to synchronise. Therefore this coordinated action would be expected to create a strong oscillatory output from the striatum and possibly cause such Parkinson's symptoms as tremors at rest, hypothesised previously.

5.3.8 Modelling the Effects of Parkinson's Treatments

Although there is no known cure for Parkinson's disease, it is not known what the root cause of it is, the symptoms are treatable [45][96]. Up to the time of writing, patients have been treated with the dopamine precursor L-DOPA. Recently the effective treatment of Parkinson's patients with Requip (ropinirole, a dopamine D2-type receptor agonist) has been demonstrated [2]. It would be interesting to incorporate the effects of these drugs into our model and see if they counteract the changes the onset of Parkinson's disease induces.

There is a contrast in the treatments of L-DOPA and ropinirole as regards dyskinesia. Dyskinesia are unwanted jerky movements often found in long-term high-dosage L-DOPA recipients. It has been hypothesised that this is due to a resulting disturbed control of the dopamine signal that leads to the preferential activation of indirect pathways to the subthalamic nucleus and then on to the thalamus. Rather than damping movement, the indirect pathway would prompt it and result in jerked movements [96]. Recent studies have shown that treating patients with ropinirole greatly reduces the incidence of dyskinesia, only 5% of the ropinirole

test group developed it compared with 90% of the L-DOPA treated group (a combination of ropinirole and L-DOPA produced a 20% dyskinesia rate)[2].

If large doses of L-DOPA can create such an imbalance in the dopamine system it is not immediately clear why another drug that boosts the dopamine input (ropinirole) does not. This may be the result of drug potency, or the different sites of action of the two. It would be interesting to see if our model responds to the two differently also.

L-DOPA

L-3-4-dihydroxyphenylalanine (L-DOPA) has been used in the treatment of Parkinson's disease patients since the 1960's. The basis behind the treatment is quite simple, if the patient is lacking dopamine releasing cells then they can be treated by replacing the lost transmitter. Dopamine will not cross the blood-brain barrier and so cannot be used, but L-DOPA does [96]. It is a dopamine precursor that may be used to synthesise new neurotransmitter. The dopamine neurons of the nigrostriatal pathway will therefore produce more dopamine, and hence release more, than normal. This upregulated release of dopamine will then counteract the reduced release caused by cell death.

Although treatment with L-DOPA is effective it does have drawbacks, such as dyskinesia. Patients also develop a tolerance to L-DOPA's effects. There may be a straightforward reason for this, since the treatment compensates for the lack of dopamine cells by getting the remainder to produce more transmitter and this may partially reverse the compensatory upregulation of dopamine synthesis. Moreover the treatment partly relies on the survival of some dopamine cells and so its effectiveness is decreased as more die.

One can see from this, that although L-DOPA compensates for the cell death by causing the remaining cells to release more dopamine, it could be capable of changing the dopamine signal in another way. Before the onset of Parkinson's, the striatal cells are subjected to input from many dopamine cells firing at similar rates that one would expect to lead to a fairly constant level of dopamine input (this is one of the assumptions on which our modelling is based and is supported experimentally [72]). However this will cease to hold as the large numbers of cells die (a stage at which large doses of L-DOPA will be required). It is possible that for very few remaining cells the signal would look more like temporally discrete peaks of dopamine at the points where these cells fire. This would create a pulsing input to the striatal neurons which could propagate on to create motor problems.

It is the author's opinion that this state is unlikely to be reached until the remaining cells can be numbered in, say, the tens rather than the hundreds and thousands, which would imply 99% depletion. Current opinion also supports the idea that the cells generally provide a steady level of synaptic dopaminergic input, based on the slow action of dopamine receptors [96]. It would be interesting to model this phenomenon and to examine whether such a gradual discretisation would make a difference to the post-synaptic signal. This would require a model with detailed temporal resolution, of our current model which tells us nothing.

So what does our model tell us about the action of L-DOPA? We must first consider how the effect of L-DOPA can be incorporated into our model. We have already stated that it increases the amount of dopamine released by the nigrostriatal neurons, but we have not explicitly included such a term. Instead we note that the cell firing at the same rate with increased dopamine release is equivalent (in our model) to the cell firing at an increased rate with the same dopamine release. Hence the application of L-DOPA can be best modelled by an increase in the parameter that converts the membrane potential into the firing rate, that is β. The model will then behave correctly, since this increased dopamine flow will also serve to cause a slight downregulation in the dopamine receptors, as detailed in section 5.3.5. In terms of our network model (5.18)-(5.19) this will cause an increase in g'_u, precisely the same parameter that is decreased by the onset of Parkinson's.

It is clear from this why L-DOPA is an effective treatment in terms of our model, as it reverses the change that the disease causes. Sufficiently large doses will cause the system to the base state described in section 5.3.5 and by Figure 5.7. The system is once more controllable by the synaptic input. Implicit in this is a reason why larger doses will be needed as the disease progresses, since L-DOPA will need to shift g'_u back from where Parkinson's has pushed it.

Since L-DOPA merely reverses the change that Parkinson's causes there is no obvious reason, in our model, as to why it can cause dyskinesia. However there is one facet of the model that we have not considered as yet that could give rise to a theoretical instability under high L-DOPA conditions. If we consider Figure 5.7, particularly high doses would be capable of shifting the steady state past its original position and further up the left branch of the $\dot{v} = 0$ nullcline. If this shift leftwards is sufficiently big, the presence of the synaptic current $I_{syn}(t)$ may not be big enough to establish the Up state, instead the steady state may lie in the unstable part of the middle branch and oscillations could ensue.

It is not apparent whether oscillations in this pseudo-Up state would cause dyskinesia. However it was observed experimentally strong hyperpolarising currents could turn the Up state

into a period of noisy and irregular depolarisation [103]. By our previous hypotheses on how tremors and rigidity come about it would instead suppose that movements the patient attempts to make are jerky, rather than causing involuntary movements. It is far from clear whether these are merely 'two sides of the same coin'. Whilst this possible reason (or contribution) towards the inducement of dyskinesia may seem rather 'wooly', it should be viewed in the light of the effects of ropinirole on our model, which we detail next.

Ropinirole

Ropinirole is very different in action to L-DOPA, although both seek to increase the dopaminergic input to the striatal neurons. Ropinirole is a dopamine D2 receptor agonist and hence its presence in the synaptic cleft will activate these receptors and inhibit the striatal neurons [11]. It should be noted that this action is independent of the firing of the dopaminergic neurons although one would imagine the two are likely to interfere; ropinirole may compete with released dopamine for receptor occupancy and ropinirole activation of the receptors may prompt their downregulation, recent studies with combined doses of L-DOPA and ropinirole suggest that their effects are additive and therefore they do not interfere significantly[2] [97].

We shall assume the concentration of ropinirole is constant and furthermore that the subsequent activation of dopamine receptors is at steady state. The conductance per synaptic connection induced by the concentration r of ropinirole is then given by

$$g_{\mathrm{Rop}}(r) = g_{\mathrm{Rop}} R(c) m \left(\frac{r}{r + K_r} \right). \tag{5.57}$$

Here g_{Rop} is the conductance per receptor per connection, with $R(c)$ and m being the number of receptors and connections. $r/(r + K_r)$ is the proportion of receptors that are activated by ropinirole, derived from the steady state of the Michaelis-Menten equations, with disassociativity constant K_r. We have assumed that the number of receptors is still dictated by the concentration of dopamine. Since ropinirole action is independent of the number of dopamine cells (excepting induced variations in $R(c)$), this will act on the original m connections. This will serve to conduct an ionic current across the voltage gradient between the membrane potential of the striatal neuron v and the reversal potential of dopamine receptor-mediated current $E_u = 0$. Therefore, with the addition of the ropinirole term, (5.18)-(5.19) becomes

$$C'_S \frac{dv}{dt} = (a - v)(v^2 + b) - g'_{\mathrm{Rop}} v - g'_u uv + I'_{syn}(t), \tag{5.58}$$

$$C'_D \frac{du}{dt} = (E_D - u) + g'_\nu v(E_\nu - u), \tag{5.59}$$

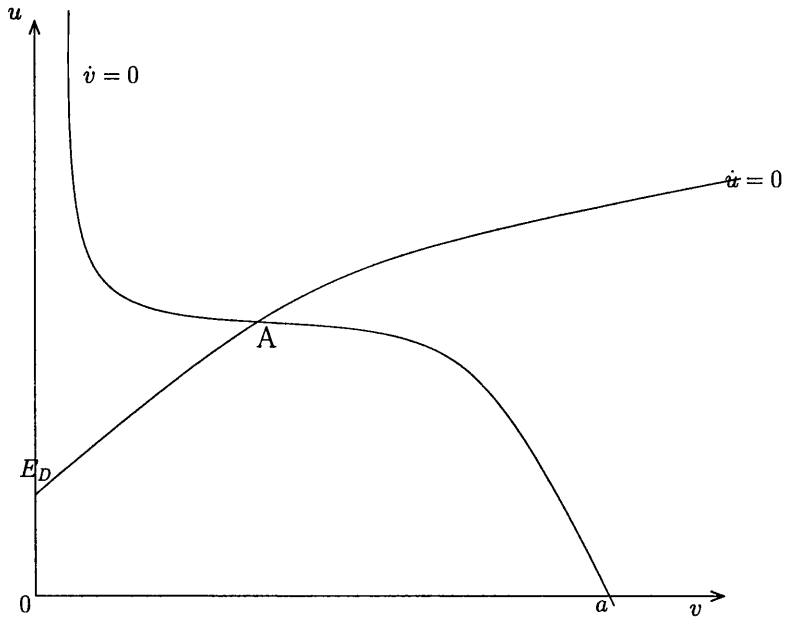

Figure 5.11: The phase plane diagram for strong ropinirole action. The steady state A remains globally stable throughout the $\dot{v}=0$ nullcline and there are no periodic orbits.

setting $g'_{\text{Rop}}(r) = g_{\text{Rop}}(r)/g_S$ as before.

If we recalculate the Jacobian for this revised system we obtain

$$\text{tr}J = -3v^2 + 2av - b - g'_{\text{Rop}}(r) - g'_u u - (1 + g'_\nu v) \tag{5.60}$$

for the trace and

$$|J| = (3v^2 - 2av + b + g'_{\text{Rop}}(r))(1 + g'_\nu v) + g'_u(u + g'_\nu v E_\nu) \tag{5.61}$$

for the determinant.

The trace remains negative for all v if $g'_{\text{Rop}}(r)$ is sufficient big, that is if the effect of ropinirole is sufficiently strong in comparison to the regulatory conductance g_S. This is certainly possible given that the original dopaminergic input is strong and the drug will act on all of the m connections. This means that our system (5.58)-(5.59) does not destabilise and the phase plane looks like Figure 5.11. In particular, there are no periodic orbits for this system.

The steady state still traverses the $\dot{v}=0$ nullcline, shifting leftwards for higher $g'_{\text{Rop}}(r)$ and so ropinirole does act to depress the striatal neurons and allow the recovery of control by the synaptic current. Moreover the situation described above, where large doses of L-DOPA could lead to oscillations in a pseudo-Up state does not occur since the steady state is always stable. While the synaptic current no longer switches between discrete Up and Down states, it will still cause large shifts in membrane potential and hence in firing rate.

We have shown that both L-DOPA and ropinirole help regain control of the striatal neurons. The only significant difference between them in terms of the model output is that ropinirole could remove the ability of the system to oscillate. Hence if the oscillatory Up state possible in high L-DOPA protocols is implicated in dyskinesia, our model shows precisely why it may not be a problem for users of ropinirole. Conversely, the presence of this oscillatory action in high L-DOPA but not ropinirole regimes suggests that this is implicated in dyskinesia.

5.3.9 A Note on Bradykinesia

We have barely mentioned one of the major symptoms of Parkinson's disease; bradykinesia, the difficulty of initiating movement and subsequent slowness of action, such as the shuffling walk seen in many sufferers. Our model has been able to suggest a reason (section 5.3.6) how the cessation of movement may come about (and why the cure works), as the abnormally high firing rate of the striatal neurons clamps the muscles into rigidity.

It has been hypothesised that degradation of the nigrostriatal pathway may slow the dopaminergic signals involved in movement and so lead to a slowing of movement[96]. However the degradation does not slow the propagation of a signal, it merely weakens it.

Whilst none of the following can be deduced directly from our model, if we suppose that our hypotheses on tremors and rigidity are correct we can then extend them to the study of bradykinesia. If we are in an advanced stage of Parkinson's then our striatal neurons will be clamped in the Up state even at rest. This high base firing rate will have the muscles tensed. One could then expect that this uncontrolled activation of opposing muscles would act as a resistor and lead to problems initiating movement and a slowness of motion. Such muscle action may also lead to the observed resistance to passive movement.

5.3.10 Anti-Psychotic Treatments

Aspects of the disorder schizophrenia are thought to arise from dysfunctions in the neighbouring mesolimbic dopamine pathway and sufferers are often treated with dopamine antagonists such as haloperidol or clozapine [43]. Haloperidol, a dopamine D2 antagonist, can have the side effect of inducing Parkinson-like symptoms on its users and these are thought to occur by its action on the nigrostriatal pathway. Clozapine does not have this side effect and is thought to not act on the nigrostriatal pathway, quite why is a different problem that we are not going to concern ourselves with here.

Since haloperidol blocks dopamine D2 receptors, it will serve to reduce the receptors available for activation by released dopamine. In terms of our model this will reduce g_u and hence g'_u, the same change that Parkinson's induces. Hence we would expect haloperidol to induce Parkinson-like effects in our model too.

5.4 Review

We have taken the neuronal network that is supposed to be involved in the action and symptomatic effects of Parkinson's disease and reduced this to a mathematical model that is essentially described in two variables. We have then considered this model in regard to the onset of Parkinson's and claim explanations for many disease symptoms in terms of this model's dynamics. This massive reduction in complexity that still retains what may be the essential features of the disease quite rightly raises questions about our approach.

5.4.1 The Model Circuitry

Firstly we must consider whether we are justified in taking a neuronal system that features thousands of neurons of at least six different types and hundreds of thousands of connections and transforming this into what amounts to a simple loop of two neurons. One of the foremost reasons is that we cannot possibly know the amount of information that would be required to model the entire circuit and even if we did (and managed to create such a model) the result would be as complex and therefore incomprehensible as the true system; we must make simplifications. The inclusion of the dopamine neurons and the striatal projection (medium spiny) neurons is essential since the former is the 'target' of Parkinson's disease and they solely innervate the latter, which also acts as the output of the system, an output which acts as our measure of the onset of the disease's effects [8][71]. The major external (to either nuclei) inputs also connect to these neurons and so we may then ask whether we need to include any other types of neuron if these two already capture the behaviour of the system.

Although the striatal projection neurons do connect directly to the dopamine neurons, and so would be thought to have an inhibitory effect, the indirect connection via the GABAergic interneurons of the substantia-nigra pars reticula is more sensitive [29]. Our approach to modelling a neuron allows us to model this as a simple excitatory input without a separate GABAergic neuron and reduces our model of the substantia nigra to this simple connection.

The striatum has a complicated circuitry and the precise nature of the connections is unknown [8]. Since the input of the dopamine neurons is inhibitory and the net effect of dopaminergic input on the striatal projection neurons is inhibitory ([52]) it is unclear what effect the other types of neurons have besides a likely weak and local modulation. From this viewpoint there is no need to model these local neurons at all. Any effects of such neurons allowing communication between projection neurons locally in the striatum is covered by the inclusion of the gap junction coupling directly between them.

We can therefore capture the essential features of the true neuronal network in this simple loop. Detailed dye-tracing would be needed to know how many dopamine neurons a single striatal neuron may innervate, and vice-versa. We do know that there is likely to be connections to many neurons from single projections and so we have formulated our idea of discrete packets within which each striatal neurons projects to, and receives inputs from, each dopamine neuron. The only inter-packet communication we allow is by gap junctions. This should cover most realities; from the entire system consisting of just one packet to hundreds or thousands of packets of two real neurons.

5.4.2 Neuron Modelling

Much of this simple loop model is enabled by our approach to modelling a single neuron, looking at in terms of average membrane potential and firing rate rather than discrete spikes. Modelling the neurons so that we can deal with individual spikes represents a layer of complication that is unnecessary since we are concerned with the long term (months to years) changes in firing as dopamine cells die. Under these long term conditions the firing rate of a cell is approximately proportional to membrane potential.

In a similar way the synaptic current input to a cell is (approximately) proportional to the number of times it is activated, which is of course proportional to the firing rate of the incident cell. This leads us to model the synaptic inputs as we do.

The model of the dopamine neuron is simple enough, with the membrane's linear current-voltage relationship being well described by a model of leakage current. However the equivalent term for the striatal neuron is more complicated and it is clear from the phase plane diagrams that this term's cubic appearance is the cause of the packet dynamics. The work of Wilson and Kawaguchi [103] reveals that striatal neurons have a combination of two types of voltage-activated potassium channels that typically lead to steady state current graphs with a cubic appearance [98]. We have explicitly used a cubic polynomial that gives this

appearance and our model fits the qualitative behaviour of striatal neurons well; we have discrete Up and Down states with a fast transition between the two and intracellular current injection will shift the time spent in each accordingly.

5.4.3 Model Dynamics

The packet dynamics follow from simple steady state and phase plane analysis. Our only problem is whether our system is likely to have a range of synaptic current inputs when it is bistable, or has a periodic orbit. The condition for a periodic orbit is simple enough but involves quantities that are intrinsic to the model rather than being biological recognisable and capable of estimation. This is not so much a fault, it is a result of the 'averaging' modelling approach that we have needed to take, but a weakness as regards allowing good quantitative estimates of the parameters involved. However we have been able to suggest that the condition for a periodic orbit is met and we have taken this to be so from thereon.

5.4.4 Parkinson's Disease

We then compare the packet dynamics with the changes in parameters that reflect the onset of Parkinson's, which will be to reduce the synaptic strength of the dopaminergic input to the striatal neurons. The cell still responds to the synaptic current input from the cortex correctly, selecting the Up or Down states appropriately, up until the Down steady state loses stability. We hypothesise that this control of the cell reflects normal, unsymptomatic behaviour and that the effects of the disease are only evident after the loss of stability. This gives the system the remaining length of the left branch of the $\dot{v} = 0$ nullcline to decay along before it becomes symptomatic.

We advance the hypothesis that this is why the symptoms of Parkinson's disease are only observable after such massive depletion of the dopamine neurons. The cell can combat the onset of Parkinson's with such compensatory mechanisms as the upregulation of dopamine production and dopamine receptors and the increased excitatory input from the striatal neurons (the latter two of which are featured in our model), all of which will serve to slow its advance into instability. The loss of inhibitory input can be seen to need be to big; the striatal neuron needs the massive excitatory input to the cells to break clear of the Down state, Wilson and Kawaguchi [103] could not with intracellular current injections.

Again we have problems with the quantitative nature of this problem. We provide a sound explanation as to why the system may remain unsymptomatic but cannot attempt to quantify

this. However by comparison to the current injections of Wilson and Kawaguchi we can demonstrate that such instability requires the loss of large amounts of inhibitory input.

Once the Down state loses stability we would expect to see the symptoms of Parkinson's appear. The early clinical signs are a tremor at rest, which is precisely what we get; activation of the striatal neurons to gain movement will still function correctly by selecting the Up state, although during rest the Down steady state is replaced with oscillations.

This raises two questions; do these oscillations exist in striatal neurons? And, can the presence of oscillations really explain tremors? For the first we claim that our oscillations arise naturally from what has so far been a good descriptive model of striatal neuron behaviour and Parkinson's disease. We do not know whether these oscillations have been observed experimentally *in-vivo*; in any case they would be difficult to distinguish from the normal oscillation between Down and Up caused by the synaptic excitation. The apparent absence of an Up state *in-vitro* suggests that this preparation may be unsuitable also.

Given that the oscillations are present in our model, can we really expect them to cause tremors? This is roughly suggesting that the appearance of oscillations and the early symptom of tremors may just be a coincidence. However, Parkinson's disease symptoms arise as a result of the death of dopamine cells whose major innervation is their link to the motor circuits; the striatal neurons. Therefore, whatever the effect the progressive lack of dopamine has, the effects must be carried by the striatal projection neurons and so we deduce the appearance of oscillations is likely to be much more than coincidence, instead we suggest it is the root cause of tremors in early stage Parkinson's disease.

We have explicitly covered the possible problem with the above; that the oscillating packets may not be synchronised and so the resulting output may appear, on the whole, more constant than oscillatory. We considered each neuron to be oscillating and so described by a single phase parameter. Then by considering the difference in phase between them, we have shown that any packets coupled together by gap junctions will indeed synchronise.

We have demonstrated that in what would correspond to late stage Parkinson's disease our model is clamped in the Up state, essentially leaving the striatal neuron permanently on. This would correspond to the transmitting of persistent attempts at movement which one would then expect to clamp muscles into rigidity and produce resistance to any movement. Whether the effect would be this dramatic is arguable, but we shall refer to our statement above that the symptoms must be transmitted through the striatal neurons. Detailed modelling of the post-striatum circuits and muscle activity would be needed to be able to answer this properly,

however we can advance this as a hypothesis for bradykinesia knowing that it is consistent, not only with the symptoms, but also with the earlier results of our model. Some preliminary feel for the viability of this hypothesis could be obtained from intracellular recording from the appropriate neurons (sufficiently accurate mapping is therefore required) and seeing if a clamp in the Up state corresponds to the sufferer's rigidity. We also feel that it provides a more adequate explanation than the degradation of the pathway slowing signals down.

Given that the model's Parkinson-like symptoms arise as a result of dopamine depletion it is not at all surprising that modelling the effect dopaminergic input-boosting drugs causes a reversal of the symptoms. It is interesting however that the different drugs do have slightly different effects and that in particular a strong ropinirole action can remove the oscillatory component of our model. It is this that prompts our investigation of dyskinesia and our subsequent hypothesis on its cause (an oscillatory pseudo-Up state).

It may seem as though we are creating this purely to fit the result of our model and so we should be careful, especially since an oscillatory (jerky?) response in movement may not be the same as a jerky (oscillatory?) unwanted movement. However these may be essentially the same thing and our hypothesis does provide a rather neat explanation for its appearance under high doses of L-DOPA and then why it may not appear for ropinirole users. Indeed motor oscillations have been seen in patients chronically treated with L-DOPA [96]. More detailed modelling of the effect of L-DOPA, featuring treatment protocols and wearing off times would be needed to examine whether over-dosing to such a likely extent is likely. Moreover, any experimental set up that could be used to observe any oscillations in the Down state, regarding tremors, could also be used here.

We have not advanced on hypotheses for some of the other symptoms of Parkinson's disease. These are such things as the stooping posture, excessive sweating and micrographia (small writing) that our model can offer no particular explanations for. Patients often suffer a loss of cognitive ability in the advanced stages of the disease and it would seem likely that this is due to the degeneration of the dopamine pathway to the cortex, rather than through the motor circuit links of the striatum, the effects of which are not addressed by our model.

5.4.5 Summary

We have produced a model of the striatonigral loop involved in the symptomatic expression of Parkinson's disease. This describes well, in a qualitative way, the average firing rates of

the output of the system, namely the striatal medium spiny neurons. Although, by its nature as a measure of averaged responses, it does not permit accurate parameter estimation.

The model allows us to advance sound and consistent hypotheses on many features of Parkinson's disease such as the robustness of the system to the large amounts of dopaminergic depletion; the causes of resting tremor; muscle rigidity in advanced-stage Parkinson's patients and the efficacy of standard treatments. By a consistent extension of these we can suggest possible causes for bradykinesia and dyskinesia, though additional experimentation and modelling is needed to further validate these hypotheses.

Bibliography

[1] The Daily Telegraph, 14th October 1999.

[2] The New Scientist, 31st July 1999.

[3] D.J.K. Balfour, M.E.M. Benwell, and C.E. Birrell. Sensitisation of the mesoaccumbens dopamine response to nicotine. *Pharmacol. Biochem. Behav.*, 59:1021–1030, 1997.

[4] D.J.K. Balfour and K.O. Fagerstrom. Pharmacology of nicotine and its theraputic use in smoking cessation and neurodegenerative diseases. *Pharmacology and Theraputics*, 72(1):51–81, 1996.

[5] M.E.M. Benwell and D.J.K. Balfour. The influence of lobeline on nucleus accumbens dopamine and locomotor responses to nicotine in nicotine-pretreated rats. *Br. J. Pharmacol.*, 125:1115–1119, 1998.

[6] M.E.M. Benwell, P.E. Holtom, R.J. Moran, D.J.K. Balfour, and C.E. Birrell. Neurochemical and behavioural interactions between ibogaine and nicotine in the rat. *Br. J. Pharmacol.*, 117:743–749, 1996.

[7] C.E. Birrell and D.J.K. Balfour. The influence nicotine-pretreatment on mesoaccumbens dopamine overflow and locomotor responses to D-amphetamine. *Psychopharmacology*, 140:142–149, 1998.

[8] J.P. Bolam and B.D. Bennett. Microcircuitry of the neostriatum. In M.A. Ariano and D.J. Surmeier, editors, *Molecular and cellular mechanisms of neostriatal function*, chapter 1, pages 1–19. R.G. Landes Company, 1995.

[9] J. G. G. Borst and B. Sakmann. Calcium influx and transmitter release in a fast CNS synapse. *Nature*, 383:431–434, October 1996.

[10] J.M. Bower and D. Beeman. *The Book of GENESIS.* TELOS, 1995.

[11] D.B. Calne. Differentiation of dopamine agonists and their role in the treatment of Parkinson's Disease. *Journal of Neural Transmission - Supplement*, 56:185–192, 1999.

[12] M. Cammarato, R. Bernabeu, M.L. de Stein, I. Izquierdo, and J.H. Medina. Learning-specific, time-dependent increases in hippocampal Ca^{2+}/calmodulin-dependent protein kinase II activity and AMPA GluR1 subunit immunoreactivity. *Eur. J. Neurosci.*, 10(8):2669–2676, 1998.

[13] W.A Carlezon, K Rasmussen, and E.J. Nestler. AMPA antagonist LY293558 blocks the development, without blocking the expression, of behavioral sensitization to morphine. *Synapse*, 31(4):256–262, 1999.

[14] C.M. Carvalho, I.L. Ferreira, C.B. Duarte, J.O. Malva, L. Tretter, V. Adam-Vizi, and A.P. Carvalho. Relation of $[Ca^{2+}]_i$ to dopamine release in striatal synaptosomes: role of Ca^{2+} channels. *Brain Res.*, 669(2):234–244, 1994.

[15] P.J. Charlety, J. Grenhoff, K. Chergui, B. De La Chapelle, M. Buda, T.H. Svensson, and G. Chouvet. Burst firing of mesencephalic dopamine neurons is inhibited by somatodendritic application of kynurenate. *Acta Physiologica Scandinavica*, 142(1):105–112, 1991.

[16] A.C. Collins and M.J. Marks. Are nicotinic receptors activated or inhibited following chronic nicotine treatment? *Drug Development Research*, 38(3-4):231–242, 1996.

[17] G. de Vries and R.M. Miura. Analysis of a class of models of bursting electrical activity in pancreatic β-cells. *SIAM Journal of Applied Mathematics*, 58(2):607–635, 1998.

[18] G. Di Chiara and A. Imperato. Drugs abused by humans preferentially increase synaptic dopamine concentrations in the mesolimbic system of freely moving rats. *Proc. Natl Acad. Sci. USA*, 85:5274–5278, 1988.

[19] F. A. Dodge and R. Rahamimoff. Co-operative action of calcium ions in transmitter release at the neuromuscular junction. *J. Physiol.*, 193:419–432, 1967.

[20] L. Edelstein-Keshet. *Mathematical Models in Biology.* New York: Random House, 1988.

[21] H. El-Bizri and P. B. S. Clarke. Blockade of nicotinic receptor-mediated release of dopamine from striatal synaptosomes by chlorisondamine and other nicotinic antagonists administered *in vitro*. *Br. J. Pharmacol.*, 111:406–413, 1994.

[22] G.B. Ermentrout and N. Kopell. Oscillator death in systems of coupled neural oscillators. *SIAM Journal of Applied Mathematics*, 50:125–146, 1990.

[23] L.W. Fitzgerald, J. Ortiz, A.G. Hamedani, and E.J. Nestler. Drugs of abuse and stress increase the expression of GluR1 and NMDAR1 glutamate receptor subunits in the rat ventral tegmental area: Common adaptations among cross-sensitizing agents. *J. Neurosci.*, 16(1):274–282, 1996.

[24] R. Fitzhugh. Impulses and physiological states in theoretical models of nerve membrane. *Biophys. J.*, 1:445–466, 1961.

[25] J. Fornaguera, J.P. Huston, R.J. Carey, and R.K.W. Schwarting. Stimulation of D1 receptors of D2 receptors in drug-naive rats with different degrees of unilateral nigrostriatal dopamine lesions. *Psychopharmacology*, 119(2):145–154, 1995.

[26] M. Garcia-Munoz, P. Patino, S.J. Young, and P.M. Groves. Effects of nicotine on dopaminergic nigrostriatal axons requires stimulation of presynaptic glutamatergic receptors. *J. Pharmacol. Exp. Ther.*, 277(3):1685–1693, 1996.

[27] A.A. Grace and B.S. Bunney. The control of firing pattern in nigral dopamine neurons: Burst firing. *J. Neurosci.*, 4:2877–2890, 1984.

[28] A.A Grace and B.S. Bunney. The control of firing pattern in nigral dopamine neurons: Single spike firing. *J. Neurosci.*, 4:2866–2876, 1984.

[29] A.A. Grace and B.S. Bunney. Opposing effects of striatonigral feedback pathways on midbrain dopamine cell activity. *Brain Res.*, 333:271–284, 1985.

[30] A.A. Grace and S-P Onn. Morphology and electrophysiological properties of immunocytochemically identified rat dopamine neurons record *in-vitro*. *J. Neurosci.*, 9(10):3463–3481, 1989.

[31] S.R. Grady, M.J. Marks, and A.C. Collins. Desensitization of Nicotine-stimulated [^{3}H]dopamine release from mouse striatal synaptosomes. *J. Neurochem.*, 62(4):848–855, 1994.

[32] S.R. Grady, M.J. Marks, S. Wonnacott, and Alan C. Collins. Characterization of nicotinic receptor-mediated [^{3}H]dopamine release from synaptosomes prepared from mouse striatum. *J. Neurochem.*, 59(3), 1992.

[33] J. Grenhoff, G Aston-Jones, and T.H. Svensson. Nicotinic effects on the firing of midbrain dopamine neurons. *Acta Physiologica Scandinavica*, 128(3):351–358, 1986.

[34] J. Grenhoff, C.S. Tung, and T.H. Svensson. The excitatory amino-acid antagonist kynurenate induces pacemaker-like firing of dopamine neurons in rat ventral tegmental area *in-vivo*. *Acta Physiologica Scandinavica*, 134(4):567–568, 1988.

[35] J. Grenhoff, L. Ugedo, and T.H. Svensson. Firing patterns of midbrain dopamine neurons - differences between A9-cells and A10-cells. *Acta Physiologica Scandinavica*, 134(1):127–132, 1988.

[36] B. Gustafsson and H. Wigstrom. Physiological mechanisms underlying long-term potentiation. *Trends Neurosci.*, 11(4):156–162, 1988.

[37] S.N. Haber and J.L. Fudge. The primate substantia nigra and VTA: Integrative circuitry and function. *Critical Reviews in Neurobiology*, 1(4):323–342, 1997.

[38] J.K. Hale and H. Koçak. *Dynamics and Bifurcations.* Springer-Verlag, 1991.

[39] B.H. Herman, F. Vocci, and P. Bridge. The effects of NMDA receptor antagonists and nitric-oxide synthase inhibitors on opioid tolerance and withdrawal - medication development issues for opiate addiction. *Neuropsychopharmacology*, 13(4):269–293, 1995.

[40] C.J. Hillard. Nicotine-induced depolarisation of cerebral cortical synaptosomes is dependent upon sodium. *Neuropharmacology*, 31(9):909–914, 1992.

[41] A. L. Hodgkin and A. F. Huxley. A quantitative description of membrane current and its application to conduction and excitation in nerve. *J. Physiol.*, 117:500–544, 1952.

[42] M.W. Holladay, M.J. Dart, and J.K. Lynch. Neuronal nicotinic acetylcholine receptors as targets for drug discovery. *Journal of Medicinal Chemistry*, 40(26):4169–4194, 1997.

[43] J. Ichikawa and H.Y. Meltzer. Differential effects of repeated treatment with haloperidol and clozapine on dopamine release and metabolism in the striatum and the nucleus accumbens. *J. Pharmacol. Exp. Ther.*, 256(1):348–357, 1991.

[44] S.A. Kaiser, L. Soliakov, S.C. Harvey, C.W. Luetje, and S. Wonnacott. Differential inhibition by α-conotoxin-MII of the nicotinic stimulation of [^{3}H]-dopamine release from rat striatal synaptosomes and slices. *J. Neurochem.*, 70(3):1069–1076, 1998.

[45] E.R. Kandel and J.H. Schwartz. *Principles of Neural Science.* Elsevier, 1981.

[46] Y. Kawaguchi, C.J. Wilson, S.J. Augood, and P.C. Emson. Striatal interneurones: chemical, physiological and morphological characterisation. *Trends Neurosci.*, 18(12):527–535, 1995.

[47] J.P. Keener and J. Sneyd. *Mathematical Physiology.* Springer-Verlag, 1998.

[48] W.R. Klemm. *Understanding Neuroscience.* Mosby, 1996.

[49] C. Koch and I. Segev (eds). *Methods in Neuronal Modelling.* MIT Press, 1989.

[50] G.F. Koob. Drugs of abuse - anatomy, pharmacology and function of reward pathways. *Trends In Pharmacol. Sci.*, 13(5):177–184, 1992.

[51] R.M. Kostrzewa. Dopamine-receptor supersensitivity. *Neuroscience and Biobehavioural Reviews*, 19(1):1–17, 1995.

[52] L.J. Krish, M.R. Palmer, and G.A. Gerhardt. Multiple single-unit recordings in the striatum of freely moving animals: effects of apomorphine and D-amphetamine in normal and unilateral 6-hydroxydopamine-lesioned rats. *Brain Res.*, 833(1):58–70, 1999.

[53] J.M. Kulak, T.A. Nguyen, B.M. Olivera, and J.M. McIntosh. α-conotoxin MII blocks nicotine-stimulated dopamine release in rat striatal synaptosomes. *J. Neurosci.*, 17(14):5263–5270, 1997.

[54] M.G. Lacey, N.B. Mercuri, and R.A. North. Dopamine acts on D2 receptors to increase potassium conductance in neurones of the rat substantia nigra zona compacta. *J. Physiol.*, 392:397–416, 1987.

[55] P.D. Lax. *Linear Algebra.* Wiley, 1996.

[56] Y.-X. Li, R. Bertram, and J. Rinzel. Modelling N-methyl-D-aspartate-induced brusting in dopamine neurons. *Neuroscience*, 71(2):397–410, 1996.

[57] P.M. Lippiello, S.B. Sears, and K.G. Fernandes. Kinetics and mechanism of L-[^{3}H]nicotine binding to putative high affinity receptor sites in rat brain. *Molecular Pharmacology*, 31:392–400, 1987.

[58] R. Maldonado, A Saiardi, O. Valverde, T.A. Samad, B.P. Roques, and E.Borrelli. Absence of opiate rewarding effects in mice lacking D2 receptors. *Nature*, 388:586–589, 1997.

[59] R.C. Malenka, J.A. Kauer, D.J. Perkel, M.D. Maud, P.T. Kelly, and R.A. Nicoll. An essential role for postsynaptic calmodulin and protein-kinase activity in long-term potentiation. *Nature*, 340(6234):554–557, 1989.

[60] M.J. Marks, S.R. Grady, and A.C. Collins. Downregulation of nicotinic receptor function after chronic nicotine infusion. *J. Pharmacol. Exp. Ther.*, 266(3), 1993.

[61] N.C.L. McNaughton and A.D. Randall. Electrophysiological properties of the human N-type Ca^{2+} channel. 1. channel gating in Ca^{2+}, Ba^{2+} and Sr^{2+} containing solutions. *Neuropharmacology*, 36(7):895–915, 1997.

[62] L. Michaelis and M.I. Menten. Die kinetik der invertinwirkung. *Biochem Z*, 49:333–369, 1913.

[63] I. M. Mintz, B. L. Sabatini, and W. G. Regehr. Calcium control of transmitter release at a cerebellar synapse. *Neuron*, 15:675–688, 1995.

[64] L. Molloy, S. Wonnacott, T Gallagher, P.A. Brough, and B.G. Livett. Anatoxin-a is a potent agonist of the nicotinic acetylcholine receptor of bovine adrenal chromaffin cells. *Eur. J. Pharmacol.*, 289:447–453, 1995.

[65] C. Morris and H Lecar. Voltage oscillations in the barnacle giant muscle fibre. *Biophys. J.*, 35:193–213, 1981.

[66] J.D. Murray. *Mathematical Biology.* Springer-Verlag, 1993.

[67] D.G. Nicholls. *Proteins, Transmitters and Synapses.* Blackwell, 1994.

[68] J.G. Nicholls. *From neuron to brain: a cellular and molecular approach to the function of the nervous system.* Sinauer, 1992.

[69] M. Nisell, G.G. Nomikos, and T.H. Svensson. Systemic nicotine-induced dopamine release in the rat nucleus accumbens is regulated by nicotinic receptors in the ventral tegmental area. *Synapse*, 16(1):36–44, 1994.

[70] M. Nisell, G.G. Nomikos, and T.H. Svensson. Nicotine dependence, midbrain dopamine systems and psychiatric disorders. *Pharmacology and Toxicology*, 76(3):157–162, 1995.

[71] R.D. Oades and G.M. Halliday. Ventral tegmental (A10) system: neurobiology. 1. anatomy and connectivity. *Brain Res. Rev.*, 12:117–165, 1987.

[72] J.A. Obeso, F. Grandas, M.T. Herrero, and R. Horowski. The role of pulsatile versus continuous dopamine-receptor stimulation for functional recovery in Parkinson's Disease. *Eur. J. Neurosci.*, 6(6):889–897, 1994.

[73] S-P Onn and A.A. Grace. Repeated treatment with haloperidol and clozapine exerts differential effects on dye-coupling betweens neurons in sub regions of striatum and nucleus-accumbens. *Journal of Neuroscience*, 15(11):7024–7036, 1995.

[74] Y. Ouyang, A. Rosenstein, G. Kreiman, E.M. Schuman, and M.B. Kennedy. Tetanic stimulation leads to increased accumulation of Ca^{2+}/calmodulin-dependent protein kinase II via dendritic protein synthesis in hippocampal neurons. *J. Neurosci.*, 19(18):7823–7833, 1999.

[75] L.D. Partridge and C.F. Valenzuela. Ca^{2+} store-dependent potentiation of Ca^{2+}-activated non-selective cation channels in rat hippocampal neurones in-vitro. *Journal of Physiology*, 521(3):617–627, 1999.

[76] G. Paxinos. *The Rat Nervous System: Forebrain and Midbrain*, volume 1. Academic Press, 1985.

[77] P. Popik, R.T. Layer, L.H. Fossom, M. Benveniste, B. Geterdouglass, J.M. Witkin, and P. Skolnick. NMDA antagonist properties of the putative antiaddictive drug, ibogaine. *J. Pharmacol. Exp. Ther.*, 275(2):753–760, 1995.

[78] P. Popik, R.T. Layer, and P. Skolnick. 100 years of ibogaine - neurochemical and pharmacological actions of a putative anti-addictive drug. *Pharmacological Reviews*, 47(2):235–253, 1995.

[79] P.Whiteaker. *Comparison of the effects of nicotine and isoarecolone on nAChR.* PhD thesis, University of Bath, 1996.

[80] W. Rall. Branching dendritic trees and motoneuron resistivity. *Exp. Neurol.*, 1:491–527, 1959.

[81] R.H. Rand, A.H. Cohen, and P.J. Holmes. Systems of coupled oscillators as models of central pattern generators. In A.H. Cohen, editor, *Neural control of rhytmic movements in vertebrates*, chapter 9, pages 333–367. Wiley, 1988.

[82] A. Randall and R.W. Tsien. Pharmacological dissection of multiple types of Ca^{2+} channel currents in rat cerebellar granule neurons. *J. Neurosci.*, 15(3):2218–2224, 1995.

[83] C. Rapier, G.G. Lunt, and S. Wonnacott. Stereoselective nicotine-induced release of dopamine from striatal synaptosomes: Concentration dependence and repetitive stimulation. *J. Neurochem.*, 50(4), 1988.

[84] C. Rapier, G.G. Lunt, and S. Wonnacott. Nicotinic modulation of [^{3}H]dopamine release from striatal synaptosomes - pharmacological characterisation. *J. Neurochem.*, 54(3):937–945, 1990.

[85] L.W. Role and D.K. Berg. Nicotinic receptors in the development and modulation of CNS synapses. *Neuron*, 16(6):1077–1085, 1996.

[86] P.P. Rowell and D.S. Duggan. Long-lasting inactivation of nicotinic receptor function *in-vitro* by treatment with high concentrations of nicotine. *Neuropharmacology*, 37:103–111, 1998.

[87] P.P. Rowell and J.A. Hillebrand. Characterization of nicotine-induced desensitization of evoked dopamine release from rat striatal synaptosomes. *J. Neurochem.*, 63(2), 1994.

[88] P. Sah, A. J. Gibb, and P. W. Gage. The sodium current underlying action potentials in guinea pig hippocampal CA1 neurons. *J. Gen. Physiol.*, 91:373–398, 1988.

[89] P. Sah, A.J. Gibb, and P.W. Gage. Potassium current activated by depolarisation of disassociated neurons from adult guinea pig hippocampus. *J. Gen. Physiol.*, 92:263–278, 1988.

[90] H.S. Schwarzwelder, C. Ferrari, W.W. Anderson, and W.A. Wilson. The drug MK-801 attenuates the development, but not the expression, of long-term potentiation and and stimulus induced bursting in hippocampal slices. *Neuropharmacology*, 28(5):441–445, 1989.

[91] A.M. Shirke and R. Malinow. Mechanisms of potentiation by calcium-calmodulin kinase II of postsynaptic sensitivity in rat hippocampal CA1 neurons. *J. Neurophysiol.*, 78(5):2682–2692, 1997.

[92] M. Shoaib, M.E.M. Benwell, M.T. Akbar, I.P. Stolerman, and D.J.K. Balfour. Behavioural and neurochemical adaptions to nicotine in rats: influence of NMDA antagonists. *Br. J. Pharmacol.*, 111:1073–1080, 1994.

[93] S.M. Simon and R.R. Llinás. Compartmentalization of the submembrane calcium activity during calcium influx and its significance in transmitter release. *Biophys. J.*, 48:485–498, 1985.

[94] L. Soliakov, T. Gallagher, and S. Wonnacott. Anatoxin-a-evoked [^{3}H]dopamine release from rat striatal synaptosomes. *Neuropharmacology*, 34(11):1535–1541, 1995.

[95] L. Soliakov and S. Wonnacott. Voltage-sensitive Ca^{2+} channels involved in nicotinic receptor-mediated [^{3}H] dopamine release from rat striatal synaptosomes. *J. Neurochem.*, 67(1):163–170, 1996.

[96] P.G. Strange. *Brain Biochemistry and Brain Disorders.* Oxford University Press, 1992.

[97] A.C. Taylor, A. Beerahee, D.R. Citerone, M.J. Cyronak, T.J. Leigh, K.L. Fitzpatrick, A. Lopez-Gil, S.D. Vakil, E. Burns, and G. Lennox. Lack of a pharmokinetic interaction at steady state between ropinirole and L-DOPA in patients with parkinson's disease. *Pharmacotherapy*, 19(2):150–156, 1999.

[98] R.D. Traub, R.K.S. Wong, R. Miles, and H. Michelson. A model of a CA3 hippocampal pyramidal neuron incorporating voltage-clamp data on intrinsic conductances. *J. Neurophysiol.*, 66(2):635–650, 1991.

[99] K.A. Trujillo and H. Aki. Excitatory amino-acids and drugs of abuse - a role for *N*-methyl-D-aspartate receptors in drug tolerance, sensitization and physical- dependence. *Drug and Alcohol Dependence*, 38(2):139–154, 1995.

[100] T.J. Turner and K. Dunlap. Pharmacological characterization of presynaptic calcium channels using subsecond biochemical measurements of synaptosomal neurosecretion. *Neuropharmacology*, 34(11):1469–1478, 1995.

[101] M. Umemiya and A.J. Berger. Single channel properties of four calcium channel types in rat motoneurons. *J. Neurosci.*, 15(4):2995–3012, 1995.

[102] P. Whiteaker, C.G.V. Sharples, and S. Wonnacott. Agonist-induced upregulation of the $\alpha 4\beta 2$ nicotinic acetylcholine receptors in M10 cells: pharmacological and spatial definition. *Mol. Pharmacol.*, 53(5):950–962, 1998.

[103] C.J. Wilson and Y. Kawaguchi. The origins of two-state spontaneous membrane potential fluctuations of neostriatal spiny neurons. *J. Neurosci.*, 16(7):2397–2410, 1996.

[104] S. Wonnacott. Presynaptic nicotinic ACh receptors. *Trends Neurosci.*, 20:92–98, 1997.